THE UNIVERSITY
of EDINBURGH

Synthesis, Characterisation and Reactivity Study of Rare Earth Metal Complexes

Kai Wang

Supervisor: Prof. Polly Arnold

Aug 2017

Declaration

Except where specific reference has been made to other sources, the work presented in this thesis is the original work of the author. It has not been submitted, in whole or in part, for any other degree.

Kai Wang

August 2017

Acknowledgements

I would like to express my special appreciation and sincere gratitude to my advisor Professor Polly Arnold. I would like to thank her for encouraging my research and for allowing me to grow as a chemist. Five years have passed since the first time I met her at Fudan University, I have learnt a lot from her through meetings, discussions and travels. Her attitude towards science has greatly influenced my way of scientific thinking, which I appreciated very much.

I would also like to thank all the people in Arnold/Love group. This is my first time studying abroad, and it is all of you who makes me feel like home in Edinburgh. I feel so privileged to meet all the great names below: Prof. Jason Love, Dr Nicola Bell, Dr Yat-Ming So, Dr Brad Cowie, Dr Tatsumi Ochiai, Philipp Altmann, Marketa Suvova, James Pankhurst, Max McMullon, Jordann Wells, Massimiliano Curcio, Jamie Purkis, Brain Shaw, Megan Seymour, Karlotta van Rees, Connor Halliday, Ryan Kerr and so on. I want to thank you for all the days we had and all the memories we enjoyed. A special thank you to Dr Catherine Weetman for her kind help in reviewing this thesis.

I would like to thank all the staff within our department who have provided magnificent support for my research. Thanks Dr Juraj Bella and Dr Lorna Murray for the help in running NMR spectroscopy and Dr Gary Nichol for the crystal related issues. I also would like to thank Prof Neil Robertson for his guidance and support in running the internationalisation group, from which I learnt a lot.

My thanks also go to my friends. I appreciate the time I travelled with Dr Ju Wang and also the philosophy discussions with him. I appreciate the days spent in the ballroom with Ross Muir and the jokes we laughed. I also appreciate the evenings I trained for badminton and the days I coached with Dr Weigang Liu and Peter Chiu. And also thanks to everyone in ECBC.

A special thanks to my family. In the place deep in my heart, you are always there. Word cannot express how grateful I am to my parents and sisters. Thanks for all your support.

Abstract

The Chapter one introduces the reported examples of rare earth metal (RE) complexes with different oxidation states. It also reviews the synthesis and reactivity study of N-heterocyclic carbene (NHC) supported transition metal and RE metal complexes.

Chapter two focusses on the synthesis and characterisation of a series of tetraaryloxide Ce and Pr complexes. With the reaction of bulky tetraphenol proligand H_4L^R(R = P, PT, M) with four equivalents of KN"(N" = $N(SiMe_3)_2$), a dimerised complex of $[K_4L^P]_2(thf)_{11}$ was synthesised and characterised. The salt metathesis reactions of this complex with $RECl_3(thf)_2$ afford bimetallic aryloxide complexes of $K_2L_2RE_2(thf)_{11}$ (RE = Ce, Pr), which display divergent structures under different conditions. Reactions of the Ce^{III} complex of $K_2L_2Ce_2(thf)_{11}$ with a variety of oxidants(I_2, $CuCl_2$ and O_2, *etc.*) lead to the oxidation of Ce^{III} to Ce^{IV}, affording purple ceric dimer of L_2Ce_2. The reaction of the Pr^{III} complexes with I_2 under 60 °C affords a mixture from which Pr^{III} iodide (LPr_2I_2) has been isolated and characterised. This chapter also discusses the reactivity of the bimetallic aryloxide complexes towards different substrates, such as MeLi, KC_8 and KBn (Bn = benzyl). Bimetallic complexes of $L(REX)_2(py)_8$ (RE = Ce, Pr; X = Cl, BH_4) are synthesised and characterised. The preliminary study on the copolymerization of cyclohexene oxide (CHO) and CO_2 is conducted for Ce^{III} and Pr^{III} complexes.

Chapter three details the work on two different types of NHC ligand. The first ligand is the β-ketoimidazolinium salts H_2LBr {L = $RC(O)CH_2${$CH[NCH_2CH_2NMes]$, R = ^{t}Bu, naphth} which reacts with $MHBEt_3$ (M = Na, K) to form carbene-borane adducts $RC(O)CH_2${$C(BEt_3[NCH_2CH_2NMes]$}. This type of reactivity differs from the previous work on imidazole derivatives. The possible mechanism of these reactions is provided and discussed. The other ligand is *p*-aryloxy-tethered imidazolinium salt H_2LX (L = *N*-3,5-di-*tert*-butyl-4-hydrooxyphenyl-N'-mesityl-imidazolinium, X = Cl, Br, PF_6), which have been synthesised and characterised. The reactions of these salts with MN"(M = Na, K) enabled the characterisation of polymerised complexes of $[NaL]_n$ and $[KL(thf)_2]_n$. The yttrium complex YL_3 is synthesised and its reactivity towards small molecules such as boranes, CO_2 and CS_2 is discussed.

Chapter four presents the primary results on the study of macrocyclic NHC based cyclophane ligand H_6LPF_6 (L = calix[4]imidazolylidene[2]pyrazolato). Investigations on the reactivity of the ligand towards different bases (NaN", KN", KBn *etc*.) are examined and subsequent metathesis reactions with RE complexes are explored.

Chapter five concludes the work presented in this thesis.
Chapter six contains all experimental and characterisation details.

Abbreviations

acac	acac = acetylacetonate
Ad	adamantyl
Ar	generic aryl group
atm	standard atmosphere
BDI	κ^2-{2,6-$^{i}Pr_2C_6H_3NCMe\}_2CH$
BINOL	1,1'-bi-2-naphthol
BMP	2,2'-methylenebis(6-tert-butyl-4-ethylphenolate)tert-butyl-4-methylphenolate)
^{n}Bu	n-butyl
^{t}Bu	tertiary-butyl
^{i}Bu	isobutyl
Bz	N,N-dimethyl-ortho-benzyl
CAN	ceric ammonium nitrate, $(NH_4)_2Ce(NO_3)_6$
cod	1,5-cyclooctadiene
Cp	cyclopentadienyl, C_5H_5
Cp*	pentamethylcyclopentadienyl, C_5Me_5
Cp"	1,3-di-$SiMe_3$-C_5H_3
Cy	cyclohexyl
DCM	dichloromethane
dip2-pyr	2,5-bis[N-(2,6-di-isopropylphenyl)iminomethyl]pyrrole
Dipp	2,6-^{i}Pr-C_6H_3
IPr	1,3-bis(2,6-di-isopropylphenyl)-imidazol-2-ylidene
L_{OEt}^{-}	$[CpCo\{P(O)(OEt)_2\}_3]^{-}$
Me	methyl
MeCN	acetonitrile
Mes	mesityl or 2,4,6-Me-C_6H_2
napth	2-naphthyl
NHC	N-heterocyclic carbene
N"	$N(SiMe_3)_2$
NN′	$N(CH_2CH_2NSiMe_2tBu)_3$
Ph	phenyl
PNP	$(^{t}Bu_2PCH_2SiMe_2)_2N$
^{i}Pr	iso-propyl
OCO	OCO = 1,3-di(2-hydroxy-5-tert-butylphenyl)imidazolyl
OTf	Trifluoromethanesulfonate (triflate)
pTsOH	p-Toluenesulfonic acid
Py	pyridine
r	CH_2SiMe_3 or CH_2CMe_3
RE	Rare earth metals/elements
THF/thf	tetrahydrofuran
TMEDA	tetramethylethylenediamine

Table of Contents

1. Introduction 1

1.1. Rare earth metals 1

1.2. Rare earth metal complexes 2

1.2.1. RE^{III} complexes 2

1.2.2. High oxidation state complexes 4

1.2.3. Low oxidation state complexes 12

1.3. N-heterocyclic carbenes 14

1.4. Reactivity of NHCs 15

1.4.1. NHC-mediated small molecule activation 15

1.4.2. NHC-borane adducts 17

1.5. Metal NHC complexes 18

1.5.1. Unfunctionalised NHC complexes 18

1.5.2. Tethered NHC complexes 18

1.5.3. Macrocyclic NHCs 26

1.6. Reactivity of rare earth metal NHC complexes 28

1.6.1. Redox chemistry 28

1.6.2. Addition - elimination reaction 28

1.6.3. C-E (E = Si, P, Sn) and C-C bond formation 29

1.6.4. Activation of CO_2 and CS_2 31

1.6.5. C-H and N-H activation 33

1.7. Aims of Project 35

1.8. References 36

2. Synthesis and Reactivity of Tetraaryloxide Rare Earth Complexes 43

2.1. Introduction 43

2.2. Reactivity of ligands towards bases 45

2.2.1. Synthesis of potassium complexes 45

2.2.2. Other deprotonations 50

2.3. Synthesis of dinuclear rare earth metal complexes 51

2.3.1. Synthesis of complex $K_2L_2RE_2$ (5) 51

2.3.2. Attempted Synthesis of Other Complexes 56

2.3.3. Comparison of complex 5 to U and Ce complexes 57

2.4. EPR study on complex 5-Ce^{PT} 58

2.5. Reactivity of complex $K_2L_2RE_2$ (5) 60

2.5.1. Complex 5 towards coordinating molecules 60

2.5.2. Oxidation of cerium complexes 5-$Ce^{P/PT}$ 64

2.5.3. Reaction of $[K_2L_2Ce_2]$ towards other substrates 70
2.5.4. Oxidation of praseodymium complexes 5-Pr^{PT} 71
2.5.5. Reactivity of $[K_2L_2Ce_2]$ with KC_8 75
2.5.6. Reactivity of $[K_2L_2Ce_2]$ towards MeLi 76
2.5.7. Synthesis and reactivity study of cerium benzyl complex 78
2.6. Synthesis and reactivity of $L(RECl)_2$ 84
2.6.1. Synthesis of $L(RECl)_2$ 84
2.6.2. Comparison of complex $L(RECl)_2$ to U^{IV} complexes 86
2.6.3. Reactivity of $L(RECl)_2$ towards $AgPF_6$ 86
2.6.4. Synthesis of RE amide complexes 88
2.7. Synthesis of $L\{Ln(BH_4)\}_2$ 90
2.8. Synthesis of Ce^{IV} complexes 93
2.9. Studies on polymerisation 94
2.10. References 96
3. Synthesis and Reactivity Study of Saturated N-Heterocyclic Carbenes 99
3.1. Introduction 99
3.2. Ligand Synthesis 100
3.3. Reactivity of imidazolinium salts 102
3.3.1. Reaction of 38e and 38f with $MHBEt_3$ 102
3.3.2. Discussion of differences in the reactions with $KHBEt_3$ 104
3.4. Reaction of imidazolinium salts with $MYN"_4$ (M = Li, K) 106
3.5. Synthesis of p-aryloxy-tethered imidazolinium salt H_2LX 107
3.6. Synthesis of $[NaL]_n$ complex 110
3.7. Synthesis of $[KL(thf)_2]_n$ complex 111
3.8. Synthesis of $YL_3(KCl)_3(thf)_6$ 114
3.9. Attempted synthesis of CeL_3 115
3.10. Synthesis of $LYCp_2$ 116
3.11. Reactivity of $YL_3(KCl)_3(thf)_6$ towards boranes 117
3.12. Reactivity of $YL_3(KCl)_3(thf)_6$ towards CO_2/CS_2 119
3.13. References 123
4. Synthesis and Reactivity of Pyrazolate- Supported Macrocyclic NHC Complexes 126
4.1. Introduction 126
4.2. Synthesis of RE complexes 127
4.2.1. Reaction of proligands with KN" 127

4.2.2. Reaction of complex 61 with $RECl_3(thf)_2$ (RE = Sc, Y, Ce) 129
4.3. Reaction proligands with $MgN"_2$ 130
4.4. Reactivity of complex 63-Me 133
4.4.1. With Ag_2O 133
4.4.2. With $SmI_2(thf)_2$ and $UI_4(dioxane)_2$ 133
4.5. Reaction of 60-Me with $REN"_3$ (RE = Sc, Ce) 134
4.6. Transmetalation reaction with pillarplex complex 135
4.7. References 136
5. Conclusions 137
6. Experimental Procedures 142
6.1. General Experimental 142
6.2. Experimental for Chapter 2 143
6.3. Experimental for Chapter 3 160
6.4. Experimental for Chapter 4 168
6.5. Crystal data and structure refinement details 173
6.6. References 183

1.Introduction

1.1. Rare earth metals

According to IUPAC Recommendations,[1] a rare earth element (RE) or rare earth metal, is one of a set of seventeen chemical elements in Group III of the periodic table, specifically scandium and yttrium, as well as fifteen lanthanides.

Amongst the REs, the lanthanides exhibit a number of features in their chemistry that differentiate them from the d-block metals.[2] For instance, the 4f orbitals are well shielded by the $5s^2$ and $5p^6$ orbitals in the Ln^{3+} ion, which makes the 4f electrons unlikely to participate directly in bonding. As a result, their spectroscopic and magnetic properties are largely uninfluenced by the ligand.[3, 4]

Due to their unique magnetic,[3, 5] luminescent,[4] and electrochemical properties,[6] these elements help make many technologies perform with reduced weight, reduced emissions and energy consumption. REs are vital to many modern technologies, including consumer electronics, computers and networks, communications, clean energy, national defence, and many others.

Scandium and yttrium are electropositive metals. The ionic radii of Sc^{3+} and Y^{3+} are 0.745 Å and 0.900 Å, respectively. (**Table 1-1**). The former is much smaller than any Ln^{3+} ion but yttrium is very similar to Ho^{3+} (radius 0.901 Å). Based on the size, it would be expected that yttrium would resemble the later lanthanides in coordination chemistry but that scandium would exhibit considerably different properties. The Sc^{3+} ion has the largest radius of the metals in its period, so that high coordination numbers (from 3 to 9) are frequently reported in its complexes.[7]

Table 1-1. Ionic radii of the rare earth metals (pm) (in six coordination).

Sc^{3+}	Y^{3+}	La^{3+}	Ce^{3+}	Pr^{3+}	Nd^{3+}	Pm^{3+}	Sm^{3+}	Eu^{3+}
74.5	90	103.2	101	99	98.3	97	95.8	94.7
Gd^{3+}	Tb^{3+}	Dy^{3+}	Ho^{3+}	Er^{3+}	Tm^{3+}	Yb^{3+}	Lu^{3+}	
93.8	92.3	91.2	90.1	89	88	86.8	86.1	

Due to the large ionic radii, yttrium and rare earth metals tend to have a very wide range of coordination numbers (generally 6-12, but numbers of 2, 3 or 4 are known). RE^{3+} ions are regarded as hard Lewis acid and they prefer anionic ligands with donor atoms of rather high electronegativity (*e.g.* O, F). In the rapidly developing field of rare earth organometallic chemistry, the use of ancillary ligands is essential for stabilising highly reactive metal complexes.[8] Sterically bulky ligands are used for the purpose of saturating the large coordination sphere of these metals which has led to the formation of remarkably stable

compounds, and also new forms of reactivity, such as sterically induced reduction.[9] In other cases, this crowding also facilitates the ligand cyclometalative C–H bond activation.[10]

1.2. Rare earth metal complexes

1.2.1. RE^{III} complexes

For most of the REs, their chemistry is dominated by the +III oxidation state due to their relatively high fourth ionisation energy, I_4, which is greater than the combined energy of first three ionisations ($I_3 + I_2 + I_1$).[7] The electron configurations of REs at different oxidation state are listed in **Table 1-2**. The bold letters highlight the oxidation states of different REs with a half full or empty shell configuration.

Table 1-2. Electron configuration of rare earth metals.

	Inner-sphere configuration	Electron configuration of different oxidation state(OS)				
		0	**+1**	**+2**	**+3**	**+4(or higher)**
Sc	[Ar]	$3d^14s^2$	$3d^14s^1$	$3d^1$	[Ar]	/
Y	[Kr]	$4d^15s^2$	$4d^15s^1$	$4d^1$	[Kr]	/
La	[Xe]	$5d^16s^2$	$5d^16s^1$	$5d^1$	[Xe]	/
Ce	[Xe]	$4f^15d^16s^2$	N/A	$4f^15d^1$	$4f^1$	**$4f^0$**
Pr	[Xe]	$4f^36s^2$	N/A	$4f^3$	$4f^2$	$4f^1$,**$4f^0$(+5)**
Nd	[Xe]	$4f^46s^2$	N/A	$4f^4$	$4f^3$	$4f^2$
Pm	[Xe]	$4f^56s^2$	N/A	$4f^5$	$4f^4$	$4f^3$
Sm	[Xe]	$4f^66s^2$	**$4f^7$**	$4f^6$	$4f^5$	$4f^4$
Eu	[Xe]	$4f^76s^2$	N/A	**$4f^7$**	$4f^6$	$4f^5$
Gd	[Xe]	$4f^75d^16s^2$	N/A	$4f^75d^1$	**$4f^7$**	$4f^6$
Tb	[Xe]	$4f^96s^2$	N/A	$4f^9$	$4f^8$	**$4f^7$**
Dy	[Xe]	$4f^{10}6s^2$	N/A	$4f^{10}$	$4f^9$	$4f^8$
Ho	[Xe]	$4f^{11}6s^2$	N/A	$4f^{11}$	$4f^{10}$	$4f^9$
Er	[Xe]	$4f^{12}6s^2$	N/A	$4f^{12}$	$4f^{11}$	$4f^{10}$
Tm	[Xe]	$4f^{13}6s^2$	N/A	$4f^{13}$	$4f^{12}$	$4f^{11}$
Yb	[Xe]	$4f^{14}6s^2$	N/A	**$4f^{14}$**	$4f^{13}$	$4f^{12}$
Lu	[Xe]	$4f^{14}5d^16s^2$	N/A	$4f^{14}5d^1$	**$4f^{14}$**	$4f^{13}$

Rare earth metal triflates (excluding Pm), $RE(OTf)_3$($OTf = CF_3SO_3^-$), are excellent catalysts in organic synthesis for C-C bond formation, C−E (E = N, O, P, etc.) bond formation, and polymerization etc.[11]

The homoleptic *tris-bis*(trimethylsilyl)amido RE^{III} complexes (**A**, **Scheme 1-1**), $REN"_3$ (RE = Y, Sc or Ln, N" = $N(SiMe_3)_2$), are extremely useful synthetic precursors in rare earth chemistry. The whole series has been prepared either by the treatment of one equivalent of $RECl_3$ with three equivalents of MN" (M = Li, Na or K) [12, 13] or via the reaction of one equivalent of $RE(OTf)_3$ (RE = Ce, La, Nd, Sm and Er) with three equivalents of NaN".[14] $REN"_3$ have been widely utilised in protonolysis reactions with more acidic protic ligands HA to form M-A bonds and eliminate less acidic HN". The treatment of $Ln[N(SiMe_3)_2]_3$ (Ln = Y, La, Nd, Gd, Tb, Dy, Er, Lu) with K leads to the reduction of dinitrogen bridging complexes, $[(Me_3Si)_2N]_2(THF)Ln\}_2(\mu\text{-}\eta^2\text{:}\ \eta^2\text{-}N_2)$, **B** (Equation b, **Scheme 1-1**).[15]

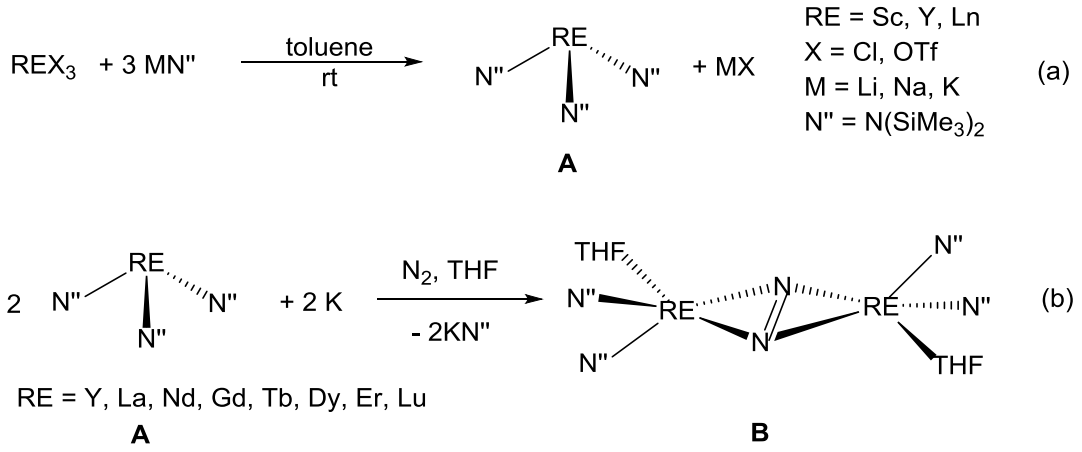

Scheme 1-1. Synthesis and reactivity of homoleptic $REN"_3$ (RE = Y, Sc or Ln) complexes.

The first example of lanthanide complex mediated C-H activation was reported by Watson in 1983.[16] In this study, lutetium methyl complex **C** (**Scheme 1-2)** reacts with ^{13}C labelled methane to yield ^{13}C labelled methyl complex **D**, as a σ-bond activation product. This reaction showed the great potential of RE^{III} alkyl complexes in small molecule activation.

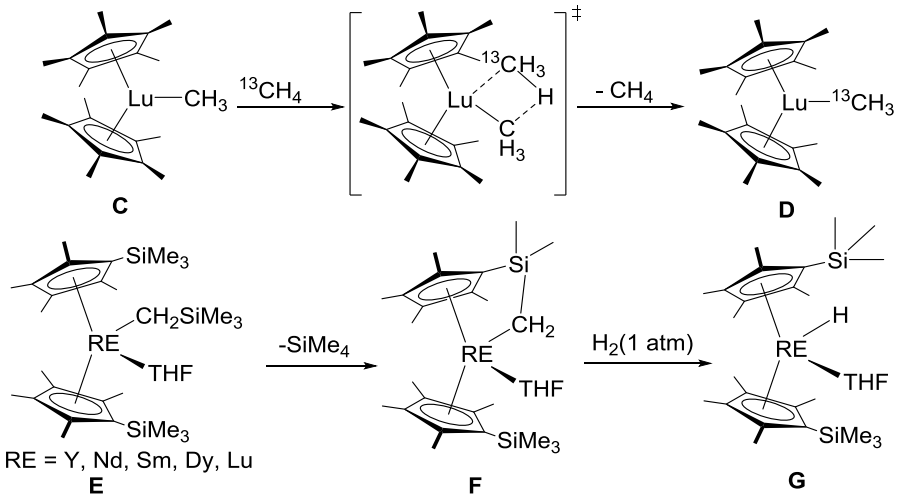

Scheme 1-2. Activation of CH_4 by Cp^*_2LuMe.

Hou *et al.* reported a series of rare earth metal alkyl complexes **E**, which readily activate the C-H bond of the trimethylsilyl group to yield the 'tuck-in' complex **F** (**Scheme 1-2**).[17] The reaction of complexes **F** with H_2 (1 atm) in toluene-d_8 at room temperature led to the methylene chelation and simultaneous formation of the corresponding metallocene hydride species **G**, which has been characterised as {[$(C_5Me_4SiMe_3)_2$REH(THF)]} (RE = Y, Nd, Sm, Dy, Lu) (**Scheme 1-2**).

1.2.2. **High oxidation state complexes**

One of the most fundamental aspects of any element is the number of oxidation states accessible to it. The limits of oxidation states for each element have been heavily probed for decades and are well established.

Amongst rare earth elements, cerium is the only exception, where a myriad of +IV oxidation state complexes has been documented. The thermodynamic basis for the isolation of cerium complexes is due to the close-shell electronic configuration of Ce^{IV} ([Xe]$4f^0$, **Table 1-2**), which contributes to the stabilisation of the complexes.

Inorganic Ce^{IV} complexes

Ce^{IV} complexes are highly oxidising, the most commonly known Ce^{IV} complex is ceric ammonium nitrate (CAN), which has been widely used in organic synthesis and catalysis for one-electron oxidation,[18] generation/cleavage of carbon-heteroatom bonds[19, 20] and formation of the carbon-carbon bond.[21] Furthermore, the CeF_4 molecule is quite stable and has an application as a fluorinating agent.[22] For example, the reaction between fullerene C_{60}(s) and CeF_4(s) at T ≈ 520 K selectively yields $C_{60}F_{36}$ (~90-95 mol %).[23]

Ce^{IV} alkoxide complexes

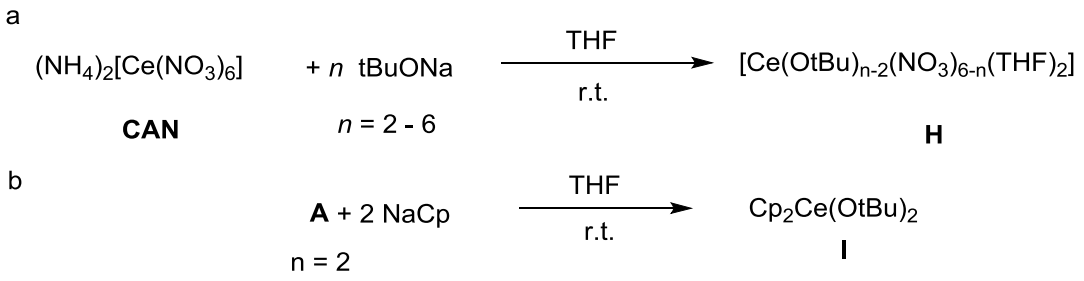

Equation 1-1. Synthesis of Ce^{IV} alkoxide complexes.

Evans and co-workers[24] reported the synthesis of Ce^{IV} alkoxide/nitrate complex, (**H**, **Equation 1-1, a**), by the reaction of CAN and NaO^tBu. Treatment of these alkoxide/nitrate complexes with NaCp (Cp = cyclopentadienyl) affords Ce^{IV} biscyclopentadienyl-bis-*ter*t-butoxide complexes (**I**, **Equation 1-1, b**) at 90% yield.[25]

Lappert and co-workers[26] reported that by treating $[Ce(O^tBu)_4(THF)_2]$ or $[Ce(O^tBu)_3(NO_3)]$ with three equivalents of $[SnCp''Me_3]$ (Cp" = 1,3-$C_5H_3(SiMe_3)_2^-$), a mixed valence trinuclear cluster, $[\{Ce(O^tBu)_2\}_2(\mu_3\text{-}O^tBu)_2\{Ce(O^tBu)(\kappa^2\text{-}NO_3)\}]$ **J**, was obtained. In the complex, the nitrate coordinated Ce atom has a formal oxidation state of +III while the other two Ce cations are tetravalent. **Scheme 1-3**.

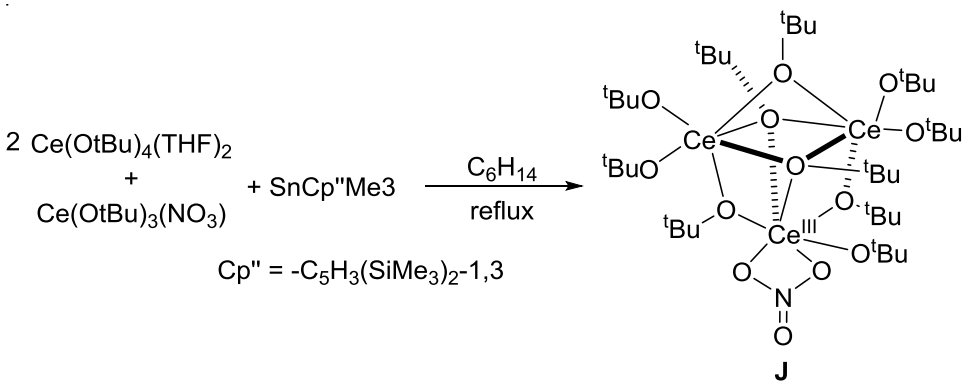

Scheme 1-3. Synthesis of mixed valence trinuclear Ce complex.

Sen and co-workers[27] reported one-electron oxidation of $Ce(OC^tBu_3)$ with di-*tert*-butyl peroxide and benzoyl peroxide to afford the Ce^{IV} complexes **K** and **L**, respectively. (**Scheme 1-4**).

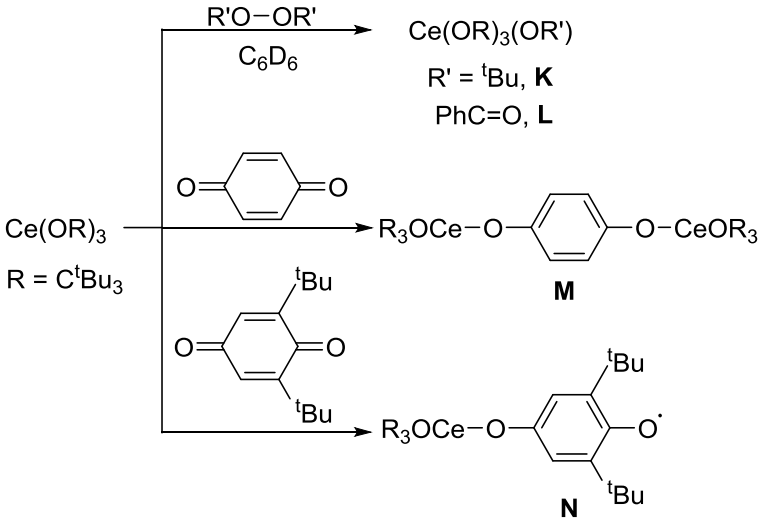

Scheme 1-4. Oxidation reactions of $Ce(OC^tBu_3)$.

The oxidation of $Ce(OCtBu_3)$ with benzoquinone yield the hydroquinonediolate bridged tetravalent binuclear complex, **M**.(**Scheme 1-4**). However, when treated with 2,6-di-*tert*-butylbenzoquinone, the only product is the hemiquinone complex **N**, ($[Ce(OR)_3(O\text{-}2,6\text{-}(^tBu)_2C_6H_2O\cdot])$. The ^1H NMR spectrum shows a paramagnetic species in which the lone electron was localised on the phenyl ring. The existence of the radical product is confirmed by ESR measurements where a single sharp line was seen at $g = 1.9993$.

Schelter and co-workers[28] reported the synthesis of rare earth/alkali metal/1,1′−BINOLate (REMB) heterobimetallic framework (**O**), which uses redox-inactive metals within the secondary coordination sphere to control ligand reorganisation.[29] The choice of alkali metal (M) alters the oxidation reactivity of the complexes. In the case of M = Li, the first general examples of inner-sphere functionalisation (**P**) were achieved through oxidative functionalisation and salt-metathesis, whereas M = Na and K undergo salt elimination pathways, affording alkali-metal "-ate" complexes (**Q**). (**Scheme 1-5**).

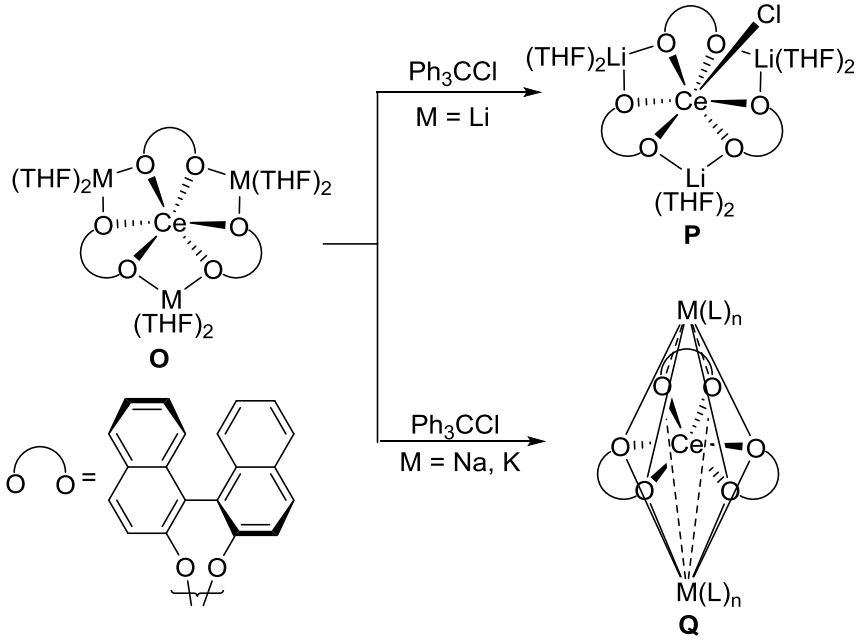

Scheme 1-5. Rare earth/alkali metal/1,1′−BINOLate (REMB) heterobimetallic framework.

Gottfriedsen and Dorokhin treated $Ce(acac)_4$ (acac = acetylacetonate) with *p*-^{t}Bu-calix[4]$(OMe)_2(OH)_2$ in toluene to give the cerium^{IV} calix[4]arene complex [*p*-^{t}Bu-calix[4]$(OMe)_2(O)_2Ce(acac)_2$], **R** (**Scheme 1-6**).[30]

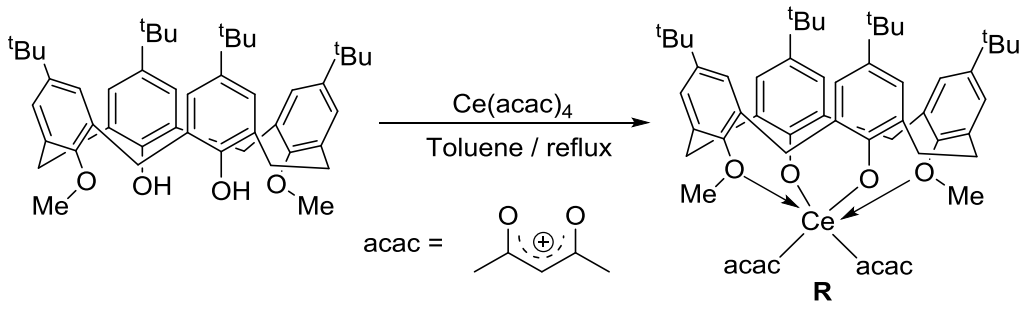

Scheme 1-6. Synthesis of cerium^{IV} calix[4]arene complex.

Ce^{IV} amide complexes

Scott and co-workers reported the oxidation of Ce^{III} amide complex **S**{$[Ce(NN')_3]$ (NN' = $N(CH_2CH_2NSiMe_2{}^tBu)_3$)} by treatment with bromine or chlorine yielded the mixed valence $Ce^{III/IV}$ complexes **T**, {$[\{Ce(NN')_3\}_2(\mu\text{-}X)]$, (X = Cl, Br)}. Treatment with iodine forms the Ce^{IV} complex $[Ce(NN')_3I]$ **U**, (**Scheme 1-7**).[31]

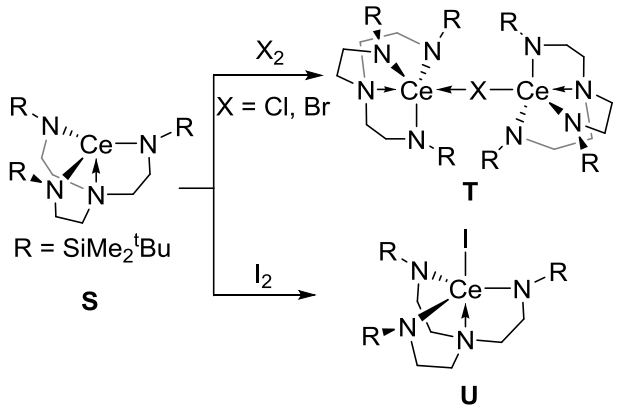

Scheme 1-7. Synthesis of $[\{Ce(NN'_3)\}_2(\mu\text{-}X)]$ and $[Ce(NN'_3)I]$.

Under oxidising conditions, cerium complexes will often undergo ligand redistribution reactions to afford rearranged products. Lappert and coworkers reported that the homoleptic Ce^{IV} amide complex $[Ce(NCy_2)_4]$, **V** (a, **Equation 1-2**), can be synthesised by reacting Ce^{III} precursors with oxygen in 35% yield.[32] The homoleptic Ce^{IV} complex $Ce[N(SiHMe_2)_2]_4$, **W** (b, **Equation 1-2**), is similarly formed through a similar process in the reaction of $Ce[N(SiHMe_2)_2]_3(THF)_x$ (x = 0, 2) with $PhICl_2$.[33]

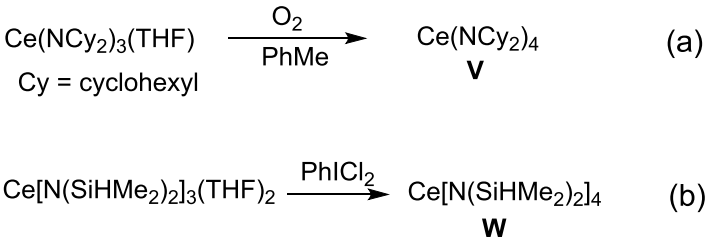

Equation 1-2. Oxidation of Ce^{III} amide complex.

Lappert and co-workers reported the first oxidation of $[Ce(N'')_3]$ to the tetravalent heteroleptic $[Ce(N'')_3Cl]$ **X**, (**Scheme 1-8**).[34] They observed that $[Ce(N'')_3]$ was inert to Cl_2 but would react with 0.25 equivalents of $TeCl_4$ to give dark purple needles of **X** in a relatively low yield of 20-30%. Arnold group improved the yield to quantitative conversion by oxidising $[Ce(N'')_3]$ with the commercially available trityl chloride, which releases Gomberg's dimer, $(Ph_3CCH(C_6H_4)CPh_2)$ **Y**, as the only byproduct, **Scheme 1-8**.[35]

Lappert and co-workers further reported no reaction of [CeN"$_3$] towards I_2 and Br_2 while it can be oxidised by $Ph_3PBr_2Ph_3$ to form the tetravalent bromide complex [Ce(N")$_3$Br] **Z**, (**Scheme 1-8**).[36]

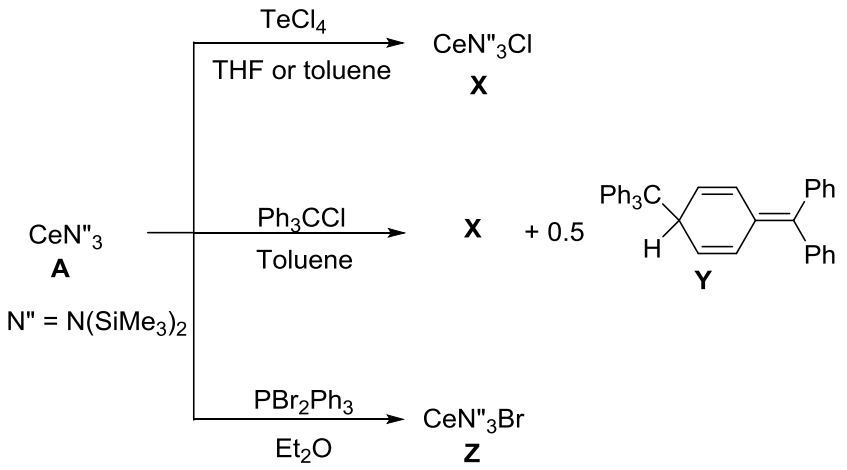

Scheme 1-8. Synthesis of [CeN"$_3$Cl] and [CeN"$_3$Br].

Lappert and co-workers reported unprecedented amido Ce^{IV} oxo-bridging complexes **AA** and **AB** (**Scheme 1-9**).[37] They found that the homoleptic [Ce(N")$_3$] can be oxidised with O_2 at -27 ˚C to form oxo-bridged complex **AA** at 38% yield. The cyclotriceroxane complex **Y** is a result of the reaction of cerium trisamide **A** with 2,6-di-^{t}Bu-1,4-benzoquinone at room temperature in a low crystalline yield of 10%. **AB** is very sensitive to temperature as it decomposes upon heating to room temperature.[37]

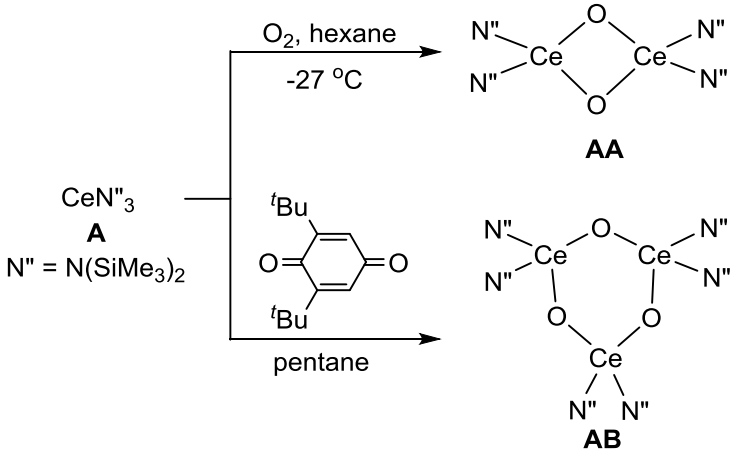

Scheme 1-9. Synthesis of the oxo-bridged Ce^{IV} amide complexes.

Cerocenium complexes

The first cerocene complex **AC**, $[Ce(COT)_2]$ (COT = cyclooctatetraenyl = η^8-C_8H_8) (**Scheme 1-10**), was synthesised by Cesca and co-workers.[38] Given the stoichiometry and formula of this complex and combined with spectral data, the compound was initially reported to be a tetravalent compound.[39] Full characterisation of this type of compound **AD** was accomplished by Streitwieser and coworkers with the methyl-substituted ligand, $[Ce(\eta^8\text{-}C_8H_7Me)_2]$.[40] However, reactivity studies on these compounds are rare due to their poor solubility in organic solvents. Edelmann and co-workers improved its solubility in organic solvents by introducing trimethylsilyl groups to the ligand to form the complex **AE** (**Scheme 1-10**).[41] Cerocenium complex with bulky triphenylsilyl groups as substituents **AF** has been synthesised by Evans and co-workers.[42]

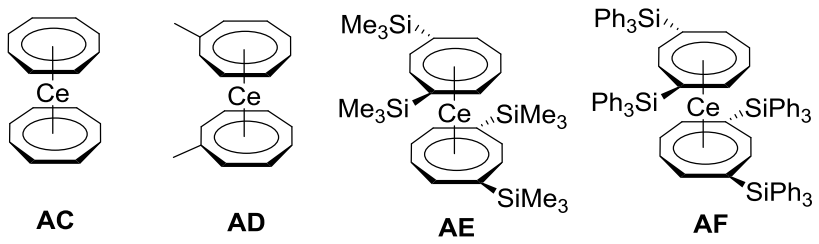

Scheme 1-10. Cerocene complexes.

Ce^{IV}=E (E = oxo, imido, carbene, etc.) multiple bond complexes

Due to the mismatch between the d_π(Ln) and p_π(E) (E = O, N, etc.) orbitals, stable isolated lanthanide (Ln) compounds with multiple bonded ligands are scarce. The nature of these multiple bonds is usually polar (i.e., $Ln^+{-}E^-$). As a result, Ln = E complexes are kinetically unstable and are prone to react with electrophiles/nucleophiles.[43]

So et al. reported that by introducing π-donating Kläui tripodal oxygen ligand L_{OEt}^- $\{[CpCo\{P(O)(OEt)_2\}_3]^-\}$, tetravalent cerium complex **AG** $\{[Ce{=}O(L_{OEt})_2(H_2O)]\cdot MeC(O)NH_2\}$ (**Scheme 1-11**), which contains a Ce=O bond can be synthesised and characterised.[44] DFT calculations of the complex revealed that the occupied bonding molecular orbitals relevant to the Ce−O π and σ bonds in **AG** are mostly localized on the oxo group. Thus, the Ce−O bond is best described as a polarized multiple bond, i.e., Ce=O ↔ $Ce^+{-}O^-$.[45] Complex AC is highly nucleophilic and reacts rapidly with carbon dioxide (CO_2) in air to give a Ce^{IV} carbonate complex **AH**. It is also redox active and can reduce carbon monoxide (CO) to form a dinuclear Ce^{III} carbonate complex **AI** (**Scheme 1-11**).

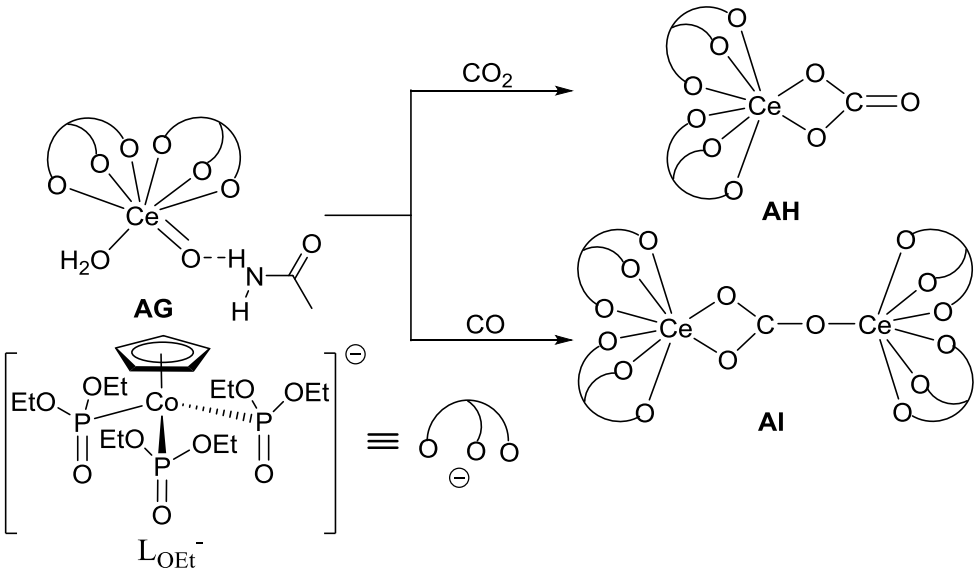

Scheme 1-11. The reaction of Ce^{IV}=O complex towards CO_2 and CO.

Schelter and co-workers expand on a new strategy for isolating terminal lanthanide cerium^{IV} imido complexes.[46] With the help of tris(hydroxylaminato) ligand framework, [$TriNOx_3^-$], which provides steric and electronic protection against side reactions, they managed to isolate the first formal Ce=N bonded moiety in the complex **AJ**, $[K(DME)_2][Ce{=}N(3,5\text{-}(CF_3)_2C_6H_3)(TriNOx)]$ (**Scheme 1-12**). In this alkali metal-capped complex, the Ce=N bond is the shortest known at 2.119(3) Å. The nucleophilic character of the Ce=N fragment in this complex is well demonstrated by its reaction with the electrophilic substrate, Me_3SiCl, which yields the Ce-containing product **AK**, $Ce(TriNOx)[N(SiMe_3)(3,5\text{-}(CF_3)_2\text{-}C_6H_3)]$, with an estimated yield of 90% by ^{1}H NMR spectroscopy.[46]

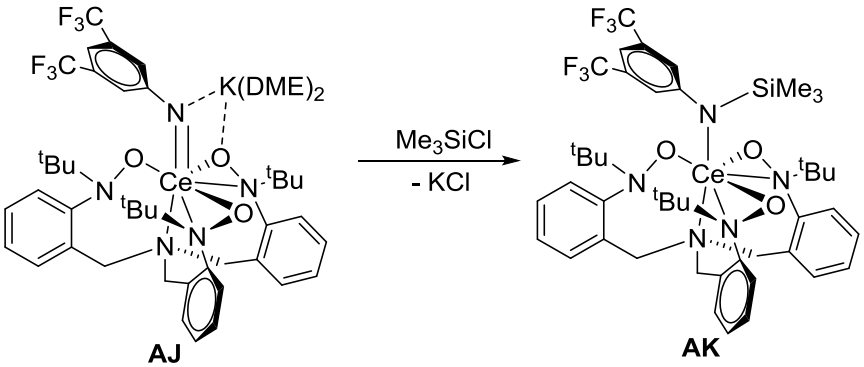

Scheme 1-12. The reaction of Ce^{IV}=NR complex towards Me_3SiCl.

Liddle and co-workers reported that by oxidising an anionic "ate" precursor (**AL**), the first example of a formal Ce^{IV}–carbene multiple bond interaction complex (**AM**, **Scheme 1-13**) can be synthesised and characterised. The $Ce{=}C_{carbene}$ bond was revealed at a length of 2.441(5)

Å. Theoretical calculations suggest a modest covalent component in the Ce=C bond with a Nale-wajski–Mrozek bond order of 1.1 in this Ce^{IV}–carbene complex.[47]

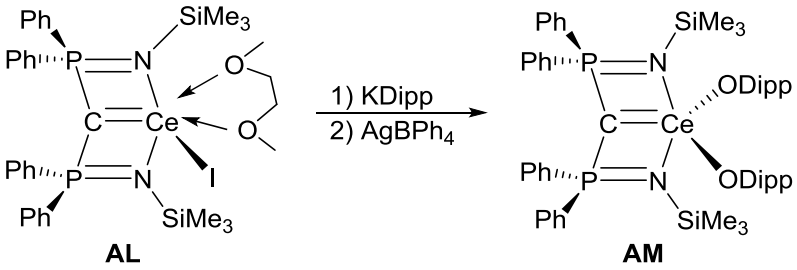

Scheme 1-13. Synthesis of first Ce^{IV}=carbene complex.

Pr^{IV} and Tb^{IV} complexes

The dominant oxidation state of praseodymium is +III, but there are also some oxides(PrO_2)[48] and fluorides (PrF_4),[49, 50] with praseodymium in the +IV oxidation state. The electron configuration of the +IV state in praseodymium is $[Xe]4f^1$, (**Table 1.1**). The synthesis of the tetrafluoride is possible at room temperature by reaction of Pr_2O_3 with KrF_2[50] or in aqueous HF under UV photolysis.[51] TbF_4 can also be synthesised by a similar procedure with a prolonged reaction time of 25 days. However, no data about the vibrational spectrum or single crystal structure of Pr^{IV} or Tb^{IV} is known so far.[51]

Pr^{V} complexes

Removal of the last f-electron of praseodymium would lead to a closed-shell system of $[Xe]f^0$ (**Table 1-2**) making the Pr in the formal oxidation state of +V.[52] In 2016, Li and co-workers[53] reported the formation of the lanthanide oxide species PrO_4 and PrO_2^+ complexes in the gas phase and in solid noble gas matrix. The generation of the linear PrO_2^+ complex is confirmed by matrix-isolation infrared spectroscopic experiments and infrared photodissociation spectroscopic experiments. This finding in the existence of the pentavalent Pr in oxides opens the doors or high oxidation state lanthanide compounds which may provide unique reactivity different from the ubiquitous di-, tri-, and tetravalent analogues.[53]

1.2.3. **Low oxidation state complexes**

Besides +III oxidation state, +II oxidation states are also possible for rare earth metals. The most common examples are samarium[54] and europium[55] complexes due to their favourable half-filled electronic configurations.(**Table 1-2.**)

There are also examples for Yb^{II} which has a full $4f^{14}$-subshell.[26, 56] Complexes of neodymium, dysprosium and thulium have also been reported.[55] A series of diiodide complexes have been synthesised such as SmI_2,[54] $NdI_2(THF)_5$[57], $DyI_2(DME)_3$[58] and $TmI_2(DME)_2$.[59] Synthesis and characterisation of EuN''_2 (N'' = bis(trimethylsilyl)amide) complexes(**AP**, **Scheme 1-14**) were first reported by Tilley and co-workers[60] through the addition of sodium naphthalenide to the chloroamide (**AO**) which is prepared *in situ* by reaction of EuN''_3 (**A**) with $EuCl_3$ (**AN**).

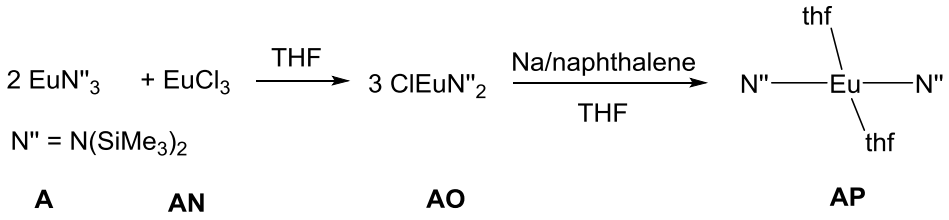

Scheme 1-14. Synthesis of $EuN''_2(thf)_2$, N" = $N(SiMe_3)_2$.

Evans and co-workers have isolated all the lanthanides in the formally +II state as 'ate' complexes, which helps in their stabilisation, *via* reduction of the $LnCp''_3$ complexes (**AQ**) by potassium metal with the presence of 2.2.2-cryptand to yield Ln^{II} complexes (**AR**) of La and Ce (**AS**).[61, 62](**Scheme 1-15**).

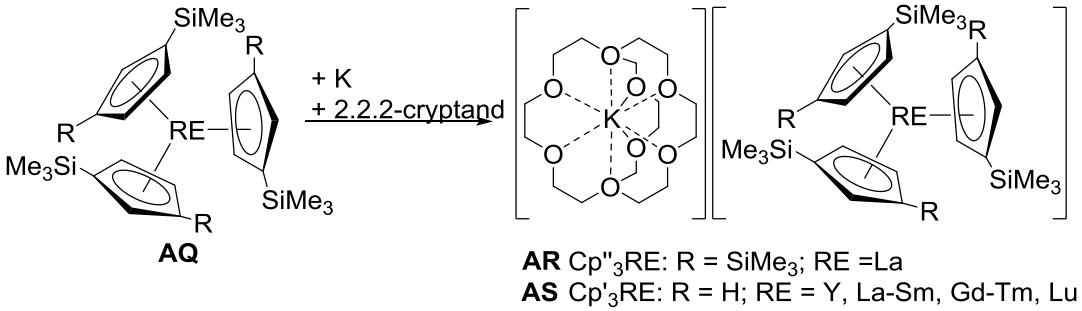

Scheme 1-15. Reduction of RE^{III} to RE^{II}.

Amongst these rare earth elements, scandium has the lowest atomic number of any transition metal, which is quite attractive for theoretical studies. However, due to the experimental difficulty of working with this small electropositive element, research on its redox chemistry lags behind the other late transition metals.[63-65] The +III oxidation state is predominant for Sc in molecular complexes in solution with only several examples reported in other oxidation states.

The first example of a formal Sc^{I} complex(**AT**, **Scheme 1-16)** was reported by Arnold *et al*.[66] through co-condensation of electron beam vaporised scandium with an excess of ^{t}BuCP at 77 K. The crystal structure shows the central 2,4,6-tri-*tert*-butyl-1,3,5-triphosphabenzene ring in the triple-decker structure lies on a crystallographic mirror plane and is planar with no significant variation in ring P-C bond lengths, indicative of binding as a $\mu,\eta^6:\eta^6$ aromatic ligand.

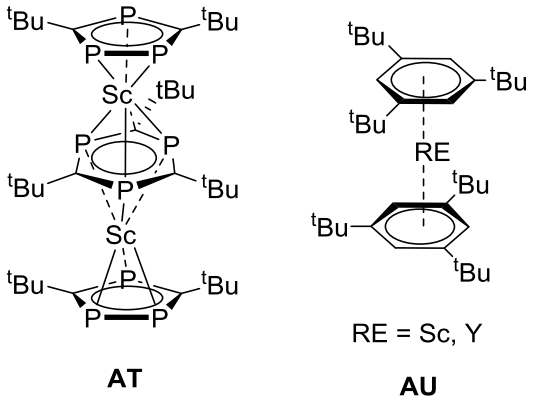

Scheme 1-16. The structure of Sc^{I} and Y^{I} complexes.

Co-condensation of electron-beam vaporised scandium with an excess of 1,3,5-tri-tert-butylbenzene afforded the first Sc^{0} complexes **AU**, ($[Sc(\eta\text{-}^{t}Bu_3C_6H_3)_2]$, **Scheme 1-16**) in *ca*. 20% yield.[67] The yttrium analogue was obtained and characterised by a similar procedure.[68]

1.3. N-heterocyclic carbenes

N-heterocyclic carbenes (NHCs) are two electron donors which contain a neutral, divalent, sp^2-hybridised carbon centre with a strongly nucleophilic lone pair.[69] Five-membered imidazolin-2-ylidene (unsaturated backbone) and imidazolidin-2-ylidene (saturated backbone) are regarded as classical NHCs. (**Figure 1-1**).

Imidazolin-2-ylidene Imidazolidin-2-ylidene

Figure 1-1. Structure and nomenclature of classical N-heterocyclic carbenes.

Similar to terminal carbenes, NHCs exist as either singlet carbenes, where both electrons are in the same orbital and paired with each other, or as triplet carbenes, where the electron are unpaired and in different orbitals. These are also known as Schrock type[70] (singlet) and Fischer type[71] (triplet). (**Figure 1-2**).

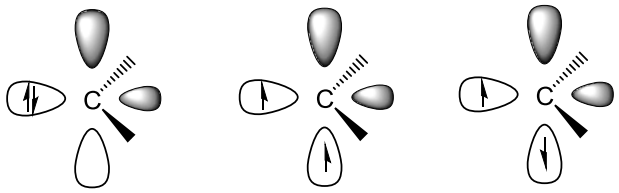

Figure 1-2. Singlet (left) and triplet carbenes.

N-Heterocyclic carbenes are usually singlet carbenes. The two α-amino substituents stabilise the singlet state in two important ways: firstly, by stabilising the formally sp^2 hybridised non-bonding lone pair through σ-inductive electron withdrawing effect (a, **Figure 1-3**); secondly, by destabilising the vacant p-orbital through mesomeric electron donation from the lone pairs on the α-amino substituents. (b, **Figure 1-3**).

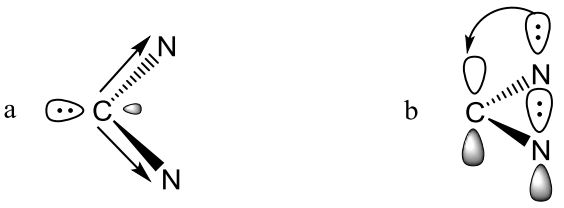

Figure 1-3. Inductive and Mesomeric effects in NHCs.

The first NHC compound was synthesised by Wanzlick and Kleiner[72] through α-elimination of chloroform from the imidazolidine (**AV**) which dimerised to form enetetramine **AW** (**Scheme 1-17**). However, attempts to isolate the free carbene were not successful.

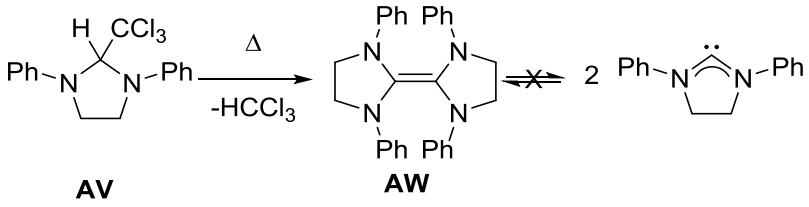

Scheme 1-17. Wanzlick's initial observation of N-heterocyclic carbenes.

Arduengo *et al.* synthesised the first stable, crystalline, free NHC (**AY**) in 1991 by deprotonation of *N,N"*-di-adamantyl imidazolium salt **U** with sodium hydride and a catalytic amount of dimethyl sulfoxide. (**Scheme 1-18**).[73]

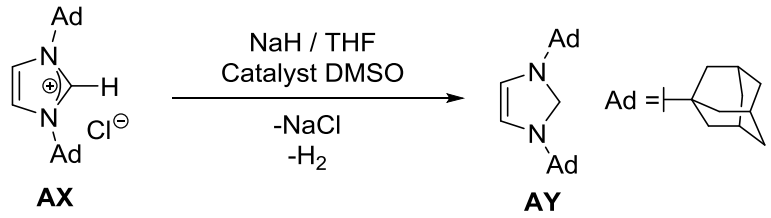

Scheme 1-18. The synthesis of the first stable, free N-heterocyclic carbene.

1.4. Reactivity of NHCs

1.4.1. **NHC-mediated small molecule activation**

Since the first report of stable nucleophilic NHC by Arduengo *et al*.,[73] the application of NHCs in organocatalytic synthesis has been greatly developed.[74, 75] NHC catalysis has also been extended to C−H bond[76], C−C bond[77, 78] and small molecule activations.[79]

It has been reported by different groups that the reaction of imidazol-2-ylidenes with chalcogen can produce imidazole-2-thiones (**BA**),[80] imidazoleselones (**BB**),[81] and telluroimidazolines (**BC**).[82] (**Scheme 1-19**)

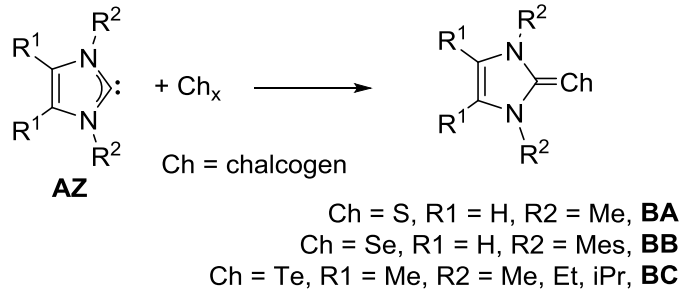

Scheme 1-19. The reaction of NHCs towards chalcogen.

Arduengo *et al.* reported the chemistry of NHCs towards pnictinidenes, which form the carbene-pnictinidene adducts(**BE**, **Scheme 1-20**). The direct formation of 'pnictaalkenes' proceeds smoothly from stable nucleophilic carbenes phosphorus and arsenic cyclic oligomers

reagents. The formation of a 'phosphaalkene' (**BG**) can also be accomplished *via* the reduction reaction between two equivalents of nucleophilic NHC and henyldichlorophosphine by which 2-chloro-1,3-dimesitylimidazolinium chloride by-product (**BH**) is formed consequently.[80, 83](**Scheme 1-20**).

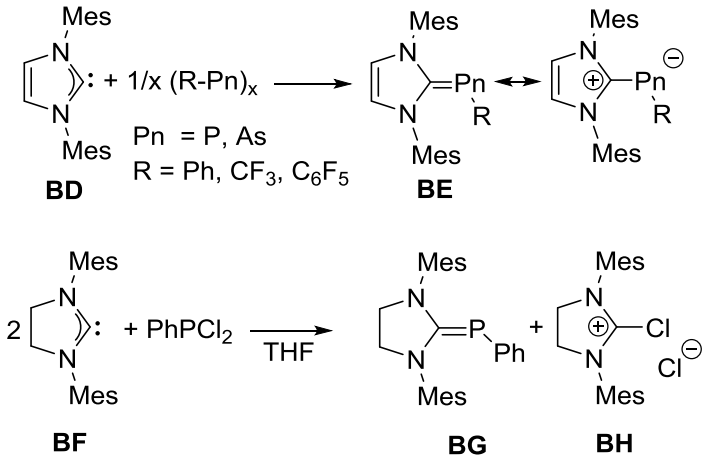

Scheme 1-20. The reaction of NHCs towards pnictinidenes.

Carbon dioxide, a weak electrophile, can also be activated by nucleophilic NHCs. Louie and co-workers reported the reversible direct fixation of CO_2 to NHCs (**BI**, **BJ**) yielding the imidazolium carboxylates.[84] (**Scheme 1-21**)

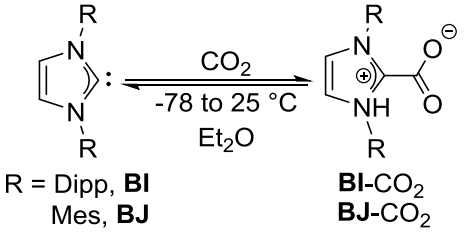

Scheme 1-21. Activation of CO_2 with NHC.

A series of similar NHCs and their carbon dioxide adducts have been successfully applied for various metal-free NHC catalysed CO_2 conversions.[79] Ying and co-workers reported the metal-free hydrosilylation of CO_2 using **BJ-CO_2** as catalyst under mild conditions.[85] Another efficient CO_2 transformation with amine to give the corresponding amide using NHC catalyst **BI** was reported by Jacquet *et al.*[86] (**Scheme 1-22**).

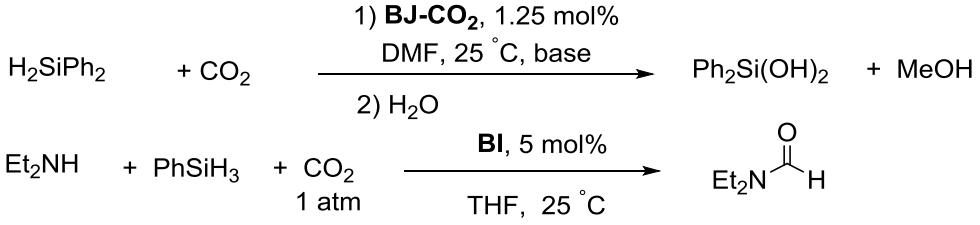

Scheme 1-22. Catalytic reduction of CO_2 mediated by NHCs.

1.4.2. **NHC-borane adducts**

Nucleophilic NHCs can also react with boranes, forming NHC-borane adducts.[87] NHC-boranes are neutral, four-coordinate species that were first synthesised by Kuhn and co-workers, **BK** (**Scheme 1-23**).[88] After that, there have been many examples (**BL**, **BM**) of NHC-borane adducts in the literature, many of these adducts are easy to handle because they are stable to air, water, base, and even mild acid. NHC-boranes have shown diverse reactivity as reagents and catalysts in organic synthesis[89] and as co-initiators in radical polymerization.[90]

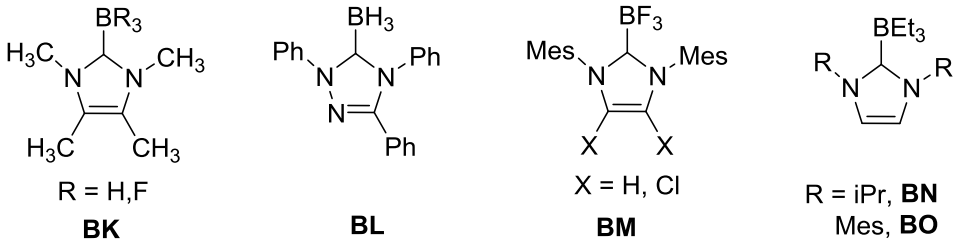

Scheme 1-23. NHC-borane complexes.

Ito and co-workers made the 1,3-diisopropyl- and 1,3-dimesitylimidazol-2-ylidene complexes of triethylborane **BN** and **BO** (**Scheme 1-23**), and showed that the BEt_3 group exchanged with BH_3 (and also BF_3 in the case of **BN**).[91] Ito and co-workers also showed BEt_3 groups of **BN** and **BO** could be exchanged for metals, forming Mo and W carbene complexes.[92, 93]

These Lewis acid-base adducts can act as frustrated Lewis pairs when their ability to form stable donor-acceptor adducts is suppressed by steric protection. This allows activation of small molecules such as dihydrogen,[94] olefins and tetrahydrofuran.[95] Tamm reported the frustrated Lewis pair (FLP), **BQ Scheme 1-24**, which can activate C-O, H-H and N-H bonds.[94]

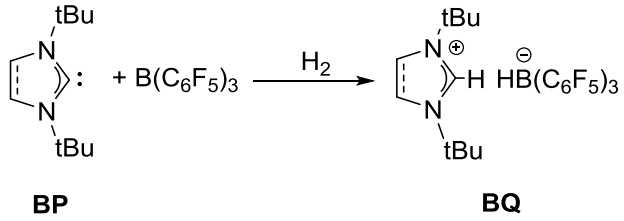

BP **BQ**

Scheme 1-24. NHC based frustrated Lewis pairs and its reactivity towards H_2.

1.5. Metal NHC complexes

1.5.1. **Unfunctionalised NHC complexes**

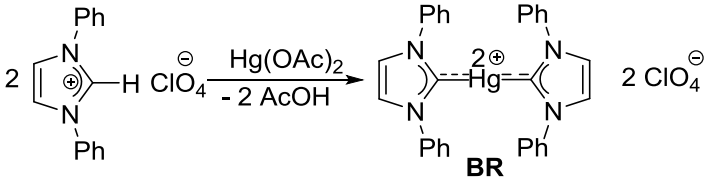

Scheme 1-25. Synthesis of metal-NHC complexes.

In 1968, Wanzlick and Schönherr[96] used a 1,4- benzylimidazole based N-heterocyclic carbene, to synthesise a mercury NHC compound by reacting the imidazolium perchlorate salt with mercury acetate. (**BR**, **Scheme 1-25**) This was the first example of the direct synthesis of a transition metal carbene complex. Soon after that Öfele[97] presented a chromium-based NHC complex using a 1,4-methylimidazolium with a chromium carbonyl complex (**BS**, **Scheme 1-26**).

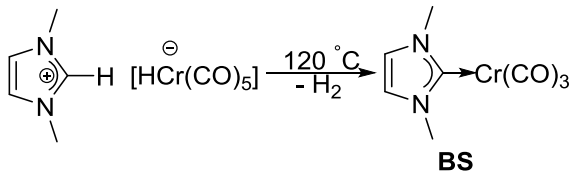

Scheme 1-26. Synthesis of metal-NHC complexes.

The strongly nucleophilic lone pair renders NHCs strong σ-donors. Therefore, they are used extensively as ligands for metal complexes in homogeneous catalysis[98] and small molecule activation.[99]

1.5.2. **Tethered NHC complexes**

Mid-late transition metal-NHC complexes are common and have been greatly studied. [98, 99] However, due to the mismatch of 'soft' σ-donors (NHCs) and 'hard' Lewis acidic elements, NHCs often require further modification in order to form stable complexes with more electropositive early transition and f-block metals. Functionalisation of the substituent groups on the nitrogen atoms allows the incorporation of a pendant anionic group and this facilitates binding to metals where interactions are primarily electrostatic in nature. It also favours binding due to the chelate effect (**Scheme 1-27**). The use of a variety of moieties to tether NHCs to the metal centre has allowed them to stabilise the complexes as well as to bring in a potentially reactive π-system proximal to the metal, which has shown rich reactivity in C-H activation,[100] small molecule activation[101] and homogeneous catalysis.[102]

R = alkyl, aryl *etc.*
E = O, S, N, Cp, *etc.*

Scheme 1-27. Anionic functionalised NHC tethered to a metal centre.

Amido-tethered NHCs

Amido-functionalised NHC complexes were first reported by Arnold *et al.* in 2003.[103] The proligands were deprotonated to form free carbene (**BT**, **Scheme 1-28**) which were reacted with $MgMe_2$, yielded the Mg-NHC complex (**BU**). Further deprotonation by n-butyllithium followed by reaction with $UO_2Cl_2(THF)_2$ afforded the uranyl-NHC complexes (**BV**).[104]

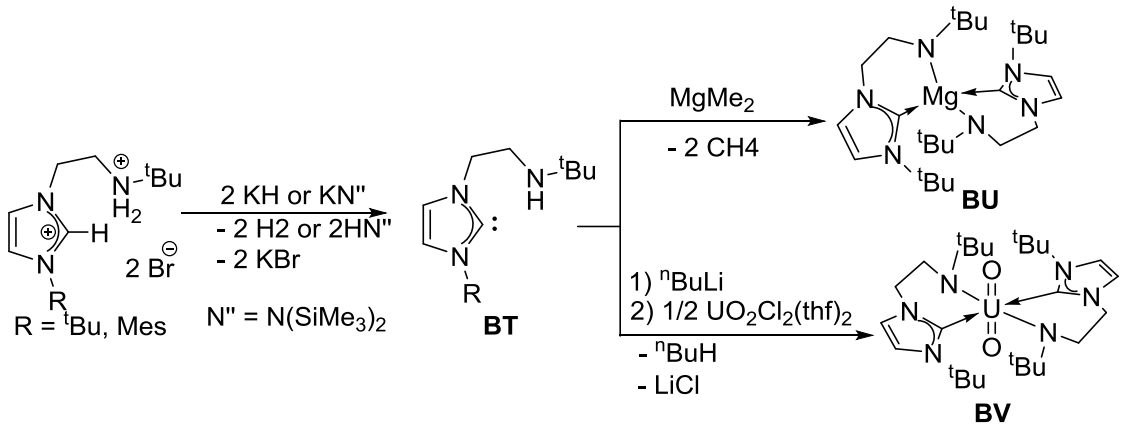

Scheme 1-28. Synthesis of first amido-tethered NHC complexes.

A series of different rare earth metal complexes(**BW**, **Scheme 1-29**) have been isolated as well as the halogen-bridged dimers (**BX**).[105](**Scheme 1-29**).

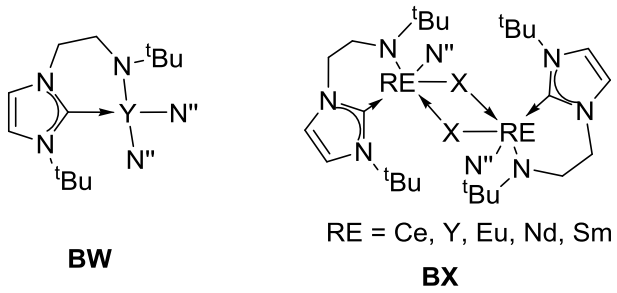

Scheme 1-29. Synthesis of amido-tethered NHC complexes.

In 2004, Fryzuk and co-workers[106, 107] reported the synthesis of free bis-amido NHC (**BY**, **Scheme 1-30**) by the deprotonation of imidazoline proligand. The reaction of AH with early transition metal tetraamide affords tridentate NHC complexes. (**BZ**, **Scheme 1-30**). These complexes can react with two equivalents of trimethylsilylchloride (TMSCl) to replace the

dimethylamide ligands for chlorides to form **CA**, which can further be replaced for alkyls using Grignard reagents to give complexes **CB**, (**Scheme 1-30**).[106, 107]

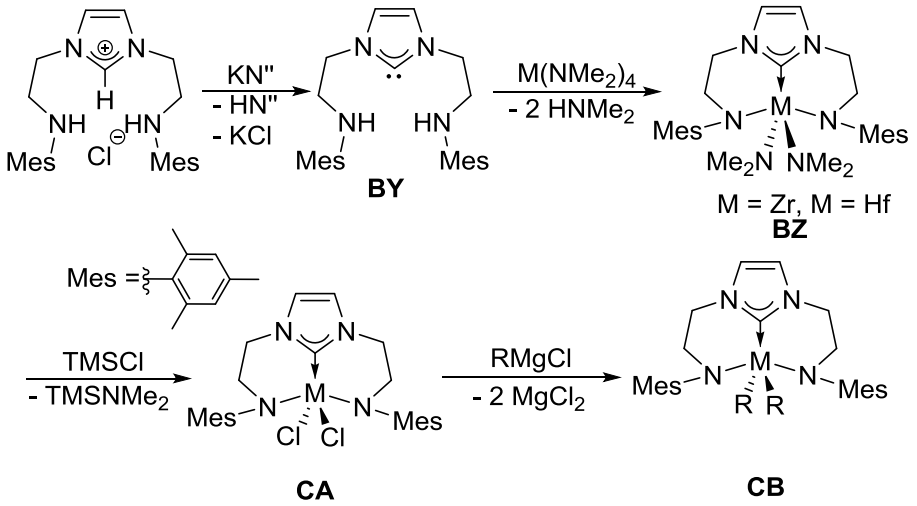

Scheme 1-30. Bis-amido-tethered NHCs and early transition metal complexes.

Alkoxy-tethered NHCs

Alkoxy-tethered carbene proligands were first synthesised by Arnold *et al*.[108] The pro-ligands can be deprotonated by KH to yield the potassium salt (**CD**). (**Scheme 1-31**).

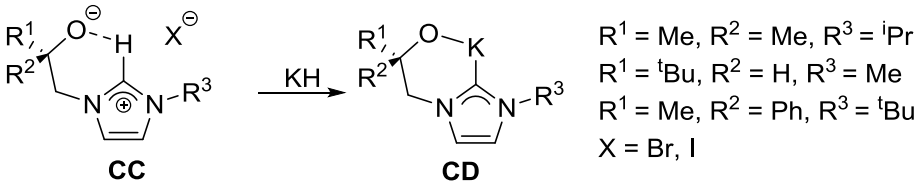

Scheme 1-31. Alkoxide-tethered NHC ligand and complexes.

The reaction of one equivalent of potassium salt **CD** with $TiCl(O^iPr)_3$ leads to the formation of the titanium alkoxy-tethered complex (**CE**, **Scheme 1-32**).[109] Scandium[110] and cerium[111] complexes (**CF**) can be synthesised in the same manner with $RECl_3(thf)_n$. Arnold *et al.* reported the reaction of uranium triiodide with **CD**. The reaction KL with 4/9 equivalents of $UI_3(thf)_4$ resulted in disproportionation which affords the uranium iodide tris(ligand) complex **CH** (L = $OCMe_2CH_2(1\text{-}C\{NCHCHN^iPr\})$) and uranium metal. Reaction of **CD** with 1/3 equivalent of $UI_3(thf)_4$ yields another tetravalent uranium complex **CI** (**Scheme 1-32**), which contains a seven-coordinate U^{IV} centre and one unbound NHC group.[112]

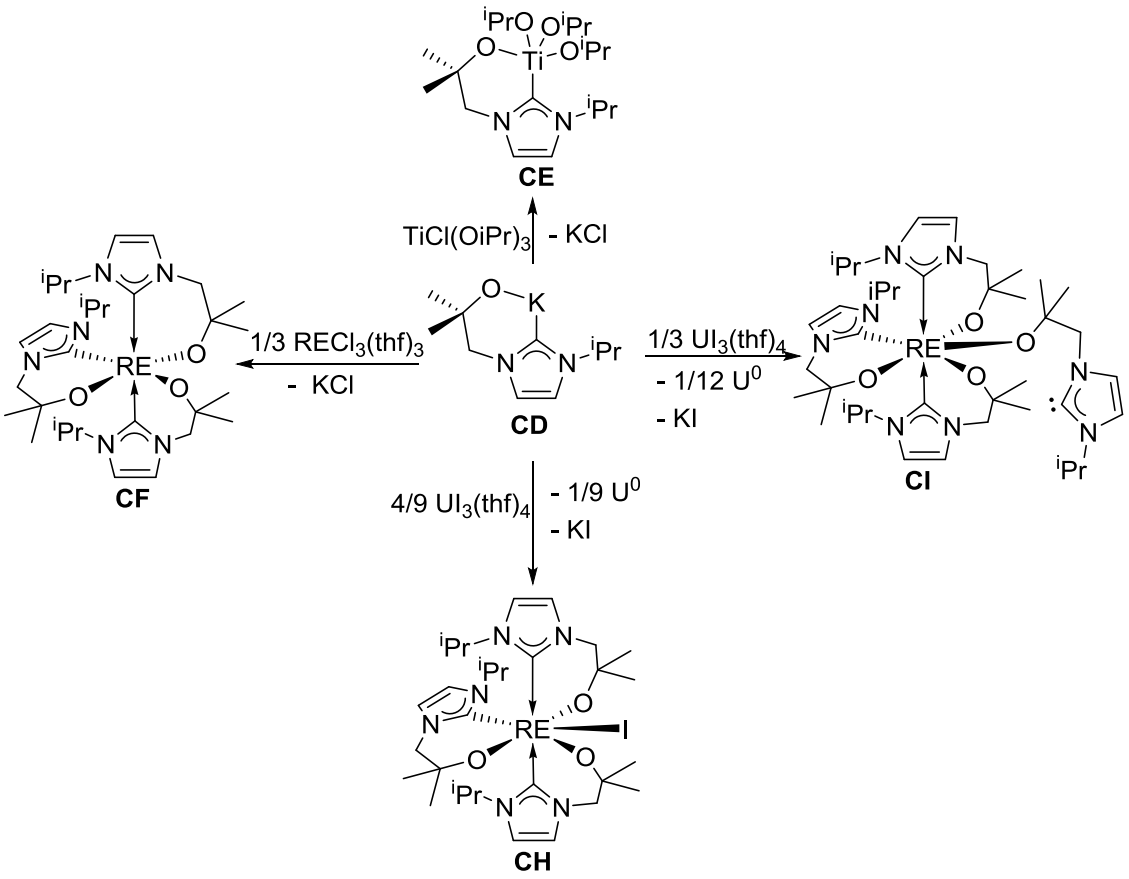

Scheme 1-32. Synthesis and reactivity of alkoxy-tethered NHC complexes.

Aryloxy-tethered NHCs

The first reported aryloxy-tethered carbene complex was synthesised by Hoveyda and co-workers.[113, 114] The proligands are converted to silver complexes and then transmetallated to form the chiral ruthenium complexes (**CK**) in >98% diastereo- and enantiomeric purity. These catalysts proved to be highly efficient in promoting asymmetric ring-opening/cross metathesis (AROM/CM). **Scheme 1-33**.

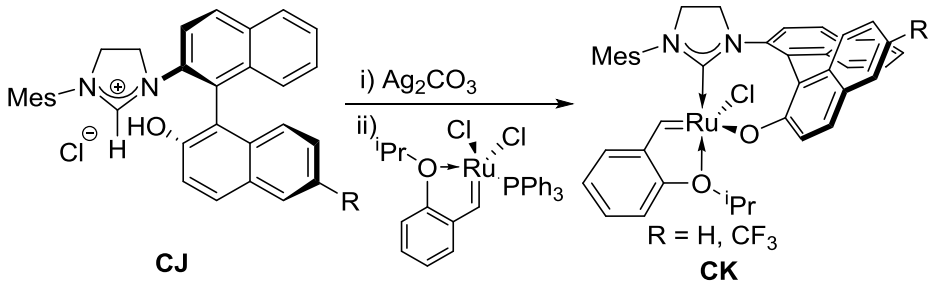

Scheme 1-33. Synthesis of aryloxy-tethered NHC ruthenium complex.

Grubbs and co-workers synthesised an Aryloxy-tethered saturated NHC proligand (**CL**) from several steps of organic synthesis.[115, 116] The proligands can be deprotonated with two

equivalents of KN" to yield the potassium salts which can react *in situ* with a number of starting materials to form resulting complexes. Reaction with [NiBrMes(PPh_3)$_2$] and [PdClMe(PPh_3)$_2$)] results in the desired aryloxide-tethered NHC complex, **CM** and **CN**, respectively. (**Scheme 1-34**).

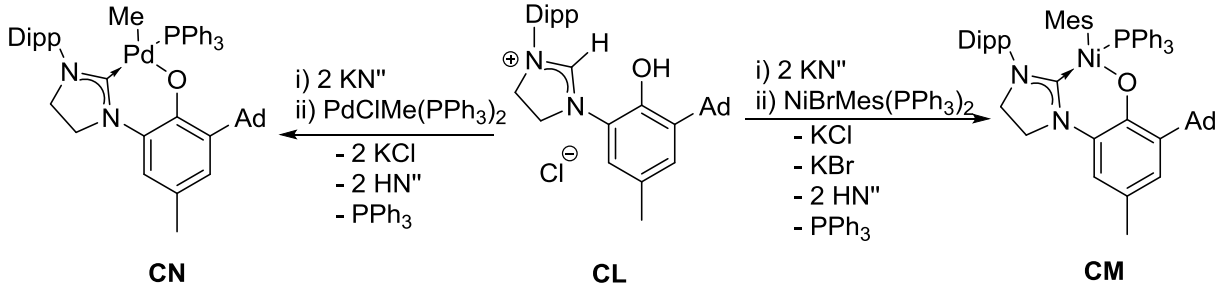

Scheme 1-34. Synthesis of aryloxy-tethered NHC palladium and nickel complexes.

Wang *et al.* reported that the deprotonation of the proligand **CO** with n-butyllithium followed by reaction with [(allyl)PdCl]$_2$ yields the mono-NHC palladium allyl complex **CP** (**Scheme 1-35**).[117] Reaction with [Pd(OAc)$_2$] yields three different complexes, **CQ**, **CR** or **CS** which are depended on the R group of the imidazole (**Scheme 1-35**). [118]

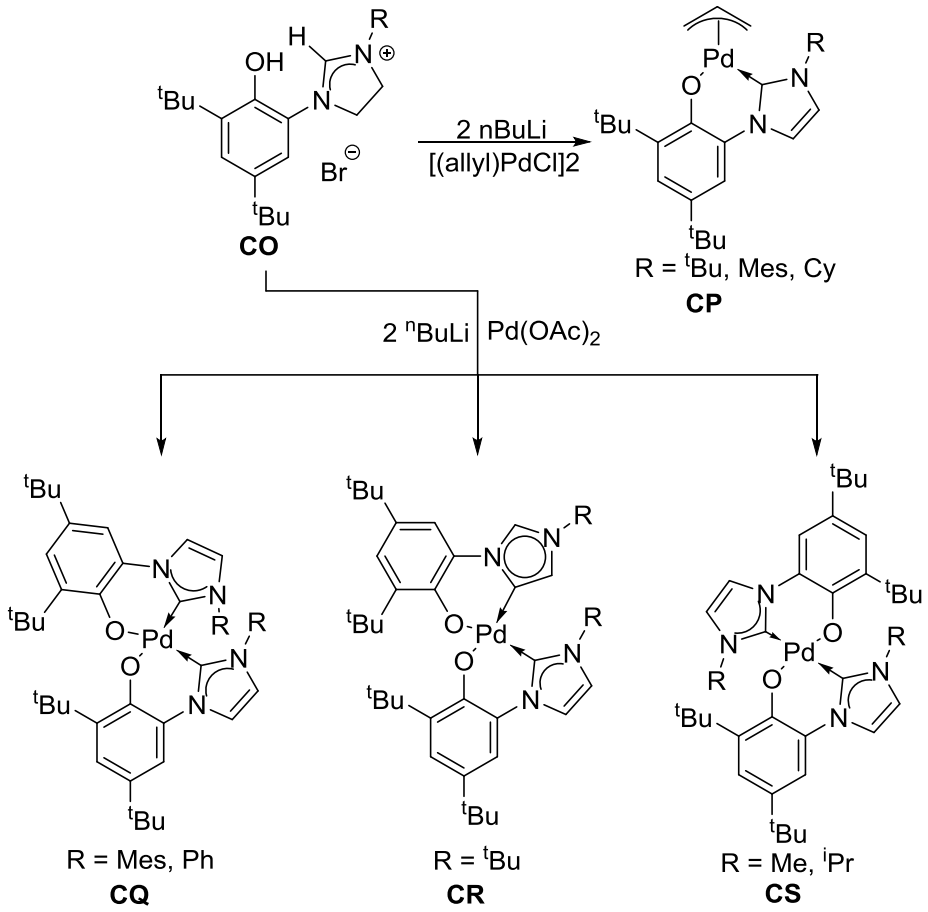

Scheme 1-35. Synthesis of aryloxy-tethered NHC proligand and palladium complexes.

Kawaguchi *et al.* have reported the synthesis of a bis-aryloxy tethered NHC ligand. The proligand can then be deprotonated with three equivalents of NaN" at -78 °C to produce the free carbene **CU**.[119] This free carbene can react with $[MCl_4(thf)_2]$ (M = Ti, Zr) at low temperature to form the corresponding metal complexes **CV**.[119, 120] Reaction with alkyl lithium or Grignard reagents replaces the chloride, affording metal alkyl complexes **CW**, **Scheme 1-36**.[120]

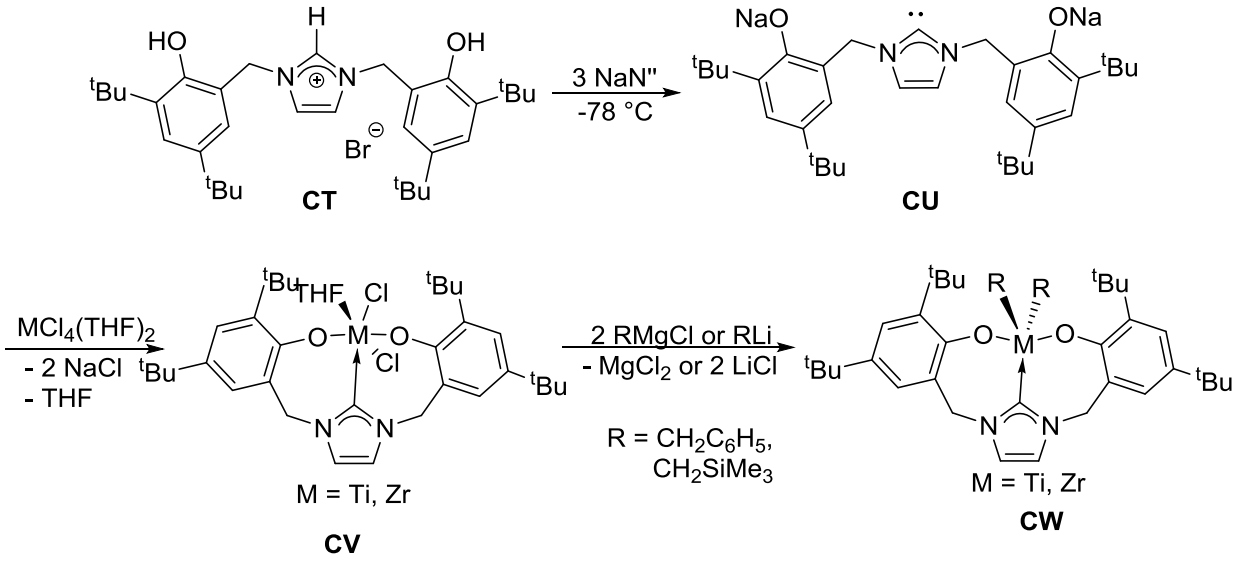

Scheme 1-36. Synthesis of (bis)aryloxy-tethered NHC complexes.

Enolate-tethered NHCs

Waymouth and co-workers reported the use of a ketone tethered proligand **CX** (R_1 = Ph, R_2 = Dipp, Mes) to form transition metal-NHC complexes.[121] After deprotonation with NaN", the ketone group transforms into enolate configuration which reacts with $[Ni(cod)_2]$ to yield the corresponding nickel enolate-tethered complexes **CY** (**Scheme 1-37**).[122] The RE analogues **CZ** are synthesised by Li and co-workers through the reaction of $RECl_3$ with four equivalents of NaN" in THF at room temperature, and then followed by treatment with one equivalent of proligand **CX**.[123]

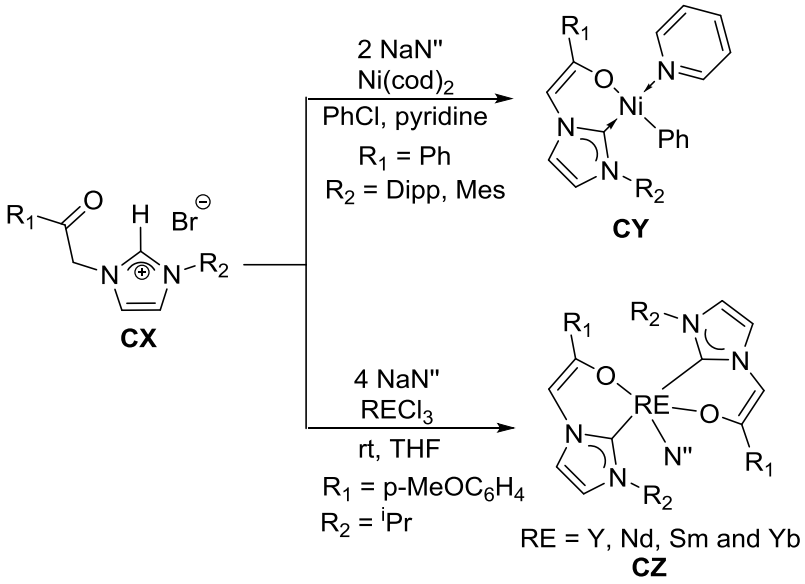

Scheme 1-37. Synthesis of enolate-tethered NHC nickel complexes.

Thiolate-tethered NHCs

Sellmann *et al.* reported the synthesis of arylthiolate-tethered nickel complexes *via* the cyclometallation of nickel complex **DA**, which upon reaction with triethyl orthoformate yielded the $[Ni_2L_2]$ dimer **DB** (**Scheme 1-38**).[124, 125] The mono-ligand complex can be obtained either by reaction with alkali metal salt to yield the anionic complexes **DC** or with strong coordinating ligands such as PPh_3, PMe_3 or CN^- to break the Ni-S bonds, forming complex **DD** (**Scheme 1-38**).[124, 125]

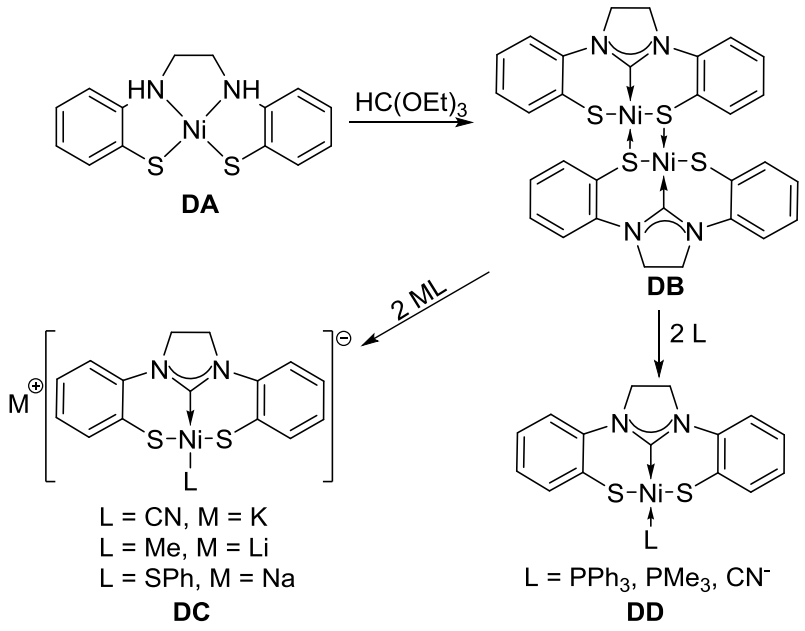

Scheme 1-38. Thiolate-tethered NHC nickel complexes.

Cyclopentadienyl-tethered NHCs

In 2006, Danopoulos and co-workers reported the first Cp based-tether by introducing fluorenyl- and indenyl-groups to NHCs.[126-128] Deprotonation of **DE** with two equivalents of KN" yields the potassium salt **DF**; this can then react with $[Ti(NMe_2)_2Cl_2]$ to yield the fluorenyl-tethered titanium NHC complex **DG**. The first RE bis-alkyl indenyl-tethered complex **DI** was synthesised directly from the reaction of imidazolium salt **DH** with $[Li(thf)_4Ln(CH_2SiMe_3)_4]$ (**Scheme 1-39**).[129]

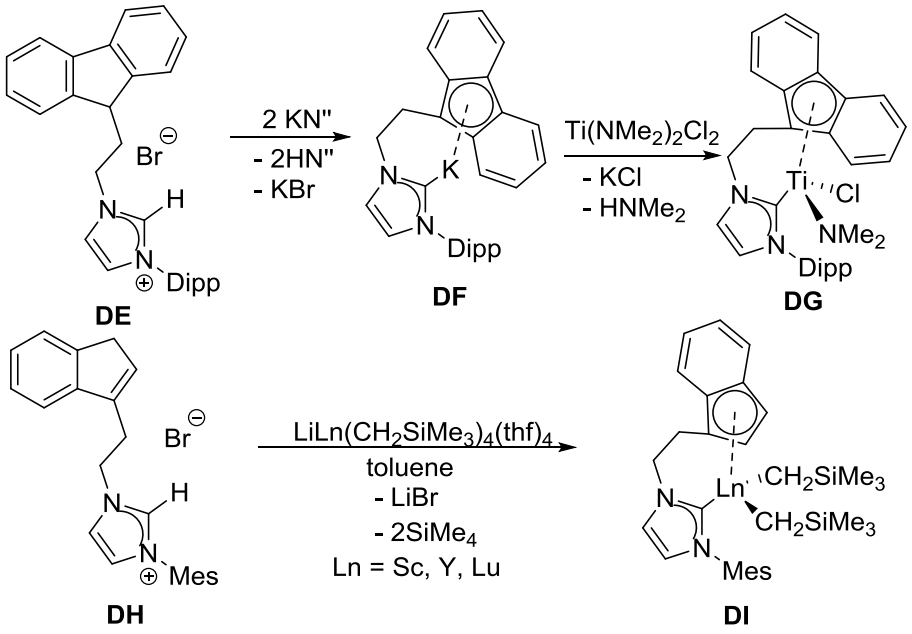

Scheme 1-39. Fluorenyl and indenyl tethered NHC complexes.

Royo and co-workers reported the Cp* functionalised imidazole **DJ** (**Scheme 1-40**).[130] Reaction of n-butyl lithium formed the lithium complex (**DK**) which can react with $[FeL_2(CO_2)]$ and MCl_2 (M = Fe, Ni) to yield complex **DL** and **DM**, respectively.[131]

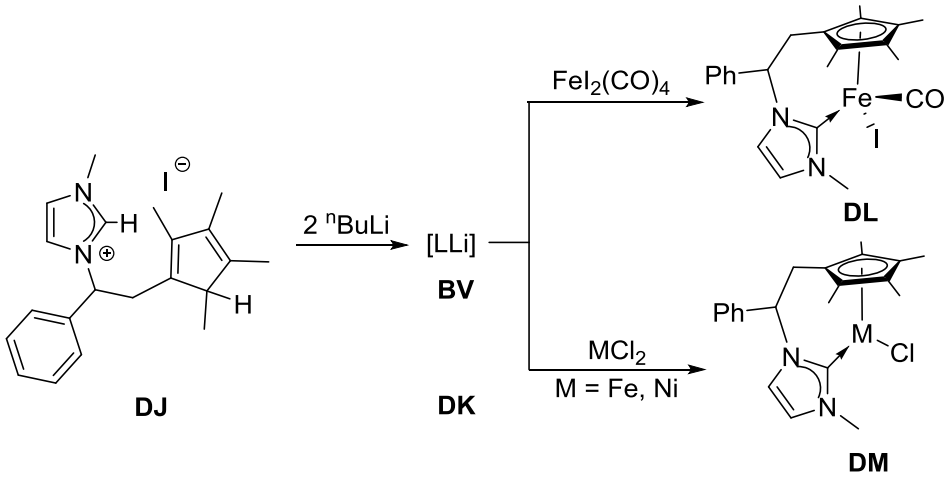

Scheme 1-40. Synthesis of Cp*-tethered NHC complexes.

1.5.3. **Macrocyclic NHCs**

Macrocyclic ligands consist at least nine atoms among which three or more of them are donor atoms, can form a continuous ring around the centre.[132] These ligands have been shown to form robust and stable complexes due to the macrocyclic effect.[133] Amongst these macrocyclic ligands, an emerging area of research is that of macrocyclic NHC ligands containing imidazolin-2-ylidene/imidazolindin-2-ylidene subunits, which form various multidentate NHC ligands, ranging from biscarbenes[134] to tetracarbenes[135] (**Scheme 1-41**). Various types of neutral or anionic ancillary coordinating donor groups, such as alkyls and heterocycles have been introduced to the ring to further support the NHC−metal ion binding, and for tuning the ring cavity or electronic properties of the NHC−metal complexes.[136]

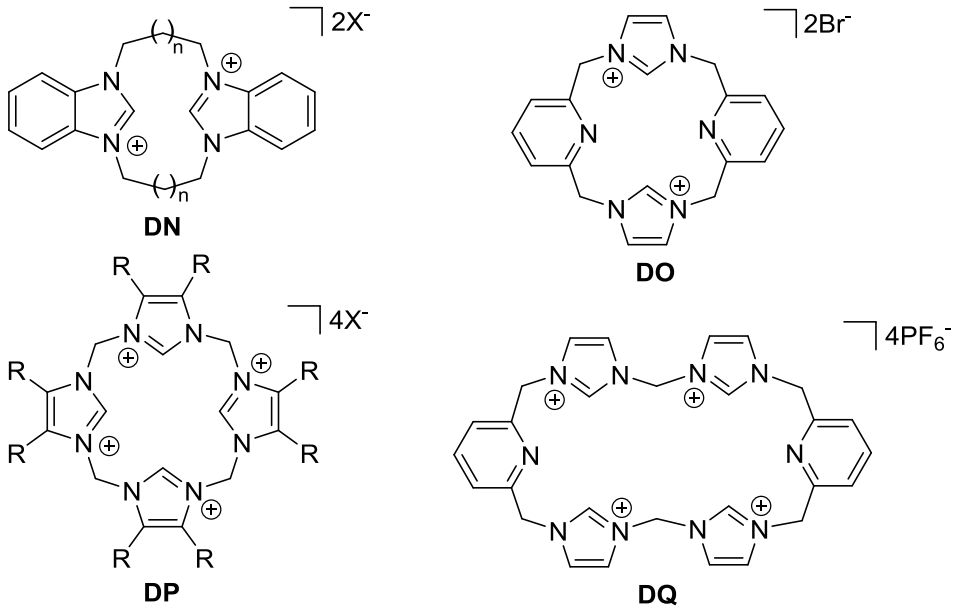

Scheme 1-41. Reported examples of macrocyclic NHCs.

There are two main strategies for the synthesis of macrocyclic NHC complexes. The first one is the template synthesis which involves the reaction of a suitable metal template with imidazolin-2-ylidene precursors. For instance, Hahn *et. al.* successfully synthesized a platinum tetracarbene complex **DS** (**Scheme 1-42**) from the reaction of $[Pt(PMe_3)_4](OTf)_2$ and 2-azidophenyl isocyanide, forming a square planar benzimidazolin-2-ylidene platinum intermediate **DR**. The intermediate **DR** was then reacted with phosgene in DMF to yield the final tetracarbene complex **DS** (**Scheme 1-42**).[137]

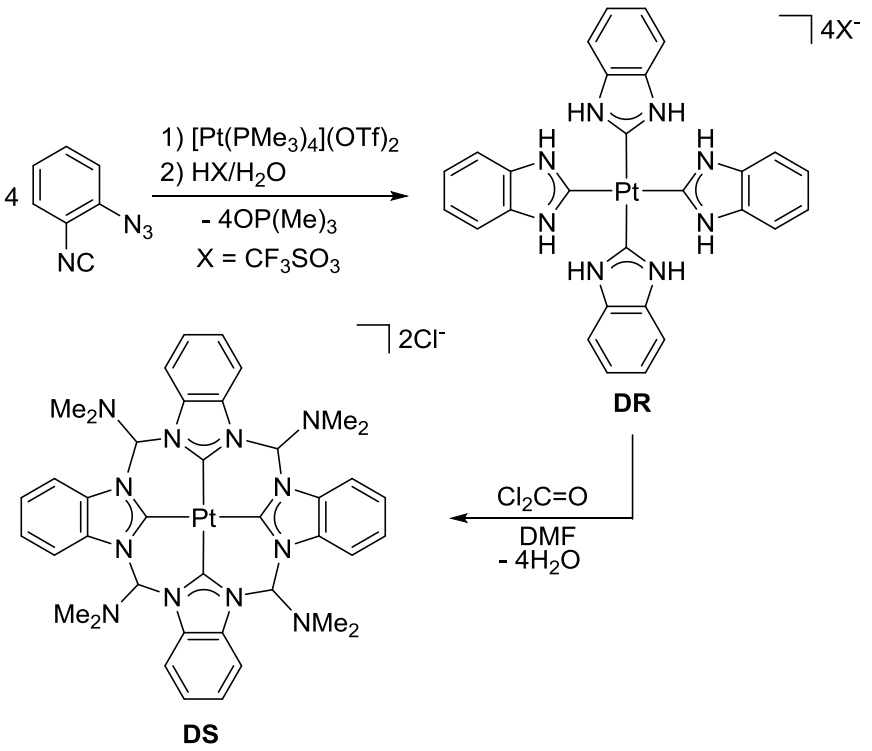

Scheme 1-42. Template synthesis of a tetradentate platinum NHC complex **DS**.

The other path is achieved by the deprotonation of the imidazolin(ium) ligands with metal base. The first pyridine-supported macrocyclic nickel NHC complex **DT** (**Scheme 1-43**) was reported by through the deprotonation of the corresponding imidazolium ligand **DO** with $Ni(OAc)_2$.[138]

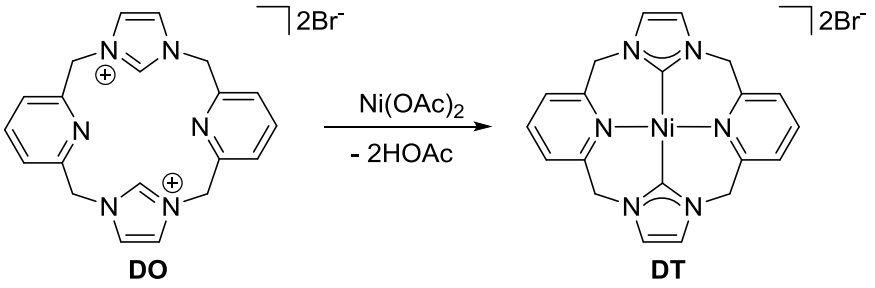

Scheme 1-43. The synthesis of the first macrocyclic nickel NHC complex **DT**.

1.6. Reactivity of rare earth metal NHC complexes

1.6.1. **Redox chemistry**

The cerium NHC complex **CF** is a good example showing how lanthanide-carbene bonds are often labile.[17] When CeL_3 (L = $[OCMe_2CH_2(1\text{-}C\{NCH{=}CHN^iPr\})]^-$) (**CF)** is treated with benzoquinone and one equivalent of KL (**CD**, **Scheme 1-31**), the product afforded is Ce^{IV} complex **DU** (**Scheme 1-44**). In the structure of **DU**, the cerium cation is coordinated by two bi-dentate ligands and two mono-dentate ligands, in which the NHC groups are unbound. Treatment of CeL_4 with borane, 9-BBN (9-borabicyclo[3.3.1]nonane), affords the carbene-borane adduct $[CeL_2(L\text{-}9\text{-}BBN)_2]$ (**DV)**.[17]

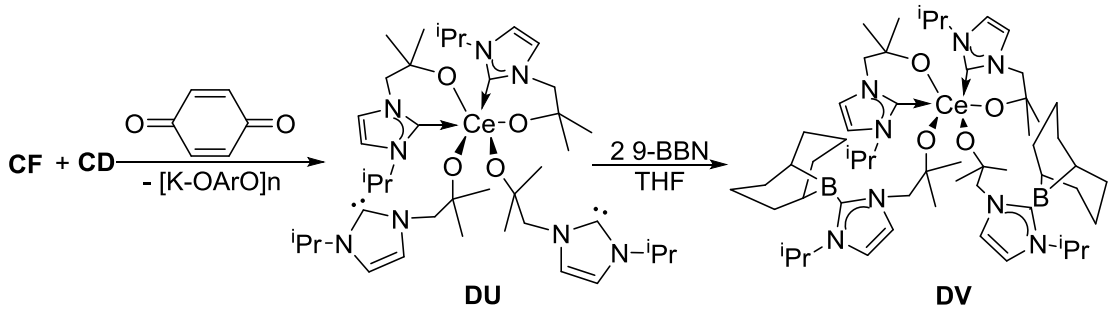

Scheme 1-44. Synthesis of Ce^{IV} carbene complex and subsequent adduct formation.

The Arnold group also reported the facile oxidation of $[Ce(L^{Ar})(N'')_2]$ (**DW**, **Scheme 1-45**) with tritylchloride to **DX**, $[Ce(Cl)(L^{Ar})(N'')_2]$ (Ar = diisopropylphenyl/mesityl).[139] In this reaction the oxidant is reduced to form Gomberg's dimer **DY** (((4-(diphenylmethylene)cyclohexa-2,5-dienyl)methanetriyl)tribenzene), which shows characteristic resonances in the ^1H NMR spectrum in C_6D_6 at $\delta = 4.92$ ppm, 5.92ppm, 6.44ppm and 7.07-7.30 ppm.

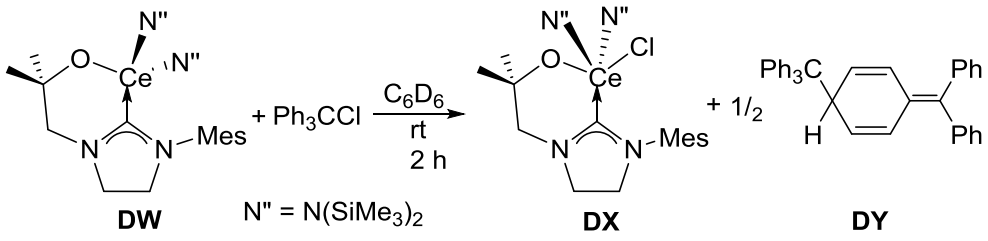

Scheme 1-45. Oxidation of $Ce(L^{Ar})(N'')_2$.

1.6.2. **Addition - elimination reaction**

Arnold and co-workers have demonstrated that by introducing tethers (i.e. anionic, alkoxy tethers) to NHCs, hemilabile tethered NHCs can be used as a reactive donor ligand which allows these redox-inactive metals to exhibit novel reactivity.[140]

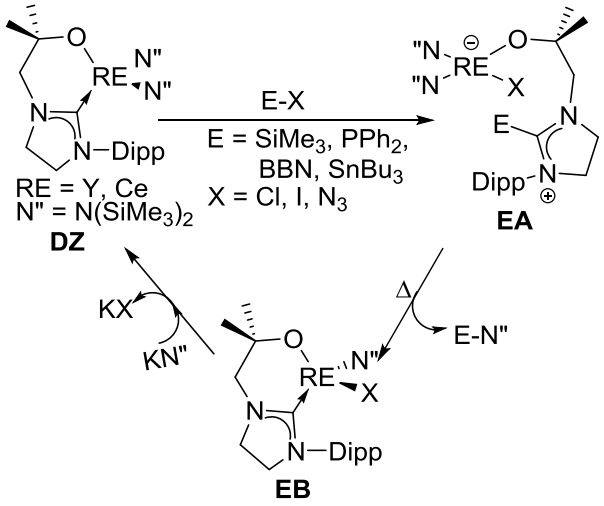

Scheme 1-46. Addition-elimination cycles of NHC complexes with E-X.

Polar substrates (such as halosilanes and haloboranes) were shown to add across the labile metal-carbene bond in d^0 group 3 and f-block metal NHC complexes (**DZ**). This 'addition' type reaction results in the formation of a zwitterionic complex (**EA**, **Scheme 1-46**) - the electrophile being coordinated to the carbene and the nucleophile to the metal centre. Subsequent elimination (induced by heating) allows reformation of the metal-carbene bond and releases amidosilane/borane rather than the halogenated products **EB**. Treatment of **EB** with KN" leads to the regeneration of **DZ** and the elimination of KX (X = Cl, I, N_3). (**Scheme 1-46**).

1.6.3. **C-E (E = Si, P, Sn) and C-C bond formation**

Treatment of scandium mono-neosilyl $[CH_2SiMe_3]^-$ or mono-neopentyl $[CH_2CMe_3]^-$ complex $Sc(R)(L^D)_2$ (**EC**) with one equivalent of Me_3SiX (X = Cl, I) in benzene, resulted in the formation of a clear, colourless solution which yielded $ScX(L)_2$ (**ED**) and corresponding silane after workup (**Scheme 1-47**).[110] The scandium mono-neosilyl complex also shows reactivity towards halophosphines and stannanes which resulted in C-P and C-Sn bond formation. However, the reaction of complex **EC** with a number of alkyl halides (MeI, ^{i}PrCl, ^{i}PrI, ^{t}BuI, Ph_3CCl, CH_2CHCH_2Cl, BnBr, Me_3SiCH_2Cl) and aryl halides (PhCl, PhI, C_6F_5I) showed no signal for the formation of C-C bonded organic product (**Scheme 1-47**).

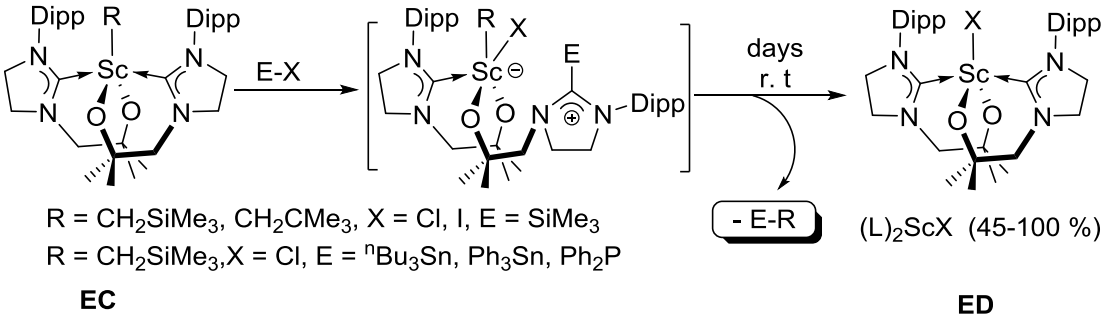

Scheme 1-47. Formation of C-E bonds from the reaction of scandium complexes.

Treatment of $ScCl_3(thf)_3$ with four equivalents of LiR(R = CH_2SiMe_3), followed by the addition of one equivalent of **EF** afforded heterobimetallic 'ate' complex **EG**, **Scheme 1-48**.[110] By using the heterobimetallic 'ate' complex **EG**, Li[(L)ScR_3], another route to the formation of C-Si bonds has been established This route also shows successful formation of C-C bond, which was not achieved by complex **DW** in **Scheme 1-47**.

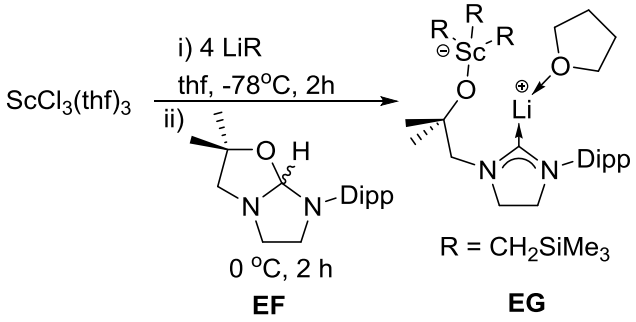

Scheme 1-48. Formation of Sc 'ate' complex.

The addition of trimethylsilylchloride or triphenylmethylchloride to this 'ate' complex at room temperature resulted in the displacement of the lithium cation, forming lithium chloride and the silylated (L^{SiMe3})$Sc(R)_3$ (**EH**) and alkylated imidazolinium complexes(L^{CPh3})$Sc(R)_3$ (**EI**). These zwitterionic complexes can then undergo the similar 'elimination' type chemistry as previously seen in **Scheme 1-47**, to release scandium complex (**EJ**) and the products of C-Si and C-C bond formation (Me_3Si-CH_2SiMe_3 and Ph_3C-CH_2SiMe_3, respectively) (**Scheme 1-49**).

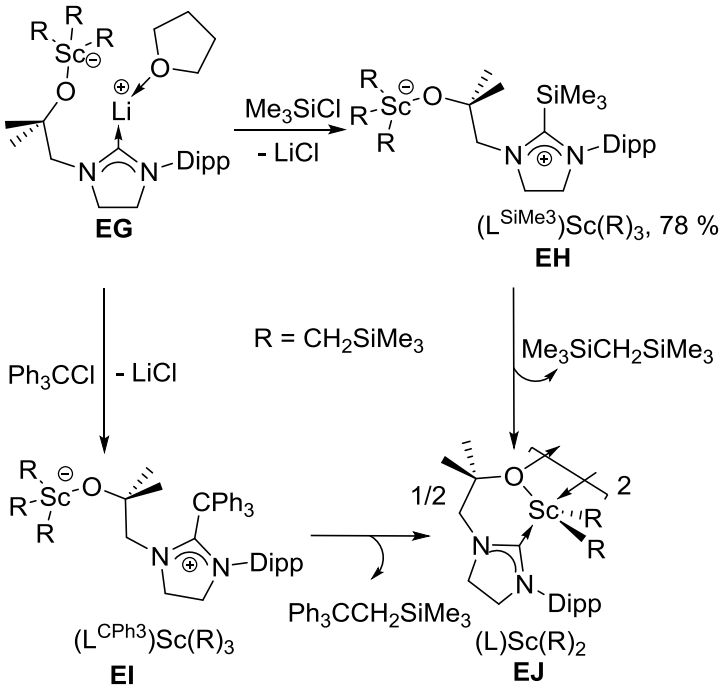

Scheme 1-49. Formation of C-C and C-Si bonds using Sc 'ate' complex.

Attempts to expand on this reactivity, using substrates such as simple alkyl halides (^{i}PrCl, ^{i}PrI, ^{t}BuI, BnBr and MeI) and aryl halides (PhCl, C_6F_5I and PhI), did not result in any reaction. This suggests that the reactivity is not dependent on C-X bond dissociation energies alone given that several of the substrates tested have C-X bond dissociation energies which are lower than that of Ph_3CCl.[110]

1.6.4. **Activation of CO_2 and CS_2**

Treatment of scandium tris(alkoxy-tethered NHC) complex **CF** (**Scheme 1-32**), $Sc(L)_3$, with one equivalent of CS_2 in toluene affords **EK**, $[Sc(L^{CS2})(L)_2]$, which contains a single dithiocarboxylate imidazolium group binding to Sc through the alkoxide group (**Scheme 1-50**). Reaction with two equivalents of CS_2 in toluene leads to the immediate formation of **EK** followed by the slow formation of **EL**. However, the addition of further equivalents of CS_2 does not lead to the formation of $Sc(L^{CS2})_3$ but instead, accelerates the rate at which **EL** is formed.[141] (**Scheme 1-50**).

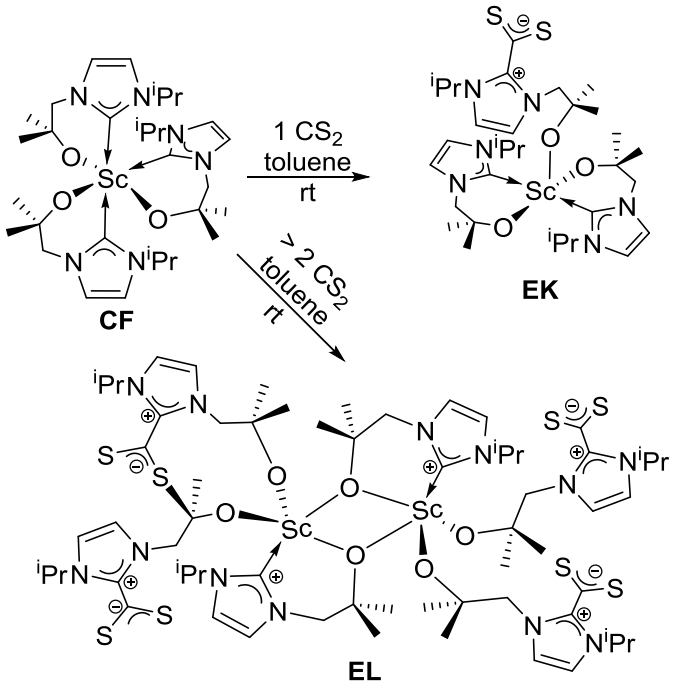

Scheme 1-50. The reaction of scandium complex **CF** towards CS_2.

When a solution of **CF** in benzene was exposed to an atmosphere of CO_2, a colourless precipitate immediately formed. The isolated precipitate was insoluble in solvents with which it does not react and assigned as the product of insertion of three equivalents of CO_2 into the Sc-C bonds. Elemental analysis, FTIR, and solid-state NMR spectroscopies indicate the formation of polymeric complex **EM**.[141] (**Scheme 1-51**).

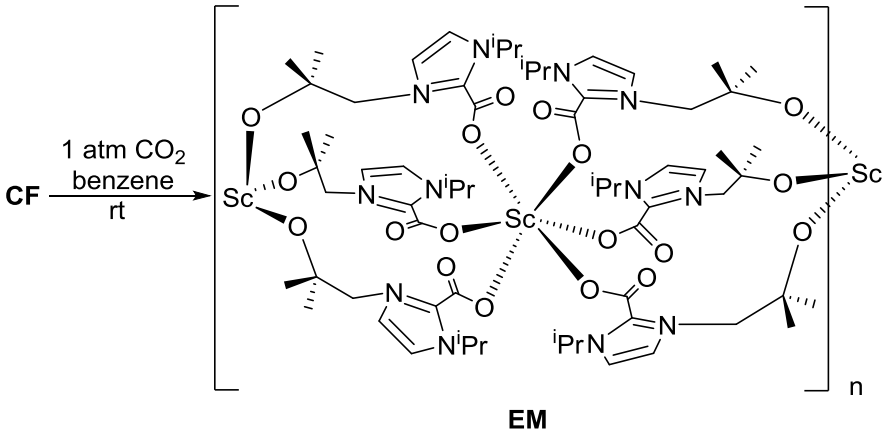

Scheme 1-51. Reaction towards CO_2.

1.6.5. **C-H and N-H activation**

The Arnold group have reported a number of hetero- and homoleptic alkoxy-tethered carbene complexes which showed interesting chemistry in the activation of C-H and N-H bonds.

The heteroleptic yttrium bis(alkoxy-tethered NHC) complex (**EO**) reacts with two equivalents of CpH over four hours' reflux, affords the extended zwitterionic polymer complex **EP** (**Scheme 1-52**). However, the scandium analogues remained unreacted under the same condition.[142]

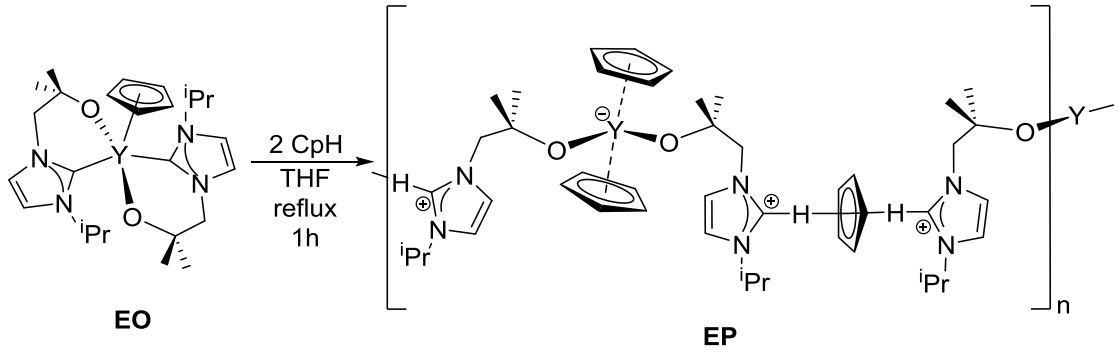

Scheme 1-52. The activation of CpH.

Treatment of heteroleptic yttrium bis(Cp)-mono-(alkoxy-tethered NHC) complex (**EP**) with acidic pyrrole and indole yields the zwitterionic insertion products **EQ** and **ER** (**Scheme 1-53**), respectively.[142] The heteroleptic yttrium complex **EP**, reacts with one equivalent of diphenylacetone to yield a zwitterionic yttrium enolate complex **ES** (**Scheme 1-53**).[142]

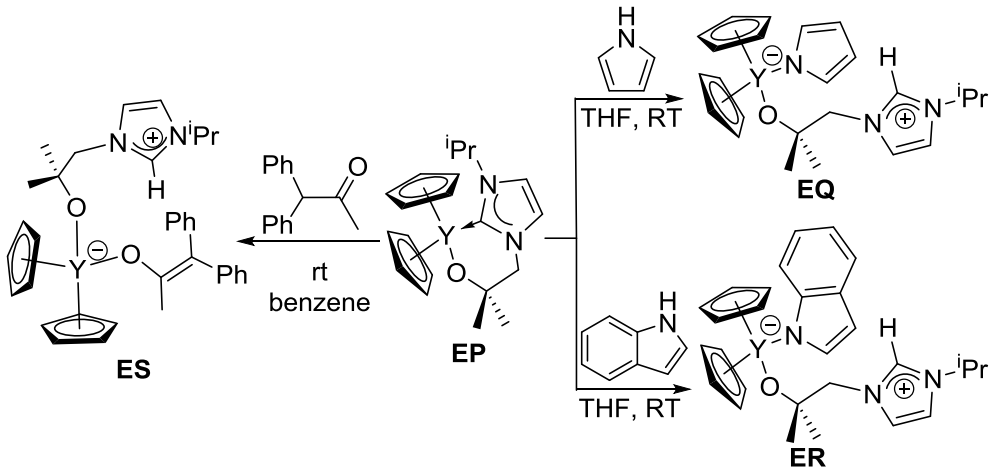

Scheme 1-53. C-H activation of yttrium complexes.

Reactions of pyrrole with homoleptic scandium complexes (**CF**, **Scheme 1-32**), leads to the formation of the hydrogen-bonded complexes **ET**, **Scheme 1-54**.

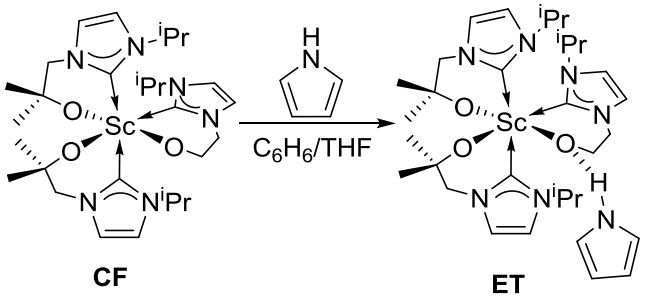

Scheme 1-54. The reaction of ScL_3 with pyrrole.

However, the cerium analogue (**EU**) of **EP** remains intact when mixed with pyrrole and indole while it shows reactivity towards alkynes to yield the cerium alkynyl complex (**EV**, **Scheme 1-55**). This alkynyl complex can react with one equivalent of CpH, affording zwitterionic complex (**EW**). The complex **EP** can also be obtained by the direct reaction of **EU** with CpH.[142] (**Scheme 1-55**).

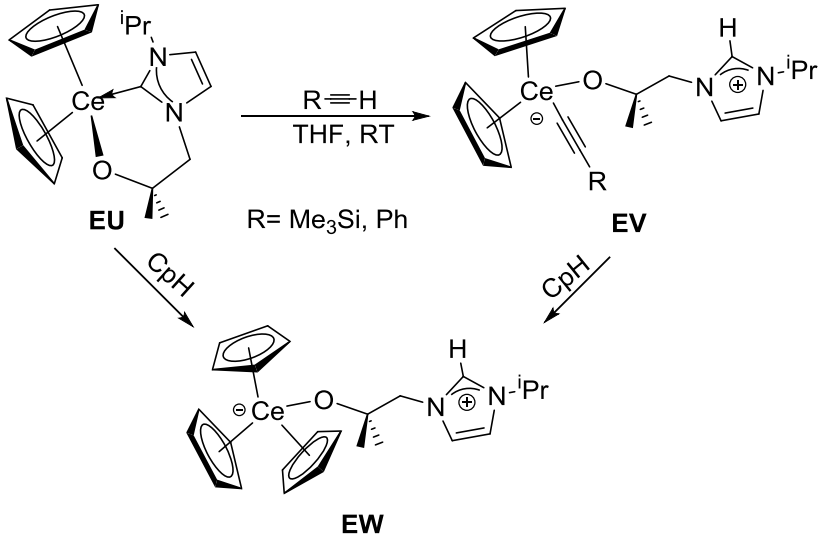

Scheme 1-55. The activation of terminal alkynes.

1.7. Aims of Project

The project will be focused on two rare earth metals: cerium, and praseodymium, which is expected to have an accessible oxidation state of +IV. As discussed in this chapter, the oxo-containing ligands (alkoxide/nitrate/aryoxide) help to stabilise the Ce^{IV} complexes. This project is aimed to introduce the tetraphenolate ligands to Ce and Pr to synthesise the metal complexes. After successful synthesis of these complexes, investigations on their redox chemistry are targeted.

The use of NHC ligands for coordination to rare earth metals has been studied much less than the transition metal counterparts. As discussed in Section 1.3, the introduction of tether groups on nitrogen atoms of NHCs allows the incorporation of a pendant anionic group and facilitates binding to rare earth metals. These modifications also favour binding due to the chelate effect. Our group's previous work has shown that alkoxy- and amido-tethered NHCs can bind to a range of rare earth metals and actinides, and the resulting complexes have been shown to exhibit unprecedented reactivity towards small molecules. Thus, this part of the project focuses on aryloxy-tethered and macrocyclic NHCs which were expected to coordinate with rare earth metals, forming the consequent rare earth metal NHC complexes.

1.8. References

1. N. G. Connelly and T. Damhus, eds., *Nomenclature of Inorganic Chemistry: IUPAC Recommendations 2005*, RSC Publ., Cambridge, 2005.
2. T. Moeller, D. F. Martin, L. C. Thompson, R. Ferrus, G. R. Feistel and W. J. Randall, *Chem. Rev.*, 1965, **65**, 1-50.
3. R. Lemaire and J. Pierre, *Rev. Chim. Miner.*, 1973, **10**, 273-290.
4. S. L. Gai, C. X. Li, P. P. Yang and J. Lin, *Chem. Rev.*, 2014, **114**, 2343-2389.
5. R. A. Layfield and M. Murugesu, *Lanthanides and Actinides in Molecular Magnetism*, Wiley-VCH, 2015.
6. A. Banerjee, *Solid State Ionics*, 2013, **253**, 70-75.
7. S. Cotton, *Lanthanide and Actinide Chemistry*, John Wiley & Sons, Ltd, 2006.
8. M. Zimmermann and R. Anwander, *Chem. Rev.*, 2010, **110**, 6194-6259.
9. W. J. Evans, *Inorg. Chem.*, 2007, **46**, 3435-3449.
10. K. R. D. Johnson and P. G. Hayes, *Chem Soc Rev*, 2013, **42**, 1947-1960.
11. S. Kobayashi, M. Sugiura, H. Kitagawa and W. W. L. Lam, *Chem. Rev.*, 2002, **102**, 2227-2302.
12. M. Westerhausen, M. Hartmann, A. Pfitzner and W. Schwarz, *Z. Anorg. Allg. Chem.*, 1995, **621**, 837-850.
13. F. T. Edelmann, A. Steiner, D. Stalke, J. W. Gilje, S. Jagner and M. Hakansson, *Polyhedron*, 1994, **13**, 539-546.
14. A. D. Frankland, P. B. Hitchcock, M. F. Lappert and G. A. Lawless, *J. Chem. Soc., Chem. Commun.*, 1994, 2435-2346.
15. W. J. Evans, D. S. Lee, D. B. Rego, J. M. Perotti, S. A. Kozimor, E. K. Moore and J. W. Ziller, *J. Am. Chem. Soc.*, 2004, **126**, 14574-14582.
16. P. L. Watson, *J. Am. Chem. Soc.*, 1983, **105**, 6491-6493.
17. Y. Takenaka and Z. Hou, *Organometallics*, 2009, **28**, 5196-5203.
18. D. P. Riley, M. R. Smith and P. E. Correa, *J. Am. Chem. Soc.*, 1988, **110**, 177-180.
19. J. L. Jiao, L. X. Nguyen, D. R. Patterson and R. A. Flowers, *Org Lett*, 2007, **9**, 1323-1326.
20. V. Nair, L. Balagopal, R. Rajan, A. Deepthi, K. Mohanan and N. P. Rath, *Tetrahedron Lett*, 2004, **45**, 2413-2416.
21. V. Nair, L. Balagopal, R. Rajan and J. Mathew, *Acc. Chem. Res.*, 2004, **37**, 21-30.
22. D. A. Rausch, R. A. Davis and D. W. Osborne, *J. Org. Chem.*, 1963, **28**, 494-&.
23. A. A. Goryunkov, Z. Mazej, B. Zemva, S. H. Strauss and O. V. Boltalina, *Mendeleev Commun*, 2006, **16**, 159-161.

24. W. J. Evans, T. J. Deming, J. M. Olofson and J. W. Ziller, *Inorg. Chem.*, 1989, **28**, 4027-4034.
25. W. J. Evans, T. J. Deming and J. W. Ziller, *Organometallics*, 1989, **8**, 1581-1583.
26. M. C. Cassani, Y. K. Gun'ko, P. B. Hitchcock, A. G. Hulkes, A. V. Khvostov, M. F. Lappert and A. V. Protchenko, *J. Organomet. Chem.*, 2002, **647**, 71-83.
27. A. Sen, H. A. Stecher and A. L. Rheingold, *Inorg. Chem.*, 1992, **31**, 473-479.
28. J. R. Robinson, P. J. Carroll, P. J. Walsh and E. J. Schelter, *Angew. Chem., Int. Ed.*, 2012, **51**, 10159-10163.
29. J. R. Robinson, Z. Gordon, C. H. Booth, P. J. Carroll, P. J. Walsh and E. J. Schelter, *J. Am. Chem. Soc.*, 2013, **135**, 19016-19024.
30. J. Gottfriedsen and D. Dorokhin, *Z. Anorg. Allg. Chem.*, 2005, **631**, 2928-2930.
31. C. Morton, N. W. Alcock, M. R. Lees, I. J. Munslow, C. J. Sanders and P. Scott, *J. Am. Chem. Soc.*, 1999, **121**, 11255-11256.
32. P. B. Hitchcock, M. F. Lappert and A. V. Protchenko, *Chem. Commun.*, 2006, 3546-3548.
33. A. R. Crozier, A. M. Bienfait, C. Maichle-Mossmer, K. W. Tornroos and R. Anwander, *Chem. Commun.*, 2013, **49**, 87-89.
34. O. Eisenstein, P. B. Hitchcock, A. G. Hulkes, M. F. Lappert and L. Maron, *Chem. Commun.*, 2001, 1560-1561.
35. P. L. Arnold, Z. R. Turner, A. I. Germeroth, I. J. Casely, R. Bellabarba and R. P. Tooze, *Dalton Trans.*, 2010, **39**, 6808-6814.
36. P. B. Hitchcock, A. G. Hulkes and M. F. Lappert, *Inorg. Chem.*, 2004, **43**, 1031-1038.
37. M. P. Coles, P. B. Hitchcock, A. V. Khvostov, M. F. Lappert, Z. N. Li and A. V. Protchenko, *Dalton Trans.*, 2010, **39**, 6780-6788.
38. A. Greco, S. Cesca and G. Bertolini, *J. Organomet. Chem.*, 1976, **113**, 321-330.
39. A. Streitwieser, S. A. Kinsley, J. T. Rigsbee, I. L. Fragala, E. Ciliberto and N. Rosch, *J. Am. Chem. Soc.*, 1985, **107**, 7786-7788.
40. T. R. Boussie, D. C. Eisenberg, J. Rigsbee, A. Streitwieser and A. Zalkin, *Organometallics*, 1991, **10**, 1922-1928.
41. U. Kilimann, R. Herbstirmer, D. Stalke and F. T. Edelmann, *Angew Chem Int Edit*, 1994, **33**, 1618-1621.
42. V. Lorenz, B. M. Schmiege, C. G. Hrib, J. W. Ziller, A. Edelmann, S. Blaurock, W. J. Evans and F. T. Edelmann, *J. Am. Chem. Soc.*, 2011, **133**, 1257-1259.
43. D. Cui, M. Nishiura and Z. M. Hou, *Angew. Chem., Int. Ed.*, 2005, **44**, 959-962.
44. Y. M. So, G. C. Wang, Y. Li, H. H. Y. Sung, I. D. Williams, Z. Y. Lin and W. H. Leung, *Angew. Chem., Int. Ed.*, 2014, **53**, 1626-1629.

45. Y. M. So, Y. Li, K. C. Au-Yeung, G. C. Wang, K. L. Wong, H. H. Y. Sung, P. L. Arnold, I. D. Williams, Z. Y. Lin and W. H. Leung, *Inorg. Chem.*, 2016, **55**, 10003-10012.
46. L. A. Solola, A. V. Zabula, W. L. Dorfner, B. C. Manor, P. J. Carroll and E. J. Schelter, *J. Am. Chem. Soc.*, 2016, **138**, 6928-6931.
47. M. Gregson, E. Lu, J. McMaster, W. Lewis, A. J. Blake and S. T. Liddle, *Angew. Chem., Int. Ed.*, 2013, **52**, 13016-13019.
48. S. D. Gabelnick, G. T. Reedy and M. G. Chasanov, *J. Chem. Phys.*, 1974, **60**, 1167-1171.
49. V. I. Spitsyn, Y. M. Kiselev, Martynen.Li, V. N. Prusakov and V. B. Sokolov, *Dokl. Akad. Nauk SSSR*, 1974, **219**, 621-624.
50. Z. Mazej, *J. Fluor. Chem.*, 2002, **118**, 127-129.
51. T. Vent-Schmidt and S. Riedel, *Inorg. Chem.*, 2015, **54**, 11114-11120.
52. W. X. Ji, W. Xu, Y. Xiao and S. G. Wang, *J. Chem. Phys.*, 2014, **141**.
53. Q. N. Zhang, S. X. Hu, H. Qu, J. Su, G. J. Wang, J. B. Lu, M. H. Chen, M. F. Zhou and J. Li, *Angew. Chem., Int. Ed.*, 2016, **55**, 6896-6900.
54. W. J. Evans, *Inorg. Chim. Acta*, 1987, **139**, 169-170.
55. F. Nief, *Monogr. Ser. Int. Conf. Coord. Bioinorg. Chem.*, 2011, **10**, 405-424.
56. P. B. Hitchcock, A. V. Khvostov, M. F. Lappert and A. V. Protchenko, *J. Organomet. Chem.*, 2002, **647**, 198-204.
57. M. N. Bochkarev, I. L. Fedushkin, S. Dechert, A. A. Fagin and H. Schumann, *Angew. Chem., Int. Ed.*, 2001, **40**, 3176-3178.
58. W. J. Evans, N. T. Allen and J. W. Ziller, *J. Am. Chem. Soc.*, 2000, **122**, 11749-11750.
59. M. N. Bochkarev, I. L. Fedushkin, A. A. Fagin, T. V. Petrovskaya, J. W. Ziller, R. N. R. Broomhall-Dillard and W. J. Evans, *Angew. Chem., Int. Ed.*, 1997, **36**, 133-135.
60. T. D. Tilley, A. Zalkin, R. A. Andersen and D. H. Templeton, *Inorg. Chem.*, 1981, **20**, 551-554.
61. M. R. MacDonald, J. E. Bates, J. W. Ziller, F. Furche and W. J. Evans, *J. Am. Chem. Soc.*, 2013, **135**, 9857-9868.
62. C. M. Kotyk, M. E. Fieser, C. T. Palumbo, J. W. Ziller, L. E. Darago, J. R. Long, F. Furche and W. J. Evans, *Chem. Sci.*, 2015, **6**, 7267-7273.
63. P. J. Shapiro, W. D. Cotter, W. P. Schaefer, J. A. Labinger and J. E. Bercaw, *J. Am. Chem. Soc.*, 1994, **116**, 4623-4640.
64. A. D. Sadow and T. D. Tilley, *J. Am. Chem. Soc.*, 2005, **127**, 643-656.
65. B. J. Burger, M. E. Thompson, W. D. Cotter and J. E. Bercaw, *J. Am. Chem. Soc.*, 1990, **112**, 1566-1577.

66. P. L. Arnold, F. G. N. Cloke, P. B. Hitchcock and J. F. Nixon, *J. Am. Chem. Soc.*, 1996, **118**, 7630-7631.
67. F. G. N. Cloke, K. Khan and R. N. Perutz, *J. Chem. Soc., Chem. Commun.*, 1991, 1372-1373.
68. F. G. N. Cloke, K. A. E. Courtney, A. A. Sameh and A. C. Swain, *Polyhedron*, 1989, **8**, 1641-1648.
69. H. W. Wanzlick and E. Schikora, *Angew. Chem., Int. Ed.*, 1960, **72**, 494-494.
70. L. J. Guggenberger and R. R. Schrock, *J. Am. Chem. Soc.*, 1975, **97**, 6578-6579.
71. E. O. Fischer and A. Maasbol, *Angew. Chem., Int. Ed.*, 1964, **3**, 580-&.
72. H. W. Wanzlick and H. J. Kleiner, *Angew. Chem., Int. Ed.*, 1961, **73**, 493-&.
73. A. J. Arduengo, R. L. Harlow and M. Kline, *J. Am. Chem. Soc.*, 1991, **113**, 361-363.
74. D. M. Flanigan, F. Romanov-Michailidis, N. A. White and T. Rovis, *Chem. Rev.*, 2015, **115**, 9307-9387.
75. D. Enders, O. Niemeier and A. Henseler, *Chem. Rev.*, 2007, **107**, 5606-5655.
76. Z. Q. Fu, J. F. Xu, T. S. Zhu, W. W. Y. Leong and Y. R. Chi, *Nat. Chem.*, 2013, **5**, 835-839.
77. B. S. Li, Y. H. Wang, Z. C. Jin, P. C. Zheng, R. Ganguly and Y. R. Chi, *Nat Commun*, 2015, **6**.
78. M. Pareek and R. B. Sunoj, *Org Lett*, 2016, **18**, 5932-5935.
79. H. Song, Y. Kim, J. Park, K. Kim and E. Lee, *Synlett*, 2016, **27**, 477-485.
80. A. J. Arduengo, J. C. Calabrese, A. H. Cowley, H. V. R. Dias, J. R. Goerlich, W. J. Marshall and B. Riegel, *Inorg. Chem.*, 1997, **36**, 2151-2158.
81. D. J. Williams, M. R. Fawcettbrown, R. R. Raye, D. Vanderveer, Y. T. Pang, R. L. Jones and K. L. Bergbauer, *Heteroatom Chem*, 1993, **4**, 409-414.
82. N. Kuhn, G. Henkel and T. Kratz, *Chem Ber-Recl*, 1993, **126**, 2047-2049.
83. A. J. Arduengo, H. V. R. Dias and J. C. Calabrese, *Chem Lett*, 1997, 143-144.
84. H. A. Duong, T. N. Tekavec, A. M. Arif and J. Louie, *Chem. Commun.*, 2004, 112-113.
85. S. N. Riduan, Y. G. Zhang and J. Y. Ying, *Angew. Chem., Int. Ed.*, 2009, **48**, 3322-3325.
86. O. Jacquet, C. D. Gomes, M. Ephritikhine and T. Cantat, *J. Am. Chem. Soc.*, 2012, **134**, 2934-2937.
87. D. Holschumacher, T. Bannenberg, C. G. Hrib, P. G. Jones and M. Tamm, *Angew. Chem., Int. Ed.*, 2008, **47**, 7428-7432.
88. N. Kuhn, G. Henkel, T. Kratz, J. Kreutzberg, R. Boese and A. H. Maulitz, *Chemische Berichte-Recueil*, 1993, **126**.
89. T. Taniguchi and D. P. Curran, *Angew. Chem., Int. Ed.*, 2014, **53**, 13150-13154.

90. D. P. Curran, A. Solovyev, M. M. Brahmi, L. Fensterbank, M. Malacria and E. Lacote, *Angew. Chem., Int. Ed.*, 2011, **50**, 10294-10317.
91. Y. Yamaguchi, T. Kashiwabara, K. Ogata, Y. Miura, Y. Nakamura, K. Kobayashi and T. Ito, *Chem. Commun.*, 2004, 2160-2161.
92. D. P. Curran, A. Solovyev, M. Makhlouf Brahmi, L. Fensterbank, M. Malacria and E. Lacôte, *Angew. Chem., Int. Ed. Engl.*, 2011, **50**, 10294-10317.
93. K. Ogata, Y. Yamaguchi, T. Kashiwabara and T. Ito, *J. Organomet. Chem.*, 2005, **690**, 5701-5709.
94. A. L. Kenward and W. E. Piers, *Angew. Chem., Int. Ed.*, 2008, **47**, 38-41.
95. D. W. Stephan, *Dalton Trans.*, 2009, 3129-3136.
96. H. W. Wanzlick and Schonher.Hj, *Angew. Chem., Int. Ed.*, 1968, **7**, 141-&.
97. K. Ofele, *J. Organomet. Chem.*, 1968, **12**, P42-43.
98. K. J. Cavell and D. S. McGuinness, *Coord. Chem. Rev.*, 2004, **248**, 671-681.
99. C. M. Crudden and D. P. Allen, *Coord. Chem. Rev.*, 2004, **248**, 2247-2273.
100. P. L. Arnold, M. W. McMullon, J. Rieb and F. E. Kuhn, *Angew. Chem., Int. Ed.*, 2015, **54**, 82-100.
101. S. Bellemin-Laponnaz and S. Dagorne, *Chem. Rev.*, 2014, **114**, 8747-8774.
102. P. L. Arnold and S. T. Liddle, *Organometallics*, 2006, **25**, 1485-1491.
103. P. L. Arnold, S. A. Mungur, A. J. Blake and C. Wilson, *Angew. Chem., Int. Ed.*, 2003, **42**, 5981-5984.
104. S. A. Mungur, S. T. Liddle, C. Wilson, M. J. Sarsfield and P. L. Arnold, *Chem. Commun.*, 2004, 2738-2739.
105. S. T. Liddle and P. L. Arnold, *Organometallics*, 2005, **24**, 2597-2605.
106. L. P. Spencer, S. Winston and M. D. Fryzuk, *Organometallics*, 2004, **23**, 3372-3374.
107. L. P. Spencer and M. D. Fryzuk, *J. Organomet. Chem.*, 2005, **690**, 5788-5803.
108. P. L. Arnold, M. Rodden, K. M. Davis, A. C. Scarisbrick, A. J. Blake and C. Wilson, *Chem. Commun.*, 2004, 1612-1613.
109. D. Patel, S. T. Liddle, S. A. Mungur, M. Rodden, A. J. Blake and P. L. Arnold, *Chem. Commun.*, 2006, 1124-1126.
110. P. L. Arnold, Z. R. Turner, R. Bellabarba and R. P. Tooze, *J. Am. Chem. Soc.*, 2011, **133**, 11744-11756.
111. I. J. Casely, S. T. Liddle, A. J. Blake, C. Wilson and P. L. Arnold, *Chem. Commun.*, 2007, 5037-5039.
112. P. L. Arnold, A. L. Blake and C. Wilson, *Chem-Eur J*, 2005, **11**, 6095-6099.
113. J. J. Van Veldhuizen, S. B. Garber, J. S. Kingsbury and A. H. Hoveyda, *J. Am. Chem. Soc.*, 2002, **124**, 4954-4955.

114. J. J. Van Veldhuizen, D. G. Gillingham, S. B. Garber, O. Kataoka and A. H. Hoveyda, *J. Am. Chem. Soc.*, 2003, **125**, 12502-12508.
115. A. W. Waltman and R. H. Grubbs, *Organometallics*, 2004, **23**, 3105-3107.
116. A. W. Waltman, T. Ritter and R. H. Grubbs, *Organometallics*, 2006, **25**, 4238-4239.
117. H. Ren, P. Yao, S. Xu, H. Song and B. Wang, *J. Organomet. Chem.*, 2007, **692**, 2092-2098.
118. Y. Kong, H. P. Ren, S. S. Xu, H. B. Song, B. Y. Liu and B. Q. Wang, *Organometallics*, 2009, **28**, 5934-5940.
119. H. Aihara, T. Matsuo and H. Kawaguchi, *Chem. Commun.*, 2003, 2204-2205.
120. D. Zhang, H. Aihara, T. Watanabe, T. Matsuo and H. Kawaguchi, *J. Organomet. Chem.*, 2007, **692**, 234-242.
121. B. E. Ketz, A. P. Cole and R. M. Waymouth, *Organometallics*, 2004, **23**, 2835-2837.
122. B. E. Ketz, X. G. Ottenwaelder and R. M. Waymouth, *Chem. Commun.*, 2005, 5693-5695.
123. Z. Li, M. Q. Xue, H. S. Yao, H. M. Sun, Y. Zhang and Q. Shen, *J. Organomet. Chem.*, 2012, **713**, 27-34.
124. D. Sellmann, W. Prechtel, F. Knoch and M. Moll, *Organometallics*, 1992, **11**, 2346-2348.
125. D. Sellmann, W. Prechtel, F. Knoch and M. Moll, *Inorg. Chem.*, 1993, **32**, 538-546.
126. S. P. Downing, S. C. Guadano, D. Pugh, A. A. Danopoulos, R. M. Bellabarba, M. Hanton, D. Smith and R. P. Tooze, *Organometallics*, 2007, **26**, 3762-3770.
127. S. P. Downing, P. J. Pogorzelec, A. A. Danopoulos and D. J. Cole-Hamilton, *Eur. J. Inorg. Chem.*, 2009, DOI: 10.1002/ejic.200801162, 1816-1824.
128. S. Conde-Guadano, A. A. Danopoulos, R. Pattacini, M. Hanton and R. P. Tooze, *Organometallics*, 2012, **31**, 1643-1652.
129. B. L. Wang, D. Wang, D. M. Cui, W. Gao, T. Tang, X. S. Chen and X. B. Jing, *Organometallics*, 2007, **26**, 3167-3172.
130. V. V. K. M. Kandepi, A. Pontes da Costa, E. Peris and B. Royo, *Organometallics*, 2009, **28**, 4544-4549.
131. B. Royo, in *Advances in Organometallic Chemistry and Catalysis*, John Wiley & Sons, Inc., 2013, DOI: 10.1002/9781118742952.ch10, pp. 133-143.
132. G. A. Melson, *Coordination Chemistry of Macrocyclic Compounds*, New York: Plenum Press, 1979.
133. D. K. Cabbiness and D. W. Margerum, *J. Am. Chem. Soc.*, 1969, **91**, 6540-+.
134. M. Poyatos, J. A. Mata and E. Peris, *Chem. Rev.*, 2009, **109**, 3677-3707.
135. H. M. Bass, S. A. Cramer, J. L. Price and D. M. Jenkins, *Organometallics*, 2010, **29**, 3235-3238.

136. O. Kuhl, *Chem Soc Rev*, 2007, **36**, 592-607.
137. F. E. Hahn, V. Langenhahn, T. Lugger, T. Pape and D. Le Van, *Angew. Chem., Int. Ed.*, 2005, **44**, 3759-3763.
138. M. V. Baker, B. W. Skelton, A. H. White and C. C. Williams, *Organometallics*, 2002, **21**, 2674-2678.
139. P. L. Arnold, Z. R. Turner, N. Kaltsoyannis, P. Pelekanaki, R. M. Bellabarba and R. P. Tooze, *Chem-Eur J*, 2010, **16**, 9623-9629.
140. Z. R. Turner, R. Bellabarba, R. P. Tooze and P. L. Arnold, *J. Am. Chem. Soc.*, 2010, **132**, 4050-4051.
141. P. L. Arnold, I. A. Marr, S. Zlatogorsky, R. Bellabarba and R. P. Tooze, *Dalton Trans.*, 2014, **43**, 34-37.
142. P. L. Arnold, T. Cadenbach, I. H. Marr, A. A. Fyfe, N. L. Bell, R. Bellabarba, R. P. Tooze and J. B. Love, *Dalton Trans.*, 2014, **43**, 14346-14358.

2. Synthesis and Reactivity of Tetraaryloxide Rare Earth Complexes

2.1. Introduction

The organometallic chemistry of rare earth elements has attracted much attention in recent years as active and selective homogeneous catalysts for a range of small molecule transformations. In particular, cerium is of major importance because of its facile $Ce^{III/IV}$ couple, which has been utilised in organic, inorganic, and materials chemistry.[1] Applications of cerium reagents in molecular chemistry have largely been focused on the strong oxidizing potential of Ce^{IV} in electron deficient ligand frameworks in stoichiometric redox reactions, while the use of electron-rich frameworks to produce Ce^{III} reductants have received considerably less attention.[2]

The concept of stabilising Ce^{IV} ion by the introduction of polyanions to the coordination sphere has been explored throughout the past decade.[3, 4] It has been shown that through the use of poly-oxo ligands (POMs), Ce^{IV} ions can be stabilised and various reactivity has been documented.[2] POMs can act as large, polyanionic ligands that coordinate cerium ions and can serve to stabilise the +IV oxidation state because of the high electronegativity of oxygen atoms (**Scheme 2-1**).[5, 6]

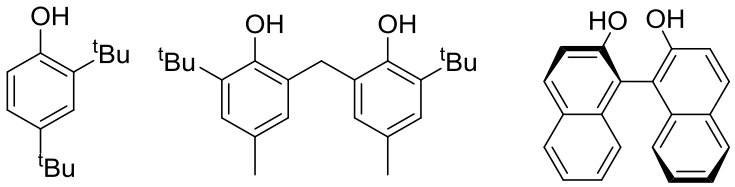

Scheme 2-1. Examples of phenol ligands.

Based on these findings for Ce^{IV} complexes and combined with the bulky phenyl groups which may help to stabilise the rare earth metal complexes, a series of tetraphenol ligands are designed and tested in this project to synthesise Ce/Pr complexes.

The tetraphenol ligands H_4L^R(R = P, PT and M) are synthesised through a modification of a literature preparation.[7] The reaction of substituted phenol and terephthalaldehyde (or isophthalaldehyde) in the presence of catalytic amount of *p*-toluenesulfonic acid afforded the ligand **1** (H_4L) in good yield (**Scheme 2-2**).

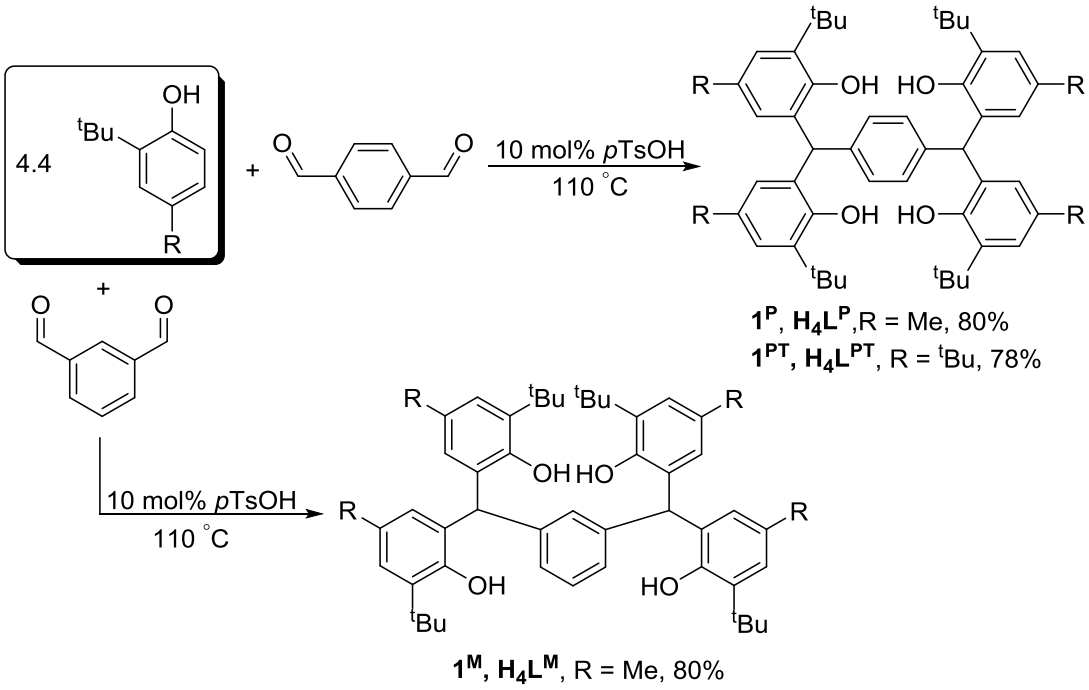

Scheme 2-2. Synthesis of tetraphenol ligand H_4L.

Zhang and co-workers reported that the reaction of H_4L with two or three equivalents of KN" (N" = $N(SiMe_3)_2$) affords partially deprotonated bimetallic complexes **EX** $\{H_2K_2L^{PT}(thf)_2\}$ and **EY** $\{K_3HL^{M}(thf)_5\}$ (**Scheme 2-3**), respectively. The *meta*-tetraphenolate lithium complexes **EZ** $\{Li_4L^{M'}(thf)_2\}$ are synthesised by the reaction of $H_4L^{M'}$ with four equivalents of *n*-butyllithium at room temperature.[8]

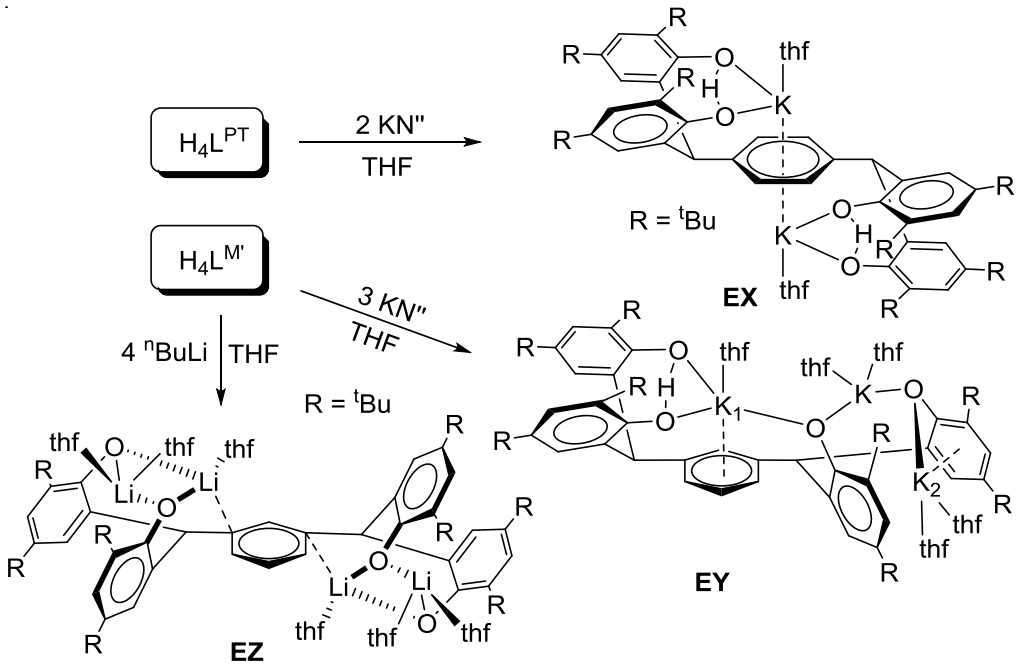

Scheme 2-3. Reported synthesis of alkali metal complexes.

These complexes have been found to be very active towards the ring-opening polymerization of *l*-lactide, in which bimetallic potassium complex **EX** serves as a highly active catalyst for the controllable ring-opening polymerisation.[8] Other bimetallic complexes of the modified phenol ligands have been synthesised and are proved to be excellent ring opening polymerisation initiators. For example, bis-Al^{III} adducts of L^{PT} have been tested for the ring-opening polymerisation of epoxide[9] while the bis-Nb (or Ta) complexes of L^{PT} and L^{M} catalyse the conversions of ε-caprolactone with excellent performance.[10, 11]

2.2. Reactivity of ligands towards bases

Zhang *et al*. have reported the partial deprotonation of the *para*-tetraphenols, however, the products of full deprotonation of these ligands have not been characterised. In this part of research, the reaction of tetraphenol ligands towards different bases are investigated to synthesise fully deprotonated phenolate complexes.

2.2.1. **Synthesis of potassium complexes**

2.2.1.1. Reaction with KN" in THF

Treatment of $\mathbf{1^P}$ with four equivalents of KN" in THF at room temperature affords a full deprotonation product $\mathbf{2^P}$ (**Scheme 2-4**), which is confirmed through the use of NMR spectroscopy.

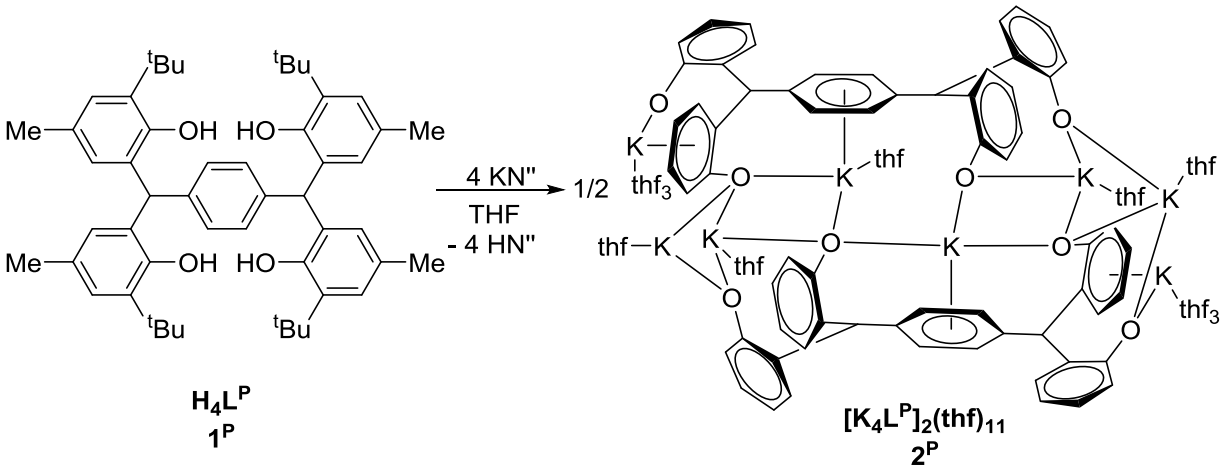

Scheme 2-4. Reaction of $\mathbf{1^P}$ towards KN". Methyl and *t*-butyl groups are omitted for clarity.

The ^{1}H NMR spectrum of the product in THF shows the absence of –O*H* groups and full consumption of KN" which confirms the full deprotonation of ligands. The phenyl protons of the phenyl linkers are observed at δ = 6.45 ppm while the benzylic-C*H* are recorded at δ = 5.76 ppm. The methyl groups are observed as doublets at δ = 2.00 ppm (J = 13.4 Hz) and the *tert*-butyls are observed at δ = 1.31 ppm (d, J = 34.0 Hz).

The full deprotonation of $\mathbf{1}^{PT}$ and $\mathbf{1}^{M}$ can also be achieved using this synthetic procedure and was confirmed by ^{1}H NMR spectrum.

Single crystals of $\mathbf{2}^{P}$ were grown from a hexane layered THF solution. The solid-state structure (**Figure 2-1**) and selected bond length (Å) and angles (°) are provided (**Table 2-1**).

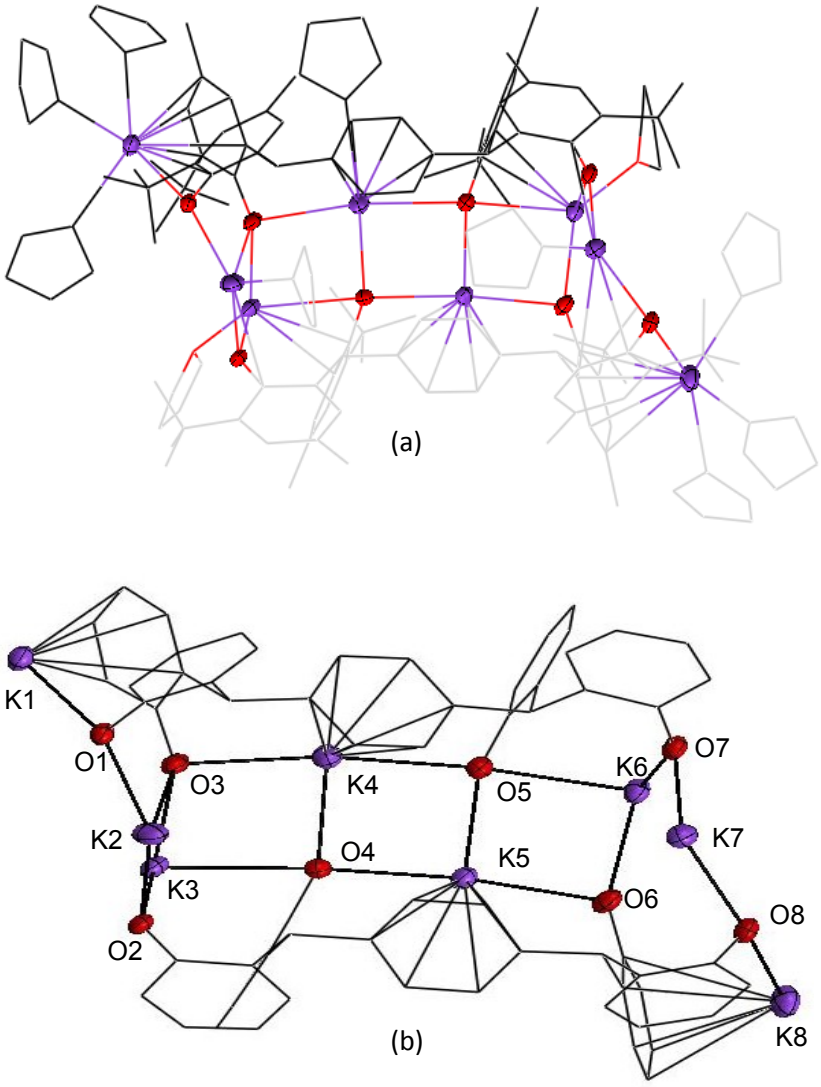

Figure 2-1. Representation of the molecular structure of complex $\mathbf{2}^{P}$(a) and the skeleton structure(b). Thermal ellipsoids of non-carbon atoms are shown at 30% probability. All hydrogen atoms and solvents (and *tert*-butyl groups in b) are omitted for clarity.

Compound $\mathbf{2}^{P}$ crystallises in the monoclinic space group $P2_1/c$, with four molecules in the unit cell. Complex $\mathbf{2}^{P}$ is a dimerised compound of K_4L^{P}. In the crystal structure (**Figure 2-1**), four K^+ ions (K3-K6) and four oxygen atoms (O3-O6) bind to each other in a staggered quadrangle mode, forming a near-planar ladder-like $[K_4O_4]$ skeleton. This type of coordination can have been reported in the family of "K(OAr)(sol), (Ar = 2,6-di-methyl, *etc.*)" species[12] and potassium *p*-halide-substituted aryloxides, $[(4\text{-X-}C_6H_4OK)_6\cdot(\text{dioxane})_6]$, (X = F, Cl, Br).[13]

Each K^+ coordinates with three phenol oxygen atoms while oxygen atoms bridge two K^+ ions. The bond length of each K-O_{Ph} bond varies from 2.552(4) Å (K4-O5) to 3.132(4) Å (K6-O5) (**Table 2-1**), which falls within the reported range of K-O bonds of 2.432(6) Å to 3.194 (Å).[12] The wide range of the bond lengths in this complex can be explained by the steric hindrance of the bulky *tert*-butyl groups on the *meta* position of phenols and the flexibility of the K-O bonds. The two ions in the middle of the skeleton, K4 and K5, coordinate with the phenyl linker through a *p*-π interaction with an average distance of 2.868 Å and 3.046 Å, respectively. It is proposed that the difference between these bonds lengths are due to the coordination of THF to K5 but not K4.

Table 2-1. Selected bond distances (Å) of complex $\mathbf{2^P}$.

Bond	Length	Bond	Length
K1-O1	2.672(4)	K8-O8	2.667(4)
K2-O1	2.652(4)	K7-O8	2.619(4)
K2-O2	2.627(4)	K7-O7	2.572(4)
K2-O3(distance)	4.811(4)	K7-O6	3.132(5)
K3-O2	2.585(4)	K6-O5	3.132(4)
K3-O3	2.991(4)	K6-O6	2.552(4)
K3-O4	2.559(4)	K6-O7	2.643(4)
K4-O3	2.735(4)	K5-O5	2.638(4)
K4-O4	2.746(4)	K5-O4	3.081(4)
K4-O5	2.552(4)	K5-O6	2.945(4)
K1-Ph ring	2.948	K8-Ph ring	2.916
K4-Ph ring	2.868	K5-Ph ring	3.046

Each terminal K^+ ion (K1, K8) is coordinated by three THF molecules, one oxygen atom of the phenol, and the phenyl ring of the ligand through a *p*-π interaction with an average distance of 2.932 Å between the K^+ and benzene ring.

These K^+-π interactions are also seen in the reported complexes (**Scheme 2-3**).[8] In complex **EQ**, the K^+ ion coordinates with the phenyl-linker at a distance of 2.743(7) Å. There are also two important *p*-π interactions in the trimetallic complex **ER**: one is the interaction between K1 and the centre of the benzene ring with a distance of 3.156(8) Å, and another is between K2 and one peripheral benzene ring with a distance of 2.577(5) Å.

2.2.1.2. Reaction with KN" in benzene

In order to study how solvents affect the deprotonation reaction and the structure of the products, a reaction of KN" with tetraphenol is carried out in a donor-free solvent, benzene.

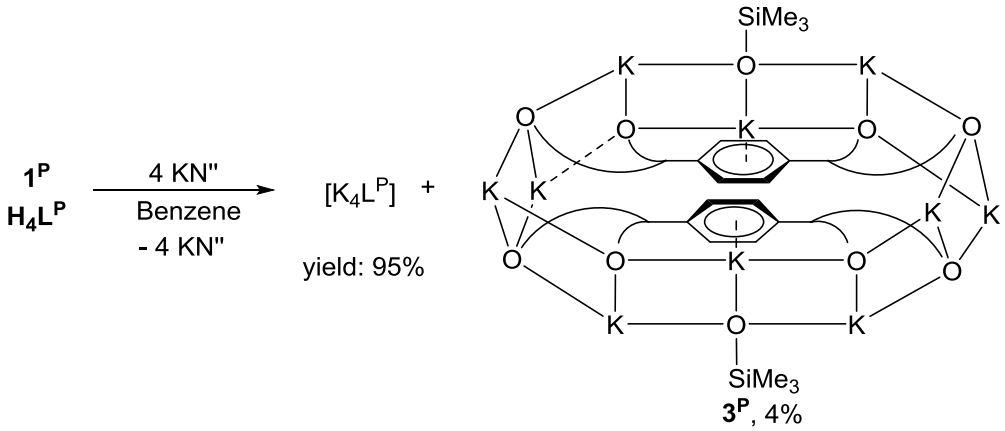

Scheme 2-5. Reaction of $\mathbf{H_4L^P}$ with KN" in benzene.

The product of an *in situ* reaction of H_4L^P with four equivalents of KN" in benzene shows similar resonances compared to complex $\mathbf{2^P}$. These complexes can be converted to complex $\mathbf{2^P}$ when several drops of THF are added. This shows that the full deprotonation of the ligand can also be achieved in donor-free conditions. In this reaction, a trace amount of a side product $\mathbf{3^P}$ can be obtained in benzene at a low yield (4% by NMR). However, attempts to synthesise this complex in a larger scale failed to yield the desired product. The colourless crystals of the side product were grown from the benzene solution at room temperature. Its solid state structure was characterised by single crystal X-ray diffraction. (**Figure 2-2**).

In the structure of complex $\mathbf{3^P}$, the staggered $[K_4O_4]$ skeleton moiety which is observed in complex $\mathbf{2^P}$ is extended to $[K_{10}O_{10}]$, and are bound from toe to head, forming a ladder-belt structure (**Figure 2-2**). Similar to the structure observed in complex $\mathbf{2^P}$, the K-O_{Ph} bonds in complex $\mathbf{3^P}$ vary from 2.591(6) Å (K5-O5) to 2.957(6) Å (K8-O7). (**Table 2-2**). In the crystal structure, each of the two Me_3SiO groups coordinates with three K^+ ions.

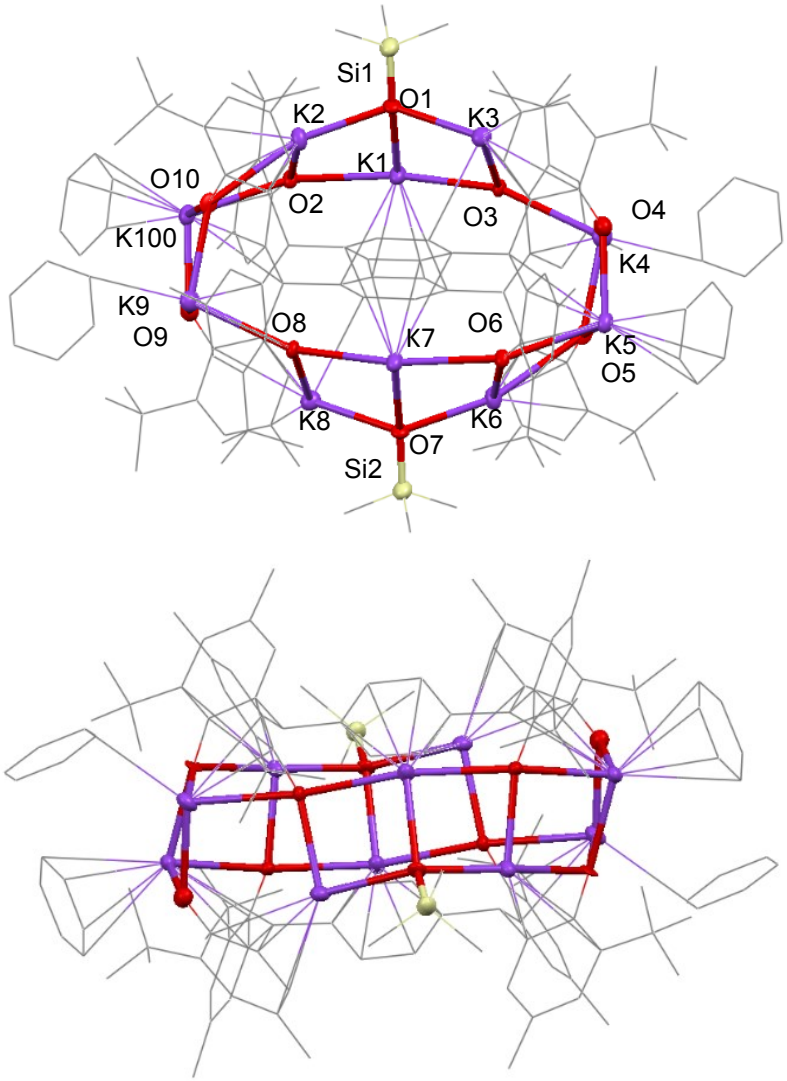

Figure 2-2. Molecular structure of complex **3^{P}**. Thermal ellipsoids of non-carbon atoms are shown at 30% probability. All hydrogen atoms and solvents are omitted for clarity.

Table 2-2. Selected bond distances of complex **3^{P}**.

Bond	Length (Å)	Bond	Length (Å)
K1-O1	2.600(6)	K7-O6	2.644(6)
K1-O2	2.793(6)	K7-O7	2.565(6)
K1-O3	2.836(6)	K8-O7	2.957(6)
K2-O1	2.722(6)	K8-O8	2.544(7)
K2-O2	2.620(5)	K9-O8	2.573(6)
K3-O3	2.643(6)	K10-O9	2.695(6)
K4-O3	2.660(6)	K10-O10	2.619(6)
K4-O4	2.558(6)	Si2-O6	1.587(6)
K5-O5	2.591(6)	Si1-O1	1.592(6)

Given the low yield of the product and the base (KN", N" = $N(SiMe_3)_2$) used in the reaction, it is proposed that the O-$SiMe_3$ groups are formed via the cleavage of Si-N bond, followed by the reaction with trace amount of water (or OH groups) in the phenol ligand, which then reacts with the complex. Similar reactivity of the Si-N bond has been reported in the reaction of ruthenium complex (PNP)Ru(OTf) (PNP = $(^tBu_2PCH_2SiMe_2)_2N$) (**ET**) with two equivalents of water which affords planar *trans*-Ru($^tBu_2PCH_2SiMe_2O)_2$ complex **EU** (**Scheme 2-6**).[14]

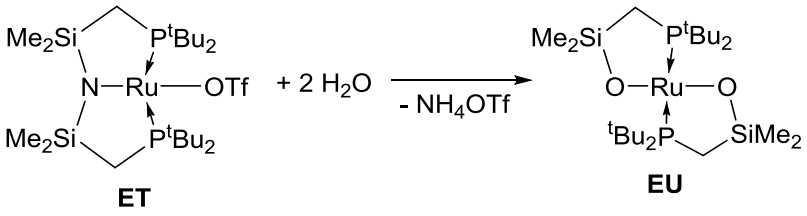

Scheme 2-6. Reported example of cleavage of the Si-N bond.

2.2.2. **Other deprotonations**

Apart from the reaction with KN", the tetraphenols can also be deprotonated by other alkali metal bases, such as LiN" or NaN", forming alkali metal complexes which are soluble in organic solvents. The ^1H NMR spectrum has shown similar patterns to that of complex **2**, which suggest the full deprotonation of phenols. However, the crystal structures of these complexes have not yet been reported. (**Scheme 2-7**)

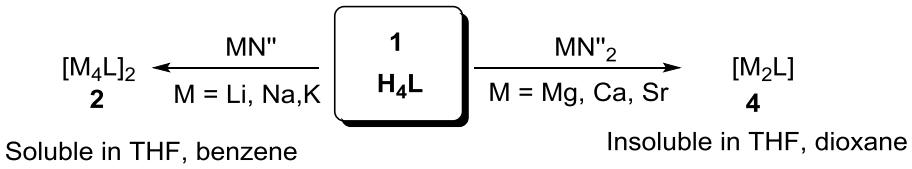

Scheme 2-7. Deprotonation of tetraphenols.

Work within the Arnold group shown that the reaction of **1** with alkaline earth metal *bis*-amide ($CaN"_2$, $MgN"_2$ or $SrN"_2$) in THF or 1,4-dioxane forms off-white suspensions from which no phenol or amide starting reagent is observed.[8] The full deprotonation of the tetraphenols is confirmed by the ^1H NMR spectroscopy where the by-product of HN" is quantitatively formed. The products are not very soluble in THF or 1, 4-dioxane, this may due to the higher coordination number of alkaline earth metals which allows the formation of polymers. This thus offers a comparison with the soluble alkali metal phenolates, from which we presume that the *p*-π interactions between metal and phenyl rings help to solubilise the complexes.

2.3. Synthesis of dinuclear rare earth metal complexes

2.3.1. Synthesis of complex $K_2L_2RE_2$ (5)

The synthesis of rare earth metal (RE) aryloxide complexes is achieved by either salt elimination from the REX_3 (X = halogen, BH_4, *etc*.) or by protonolysis between phenols and rare earth metal amides or alkyl complexes. In this part of project, the salt elimination reactions towards complex $\mathbf{2^P}$ and $\mathbf{2^{PT}}$ are carried out to make Ce^{III} and Pr^{III} complexes.

The reaction of complex $\mathbf{2^P}$ or $\mathbf{2^{PT}}$ with two equivalents of $RECl_3(THF)_2$ (RE = Ce, Pr) in THF affords a cloudy suspension after being stirred at room temperature for 12 hours. The KCl salt is removed by centrifugation and the volatiles of the solution are removed under reduced pressure to yield a white solid. This was washed with hexane and dried under reduced pressure. The products are obtained in good yields (~ 80%).

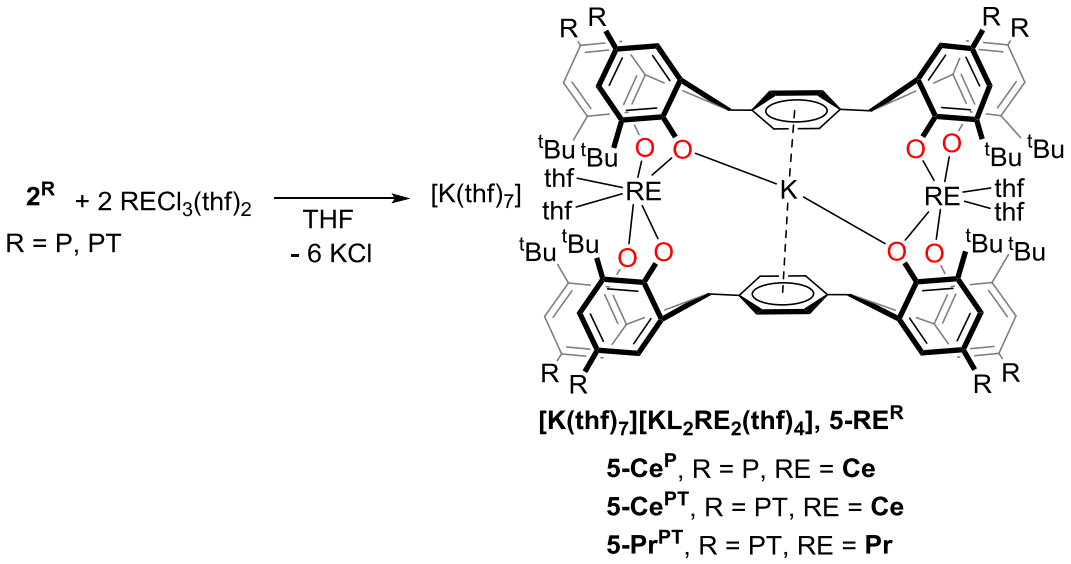

$[K(thf)_7][KL_2RE_2(thf)_4]$, 5-$RE^R$

5-Ce^P, R = P, RE = **Ce**
5-Ce^{PT}, R = PT, RE = **Ce**
5-Pr^{PT}, R = PT, RE = **Pr**

Scheme 2-8. Synthesis of complex **5**.

The ^{1}H NMR spectrum of complex **5-Ce^P** at 300 K shows paramagnetically shifted resonances, which agree with the unpaired electrons of Ce^{III} ions. In order to investigate how temperature affects the configuration of the complexes, variable temperature ^{1}H NMR spectra of **5-Ce^{PT}** has been carried out in d_8-THF at the temperature from 243K to 328K (**Figure 2-3**).

The phenyl protons on phenol rings are observed at δ = 9.74 (s, 4H), 8.89 (s, 4H), 7.82 (s, 4H) and 5.48 (s, 4H). The resonances of phenyl-linker can be ascribed to the broad signal at 3.82 ppm (asterisk), which become obvious at higher temperatures (318 K and 328 K). The protons of the benzylic CH groups are not obvious in these spectra, which may due to the broadening effect from the paramagnetic metal ions and being overlapped by the broad phenyl-linker signals. The methyl groups resonate as two singlets at δ = 3.77 and 2.00 ppm. The *tert*-butyls

are greatly shifted to 3.45 and -0.35 ppm as two singlets. When the THF solution of **5-Ce^{PT}** was cooled to 243 K, the ^{1}H NMR showed a desymmetrised pattern compared to all the NMR spectra recorded above 278 K where several new broad singlets for *tert*-butyl groups are observed at δ = 9.3, 0.62, -1.65 and -2.11 ppm. The phenyl protons are also broadened and are shifted to δ = 14.16, 11.24, 7.18 ppm. This suggests a possible reversible change of configurations at a lower temperature. (**Figure 2-3**).

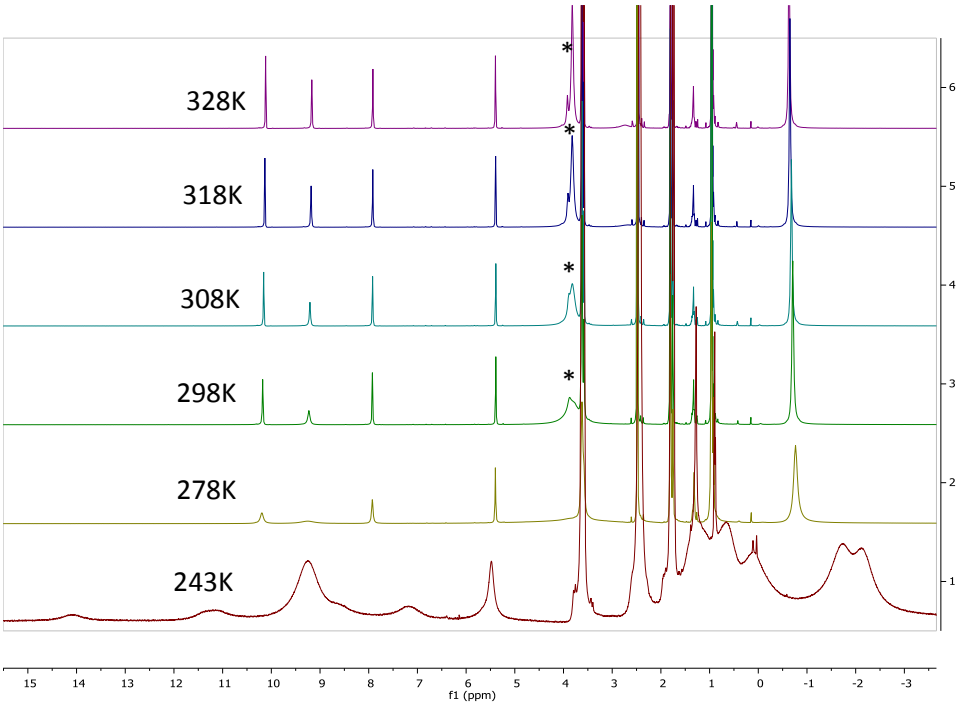

Figure 2-3. Variable-temperature ^{1}H NMR of complex **5-Ce^{PT}**.

The ^{1}H NMR spectrum of complex **5-Pr^{PT}** also displays paramagnetic shifts. Due to the two uncoupled electrons on the 4f sub-orbital, the phenyl protons on phenol rings are greatly shifted to δ = 34.58, 27.92 and -11.41 ppm. The tert-butyls are also greatly shifted from 1.32 ppm in **2^{PT}** to 26.72, 13.14, -2.59 and -17.64 ppm. The protons of the benzylic CH groups are also not observed in this spectrum.

Crystals of complexes **5-Ce^{P}**, **5-Ce^{PT}** and **5-Pr^{PT}**, which were suitable for single crystal X-ray analysis were grown from their concentrated THF solution at -30 °C. The solid-state structures are provided in **Figure 2-4** and **Figure 2-5**. Selected bond distances (Å) and angles (°) are listed in **Table 2-3**.

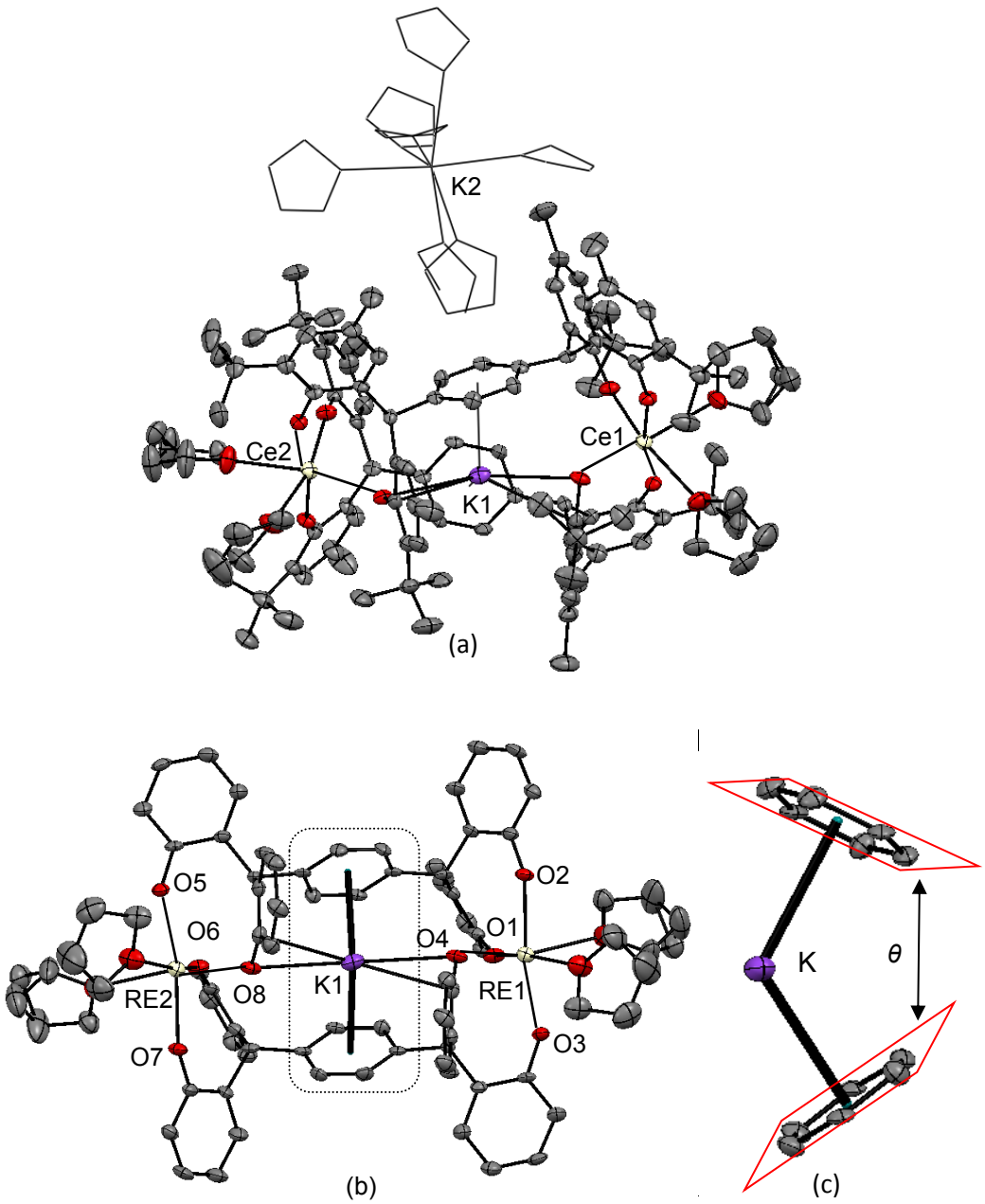

Figure 2-4. Representation of the molecular structure of complex **5-Ce^{P}** (a). Thermal ellipsoids of non-carbon atoms are shown at 30% probability. All hydrogen atoms and solvents are omitted for clarity. The skeleton structure (b) with highlighted internal K^{+} ion coordination (c) are provided.

In the solid structure of complex **5-Ce^{P}**, a free K^{+} counter ion is coordinated by seven THF molecules. Each Ce^{3+} ion is coordinated by four oxygen atoms from the phenol ligand and two THF molecules, displaying a distorted octahedral configuration. The bond length of the Ce-O_{Ph} range from 2.235(5) Å to 2.394(5) Å **(Table 2-3)**, which are comparable to previously reported cerium^{III} bis-aryloxy complexes such as $[Li(THF)_2Ce(MBP)_2(THF)_2]$ (BMP = 2,2'-methylenebis(6-*tert*-butyl-4-methylphenolate)) with an average Ce-O_{Ph} bond length of 2.3570 Å.[6]

The K^+ ion is bridged to the Ce^{3+} ion by one oxygen atom from each ligand at a distance of 3.021(6) Å and is encapsulated by two phenyl-linkers through η^6-coordination, forming a V-shape cage (c, **Figure 2-4**). The distance of the K^+ to the phenyl ring centroid is calculated at 2.969 Å while the dihedral angle between the two phenyl rings is calculated as $\theta = 62.94°$.

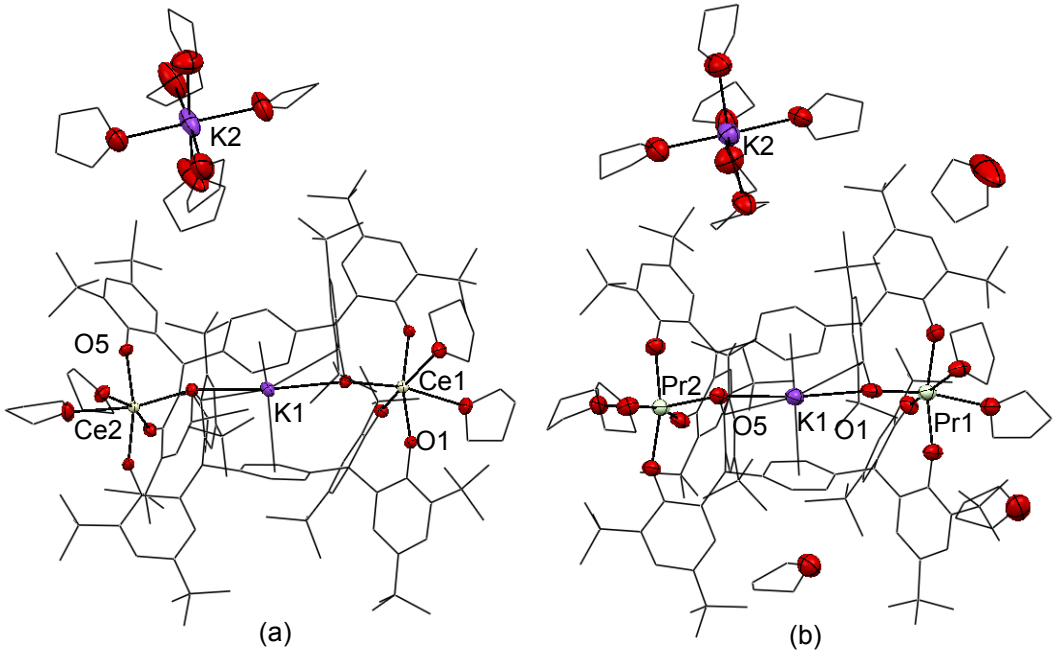

Figure 2-5. Representation of the molecular structure of complex **5-Ce^{PT}** (a) and **5-Pr^{PT}** (b). Thermal ellipsoids of non-carbon atoms are shown at 30% probability. All hydrogen atoms and solvents are omitted for clarity.

Table 2-3. Selected bonds lengths (Å) and angles (°) of complex **5**.

	5-Ce^{P}	**5-Ce^{PT}**	**5-Pr^{PT}**
RE1-O1	2.394(5)	2.382(3)	2.348(10)
RE2-O5		2.371(3)	2.396(7)
K1-O1	3.021(6)	2.872(3)	2.903(10)
K1-O5		2.845(3)	2.854(9)
RE1-O2	2.319(5)	2.313(3)	2.272(9)
RE2-O6		2.317(3)	2.291(9)
RE1-O3	2.235(5)	2.245(3)	2.267(7)
RE2-O7		2.302(3)	2.211(9)
RE1-O4	2.333(5)	2.305(3)	2.285(8)
RE2-O8		2.247(3)	2.303(8)
K- Ph ring	2.969	3.012	3.006
K- Ph ring		3.006	3.017
RE1-O1-K1	141.2(2)	146.57(13)	141.3(4)
RE2-O5-K1		143.10(13)	146.2(4)
O1-K1-O5	162.3(2)	161.96(10)	162.2(3)
dihedral angle (θ)	62.94	72.08	71.7

The complexes of **5-Ce^{PT}** and **5-Pr^{PT}** (**Figure 2-5**) display an isomorphism character where the unit cell parameters of these complexes are very similar (see Appendix). This is due to the similar ionic radii of Ce^{3+} and Pr^{3+} ions (**Table 1.1**, **Chapter 1**).

In the both of the crystal structures in **Figure 2-5**, the free K^+ counterion is coordinated by six THF molecules. The Ce-O_{Ph} bonds of **5-Ce^{PT}** are similar to that of **5-Ce^{P}** while the distance of K^+ ions to the bridging oxygen atoms is slightly shorter. The Pr-O_{Ph} bonds (2.348(10) Å and 2.396(7) Å) are longer than the reported values (average 2.16 Å) in complex Pr(O-2,6-$^{i}Pr_2C_6H_3)_3(THF)_2$[15] but shorter than those in the complexes of $(EtZn)_3(THF)_2(BINOLate)_3$-Pr(THF) at 2.412(32) Å.[16] The dihedral angles between the two phenyl rings are calculated as $\theta = 72.08°$ (**5-Ce^{PT}**) and 71.7° (**5-Pr^{PT}**), which is 10° greater than the **5-Ce^{P}** counterpart. This is probably due to the steric difference between the bulkier *tert*-butyl groups of the ligand (**Table 2-3**).

2.3.2. **Attempted Synthesis of Other Complexes**

Schelter and co-workers have reported that the choice of the alkali metal attached to the rare earth/1,1′−BINOLate (REMB) heterobimetallic framework greatly affects the oxidation reactivity of those cerium complexes (**Scheme 1-6**, **Chapter 1**).[2, 17]

As discussed in **Chapter 2.3.1**, the tetraphenol ligand can also be deprotonated by alkali metal amide (LiN" or NaN") as well as alkaline earth metal bis-amide ($CaN"_2$, $MgN"_2$ or $SrN"_2$), forming alkali (or alkaline earth) metal complexes.

An NMR scale study of the reaction of $[Li_4L]_2$ or $[Na_4L]_2$ with four equivalents of $RECl_3$ shows a similar pattern compared to complex **5**, indicating the formation of similar products. However, the reaction with the alkaline earth metal complexes generates insoluble white precipitate after stirring in THF at room temperature, which shows multiple paramagnetic peaks when dissolved in pyridine (**Scheme 2-9**).

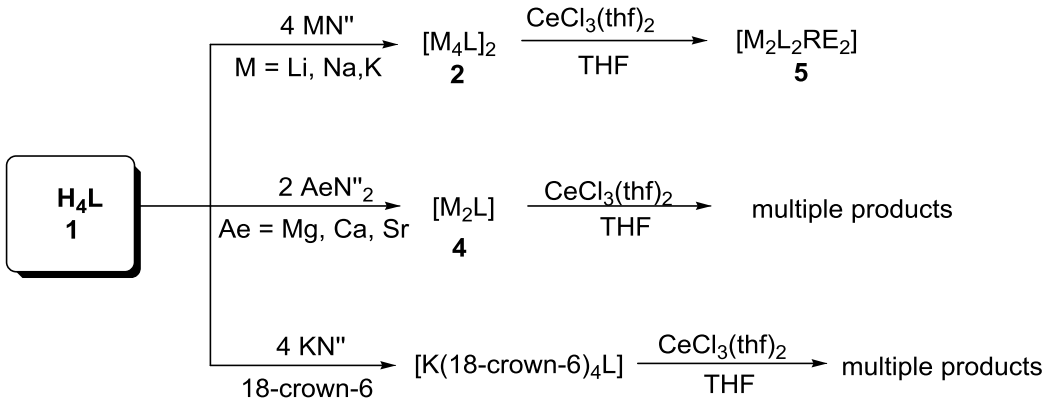

Scheme 2-9. Reactions of group 1 and 2 metal salts with $RECl_3(thf)_2$.

In order to test how the K^+ ion is encapsulated in the complex, a THF solution of $\mathbf{2^P}$ is treated with 18-crown-6 and then transferred to the THF suspension of $CeCl_3$. After being stirred for 8 hours, a white precipitate is formed which displays multiple paramagnetic resonances in pyridine whilst no signal of $\mathbf{5\text{-}RE^P}$ is observed in the THF solution by ^1H NMR spectroscopy. This shows that with the strong coordination of 18-crown-6 to K^+ ion, the *p*-π interactions between alkali metal ions and phenyl rings are disfavoured. As a consequence, the dinuclear complex similar to complex **5** could not be obtained.

2.3.3. **Comparison of complex 5 to U and Ce complexes**

Research carried out by Jordann Wells in the Arnold group have shown different chemistry when the salt metathesis strategy is applied to uranium counterpart. In the reaction of **4^{P}-Ca** with one equivalent of UI_3 in 1,4-dioxane, no sign of the expected [$CaLU_2$] is observed. Instead, bimetallic U^{IV} complex **FA** and uranium metal is obtained, which suggests a disproportionation reaction of the U^{III} complex (**Scheme 2-10**).

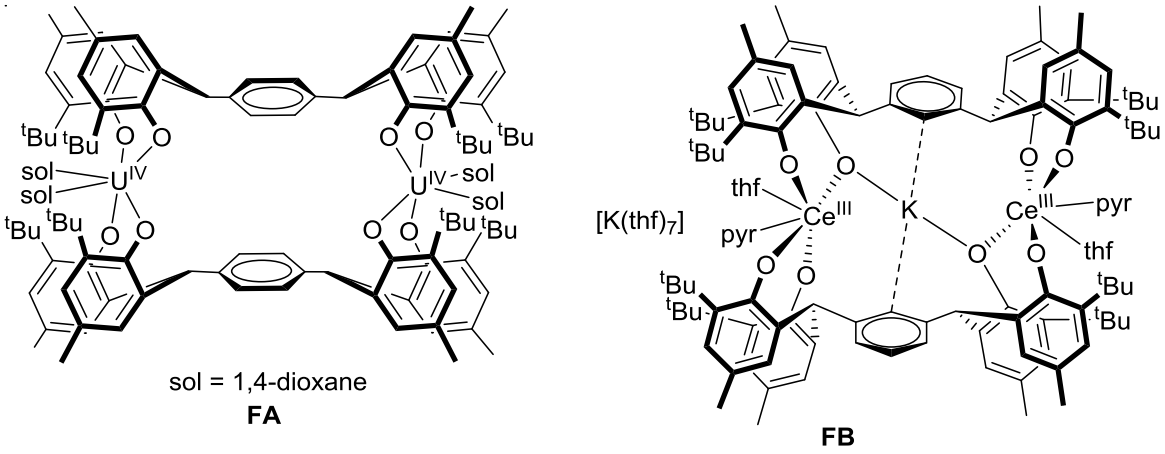

Scheme 2-10. Examples of tetraaryloxide complexes within the Arnold group.

The reaction of *meta*-substituted precursor **2^{M}-K** with one equivalent of $CeCl_3$ has been carried out by Megan Seymour from the Arnold group. In the structure of the complex **FB**, $K(thf)_7KCe_2(L^{M'})_2(thf)_2(py)_2$ (**Scheme 2-10**), the cerium atom and the free K^+ ion shows similar coordination mode to complex **5^{P}**. The Ce-O_{Ph} bonds are similar to those in complex **5**, however, due to the *meta*-substitution of the ligands, the K^+ ion in the middle of the molecule displays a different configuration. The K^+ ion shows weak η^1-phenyl interactions to the nearest carbon atom on the phenyl rings at a distance of 3.103(6) Å. The bridging K-O_{Ph} bond (2.747(3) Å) is 0.1 Å shorter than those observed in complex **5**. Unlike the two phenyl rings in complex **5**, these two phenyl rings in complex **FB** are parallel to each other at a distance of 6.206(7) Å.

2.4. EPR study on complex 5-Ce^{PT}

A primary EPR study on the magnetism properties of complex **5-Ce^{PT}** was carried out. The data are collected at 298K, 97K and 9K at solid state. (**Figure 2-6**)

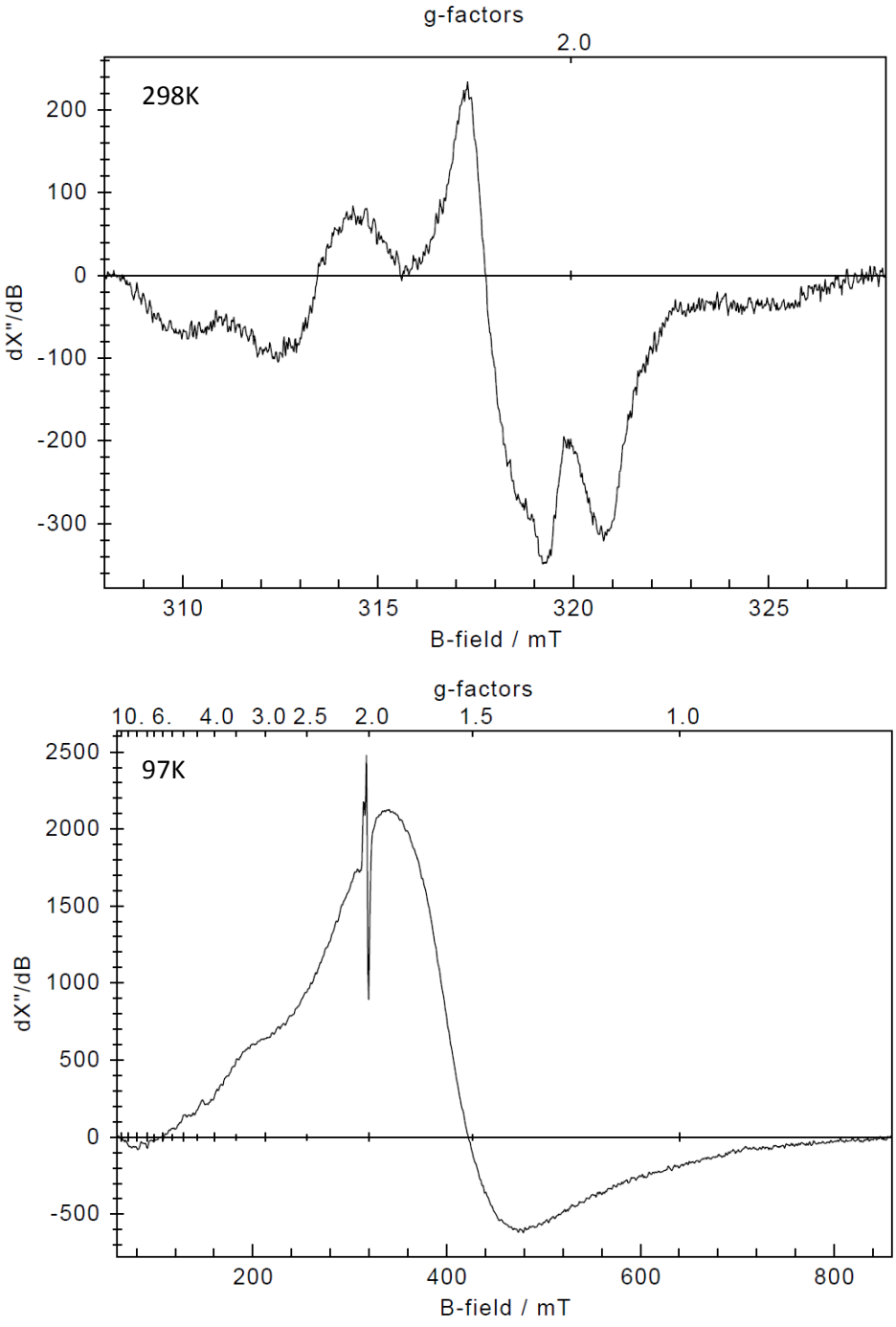

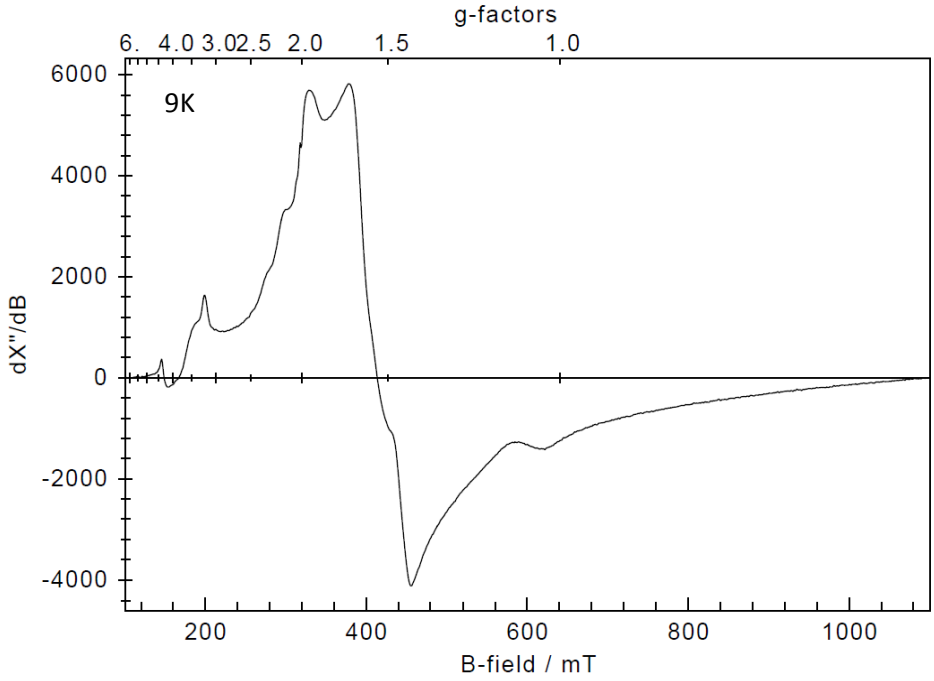

Figure 2-6. EPR measurement of complex **5-Ce^{PT}**.

The EPR data recorded at a lower temperature (97K and 9K) shows different patterns compared to the one obtained at 298 K. This suggests a possible configuration change of the complex which is observed in the low temperature (243K) ^{1}H NMR spectrum in **Figure 2-3**. Although the influence of the caged K^{+} ion to the magnetic properties of Ce^{III} ions is not clear based on these data, the changes of the g values observed under different temperature suggest possible electron interactions in the complex **5-Ce^{PT}** and further studies on their magnetism properties are ongoing.

2.5. Reactivity of complex $K_2L_2RE_2$ (5)

2.5.1. **Complex 5 towards coordinating molecules**

Given the interesting structure of complex **5**, we intend to replace the encapsulated K^+ cation with other metal ions to make different complexes. Thus a study on the solvent dependence of the complex was carried out.

When complex **5-Ce^P** was treated with pyridine, the clean ^{1}H NMR spectrum shows a shift to a lower frequency of the protons on the phenol groups which are observed at δ = 10.27, 10.20, 9.74 and 5.51ppm. The signals of phenyl-linker remain at δ = 5.44 ppm while the two methyl groups also shift to 4.17 and 2.33 ppm, respectively. The *tert*-butyl groups show different trend while one set is shifted from 3.45 to 2.91 ppm and the other changed from -0.35 to -0.48 ppm.

The addition of excess amount of 18-crown-6 to **5-Ce^P** affords complex **7-Ce^P** (**Scheme 2-11**). The ^{1}H NMR data of the product remain identical to the starting material and no change of the ^{1}H NMR data is observed even when the solution is heated to reflux at 80 °C for 24 hours. This suggests the strong coordination to the K^+ ion which prevents the extraction of the ion from the core skeleton.

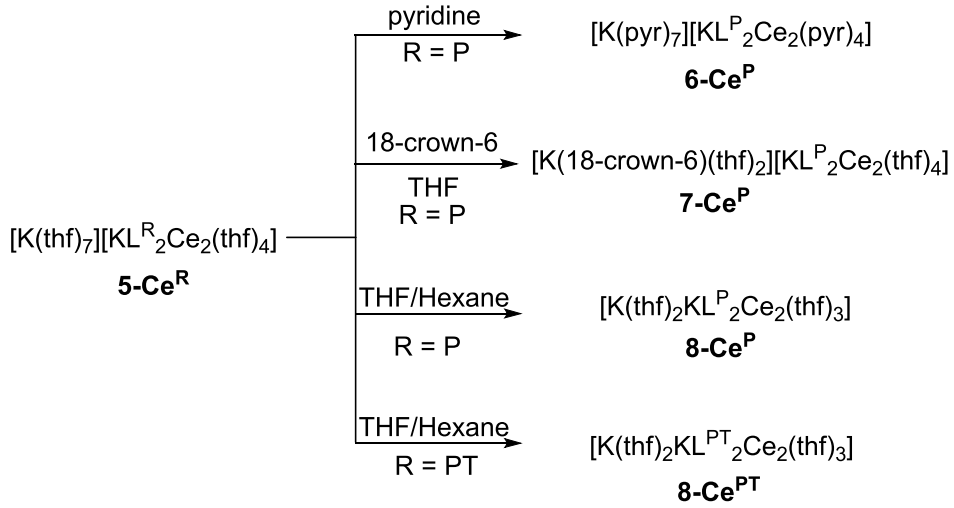

Scheme 2-11. Solvation studies on complex **5**.

Crystals of complexes **6-Ce^P**, **7-Ce^P** were grown by slow evaporation of hexane into the concentrated THF solutions at room temperature. The solid-state structure of compound **6-Ce^P** and **7-Ce^P** are shown in **Figure 2-7** and Selected bond distances (Å) and angles (°) are provided in **Table 2-4**.

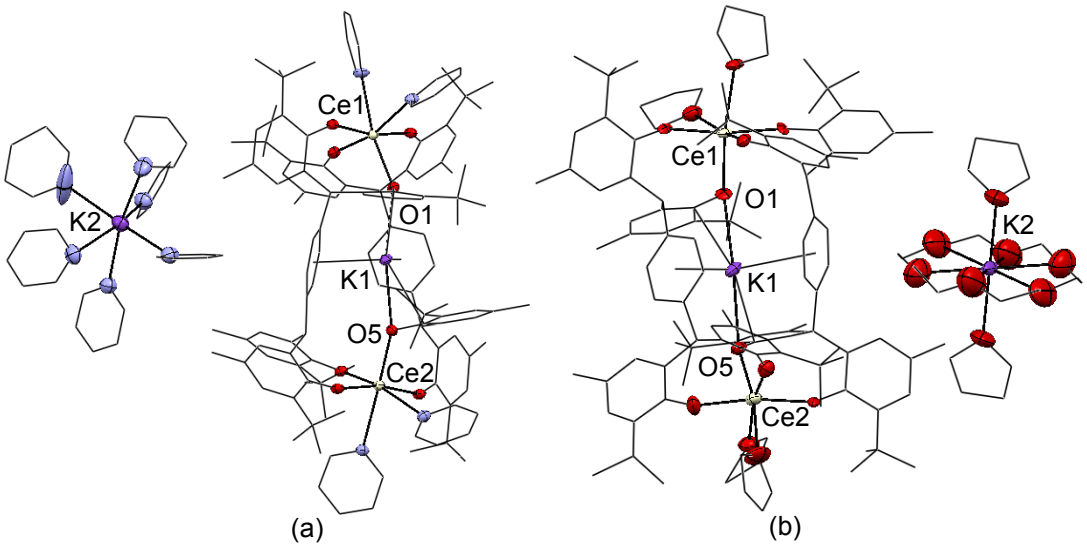

Figure 2-7. Solid state structure of complex **6-Ce^{P}** (a) and **7-Ce^{P}** (b). Thermal ellipsoids of non-carbon atoms are shown at 30% probability. All hydrogen atoms and solvents are omitted for clarity.

In the solid-state structure of complex **6-Ce^{P}**, all the THF molecules from complex **5-Ce^{P}** are replaced by pyridine molecules. The cerium centre in **6-Ce^{P}** is six-coordinate and adopts distorted octahedral geometry. The bond length of the Ce-O_{Ph} bond or the distance of the K^{+} ion to the phenyl ring centroid is similar to that of **5-Ce^{P}**. The dihedral angle between the two phenyl rings is recorded at θ = 71.87°, which is 9 degrees greater than that of **5-Ce^{P}**. The complexes of **7-Ce^{P}** display a similar trend where the dihedral angle between the two phenyl rings are calculated at θ = 72.27° (**Table 2-4**).

Table 2-4. Selected bond distances (Å) and angles (°) of complex **6-Ce^{P}** and **7-Ce^{P}**.

	6-Ce^{P}	**7-Ce^{P}**
Ce1-O1	2.380(4)	2.366(7)
Ce2-O5	2.384(4)	2.357(6)
K1-O1	2.892(4)	2.946(7)
K1-O5	2.906(4)	2.956(7)
Ce1-O2	2.355(4)	2.305(6)
Ce2-O6	2.316(4)	2.315(7)
Ce1-O3	2.252(4)	2.319(8)
Ce2-O7	2.250(4)	2.227(7)
Ce1-O4	2.325(4)	2.246(9)
Ce2-O8	2.344(4)	2.301(6)
K-Ph ring	3.005	3.062
K-Ph ring	3.019	3.084
Ce1-O1-K1	148.32(18)	144.2(3)
Ce2-O5-K1	147.79(18)	148.1(3)
O1-K1-O5	165.16(13)	162.9(2)
dihedral angle (θ)	71.87	72.27

The recrystallisation of **5-Ce^{P}** by slow diffusion of hexane into a concentrated THF solution at room temperature afforded crystals of complex **8-Ce^{P}** (a, **Figure 2-8**). The Selected bond distances (Å) and angles (°) are provided in **Table 2-5**.

In the crystal structure, the coordination environments of the cerium centres and the caged K^+ ion is similar to complex **5-Ce$^{P/PT}$**. The free K^+ ion is now coordinated by two phenyl rings of the ligand and three THF molecules.

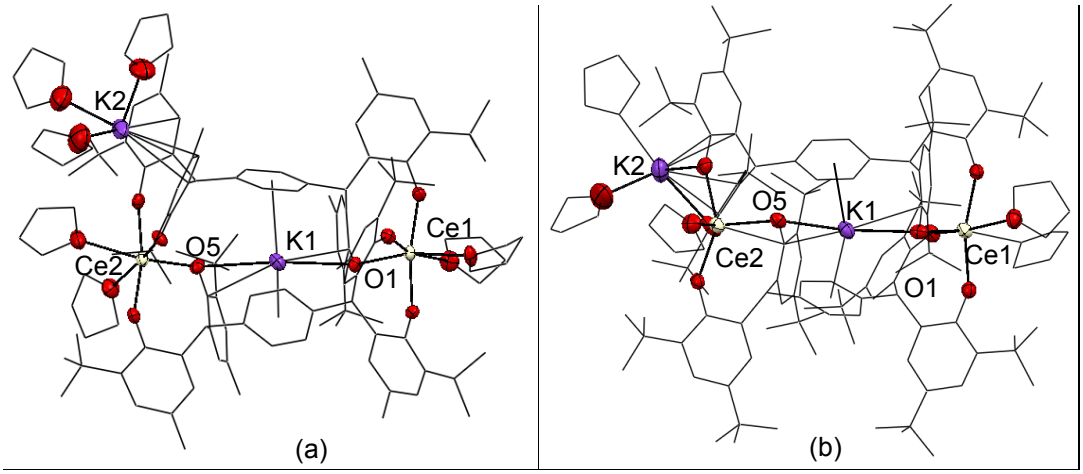

Figure 2-8. Solid state structure of complex **8-Ce^{P}**(a) and **8-Ce^{PT}**(b). Thermal ellipsoids of non-carbon atoms are shown at 30% probability. All hydrogen atoms and solvents are omitted for clarity.

Table 2-5. Selected bonds lengths (Å) and angles (°) of **8-Ce^{P}** and **8-Ce^{PT}**.

	8-Ce^{P}	**8-Ce^{PT}**
Ce1-O1	2.369(6)	2.353(5)
Ce1-O2	2.329(7)	2.304(5)
Ce1-O3	2.294(7)	2.231(5)
Ce1-O4	2.235(7)	2.274(5)
Ce2-O5	2.342(7)	2.316(5)
Ce2-O6	2.292(7)	2.267(5)
Ce2-O7	2.259(7)	2.313(5)
Ce2-O8	2.322(7)	2.258(5)
K1-O1	2.925(7)	2.771(6)
K1-O5	3.052(7)	2.807(5)
K2-O7		2.889(6)
K2-O8		2.898(7)
O1-K1-O5	162.7(2)	162.99(16)
Ce1-O1-K1	143.9(3)	143.0(2)
Ce2-O5-K1	143.9(3)	152.0(2)
dihedral angle (θ)	68.17	67.92

When complex **5-Ce^{PT}** is recrystallised by slow diffusion of hexane into its THF solution at room temperature, crystals of complex **8-Ce^{PT}** are obtained (b, **Figure 2-8**). In the solid-state

structure of **8-Ce^{PT}**, the K1 binds the bridging-O_{Ph} atom at a slightly shorter distance while the dihedral angle (θ) of phenyl linker decreases to 67.92° (**Table 2-5**). The K2 ion not only coordinates the phenyl rings of the ligand but also binds two phenol oxygen atoms at a distance of 2.889(6) Å and 2.898(7) Å, respectively. The Ce2 centre is now surrounded by five oxygen atoms, displaying a distorted a square pyramid coordination. This result shows the versatile coordination ability of the ligand and the K^+ ion.

2.5.2. **Oxidation of cerium complexes 5-Ce$^{P/PT}$**

2.5.2.1. Oxidation with I_2, CuX_2 and HgI_2

The treatment of complex **5-Ce** with oxidants, such as I_2 or CuX_2 (X = Cl or OTf), leads to the formation of a blue solution of Ce^{IV} products at room temperature. The blue colour observed in these complexes can be explained by the ligand-to-metal-charge-transfer (LMCT), which has been observed in many Ce^{IV} complexes.[18] The reaction with I_2 yields KI as a by-product while the reaction with CuX_2(X = Cl or OTf) affords Cu^0 metal. This reaction can be monitored by ^{1}H NMR spectroscopy as the paramagnetic shifts of starting material disappear immediately, and are replaced by diamagnetic spectrum for Ce^{IV} complexes.

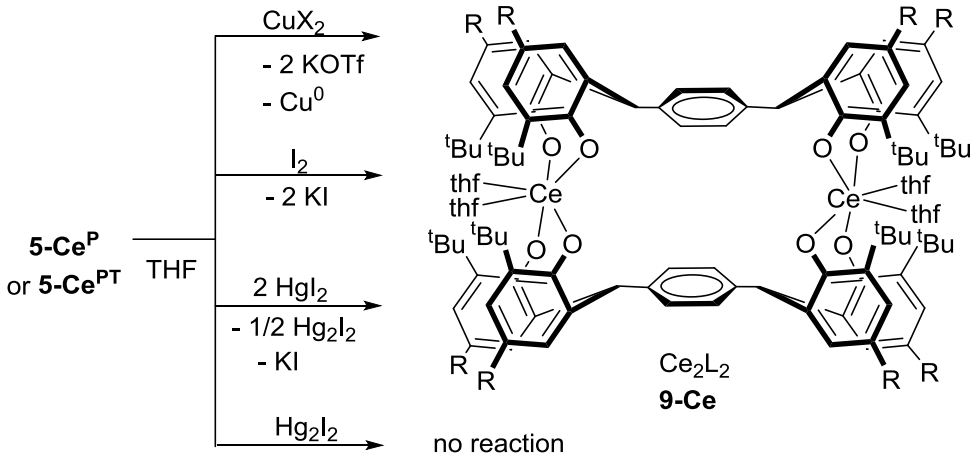

Scheme 2-12. Oxidation of **5-Ce** towards I_2/$Cu(OTf)_2$/2 HgI_2.

In complex **9-Ce^P**, the protons of the phenyl groups resonate at δ = 7.31, 6.91, 6.79, 6.75 and 6.72 ppm while the benzylic protons are seen at δ = 6.49 ppm. Two sets of methyl groups are recorded at 2.27 and 2.11 ppm while the tert-butyls are observed at 1.38 and 0.92 ppm (a, **Figure 2-11**). The oxidation of **5-Ce^{PT}** with HgI_2 occurred immediately at -30 °C. ^{199}Hg NMR spectrum shows a resonance at -3132 ppm which is different from that of HgI_2 at -3400 ppm and could be ascribed to the by-product Hg_2I_2. The reaction of **5-Ce** towards Hg_2I_2 showed no reactivity which confirmed the 2-electron oxidation. The ^{1}H NMR spectrum of **9-Ce^P** also shows diamagnetic patterns for phenyl protons at δ = 7.67, 7.36, 7.09 and 6.96 ppm which is similar to that of complex **9-Ce^{PT}**. The benzylic protons are shown at 6.84 ppm. The tert-butyls are split into 4 singlets at δ = 1.52, 1.28, 1.15 and 0.99 ppm, which suggests a decrease of molecule symmetry in solution when compared to **2^{PT}**.

A single crystal of **9-Ce^{PT}** was grown by slow evaporation of hexane into a concentrated THF solution. The crystal turned out to be heavily disordered and thus only connectivity can be deduced from the crystallographic data. The solid-state structure is shown in **Figure 2-9**. Selected bond distances (Å) and angles (°) are provided in **Table 2-6**.

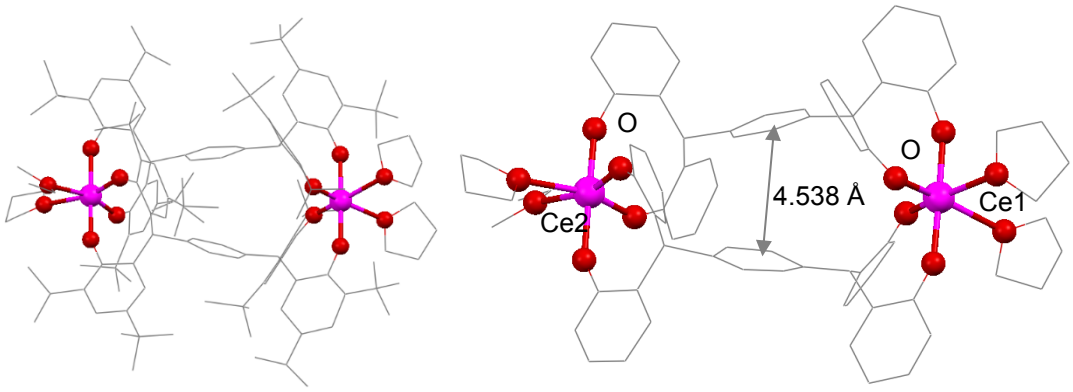

Figure 2-9. Representation of the crystal structure of complex **9-Ce^{PT}** (left). All hydrogen atoms and solvents are omitted for clarity. The skeleton structure (right) is provided.

Table 2-6. Selected bond length (Å) and angles (°)of complex **9-Ce^{PT}**.

Bond	Length
Ce1-O1	2.148(15)
Ce1-O2	2.154(13)
Ce1-O3	2.126(11)
Ce1-O4	2.194(13)
Ce2-O5	2.128(16)
Ce2-O6	2.08(2)
Ce2-O7	2.140(17)
Ce2-O8	2.254(13)
Distance of two Ph rings	4.538
dihedral angle (θ)	25.18

In the crystal structure, each Ce atom is coordinated by four phenolate oxygen atom and two THF solvent molecules. These oxidation reactions show the examples of losing the K^+ ion in the middle V-shape cage. With the loss of K^+ ion in the middle, the dihedral angle between the two phenyl rings decreases to 25° while their distance increases to 4.538 Å. The average Ce-O_{Ph} bond length of 2.151 Å is shorter than that in Ce^{III} complexes (2.382 Å for **5-Ce^{P}**, 2.350 Å for **5-Ce^{PT}**), which is consistent with the reported values. This bond contraction is due to the change of the cerium atom oxidation state from f^1 to f^0 configuration which results in a decrease in ionic radius from 1.01 ˚A to 0.87 ˚A.[19]

The electronic absorption spectrum of a THF solution of **9-Ce^{PT}** (blue line, **Figure 2-10**) reveals several broad features in the UV/visible region centred at 283, 326, and 576 nm. The broad band at 576 nm corresponds to a ligand-π to vacant Ce-4f charge-transfer (LMCT),[5, 6] which is the electronic transition underlying the compound's dark blue colour and has been regarded as a characteristic indicator for Ce^{IV} complexes.[6, 20] Regardless of this, the absorption band at 576 nm shows a longer wavelength compared to that of 487 nm in complex

$[Li_3(thf)_3(BINOLate)Ce^{IV}Cl]$, which is due to the difference of the coordination environment.[2] This is supported by the addition of diluted aqueous HNO_3 into the THF solution of **9-Ce^{PT}** where the broad peak and purple colour disappears immediately due to the protolysis of the ligand (red line, **Figure 2-10**).

The spectrum of the complex **5-Ce^{PT}** is shown for comparison and displays only transitions in the UV/vis region associated with ligand-centred transitions at 297 nm.[21]

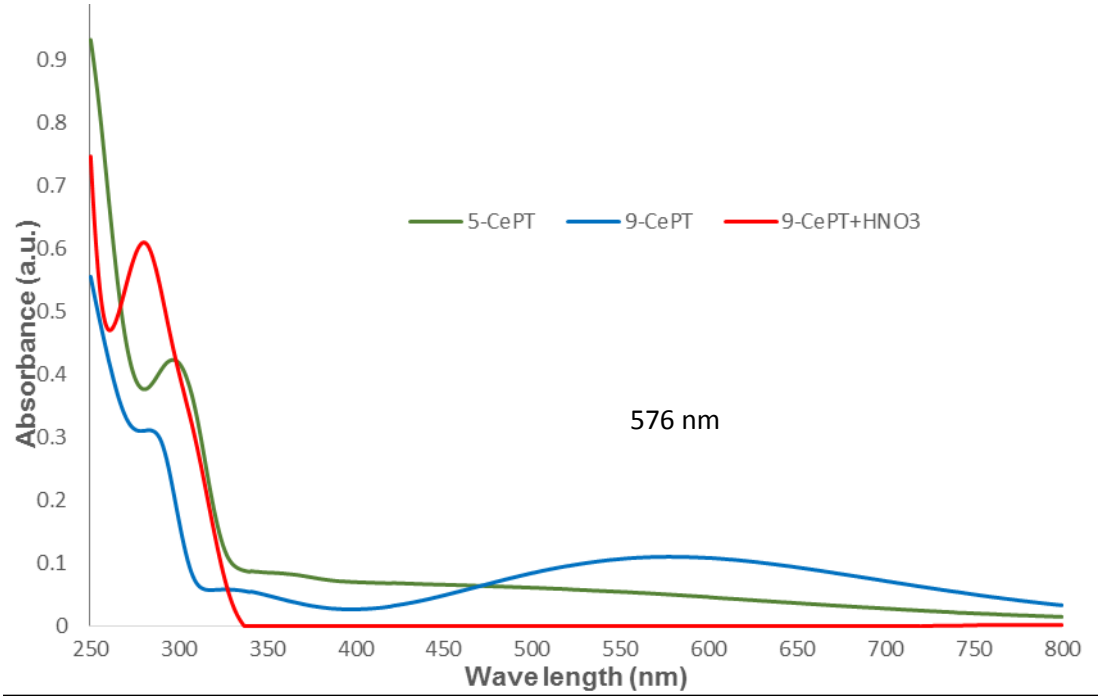

Figure 2-10. Electron absorption spectra showing a ligand to Ce charge transfer absorption for the Ce^{IV} complex **9-Ce^{PT}** (blue line) in the visible range (λ_{max} = 576 nm) in comparison with Ce^{III} complex **5-Ce^{PT}** (green line) and the solution of **9-Ce^{PT}** with HNO_3 (red line).

2.5.2.2. Oxidation with other Hg^{II} oxidants

In the reaction with two equivalents of $HgCl_2$ at -30 °C, paramagnetic shifts at 13.04, 10.86 9.8 and -1.93 ppm *etc.* are observed which suggest the possible formation of new products (a, **Figure 2-11**). Given the paramagnetic ^{1}H NMR spectrum, an intermediate which consists Ce^{III} ions and Hg ions can be induced. However, no signal for Hg could be found in the range from +3300 to -3300 ppm in the ^{199}Hg NMR spectroscopy. These paramagnetically shifted products transformed to diamagnetic species when warmed up to room temperature. As shown in **Figure 2-11**, two species can be identified upon warming. One set of the peaks (asterisk) are identical to those of **9-Ce^{PT}** (d) whilst the other species could not be determined (b, **Figure 2-11**). The diamagnetic ^{1}H NMR spectrum of the unidentified species suggests the formation

of the new Ce^{IV} complex **10-Ce**. Reaction with one equivalent of $HgCl_2$ at room temperature afforded the same product, leaving half equivalent of $K_2L_2Ce_2$ unreacted.

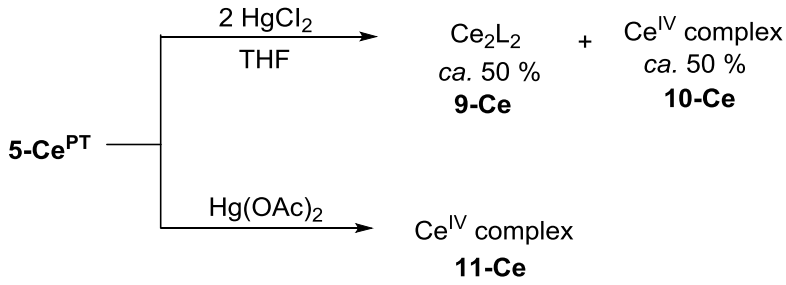

Scheme 2-13. Reaction of **5-Ce^{PT}** towards $HgCl_2$ and $Hg(OAc)_2$.

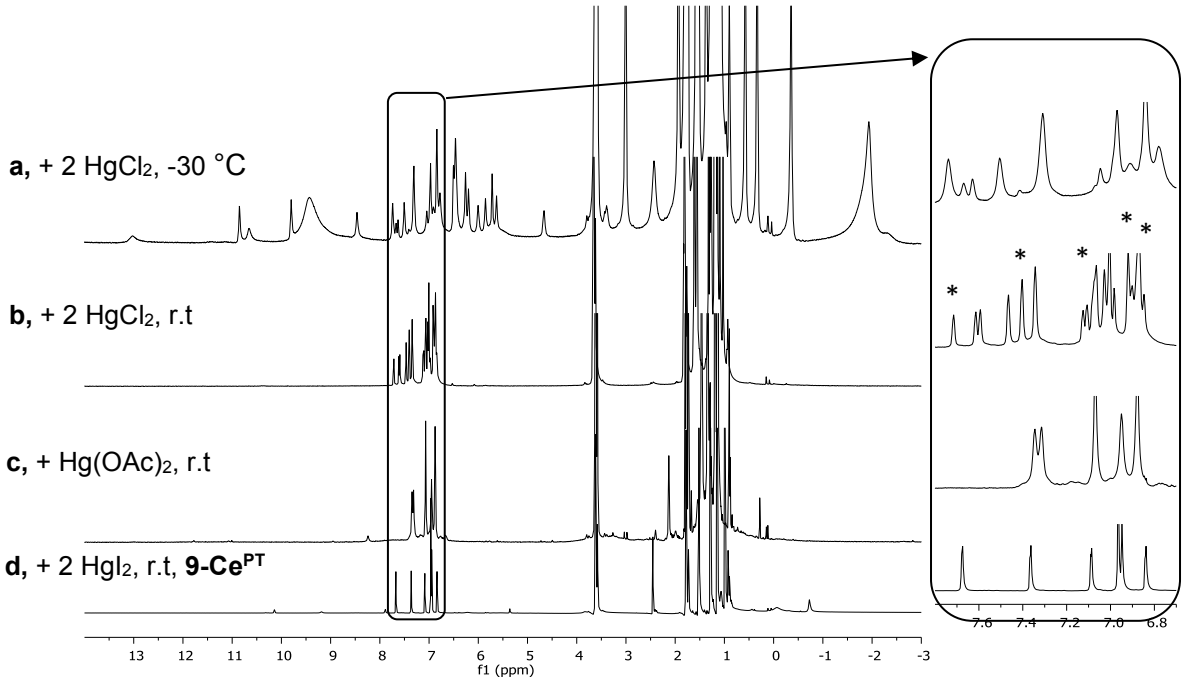

Figure 2-11. Reaction of **5-Ce^{PT}** toward HgX_2 (X = OAc, Cl, I).

The reaction of **5-Ce^{PT}** with one equivalent of $Hg(OAc)_2$ at -30 °C takes 8 hours to reach completion. The ^{1}H NMR spectrum of the product (c, **Figure 2-11**) shows different resonances to any of those species discussed above. After compared with the NMR spectrum of **9-Ce^{PT}** and the starting material **5-Ce^{PT}**, the diamagnetic resonances suggest the formation of a new Ce^{IV} complex **11-Ce^{PT}** (**Scheme 2-13**).

2.5.2.3. Oxidation with other oxidants

After investigating the reactions with mercury oxidants described above, a range of other potential oxidants was introduced to react with the Ce^{III} complexes (**Scheme 2-14**).

Upon the addition of two equivalents of Ph_3CCl into the solution of **5-Ce^{PT}**, an instant colour change from colourless to purple was observed. The ^{1}H NMR spectrum shows the formation

of Gomberg's dimer $\{Ph_3CCH(C_6H_4)CPh_2\}$ and complex **12** which displays different resonances compared to aforementioned complexes. The reaction of **5-Ce^{PT}** with one equivalent of 1,4-benzoquinone afforded precipitate immediately upon addition. The ^{1}H NMR spectrum of this reaction also shows new peaks for unidentified new products.

The electronic absorption spectrum of the products of reactions of **5-Ce^{PT}** with Ph_3CCl (blue line, **Figure 2-12**), 1, 4-benzoquinone (red line) and O_2 (purple line) are recorded in THF. The spectrum of the complex **9-Ce^{PT}** (orange line) is shown for comparison. All these spectra display broad bands within the range from 400 nm to 700 nm. The products from the reaction with Ph_3CCl and 1,4-benzoquinone show similar patterns with absorption maxima at λ = 512 and 513 nm, respectively. Due to the change in the coordination environment, these complexes display different absorption bands compared to the reported value of 480 nm in $[Li_3(Et_2O)_{3.5}\{(BINOLate)_6Ce\}_2(\mu\text{-}O_2C_6H_4))]\cdot Et_2O$.[22, 23] Although the solid state structure of these complexes are not obtained, the possible formula of the products are deduced based on the observations and literature comparisons (**Scheme 2-14)**.

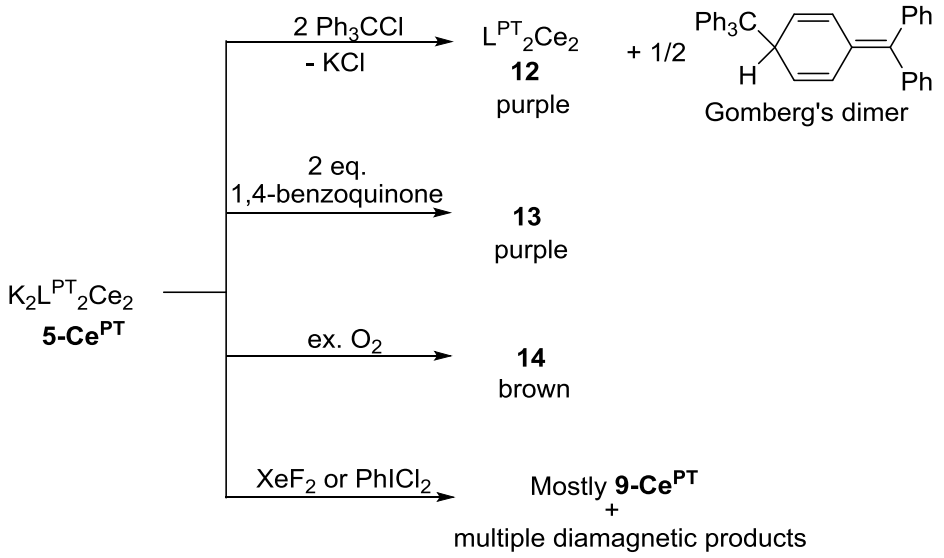

Scheme 2-14. Oxidation reactions of **5-Ce^{PT}**.

The reaction of complex **5-Ce^{PT}** with column-dried air in THF shows an instant colour change from pale yellow to red-brown. This reaction affords complex **14** as brown solid after work-up. The ^{1}H NMR spectrum of the product shows diamagnetic resonances which are different from those complex mentioned. The THF solution of complex **14** shows a broad peak at λ = 472 nm in the UV-vis spectrum (**Figure 2-12**), which is different from that of complex **9-Ce^{PT}** (576 nm), suggesting a different structure of the Ce^{IV} complex. Other reactions carried out with XeF_2 and $PhICl_2$ did not result in clean oxidation and gave a mixture of **9-Ce** and other multiple unidentified diamagnetic Ce^{IV} products which were observed by ^{1}H NMR spectroscopy.

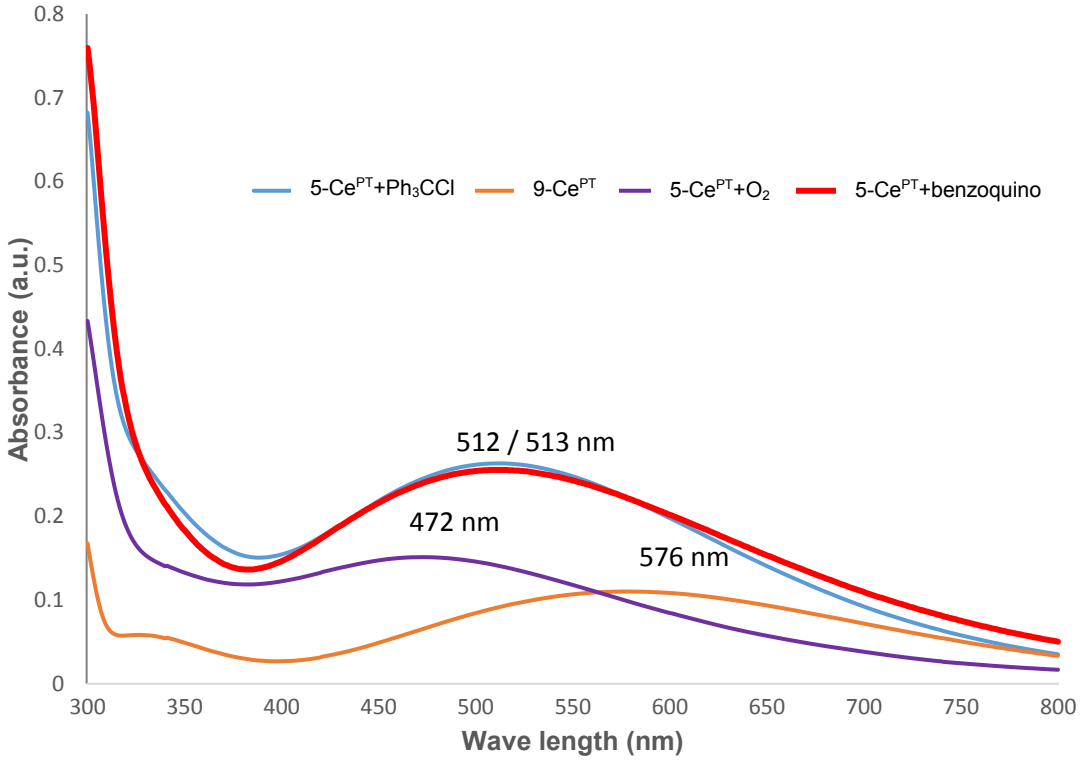

Figure 2-12. Electron absorption spectra for the Ce^{IV} complex **9-Ce^{PT}** (orange line) in the visible range in comparison with reactions of Ce^{III} complex **5-Ce^{PT}** with Ph_3Cl (blue line), 1, 4-benzoquinone (red line) and O_2 (purple line).

In order to test another path to oxidise the Ce^{III} complex to Ce^{IV} complexes, a solution of complex **2^{PT}** was treated with one equivalent of $CuCl_2$, making $[K_2CuL]$ *in situ* (**Scheme 2-15**). This solution is then added to a THF suspension of $CeCl_3(thf)_2$. However, after allowing the mixture to stir for 12 hours, no sign for the product **9-Ce^{PT}** is observed in the NMR spectrum. This can be explained by the fact that the redox chemistry of cerium complexes are highly influenced by the ligand coordination environment. The redox potential of $CeCl_3$ is reported at +1.22 V vs SCE (saturated calomel electrode) under the condition of 1 M HCl, which is much higher than the standard potential of Cu^{2+}/Cu couple of +0.34 V.[3]

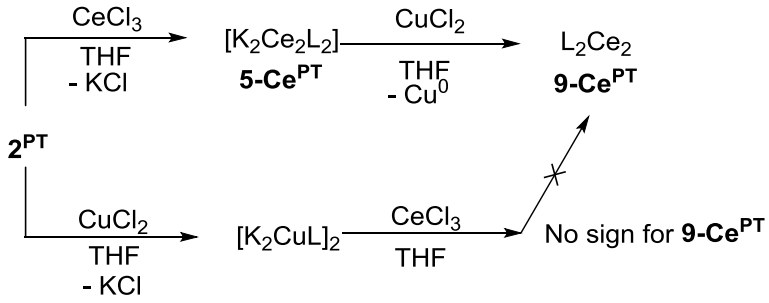

Scheme 2-15. Attempted reaction with Cu^{2+} complexes.

2.5.3. **Reaction of $[K_2L_2Ce_2]$ towards other substrates**

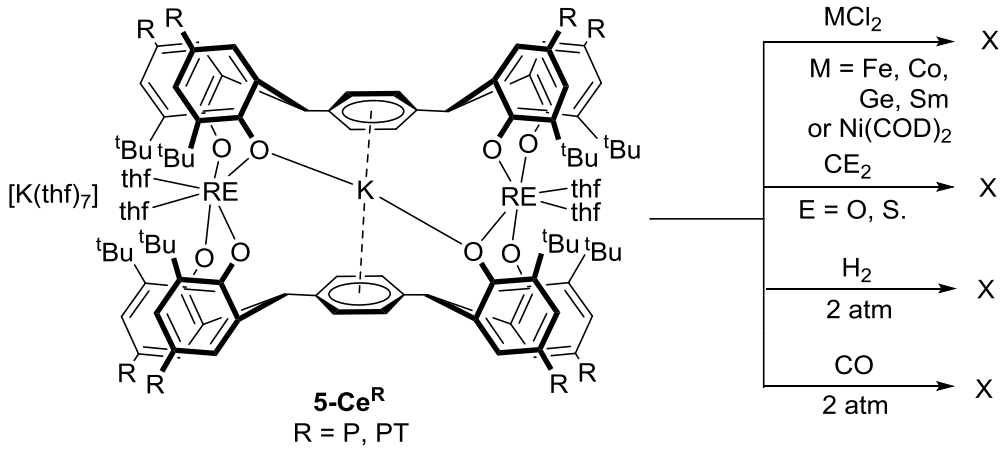

Scheme 2-16. The reaction of complex **5-Ce** towards small molecules.

Treatment of complex **5-Ce** with one or two equivalents of transition metal chloride $MCl_2(thf)_n$ (M = Fe, Co, Ge, Sm) or $Ni(COD)_2$ in THF showed no change in the ^1H NMR spectroscopy. Complex **5-Ce** also did not show any reactivity towards small molecules such as CO_2, CS_2, H_2 or CO under room temperature (**Scheme 2-16**).

In order to fully understand the redox chemistry of complex **5-Ce**, several attempts to measure its electrochemical properties were carried out. However, the resulting cyclic voltammetry data showed no oxidation/reduction couple in different solvents (THF, CH_2Cl_2) and electrolytes($[^nBu_4N][PF_6]$ or $[^iPr_4N][BPh_4]$).

Based on the oxidation chemistry of complex **5-Ce$^{P/PT}$** discussed in **Chapter 2.5.2**, and combined with the inertness of these complexes towards transition metal complexes, we can possibly draw a potential window for the redox couple for the complex. The data in **Chart 2-1** are reported in aqueous solution at 25°C but are calibrated versus SCE (saturated calomel electrode).[24-26] The possibly potential window for complex **5-Ce$^{P/PT}$** is between -0.25 to +0.27 V.

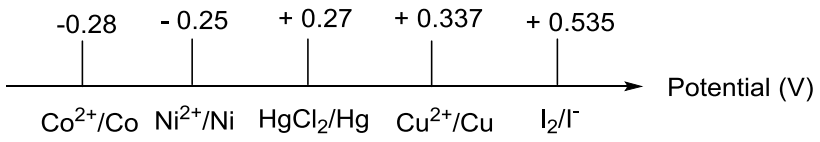

Chart 2-1. Redox potentials of reagents.

2.5.4. **Oxidation of praseodymium complexes 5-Pr^{PT}**

2.5.4.1. Oxidation with I_2

As discussed in **Chapter 1.2**, the complexes of Pr^{IV} and Pr^{V} are scarce. The direct synthesis and characterisation of these complexes have not been reported yet. Thus, investigations on the oxidation of the Pr^{III} complex are carried out.

Unlike its cerium counterpart, the praseodymium complex **5-Pr^{PT}** showed inertness to some of the oxidants under ambient conditions. The attempted reactions with oxidants such as O_2, CuX_2 (X = Cl, OTf), Ph_3CCl or benzoquinone showed no reactivity when monitored by ^{1}H NMR spectroscopy.

Addition of I_2 to complex **5-Pr^{PT}** showed no reaction at room temperature, however, this mixture showed a clear colour change from brown to green when heated at 60 °C for 8 hours. A monitored reaction showed the full transformation of starting material into several different products (

Figure 2-13). The ^{1}H NMR spectrum of the reaction mixture contains products display paramagnetically shifted resonances where two different sets of major products can be identified. In a scaled-up reaction (0.50 g of **5-Pr^{PT}**), after the removal of volatiles under reduced pressure, a green paste was obtained. After work-up, a white powder was isolated from the green paste. The ^{1}H NMR spectrum of the white solid shows singlets at δ = 13.67 (4H), 12.46 (4H) and 5.15 (4H) ppm for protons on phenyl rings while the benzylic-CH groups are observed at 4.48 ppm. Two singlets at δ = 10.33 (36H) and 1.17 ppm (36H) can be ascribed to the *tert*-butyls. These peaks observed are identical to one set of peaks observed in the mixture (asterisk peaks in **Figure 2-13**), which shows the successful separation of the product **16-Pr^{PT}** ($L^{PT}Pr_2I_2(thf)_6$) (**Scheme 2-17**). The total yield of this complex is *ca.* 30%.

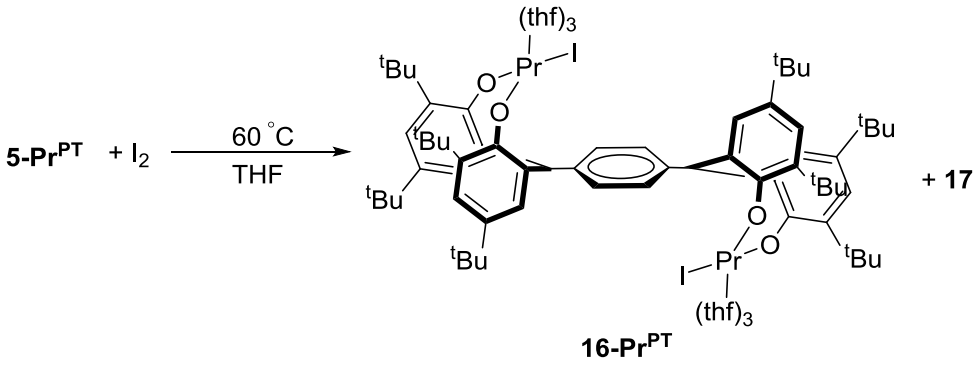

Scheme 2-17. The reaction of **5-Pr^{PT}** towards I_2.

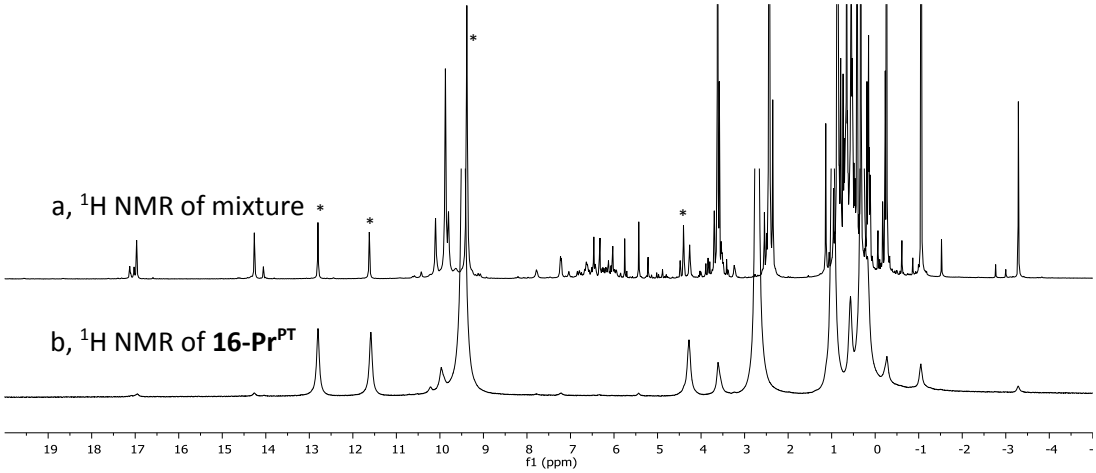

Figure 2-13. ^{1}H NMR spectrum of the reaction of **5-Pr^{PT}** with I_2 (60 °C).

Recrystallisation of the white solid from THF affords colourless crystals of **16-Pr^{PT}**. The crystal structure reveals the complex as a dinuclear Pr^{III} phenolate complex. In the structure, each Pr atom displays a *pseudo*-octahedral configuration through the coordinating of three THF molecules, two phenol oxygen atoms and one iodine atom. The two metal centres are bonded to the different side of the plane of the phenyl-linker, displaying a *trans*-configuration. The bond length of Pr-I bond is recorded as 3.1697(5) Å (**Table 2-7**). The two Pr-O bonds are shown at a distance of 2.176(4) Å and 2.202(4) Å. These Pr-O bonds are slightly longer than those observed in complex $Pr(O\text{-}2,6\text{-}^iPr_2C_6H_3)_3(THF)_2$[9, 15] but are ~0.1 Å shorter than the average length (2.30 Å) observed in complex **5-Pr^{PT}**(**Table 2-3**).

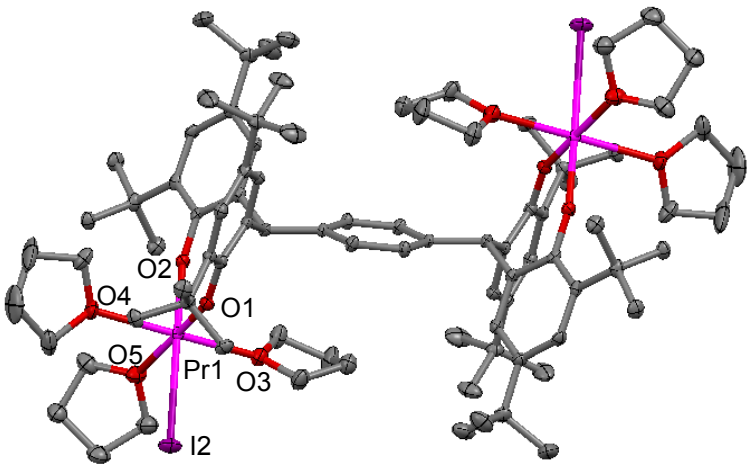

Figure 2-14. Solid state structure of complex **16-Pr^{PT}**. Thermal ellipsoids are shown at 30% probability. All hydrogen atoms and solvents are omitted for clarity.

Table 2-7. Selected bond distances (Å) of complex **16-Pr^{PT}**.

Bond	Å	Bond	Å
Pr1-I1	3.1697(5)	Pr1-O3	2.567(5)
Pr1-O1	2.176(4)	Pr1-O4	2.458(5)
Pr1-O2	2.202(4)	Pr1-O5	2.461(5)

The green hexane supernatant was collected and dried to afford a greenish solid of complex **17** at a 35% yield. The ^{1}H NMR spectrum is not as clean as expected, however, some paramagnetic resonances can be identified which suggest the possible valance state of Pr is either +III or +IV. The resonances at δ = 17.94, 15.23 and 11.07 ppm can be assigned to the phenyl protons. The *tert*-butyl groups are recorded at δ = 10.85 (18H), 0.71 (18H) and -0.09 ppm (18H). Attempts to purify and characterise the green complex were unsuccessful in this time frame.

2.5.4.2. Oxidation with XeF_2

Given the inertness of the Pr^{III} complex towards those oxidants that can oxidise Ce^{III} counterparts, a stronger oxidant, XeF_2, was used.

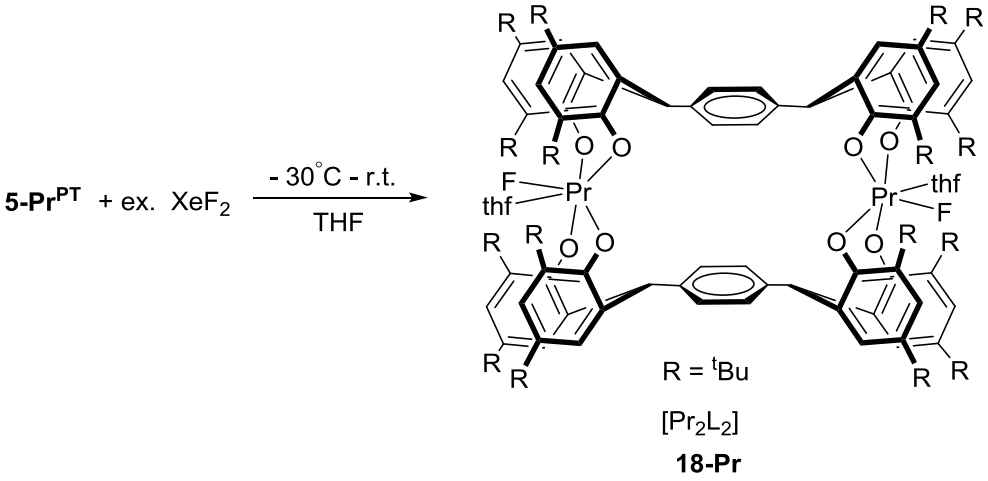

Scheme 2-18. The reaction of **5-Pr^{PT}** with XeF_2.

The reaction of **5-Pr^{PT}** with two equivalents of XeF_2 showed the peaks for the unreacted starting material and paramagnetic product. When an excess of XeF_2 is added to the THF solution of **5-Pr^{PT}** at -30 °C, the colourless solution changed to bright green gradually with the formation of an insoluble white solid. The ^{1}H NMR spectrum of this green solution shows the absence of paramagnetic starting material, and displays multiple diamagnetic species which suggests either the oxidation from Pr^{III} to Pr^{IV} or the decomposition of the complex itself. However, this green solution gradually decomposes to an orange-brown solution when stored in a freezer at -30 °C for overnight.

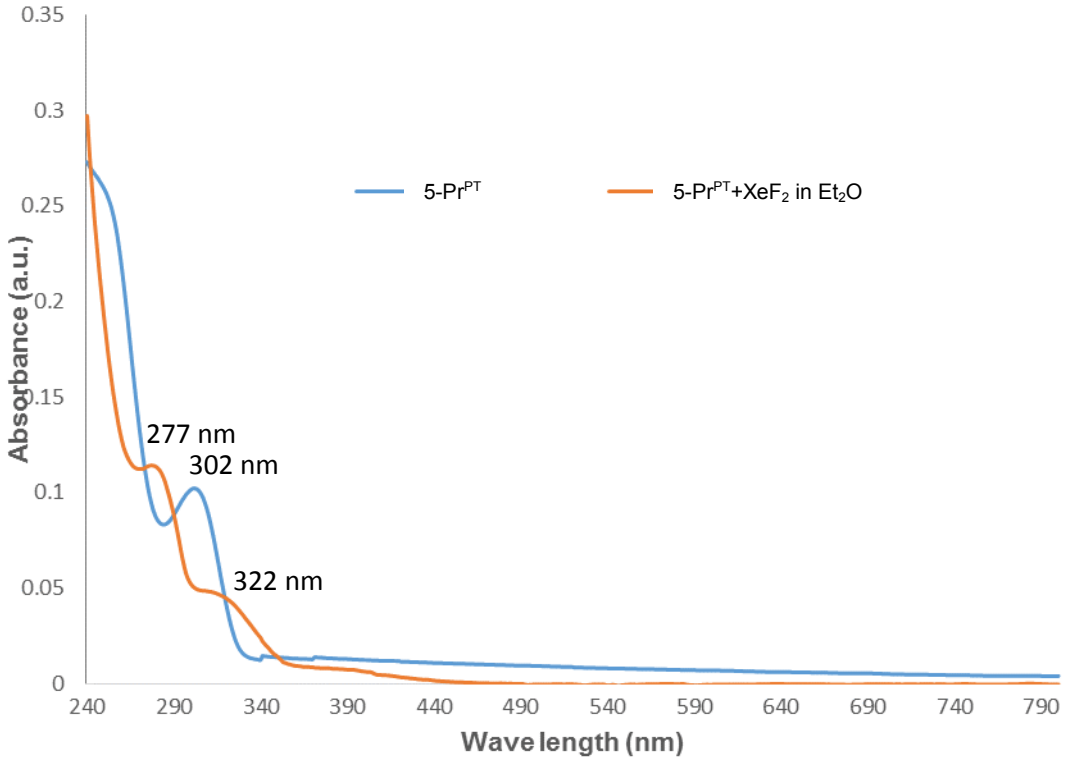

Figure 2-15. Electron absorption spectra for the Pr^{III} complex **5-Pr^{PT}** (blue line) and its reaction towards XeF_2 in Et_2O (orange line).

The electronic absorption spectrum of the Pr^{III} complex **5-Pr^{PT}**(blue line, **Figure 2-15**) shows a peak at λ = 302 nm which may due to the ligand-centred transitions which are similar to those in Ce^{III} complex of **5-Ce^{PT}** (**Figure 2-10**).[21]

The spectrum of the complex towards XeF_2 shows the disappearance of the peak observed in complex **5-Pr^{PT}** and the emergence of two new peaks at λ = 277 and 322 nm. However, due to the lack of reported spectroscopic data on Pr complexes, it is difficult to elucidate the possible assignments for these peaks.[27]

2.5.5. **Reactivity of $[K_2L_2Ce_2]$ with KC_8**

Evans and co-workers reported the reduction of $Ce(Cp')_3$ ($Cp' = C_5H_4SiMe_3$) complexes by potassium metal to make Ce^{II} complexes **AS**, [K(2.2.2-cryptand)][Cp'_3Ln] (**Scheme 1-16**).[28-30] This method has proven to be successful in isolating lanthanide complexes in the +II state. Thus, the attempted reduction of the Ce^{III} complexes to Ce^{II} was carried out.

Treatment of **5-Ce^{PT}** with two equivalents of KC_8 in THF resulted in the formation of a bright orange solution after allowing to stir for 8 hours. Work-up from this reaction afforded an orange solid which was collected and dried under reduced pressure. (**Scheme 2-19**)

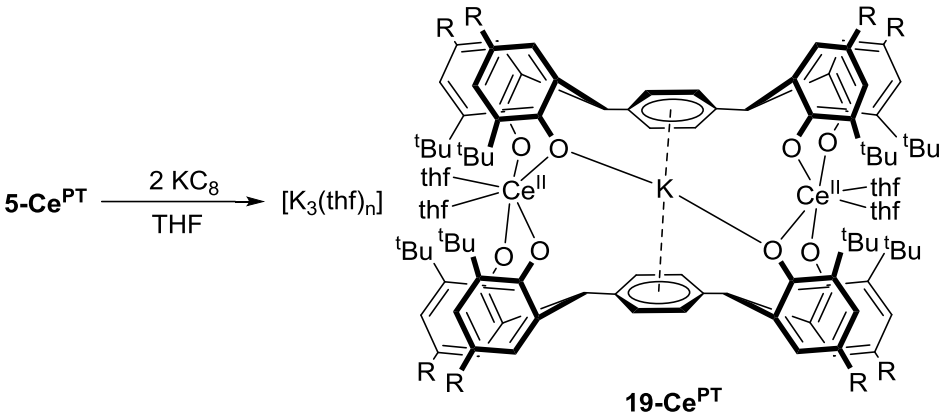

Scheme 2-19. The reaction of **5-Ce^{PT}** with KC_8.

The ^{1}H NMR spectrum of the isolated material shows a set of paramagnetic resonances that are widely shifted when compared to the **5-Ce^{PT}** starting material. The protons on the phenyl rings have greatly shifted to a higher frequency at δ = 21.52 (2H), 14.99 (2H), 11.51 (2H) and 6.28 ppm (4H) when compared to that of complex **5-Ce^{PT}** (9.74 to 5.48 ppm). The *tert*-butyls groups are recorded at a lower frequency at δ = -1.83, -2.92, -3.57 and -6.97 ppm, which suggest a stronger paramagnetic effects from the cerium ion. When this reaction is carried out in a sealed Young's tap NMR tube, no sign of H_2 is observed. This observation excludes the possible reaction on the benzylic-CH. The solid is sensitive to the trace amount of oxygen and decomposes gradually in the glove box. Due to the lack of crystal data and the difficulty in assigning paramagnetic ^{1}H NMR spectrum, it is hard to determine the valence state of the complex, yet it is suggested to have formed a Ce^{II} species **19-Ce^{PT}** as depicted in **Scheme 2-19**. Attempts to recrystallise this product from different solvents were not successful.

2.5.6. **Reactivity of $[K_2L_2Ce_2]$ towards MeLi**

Treatment of **5-Ce^{PT}** with four equivalents of MeLi in THF at -30 °C resulted in the formation of CH_4 which was observed as bubbles and confirmed by the appearance of a singlet at δ = 0.16 ppm in the ^{1}H NMR spectrum. The ^{1}H NMR spectrum of the product shows paramagnetic shifts which support the formation of Ce^{III} complexes. The characteristic phenyl protons are greatly shifted to a higher frequency to δ = 18.88, 13.66, 10.61 and 10.03 ppm when compared to that of complex **5-Ce^{PT}**. However, the opposite trend is seen for the *tert*-butyls which are recorded at δ = -3.77 and -5.32 ppm as two broad singlets. According to the character (shape and symmetry) deduced from the ^{1}H NMR data and combined with the emission of methane, the core structure of the molecule is proposed to be maintained while the benzylic-CH are deprotonated, forming complex **20**, where the lithium ions are bridged by the benzylic carbons and the phenol oxygens (**Scheme 2-20**).

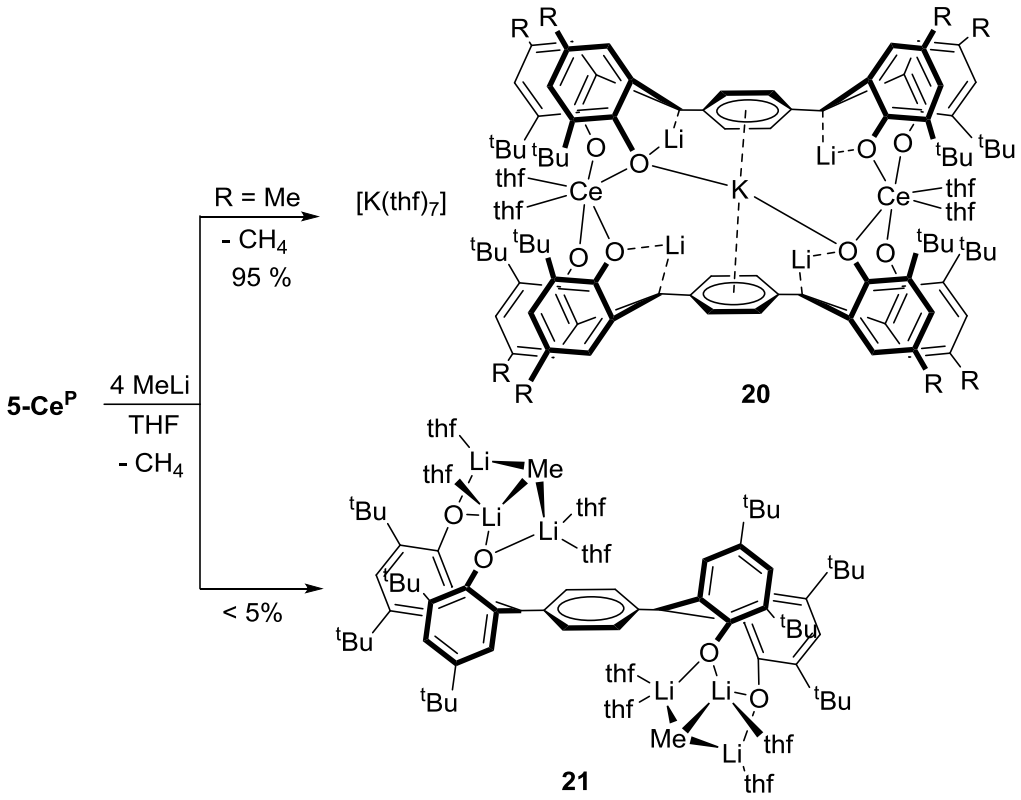

Scheme 2-20. The reaction of **5-Ce^P** towards LiMe.

The ^{1}H NMR data suggest the full conversion of the starting material but attempts to crystallise the product were not successful yet. Interestingly, after workup of the reaction solution, a lithium complex **21** is obtained as a colourless prism with a yield of less than 5% (**Scheme 2-20**). The solid-state structure is shown in **Figure 2-16**. Selected bond distances (Å) and angles (°) are provided in **Table 2-8**.

In the solid-state structure, the Li1 atom is bridging the two phenol oxygen atoms at a distance of 1.888(10) Å and 1.852(10) Å, respectively. Each phenol oxygen atom also bounds to another lithium ion, while the methyl group connects with all three lithium ions at a μ_3-bridging mode. The Li-O bonds lengths fall in the reported values from 1.854(3) Å to 2.308(12) Å.[31] The Li1 and Li2 ions have a coordination number of four while the Li3 ion displays a planar three coordination. The three C-Li bonds display different bond lengths. The shortest bond of 2.122(14) Å is shorter than the reported μ_3-bridging bonds range of 2.213 (5) Å to 2.444(6) Å while the other two bonds (2.255(13) Å and 2.302(14) Å) fall in this range.[32, 33]

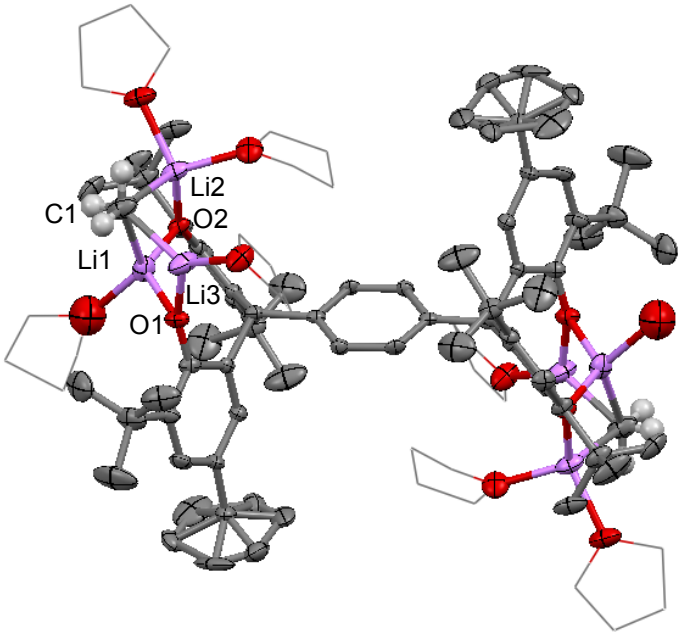

Figure 2-16. Solid state structure of complex **21**. Thermal ellipsoids are shown at 30% probability. All hydrogen atoms except those on C1 atom are omitted for clarity.

Table 2-8. Selected bond length (Å) and angles (°) of complex **21**.

Bonds	Length(Å)	Angles	(°)
Li1-C1	2.302(14)	Li2-O1-Li1	83.9(5)
Li2-C1	2.122(14)	Li1-O2-Li3	86.3(5)
Li3-C1	2.255(13)	Li3-C1-Li1	68.0(4)
Li1-O1	1.888(10)	Li2-C1-Li1	66.8(4)
Li2-O1	1.756(12)	O1-Li1-C1	95.4(5)
Li1-O2	1.852(10)	O2-Li1-O1	125.6(6)
Li3-O2	1.874(10)	O1-Li1-C1	101.9(5)

2.5.7. **Synthesis and reactivity study of cerium benzyl complex**

2.5.7.1. Synthesis of cerium benzyl complex in THF

The reaction of **5-Ce^{P}** with four equivalents of KBn (Bn = benzyl) in THF affords a red solution. After work-up, a red solid was collected with a yield of 72 %.

The ^{1}H NMR spectrum of the product shows two major different sets of resonances for the products. After fractional precipitation with hexane, two different products can be isolated. The ^{1}H NMR spectrum of the red crystals shows paramagnetic resonances of singlets at δ = 9.80, 9.11, 8.37 and 6.00 ppm which can be ascribed to protons of the phenol rings. Two doublets at δ = 7.20 (d, *J* = 7.5 Hz) and 7.15 (d, *J* = 7.5 Hz) shows the phenyl linkers. The peaks at 7.11 (m, 4H) and 6.98 (m, 4H) are assigned as the phenyl protons of the benzyl groups. The methylene groups (4H) are shown as a broad singlet at 2.03 ppm. The methyl groups are recorded at 2.35 as doublets with the *tert*-butyl groups shown at δ = 3.80, 1.15, -0.16 and -2.27 ppm. All these paramagnetic data suggest the formation of a Ce^{III} containing the product of complex **22-Ce^{P}**, [$K_3L^{P}{}_2Ce_2Bn_2(thf)_4$].

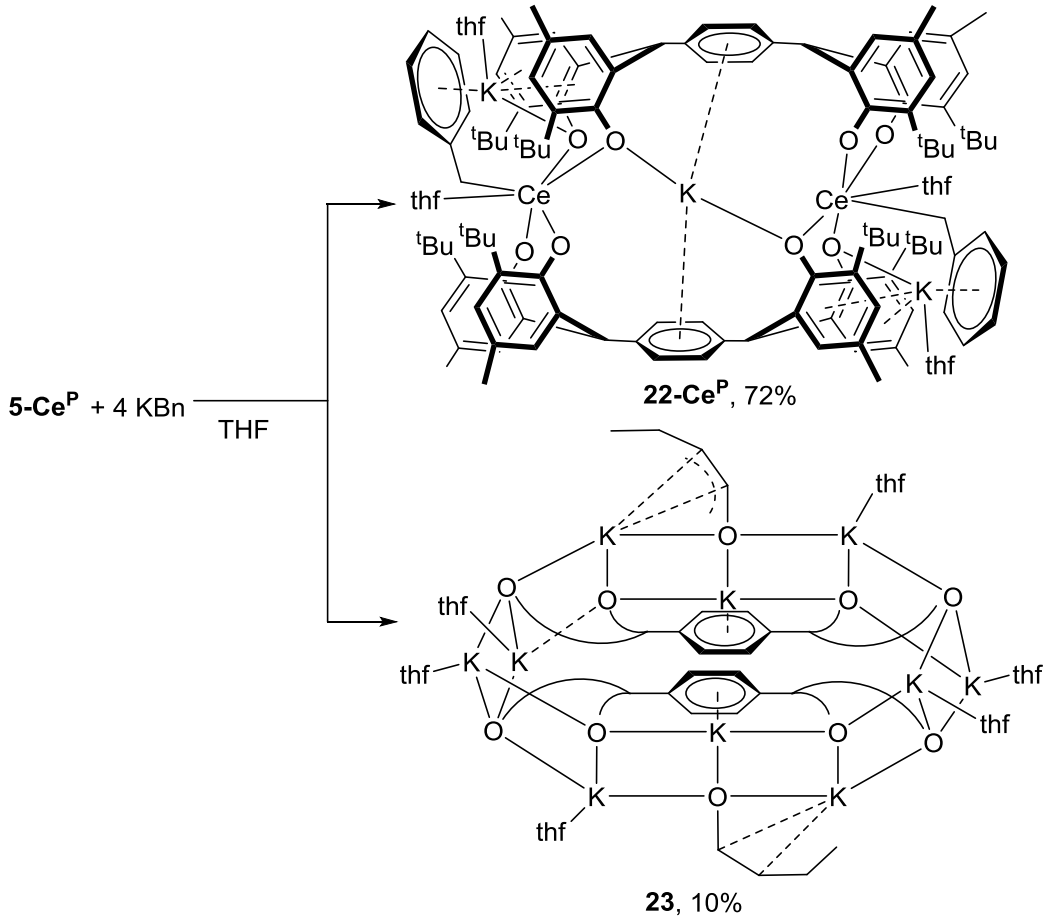

Scheme 2-21. The reaction of **5-Ce^{P}** towards KBn.

After recrystallisation of the mixture from THF, two types of crystals are obtained, one is red while the other is colourless. Crystals suitable for single-crystal X-ray diffraction are separated manually. The red crystals are characterised as *bis*-cerium complex **22-Ce^{PT}** while the colourless crystals are characterised as complex **23**. (**Scheme 2-21**)

In the crystal structure, the skeleton of the [KCe_2] core displays similar patterns as those aforementioned **5-Ce** complexes. Each cerium atom is coordinated by four phenol oxygens, one THF molecule and one methylidene carbon of the benzyl group, forming a pseudo-octahedral configuration. The K^+ ions are coordinated by three phenyl groups. The methylidene carbon of the benzyl groups bond to the cerium atom in a η^1 manner with a distance of 2.806(13) Å, which is ~0.2 Å longer than the Ce^{III}-C δ-bond observed in complex $Ce(Bn)_3(THF)_2$.[34] The slightly longer distances of the Ce-C bond in complex **22-Ce^{P}** also suggests the oxidation state of the Ce ion to be Ce^{III} rather than Ce^{IV} where much shorter bonds are expected due to contraction of ionic radii at a higher oxidation state.

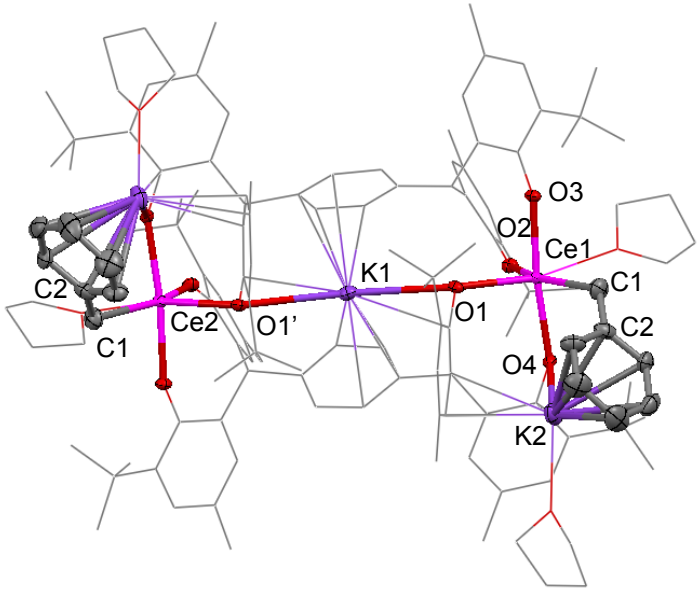

Figure 2-17. Solid state structure of complex **22-Ce^{P}**. Thermal ellipsoids are shown at 30% probability. All hydrogen atoms and solvents are omitted for clarity.

Table 2-9. Selected bond distances (Å) and angles (°) of complex **22-Ce^{P}**.

Ce1-O1	2.396(7)	Ce1-C1	2.806(13)
Ce1-O2	2.371(7)	K1-O1	3.028(7)
Ce1-O3	2.293(7)	K2-O4	2.777(8)
Ce1-O4	2.281(7)	C2-C1	1.394(18)
O1-K1-O1'	163.0(3)	C2-C1-Ce1	131.4(10)
Ce2-O5-K1	147.0(3)	dihedral angle (θ)	64.22

According to the solid-state structure, the product formula can be concluded as $K_3L^PCe_2(Bn)_2$, which suggests the mixed valence state (+III and +IV) of Ce ions. However, the results from the crystal structure show different character as the bond lengths of the terminal Ce-O_{ph} bonds of 2.371(7) Å, 2.293(7) Å and 2.281(7) Å are similar to those in complex **5-Ce^P**, which suggest the existence of Ce^{III} complexes rather than Ce^{IV} complexes where shorter distances of Ce^{IV}-O_{ph}(*ca.* 2.15 Å) are observed in complex **9-Ce** (**Table 2-6**). Attempts to purify this complex failed as the complex decomposes in THF and also gets oxidised to Ce^{IV} complexes by the trace amount of O_2 in the glovebox.

Analysis of the colourless crystals from the reaction revealed a THF-ring opening product, $[K_{10}L_2(OCH{=}CHCH_2CH_3)_2(THF)_6]$, complex **23**. In the structure of complex **23**, the staggered ladder-like skeleton o $[K_{10}O_{10}]$, which is similar to the structure observed in complex **3**. The K-O bonds in complex **23** vary from 2.524(4) Å (K1-O1) to 3.096(4) Å (K3-O10). The oxygen atom of the ring-opened THF is bridging three K^+ ions. The short C1-O1 bond of 1.315(3) Å and C1-C2 bond of 1.333(5) Å suggests a delocalised double bond between these atoms. The C2-C1 bond also displays weak interactions to the neighbouring K^+ ion.

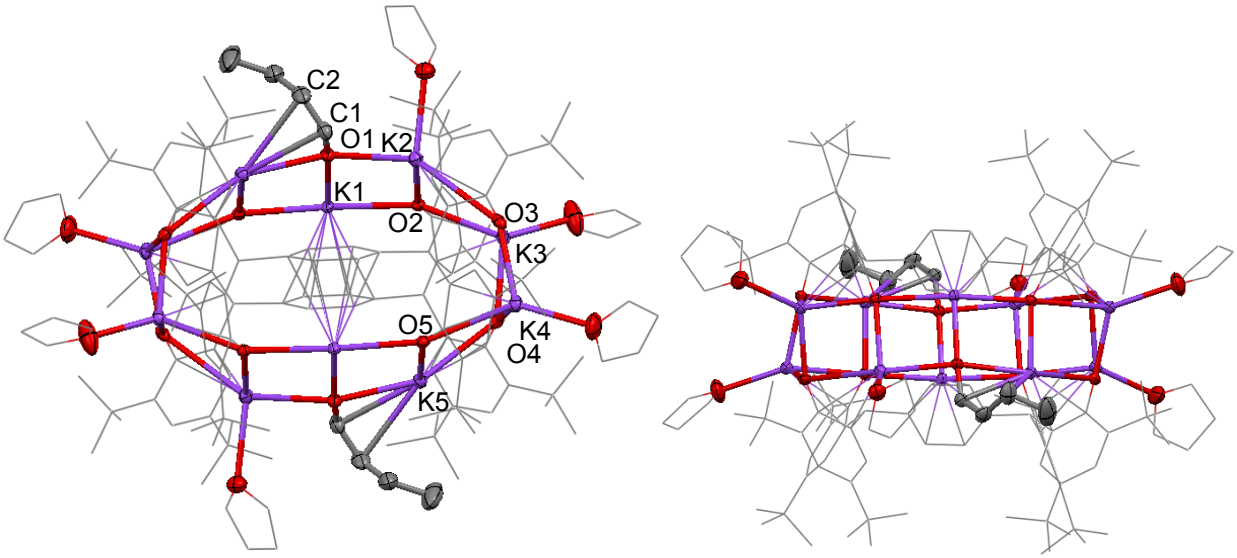

Figure 2-18. Representation of the crystal structure of complex **23**. Thermal ellipsoids are shown at 30% probability. All hydrogen atoms are omitted for clarity.

Table 2-10. Selected bond distances (Å) of complex **23**.

K1-O1	2.524(4)	K3-O3	3.096(4)
K1-O2	2.904(3)	K3-O4	2.689(4)
K1-O10	2.601(3)	K4-O3	2.760(3)
K2-O1	2.898(3)	K4-O4	2.686(4)
K2-O2	2.884(3)	K4-O5	2.842(5)
K2-O3	2.608(4)	K5-O4	2.618(3)
K3-O2	2.571(3)	K5-O5	2.792(3)
C1-O1	1.315(3)	C2-C1	1.333(5)

2.5.7.2. Synthesis of cerium benzyl complex in Et_2O

The reaction of **5-Ce^{PT}** with four equivalents of KBn (Bn = benzyl) in diethyl ether affords a red solution. After the removal of volatiles, yellow solid was formed. The ^{1}H NMR spectrum of the product shows paramagnetic phenyl protons at δ = 9.16, 6.31, 4.38 and 3.93 ppm. The benzyl protons are observed as one triplet at 7.07 ppm with a coupling constant of J = 7.7 Hz) and a doublet at 6.99 ppm with a coupling constant of J = 7.5 Hz. The methylidene group of the benzyl is recorded as a singlet at 2.15 ppm while the tert-butyl groups are shown at 2.01 and -2.99 ppm. All these paramagnetic ^{1}H NMR data are different from those in the reaction with KBn in THF in **Scheme 2-21**, which suggests the formation of another Ce^{III} containing product of $[K_6L^{PT}_2Ce_2Bn_4(Et_2O)_4]$, complex **24-Ce^{PT}**.

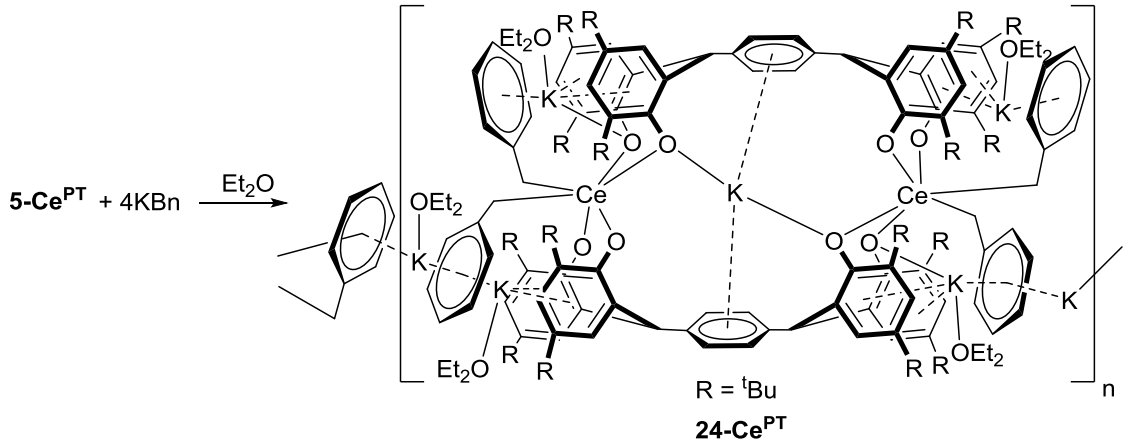

Scheme 2-22. The reaction of **5-Ce^{PT}** towards KBn in diethyl ether.

The yellow crystals of **24-Ce^{PT}** were grown by slow evaporation of a concentrated diethyl ether solution in a vial in the glovebox. The solid-state structure is shown in

Figure 2-19. Selected bond distances (Å) and angles (°) are provided in **Table 2-11**.

Compound **24-Ce^{PT}** crystallises in the triclinic space group P-1, with six molecules in the unit cell. The solid-state structure shows a polymeric molecule of complex **24-Ce^{PT}**. In the structure, each Ce atom displays a pseudo-octahedral configuration by coordinating with two benzyl groups and four phenol oxygen atoms. The carbon of the benzyl groups bond to the cerium atoms at distances from 2.7541(4) Å to 2.9736(3) Å, which is similar to those in complex **22-Ce^{P}** with a distance 2.806(13) Å.

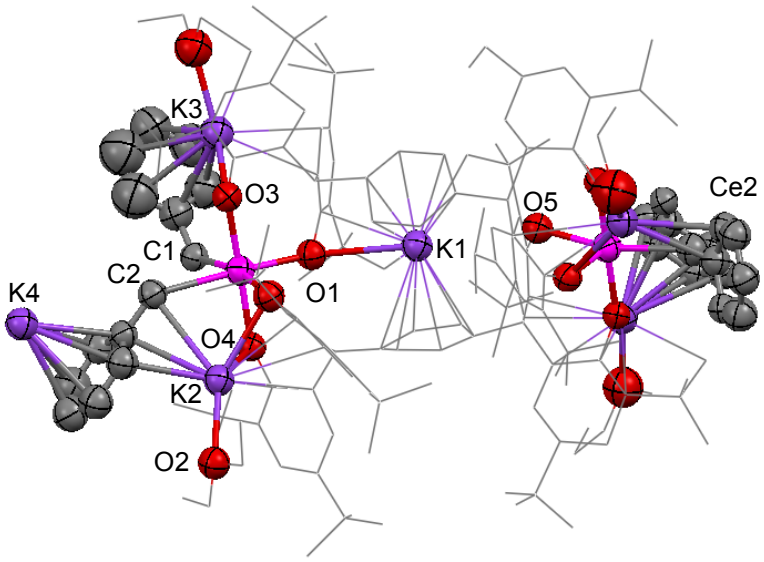

Figure 2-19. Solid state structure of complex **24-Ce^{PT}**. Thermal ellipsoids are shown at 30% probability. All hydrogen atoms and solvents are omitted for clarity.

The distances of the K+ cation in the V-shape cage to the two phenyl rings (2.868 and 2.906 Å) are similar to previous complexes while the distance to the bridging oxygen atom has greatly elongated from 2.90 Å in complex **5-Ce^{PT}** to 3.19 Å (ava). The other K^+ ions (K2, K3, K5 and K6) are coordinated by three phenyl groups and also have interactions with neighbouring phenol oxygen atoms. In the crystal structure, the molecule is connected to benzyl groups of other molecules via the K^+ ions from both sides, forming a two-dimensional polymer.

Table 2-11. Selected bond distances (Å) and angles (°) of complex **24-Ce^{PT}**.

K1-O1	3.1845(2)	K1-O5	3.2037(4)
Ce1-O1	2.3738(2)	Ce2-O5	2.4425(3)
Ce1-O2	2.3779(2)	Ce2-O6	2.2828(2)
Ce1-O3	2.4173(3)	Ce2-O7	2.2662(2)
Ce1-O4	2.3691(2)	Ce2-O8	2.2437(2)
Ce1-C1	2.8904(4)	Ce2-C4	2.8003(5)
Ce1-C2	2.7541(4)	Ce2-C3	2.9736(3)
Ce1-O1-K1	144.1(10)	Ce2-O5-K1	140.9(9)
K1-ring	2.868	K1-ring	2.906
dihedral angle (θ)	66.09		

This reaction shows the interesting chemistry of the complexes towards KBn, which undergoes an addition reaction to the molecule rather than deprotonating the benzylic-CH of the ligand in the reaction of **5-Ce^{PT}** with MeLi in **Scheme 2-20**.

2.5.7.3. Reactivity study of cerium benzyl complex

Through the introduction of benzyl groups to the complex, a myriad of reactions targeting the reactivity of Ce-C bond has been tested. The reaction of **22-Ce^{P}** with two equivalents of phenylacetylene in THF showed an immediate colour change from red to yellow. After work-up, a yellow solid of complex **25** was obtained at a yield of 75%. The ^{1}H NMR spectrum of the product shows the full consumption of the starting material and the formation of toluene. and multiple paramagnetic signals from δ = 21.17 ppm to -5.24 ppm suggests the formation of a phenylacetylenyl product **25**.

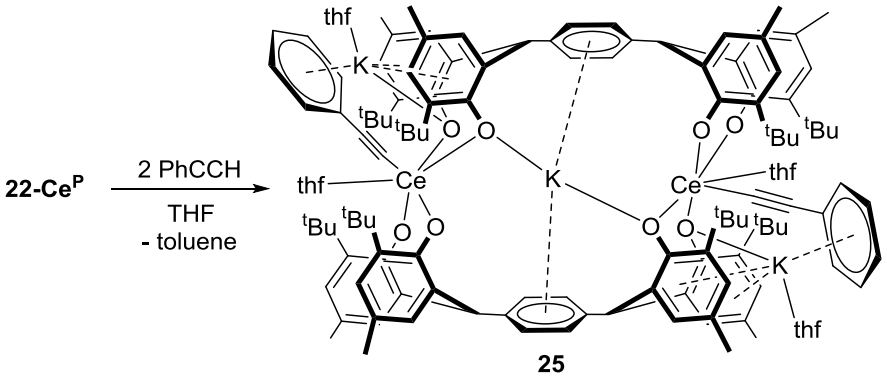

Scheme 2-23. The reaction of **22-Ce^{P}** with PhCCH.

When the CO_2 gas was passed through a drying column to the THF solution of complex **22-Ce^{P}**, an instant pale yellow precipitate was formed. The ^{1}H NMR spectrum shows the disappearance of the starting material in the solution which suggests the formation of CO_2 insertion complex **26**. Similar reactivity was observed in the reaction with CS_2, which suggests a CS_2 insertion to the Ce-C bond, forming product **27**.

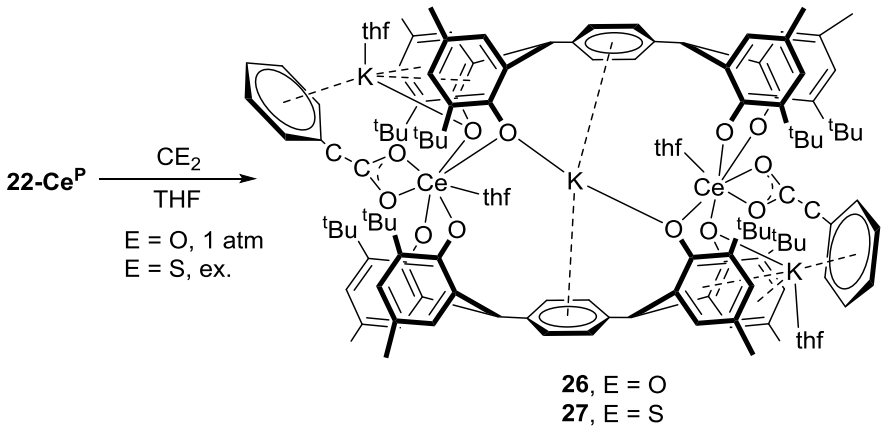

Scheme 2-24. The reaction of **22-Ce^{P}** with CO_2 and CS_2.

2.6. Synthesis and reactivity of L(RECl)$_2$

2.6.1. **Synthesis of L(RECl)$_2$**

In the reaction of complex **2^{PT}** with four equivalents $RECl_3(THF)_2$, (RE = Ce, Pr)in THF, a white suspension is formed. The solution is decanted by centrifuge and then the solids are extracted by pyridine. After the removal of solvents and washing with hexane, a white precipitate was isolated and dried under reduced pressure. The ^{1}H NMR spectrum of complex **28-Ce^{PT}** in pyridine shows peaks at δ = 10.62, 9.61 and 5.02 ppm, which are similar to those in complex **5-Ce^{PT}** and can be ascribed to the phenyl rings. The benzylic protons are recorded as a singlet at 3.68 ppm. Tert-butyl groups are shown at 2.03 and 0.20 ppm, respectively. The phenyl protons of complex **28-Pr^{PT}** are shown at a lower field (δ = 15.35 and 14.18 ppm) compared to complex **28-Ce^{PT}**, with the middle ring overlapping with pyridine solvent at 8.57 ppm. The similar trend is observed for benzylic protons which are displayed at 5.33 ppm while the tert-butyls are recorded at 3.91 and 2.30 ppm.

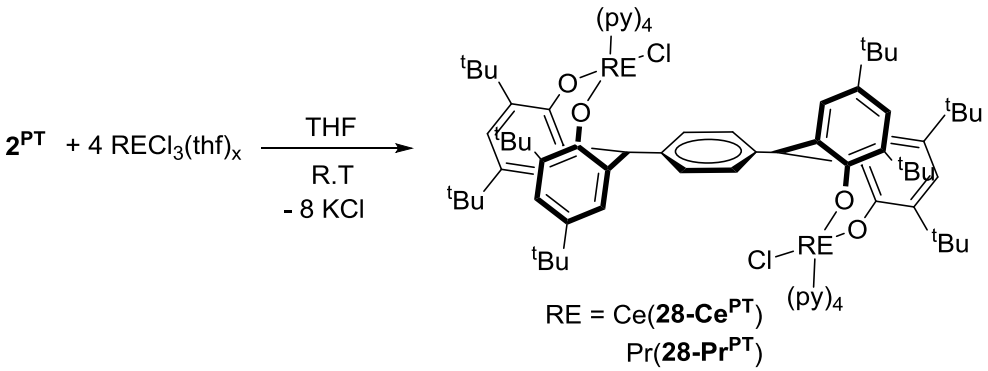

Scheme 2-25. Synthesis of complex **28**, L(RECl)$_2$, RE = Ce, Pr.

Single crystals suitable for X-ray diffraction were grown by vapour diffusion of hexane into a saturated pyridine solution at ambient temperature. The solid-state structure is shown in **Figure 2-20**.

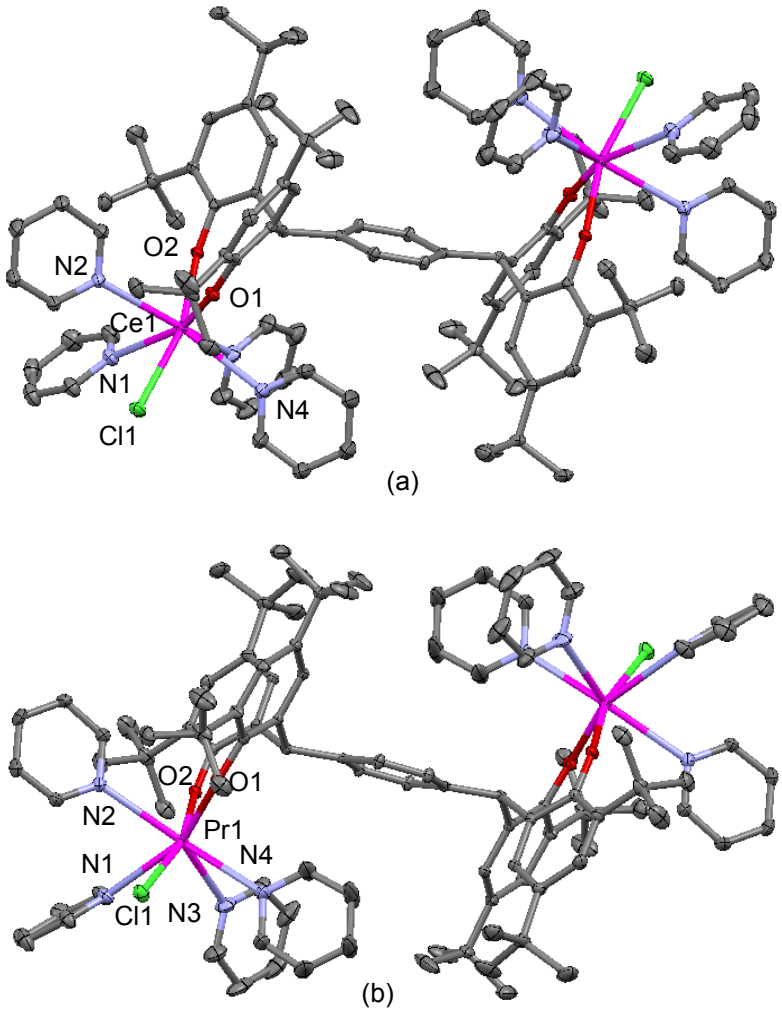

Figure 2-20. Solid state structure of complex **28-Ce^{PT}** (a) and **28-Pr^{PT}** (b). Thermal ellipsoids are shown at 30% probability. All hydrogen atoms and solvents are omitted for clarity.

Both complexes display isomorphic crystals. Due to the minor differences between the radii of Ce^{3+} and Pr^{3+} ion, the bond lengths of RE-Cl bonds in complex **28** are slightly different (~0.02 Å). The coordination of the metal ions in complex **28-Pr^{PT}** is also similar to the *trans*-configuration that observed in complex **17-Pr^{PT}**. However, due to the large radii of iodine anion, the distance between Pr1 and I1 in complex **17-Ce^{PT}** (3.1697 Å) is much greater than those in complex **28** (**Table 2-12**).

Table 2-12. Comparison of Selected bond distances (Å) of complex **28** and **17**.

Bond	**28-Ce^{PT}**	**28-Pr^{PT}**	Bond	**17-Pr^{PT}**
RE1-Cl1	2.7789(6)	2.7601(14)	Pr1-I1	3.1697(5)
RE1-O1	2.2922(15)	2.218(4)	Pr1-O1	2.176(4)
RE1-O2	2.2337(15)	2.276(4)	Pr1-O2	2.202(4)
RE1-N1	2.6797(19)	2.704(5)	Pr1-O3	2.567(5)
RE1-N2	2.782(2)	2.765(5)	Pr1-O4	2.458(5)
RE1-N3	2.714(2)	2.660(5)	Pr1-O5	2.461(5)

RE1-N4	2.725(2)	2.716(5)

2.6.2. Comparison of complex L(RECl)$_2$ to U^{IV} complexes

A similar *trans*-coordination of the ligand toward f-elements are observed in the work carried out in the Arnold group, where a series of U^{IV} halide complexes can be synthesised *via* the similar methods. The U^{IV} counterparts (**FC**, **Scheme 2-26**) for the **17-Pr^{PT}** displays the similar *trans*-bonding towards the ligand while the *meta*-substituted complex **FD** shows different symmetry.

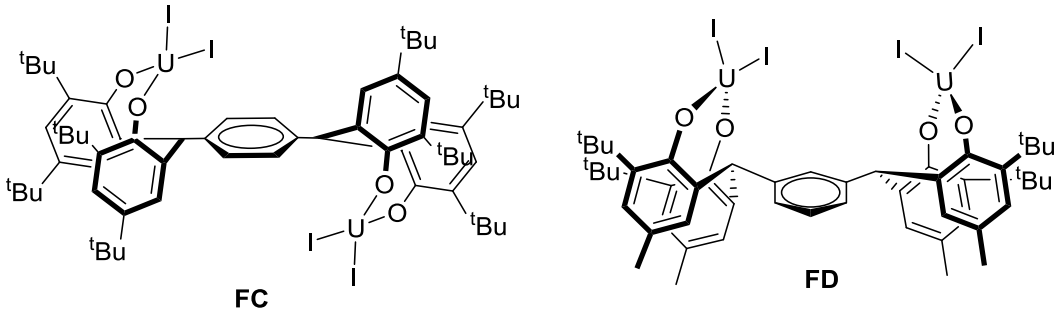

Scheme 2-26. Examples of the U^{IV} phenolate complex.

2.6.3. Reactivity of L(RECl)$_2$ towards AgPF$_6$

In inorganic synthetic chemistry, the approach to cationic rare earth species via salt elimination is a common strategy. In order to make the cationic complexes of the tetraphenol ligands, the RE halide complexes **28**, L(RECl)$_2$, are treated with silver reagents.

Treatment of **28-Ce^{PT}** with two equivalents of $AgPF_6$ at room temperature resulted in an instant colour change from colourless to blue, which suggests the oxidation of Ce^{III} to Ce^{IV}(**Scheme 2-27**). This is also confirmed by the formation of a silver film after the reaction. The ^{1}H NMR spectrum also shows diamagnetic peaks where phenyl protons are observed at δ = 7.43, 7.32 and 7.08 ppm while the tert-butyl groups are recorded at δ = 1.34 and 1.21ppm. These resonances are similar to that of complex **9-Ce^{PT}**.

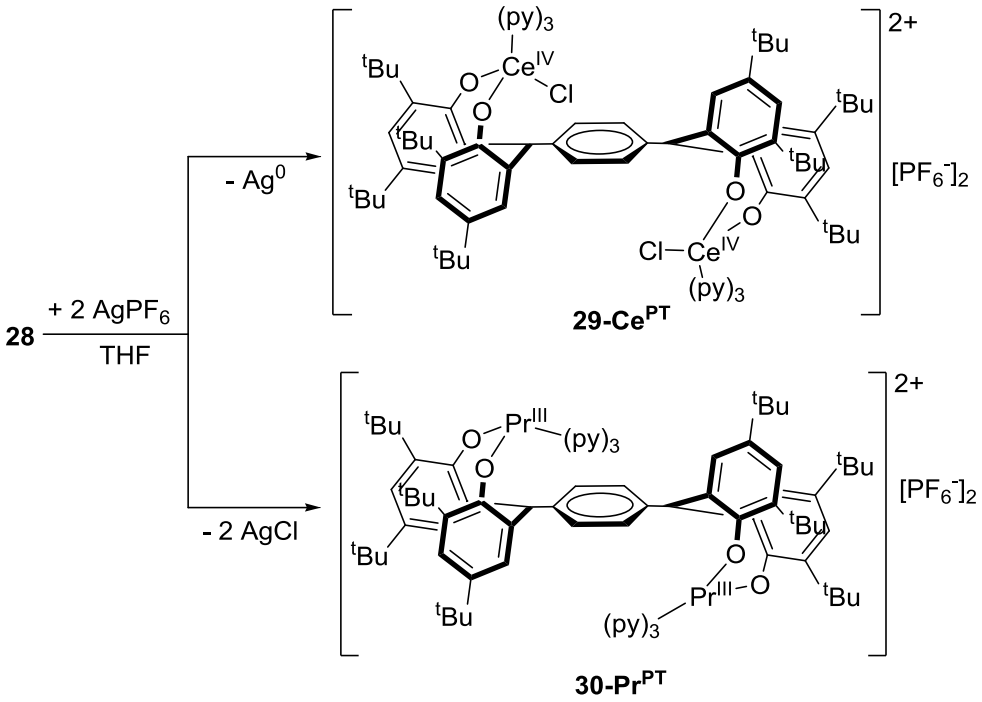

Scheme 2-27. The reaction of $L(RECl)_2$, (RE = Ce, Pr) towards $AgPF_6$.

However, the reaction of **28-Pr^{PT}** towards two equivalents of $AgPF_6$ yielded white solid of AgCl and other products which show paramagnetic shifts in the ^{1}H NMR spectrum (**Scheme 2-27**).

From this spectrum, based on the symmetry of the ligand and the integral of the peaks, two products can be identified. One of the product has a 75% NMR yield and displays singlets at δ = 19.47, 7.51 and 7.55 ppm, which can be assigned to the phenyl protons. The two sets of *tert*-butyl groups are observed as singlets at 1.65 and 1.37 ppm, respectively. The other product displayed widely shifted resonances s at δ = 28.35, 22.49, 14.78 (s, 4H) and 0.73 ppm (s, 4H) for the phenyl protons. Peaks at δ = 5.51 (s, 36H), 0.30 (d, J = 37.4 Hz, 18H) and -0.24, (s, 18H) are ascribed for *tert*-butyl groups. The ^{19}F NMR spectrum of the product shows a doublet at δ = -71.30 ppm (d, J = 710.4 Hz).

All these paramagnetically shifted resonances are different to any of the starting materials or previously studied complexes, which suggest the formation of new Pr^{III} product **30-Pr^{PT}** (**Scheme 2-27**).

2.6.4. **Synthesis of RE amide complexes**

Treatment of a slurry suspension of complexes **28** in THF with two equivalents of KN" resulted in the formation of a cloudy solution. Removal of the salt by filtration afforded a clear solution, which, after the removal of volatiles under reduced pressure, yielded a white powder of complex **31**. Formation of these complexes is confirmed by the ^{1}H NMR spectroscopy. The spectrum of the product is identical to that of the reaction of phenol ligand with CeN"$_3$ which suggests an alternative path for the synthesis of dinuclear rare earth metal amide complex (**Scheme 2-28**).

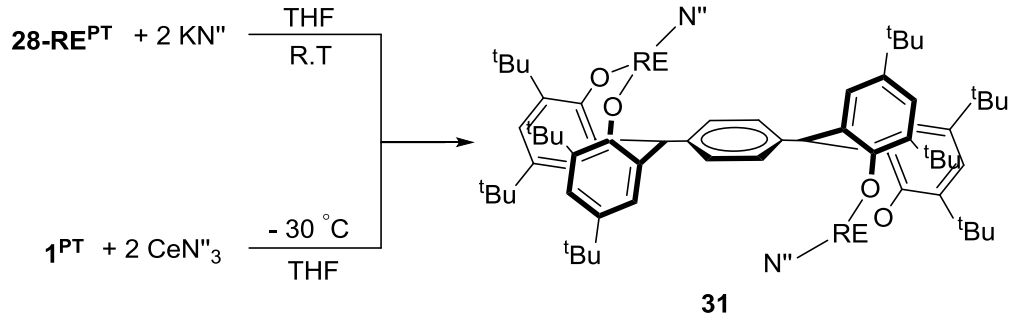

Scheme 2-28. Synthesis of L(REN")$_2$.

Single crystals of complex **31-Ce^{PT}** were grown by slow diffusion of hexane into the toluene solution at room temperature. In the crystal structure, the two N" groups take a 1/2 occupancy in the structure, which is due to the disorder. However, the connectivity of the complex can be deduced. In the solid-state structure, N" groups reside at the different side of the phenyl linker, which is similar to what observed in the halide complexes. The Ce-N bond length of 2.405(18) Å is consistent with reported results (2.357 (4)) Å in Ce[N(SiMe$_3$)$_2$]$_3$.[35]

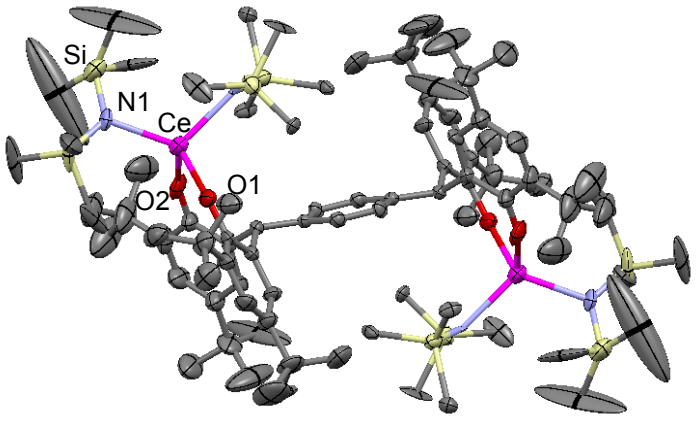

Figure 2-21. Solid state structure of complex **31-Ce^{PT}**. Thermal ellipsoids are shown at 30% probability. All hydrogen atoms and solvents are omitted for clarity.

Table 2-13. Selected bond length (Å) of complex 31-**Ce^{PT}**.

Bond	Length	Bond	Length
Ce-O1	2.253(9)	Ce-N1	2.405(18)
Ce-O2	2.193(13)	Si-N1	1.76(3)

Given the successful synthesis of the stable complex **31-Ce^{PT}**, reactions of this complex towards amines (H_2NR, R = Dipp and Mes*) are carried out in order to make the substituted amide complexes. However, the ^{1}H NMR and ^{29}Si NMR suggested no reaction occurred. When the halide complex **28-Ce^{PT}** was treated with the KNHR (R = Dipp, Mes*), a white solid was formed with no starting material in the solution which was confirmed by ^{1}H NMR spectroscopy. The white solid is insoluble in organic solvents such as THF, pyridine or acetonitrile which may due to the oligomerisation of the products **32** (**Scheme 2-29**).

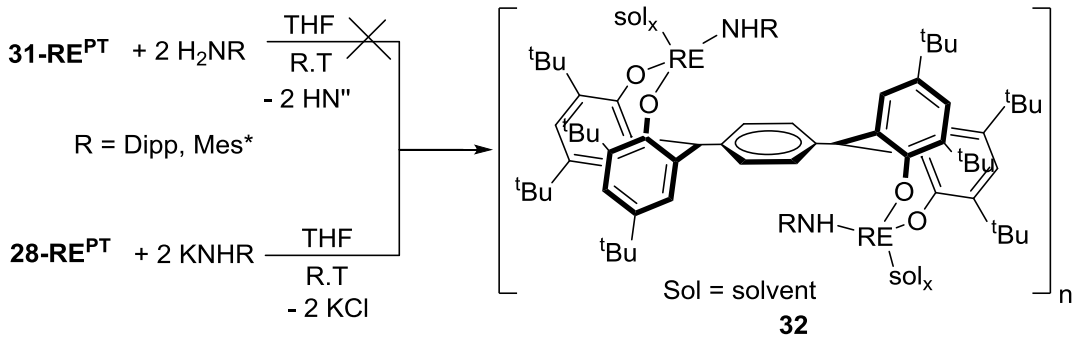

Scheme 2-29. Synthesis of amide complexes.

2.7. Synthesis of L{Ln(BH4)}2

Trivalent rare earth borohydrides, $[RE(BH_4)_3(thf)_2]$, not only have been widely studied for their applications in various polymerisation reactions,[36, 37] but also have served as valuable starting materials to make organometallic borohydride derivatives.[38] In most cases, the BH_4^- group reacts as a pseudohalide which can undergo a salt metathesis reaction with alkali metal reagents, forming borohydride derivatives and the easily removable MBH_4 (M = Li, Na, K) byproducts.[39, 40] By using this approach, rare earth borohydride derivatives, such as mono cyclopentadienyl,[41, 42] alkoxides,[40] guanidinates[43] and bis(phosphinimino)methanide[44] complexes were prepared according to literature.

By using this method, the reaction of complex $\mathbf{2^{PT}}$ with four equivalents of $Ce(BH_4)_3(thf)_2$ resulted in the formation of salt metathesis product **33-Ce^{PT}**, $L(Ce(BH_4))_2(py)_6$ (**Scheme 2-30**). The ^{1}H NMR spectrum shows paramagnetic peaks at δ = 10.49 and 9.62 ppm, which can be ascribed to the protons of the phenol rings. The phenyl linker is observed as a singlet at δ = 4.13 ppm while the benzylic groups are recorded as a triplet at 3.69 ppm with a coupling constant of J = 7.4 Hz. The tert-butyl groups are shown as two singlets at δ = 2.09 and 0.02 ppm. The ^{11}B NMR shows a broad singlet at δ = 29.08 ppm while the protons are greatly broadened and cannot be identified due to the paramagnetic Ce^{III} centre.[45]

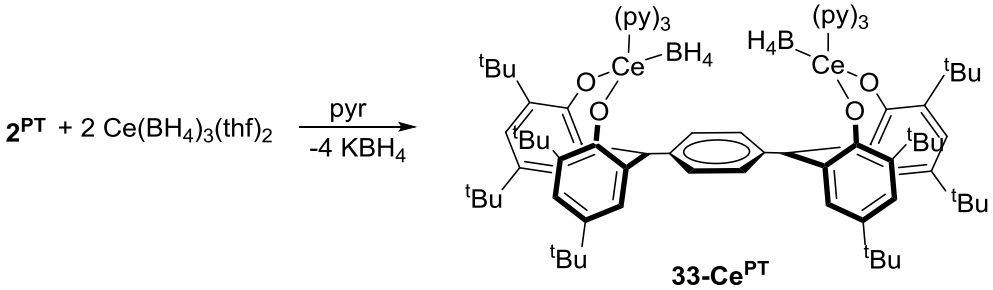

Scheme 2-30. Synthesis of cerium borohydride complex.

Single crystals of complex **33-Ce^{PT}** were grown by slow diffusion of hexane into the toluene solution at room temperature. The solid-state structure is shown in **Figure 2-22**.

Interestingly in the crystal structure, the two borohydride groups reside on the same side of the phenyl linker, displaying a '*cis*' configuration which is different to all the mono-ligand complexes synthesised in this project. This demonstrates the ligand flexibility that enables the metals to reside on the same or opposite sides of the central phenyl bridge.[11]

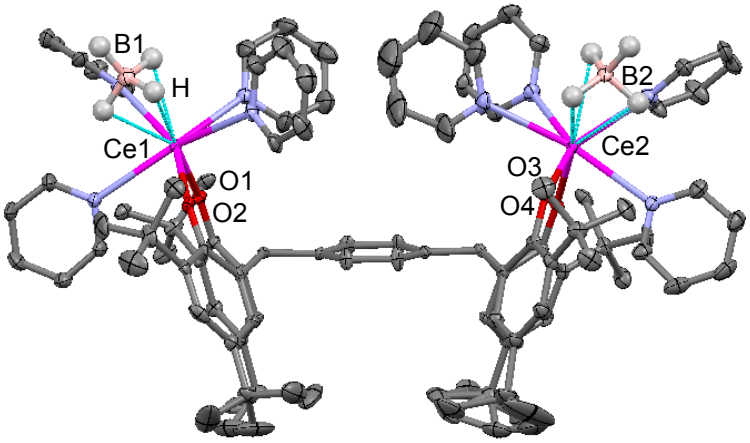

Figure 2-22. Solid state structure of complex **33-Ce^{PT}**. Thermal ellipsoids are shown at 30% probability. All hydrogen atoms and solvents are omitted for clarity.

The Ce centres are seven coordinate, adopting a distorted pentagonal bipyramidal geometry. The Ce-O bonds in complex **33-Ce^{PT}** are slightly shorter than those in complex **5-Ce^{PT}**. The Ce-B distance of 2.827(11) Å and 2.853(10) Å is 0.12 Å longer than those reported values of 2.678(6) Å and 2.704(7) Å in the complex $[Ce(BH_4)_2(THF)_5][BPh_4]$.[45]

Table 2-14. Selected bond distances (Å) of complex **33-Ce^{PT}**.

Bond	Length	Bond	Length
Ce1-B1 (distance)	2.827(11)	Ce2-B2 (distance)	2.853(10)
Ce1-O1	2.223(5)	Ce2-O3	2.276(5)
Ce1-O2	2.271(5)	Ce2-O4	2.222(5)

The treatment of two equivalents of $Ce(BH_4)_3(THF)_2$ with one equivalent of H_4L in pyridine gradually liberates hydrogen gas as verified by ^{1}H NMR spectroscopy. After 12 hours' reaction, the ^{1}H NMR spectrum shows the formation of **34-Ce^{PT}** and by-product BH_3·pyr adduct which shows a quartet at δ = -12.02 ppm in ^{11}B NMR. The ^{11}B NMR spectrum of **35-Ce^{PT}** shows a broad peak at δ = 12.26 ppm which is similar to that of 29.08 ppm in complex **34-Ce^{PT}** and 18.2 ppm in $Ce(BH_4)_3$. The difference in the ^{11}B NMR spectrum suggests a new configuration of the complex which is proposed in **Scheme 2-31**. Given the flexibility of the ligand, and combined with the solid-state structures of complex **33-Ce^{PT}**, a *trans*-configuration of the BH_4^- groups is proposed for the complex **34-Ce^{PT}**. However, due to the lack of solid state structure of this compound, the differences in ^{11}B NMR spectra could also result from the bridging BH_4^- moieties or oligomerisation of the complex.

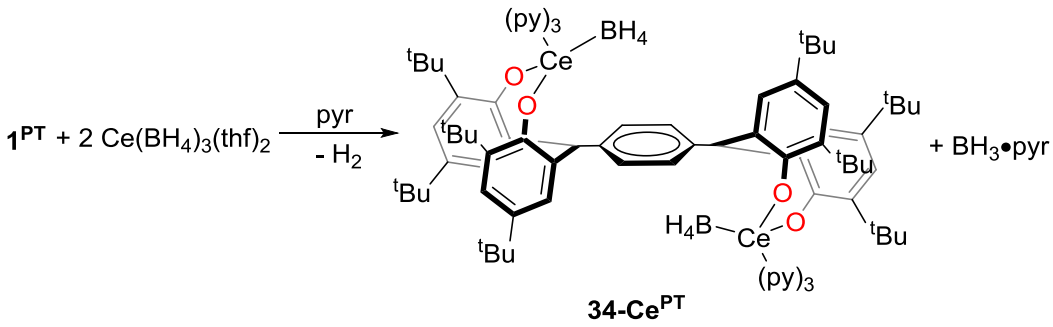

Scheme 2-31. The reaction of $Ce(BH_4)_3$ with $\mathbf{1^{PT}}$.

As discussed earlier, the BH_4^- group normally reacts like a pseudohalide. The chemistry of this reaction shows the first example of rare earth borohydride complex to serve as an active base which reacts with acidic protons to form hydrogen gas. The only similar reactivity of rare earth borohydride is observed in the reaction of K(dip2-pyr) (dip2-pyr = 2,5-bis[N-(2,6-di-isopropylphenyl)iminomethyl]pyrrole) (**FE, Scheme 2-32**) with $RE(BH_4)_3(THF)_2$ (RE = Sc, Lu), where the imino groups are reduced to amido groups, and forms a =N-BH_3 group which coordinates in a η^2-fashion to the metal atom (**FF**, **Scheme 2-32.**).[46, 47]

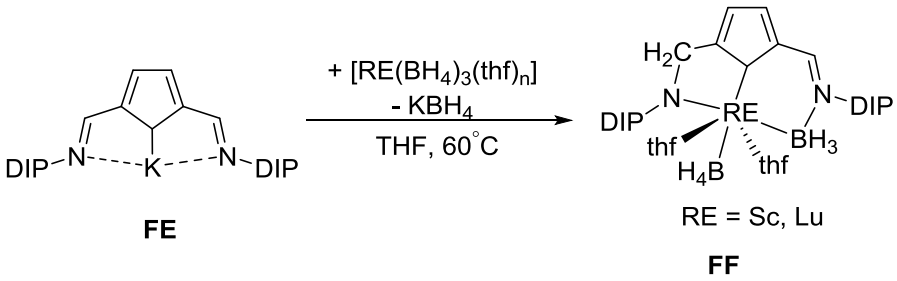

Scheme 2-32. A reported example of RE borohydride complex.[46, 47]

2.8. Synthesis of Ce^{IV} complexes

In the reaction of complex $\mathbf{2^{PT}}$ with two equivalents of $(Et_4N)_2CeCl_6$ in THF, an immediate deep blue colour solution was obtained. After the removal of inorganic salts and volatiles, complex **9-Ce^{PT}** is obtained at 70% yield.

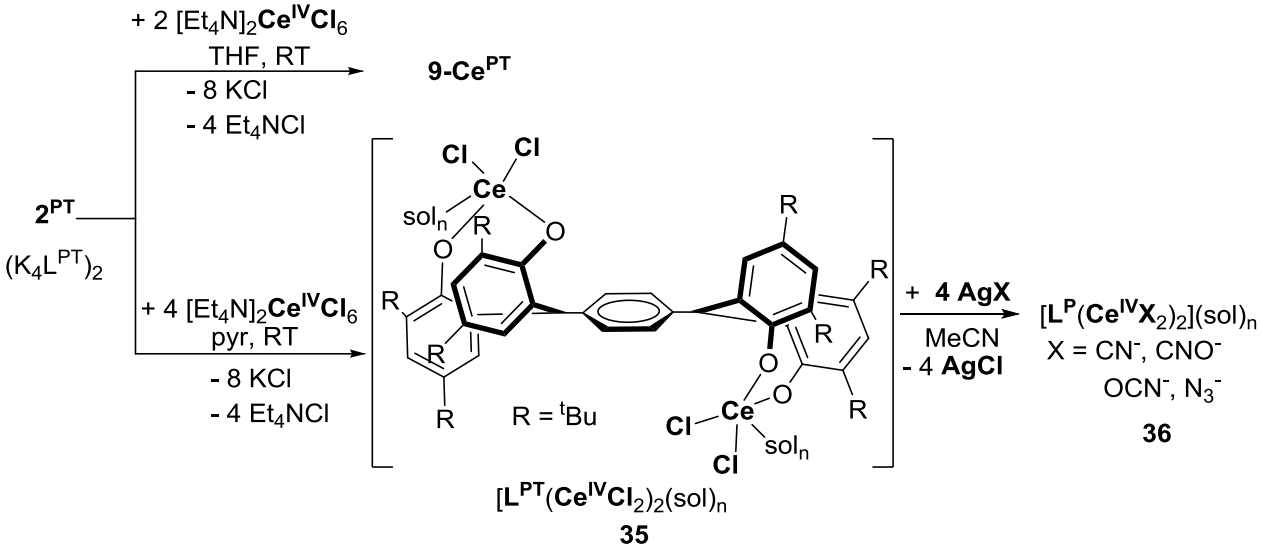

Scheme 2-33. Synthesis of Ce^{IV} complexes.

The treatment of $\mathbf{2^{PT}}$ with four equivalents of $(Et_4N)_2CeCl_6$ afforded blue solid in THF. The ^{1}H NMR in pyridine-d_5 showed diamagnetic peaks which confirmed the synthesis of Ce^{IV} complex. Unlike the complex **9-Ce^{PT}**, the spectrum of complex **35** ($[L^{PT}(CeCl_2)_2(sol)_n$) showed unsymmetrical peaks for the phenyl protons at δ = 8.14, 8.08, 7.82, 7.60, 7.48 and 7.16 ppm, which suggest the unsymmetrical configurations in solution. This unsymmetrical fashion is also observed for *tert*-butyl groups which shows four different chemical environments at δ = 1.91, 1.53, 1.41 and 1.40 ppm.

The reaction of complex **35** with silver reagents AgX (X = CN^-, CNO^-, OCN^- and N_3^-) afforded the subsequent cerium complexes with different anions and AgCl as a by-product. The formation of these complexes is confirmed by ^{1}H NMR spectroscopy.

2.9. Studies on polymerisation

In order to explore the application of the RE^{III} (RE = Ce, Pr) phenolate complexes in the field of catalytic polymerisation reactions, a study on the copolymerization of cyclohexene carbonate (CHO) and CO_2 is conducted in collaboration with Dr Sumesh K. Raman at The University of Oxford.

The catalysts tested are listed in **Figure 2-23**.

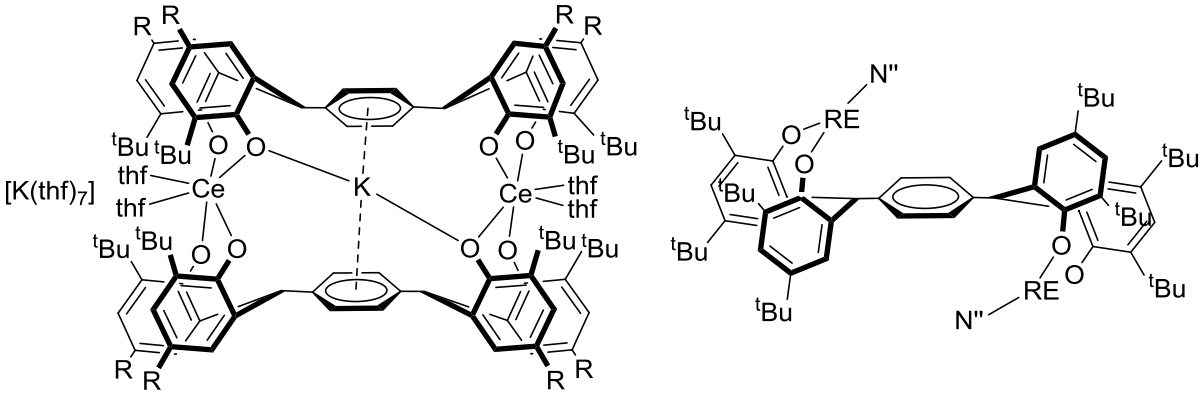

5-Ce^{PT}, R = ^{t}Bu

RE = Ce, **31-Ce**
RE = Pr, **31-Pr**

Figure 2-23. The catalysts tested for CHO-CO_2 copolymerization.

Representative CHO-CO_2 copolymerization procedure:

All the manipulations were performed in a glove box under dry nitrogen atmosphere. In a 10 mL glass vial, catalyst (0.011 mmol, 0.033 g for **5-Ce^{PT}** or 0.0168 g for **31-Ce** or 0.0170 g for **31-Pr**) cyclohexene oxide (5.82 g, 59.4 mmol), and *iso*-propanol (1.7 μL, 0.022 mmol) were mixed and allowed to stir for 5 minutes. This was then transferred to a 25 mL Parr reactor inside the glove box. The properly closed reactor was then taken outside the glove box and fitted with a high-pressure CO_2 line in a fume hood. The reactor was gently purged using CO_2 in order to ensure a complete CO_2 atmosphere inside the reactor. The reactor was then filled with 20 bars of CO_2 and heated up to 80 °C with continuous stirring. The CO_2 pressure was then adjusted to 40 bar. The polymerization stopped after desired time by a rapid cooling of the reactor. The excess carbon dioxide was released. An aliquot was taken from the crude mixture to perform the ^{1}H NMR in order to estimate the conversion and product distribution (Spectrum see **Chapter 6**, **Figure. 6-1 - 6-5**). The crude polymerization mixture was then precipitated from cold pentane. The precipitated polymer dried under vacuum at 50 °C for 48 hours. The dried polymer was used to perform GPC and other analyses.

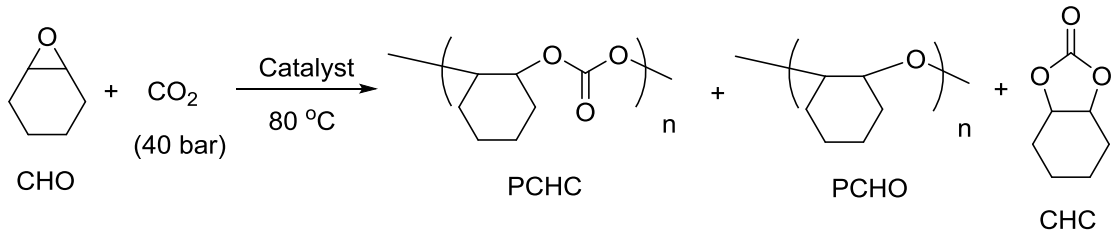

Scheme 2-34. CHO-CO_2 copolymerization.

Table 2-15. CHO-CO_2 copolymerization using Ce catalysts

Entry	Catalyst	[M]/[ROH] /Cocat	[CHO]/ [M]	Temp (°C)	Time (h)	Conv CHO (%)	PCHC/PCHO/CHC (%)	$M_{n,calc}$ [g.mol^{-1}]	$M_{n,exp}$ [g.mol^{-1}]	M_w/M_n
1	**5-Ce^{PT}**/IP	1/1/0	2700	80	48	21	1/20/0	55600	72500	1.30
2	**31-Ce**/IP	1/1/0	2700	80	48	18	1/17/0	66100	137377	1.28
3	**31-Ce**/IP/[PPN]Cl	1/1/1	2700	80	48	10	?/0/10	-	1100	1.29

IP = isopropanol, [PPN]Cl = Bis(triphenylphosphine)iminium chloride, CHC = cyclohexene carbonate. Entry 3- observed that *cis*-cyclohexene carbonate was formed together with some amount of polycyclohexene carbonate

Amongst these three complexes, the Pr complex **31-Pr** polymerised when added into the solution and showed no reactivity in this test. In the reaction with complex **5-Ce^{PT}**, a total conversion of 21% is recorded after 48 h. The ^{1}H NMR spectrum showed the product consists of 1% of poly-cyclohexene carbonate (PCHC) and 20% of polycyclohexene oxide (PCHO). The PCHO formed has a number average molecular weight of 72500 g.mol^{-1} and also shows good molecular weight distribution with a polydispersity index of 1.30.

A similar result is obtained in the trial with complex **31-Ce**, which showed the formation of 1% of PCHC and 17% of PCHO. In this reaction, the number average molecular weight of the product (137377 g.mol^{-1}) is almost doubled compared to the one with complex **5-Ce^{PT}**. The addition of co-catalyst [PPN]Cl leads to the formation of a trace amount of PCHC and 10% of cyclohexene carbonate monomer.

These results show that the complexes tested are not as active as some other systems recently reported in the literature.[48, 49] Thus further modifications on the complexes should be introduced to form the well-protected catalysts.

2.10. References

1. P. Drose, A. R. Crozier, S. Lashkari, J. Gottfriedsen, S. Blaurock, C. G. Hrib, C. Maichle-Mossmer, C. Schadle, R. Anwander and F. T. Edelmann, *J. Am. Chem. Soc.*, 2010, **132**, 14046-14047.
2. J. R. Robinson, P. J. Carroll, P. J. Walsh and E. J. Schelter, *Angew. Chem., Int. Ed.*, 2012, **51**, 10159-10163.
3. N. A. Piro, J. R. Robinson, P. J. Walsh and E. J. Schelter, *Coord. Chem. Rev.*, 2014, **260**, 21-36.
4. L. Clark, M. G. Cushion, H. E. Dyer, A. D. Schwarz, R. Duchateau and P. Mountford, *Chem. Commun.*, 2010, **46**, 273-275.
5. J. A. Bogart, A. J. Lewis, S. A. Medling, N. A. Piro, P. J. Carroll, C. H. Booth and E. J. Schelter, *Inorg. Chem.*, 2013, **52**, 11600-11607.
6. B. D. Mahoney, N. A. Piro, P. J. Carroll and E. J. Schelter, *Inorg. Chem.*, 2013, **52**, 5970-5977.
7. J. A. L. Wells, M. L. Seymour, M. Suvova and P. L. Arnold, *Dalton Trans.*, 2016, **45**, 16026-16032.
8. J. J. Zhang, C. L. Jian, Y. Gao, L. Wang, N. Tang and J. C. Wu, *Inorg. Chem.*, 2012, **51**, 13380-13389.
9. L. H. Tang, E. P. Wasserman, D. R. Neithamer, R. D. Krystosek, Y. Cheng, P. C. Price, Y. Y. He and T. J. Emge, *Macromolecules*, 2008, **41**, 7306-7315.
10. Y. Al-Khafaji, T. J. Prior, M. R. J. Elsegood and C. Redshaw, *Catalysts*, 2015, **5**, 1928-1947.
11. Y. Al-Khafaji, X. S. Sun, T. J. Prior, M. R. J. Elsegood and C. Redshaw, *Dalton Trans.*, 2015, **44**, 12349-12356.
12. T. J. Boyle, N. L. Andrews, M. A. Rodriguez, C. Campana and T. Yiu, *Inorg. Chem.*, 2003, **42**, 5357-5366.
13. J. J. Morris, B. C. Noll and K. W. Henderson, *Inorg. Chem.*, 2008, **47**, 9583-9591.
14. A. Walstrom, M. Pink and K. G. Caulton, *Inorg. Chem.*, 2006, **45**, 5617-5620.
15. D. M. Barnhart, D. L. Clark, J. C. Gordon, J. C. Huffman, R. L. Vincent, J. G. Watkin and B. D. Zwick, *Inorg. Chem.*, 1994, **33**, 3487-3497.
16. A. J. Wooten, P. J. Carroll and P. J. Walsh, *J. Am. Chem. Soc.*, 2008, **130**, 7407-7419.
17. J. R. Robinson, Z. Gordon, C. H. Booth, P. J. Carroll, P. J. Walsh and E. J. Schelter, *J. Am. Chem. Soc.*, 2013, **135**, 19016-19024.
18. J. A. Bogart, A. J. Lewis, M. A. Boreen, H. B. Lee, S. A. Medling, P. J. Carroll, C. H. Booth and E. J. Schelter, *Inorg. Chem.*, 2015, **54**, 2830-2837.
19. R. D. Shannon, *Acta Crystallogr A*, 1976, **32**, 751-767.

20. A. Vogler and H. Kunkely, *Inorg. Chim. Acta*, 2006, **359**, 4130-4138.
21. G. Mandel, R. P. Bauman and E. Banks, *J. Chem. Phys.*, 1960, **33**, 192-193.
22. J. R. Robinson, C. H. Booth, P. J. Carroll, P. J. Walsh and E. J. Schelter, *Chem-Eur J*, 2013, **19**, 5996-6004.
23. D. Werner, G. B. Deacon, P. C. Junk and R. Anwander, *Dalton Trans.*, 2017, **46**, 6265-6277.
24. W. M. Haynes, *Handbook of Chemistry and Physics: 93rd Edition*, Chemical Rubber Company, 93 edn., 2012.
25. G. Aylward; T. Findlay, *SI Chemical Data*, John Wiley & Sons, Australia, 6th edition edn., 2008
26. N. G. Connelly and W. E. Geiger, *Chem. Rev.*, 1996, **96**, 877-910.
27. T. Vent-Schmidt and S. Riedel, *Inorg. Chem.*, 2015, **54**, 11114-11120.
28. F. Nief, *Monogr. Ser. Int. Conf. Coord. Bioinorg. Chem.*, 2011, **10**, 405-424.
29. M. R. MacDonald, J. E. Bates, J. W. Ziller, F. Furche and W. J. Evans, *J. Am. Chem. Soc.*, 2013, **135**, 9857-9868.
30. C. M. Kotyk, M. E. Fieser, C. T. Palumbo, J. W. Ziller, L. E. Darago, J. R. Long, F. Furche and W. J. Evans, *Chem. Sci.*, 2015, **6**, 7267-7273.
31. B. H. Huang, B. T. Ko, T. Athar and C. C. Lin, *Inorg. Chem.*, 2006, **45**, 7348-7356.
32. B. Walfort, L. Lameyer, W. Weiss, R. Herbst-Irmer, R. Bertermann, J. Rocha and D. Stalke, *Chem-Eur J*, 2001, **7**, 1417-1423.
33. C. A. Ogle, B. K. Huckabee, H. C. Johnson, P. F. Sims, S. D. Winslow and A. A. Pinkerton, *Organometallics*, 1993, **12**, 1960-1963.
34. A. J. Wooles, D. P. Mills, W. Lewis, A. J. Blake and S. T. Liddle, *Dalton Trans.*, 2010, **39**, 500-510.
35. H. L. Yin, P. J. Carroll, J. M. Anna and E. J. Schelter, *J. Am. Chem. Soc.*, 2015, **137**, 9234-9237.
36. F. Bonnet, C. E. Jones, S. Semlali, M. Bria, P. Roussel, M. Visseaux and P. L. Arnold, *Dalton Trans.*, 2013, **42**, 790-801.
37. I. Palard, M. Schappacher, B. Belloncle, A. Soum and S. M. Guillaume, *Chem-Eur J*, 2007, **13**, 1511-1521.
38. M. Visseaux and F. Bonnet, *Coord. Chem. Rev.*, 2011, **255**, 374-420.
39. G. G. Skvortsov, M. V. Yakovenko, P. M. Castro, G. K. Fukin, A. V. Cherkasov, J. F. Carpentier and A. A. Trifonov, *Eur J Inorg Chem*, 2007, 3260-3267.
40. F. Bonnet, A. R. Cowley and P. Mountford, *Inorg. Chem.*, 2005, **44**, 9046-9055.
41. S. M. Cendrowski-Guillaume, G. Le Gland, M. Nierlich and M. Ephritikhine, *Organometallics*, 2000, **19**, 5654-5660.

42. J. Kratsch, M. Kuzdrowska, M. Schmid, N. Kazeminejad, C. Kaub, P. Ona-Burgos, S. M. Guillaume and P. W. Roesky, *Organometallics*, 2013, **32**, 1230-1238.
43. N. Ajellal, D. M. Lyubov, M. A. Sinenkov, G. K. Fukin, A. V. Cherkasov, C. M. Thomas, J. F. Carpentier and A. A. Trifonov, *Chem-Eur J*, 2008, **14**, 5440-5448.
44. J. Jenter, G. Eickerling and P. W. Roesky, *J. Organomet. Chem.*, 2010, **695**, 2756-2760.
45. T. Arliguie, L. Belkhiri, S. E. Bouaoud, P. Thuery, C. Villiers, A. Boucekkine and M. Ephritikhine, *Inorg. Chem.*, 2009, **48**, 221-230.
46. J. Jenter, N. Meyer, P. W. Roesky, S. K. H. Thiele, G. Eickerling and W. Scherer, *Chem-Eur J*, 2010, **16**, 5472-5480.
47. N. Meyer, J. Jenter, P. W. Roesky, G. Eickerling and W. Scherer, *Chem. Commun.*, 2009, 4693-4695.
48. N. D. Harrold, Y. Li and M. H. Chisholm, *Macromolecules*, 2013, **46**, 692-698.
49. W. M. Ren, G. P. Wu, F. Lin, J. Y. Jiang, C. Liu, Y. Luo and X. B. Lu, *Chem. Sci.*, 2012, **3**, 2094-2102.

3. Synthesis and Reactivity Study of Saturated *N*-Heterocyclic Carbenes

3.1. Introduction

As shown in *Chapter 1*, the strategy of introducing anionic tethers to *N*-heterocyclic carbenes such as thiolate, [1, 2] alkoxide, aryloxide and amido groups,[3-5] allows the ligand to be better retained through its strong covalent bond to early transition metals and rare earth metals.[5]

She[6] and Hamilton[7] from the Arnold group synthesised a range of *β*-ketoimidazolium salts (**FG-a-d**) (**Scheme 3-2**). These unsaturated imidazolium salts with different substituents have shown interesting reactivity towards alkali metal triethylborohydrides ($MHBEt_3$, M = Na, K).

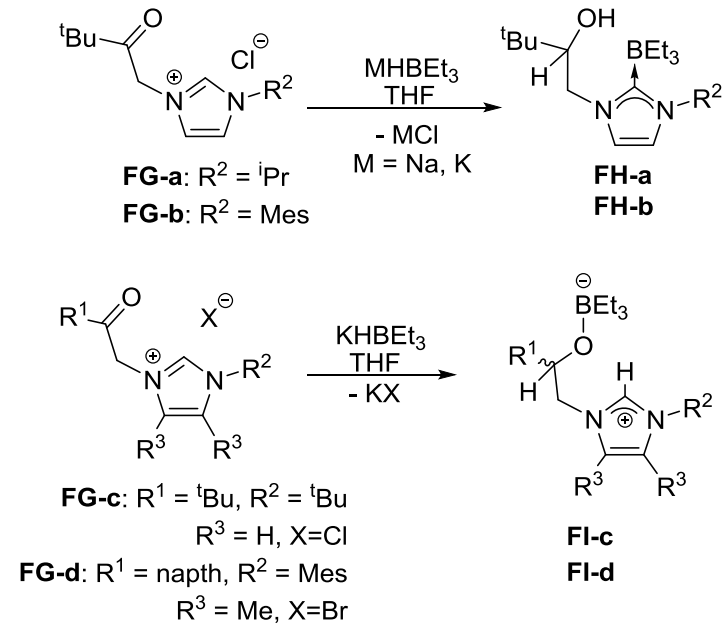

Scheme 3-1. Reactivity of imidazolium precursor with triethylborohydrides.

She[6] reported the reaction of **FG-a** (or **b**) with either $KHBEt_3$ or $NaHBEt_3$ which afforded the alcohol-functionalised carbene-borane adduct **FH-a** (or **b**), (**Scheme 3-1**). The ^1H NMR spectrum shows the reduction of the ketone and the deprotonation of the imidazolium group CH. Regardless of the number of equivalents of borohydride used or reaction temperature, complex **FH** is the only organic product formed.

However, Hamilton[7] reported that the reaction of **FG-c** (or **d**) with $KHBEt_3$ yielded a pale yellow solid, which was characterised as the imidazolium borates **FI-c** (or **d**) (**Scheme 3-1**). Complex **FI** shows the reduction of ketone bond by the formation of an alcohol-borate bond with the imidazolium CH intact. These observations show that the substituents on the N-arm greatly affect the reactivity.

To fully understand the influence of substituents on the reaction selectivity of these compounds, modifications on the R-groups and the electronic properties of the backbone are taken into consideration. Here in the first part of this chapter, saturated imidazolinium groups are introduced to the ligands to test the backbone influence on the reactivity and the mesityl groups are attached to the nitrogen atom to stabilise the molecule (**Scheme 3-2**). This part of work has been published in Dalton Trans.

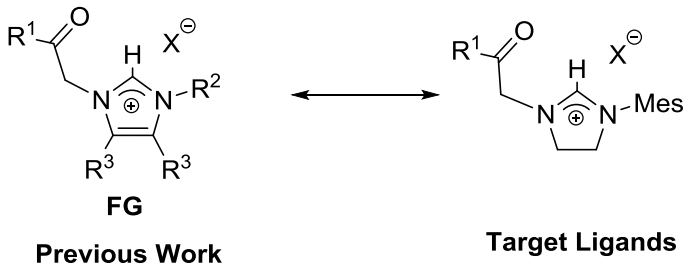

Scheme 3-2. Target ligands.

3.2. Ligand Synthesis

Firstly, diamine ($H_2NCH_2CH_2NHMes$) was synthesised through reaction of 2-bromoethylamine hydrobromide and 2,4,6-trimethylaniline in toluene for 12 hours. After distillation under reduced pressure (110 °C, 6 mbar), the diamine was then refluxed with trimethyl orthoformate to form N-mesitylimidazoline (**Scheme 3-3**).

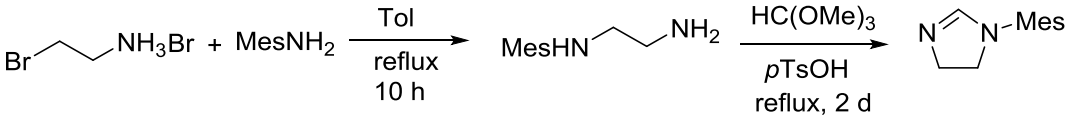

Scheme 3-3. Synthesis of N-mesitylimidazolene.

The reaction of N-mesitylimidazol(in)e with one equivalent of the respective halomethylketone derivative at 120 °C for 24h, afforded the products in decent yields (**38-a-f**, **Scheme 3-4**). A list of the previously synthesised ligands and their spectral data are summarised in this chapter to serve as a comparison in **Table 3-1**, **FG-a-d**.

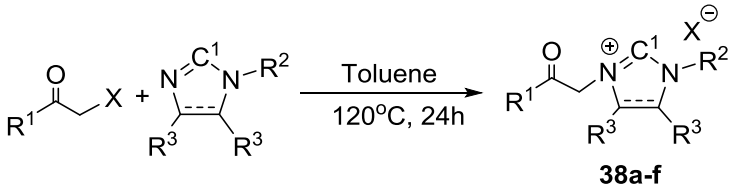

Scheme 3-4. Synthesis of *β*-ketoimidazol(in)ium salts.

Table 3-1. Spectral data of *β*-ketoimidazol(in)ium salts.

	R^1	R^2	R^3	X	^{1}H NMR δ(NC*H*N) ppm	^{13}C NMR δ(N*C*HN) ppm	Yield (%)
FG-a	^{t}Bu	^{i}Pr	H	Cl	10.53	137.3	80
FG-b	^{t}Bu	Mes	H	Cl	10.79	141.5	86
FG-c	^{t}Bu	^{t}Bu	H	Cl	10.01	137.2	93
FG-d	Napth	Mes	CH_3	Br	9.78	136.6	80
38e	^{t}Bu	Mes	H_2	Cl	9.68	137.8	83
38f	Napth	Mes	H_2	Cl	9.27	135.3	90

In the ^{1}H NMR spectrum, the resonances for the protons at the C1 (NC*H*N) position were observed at a range from 10.79 ppm to 9.27 ppm (**Table 3-1**). For imidazolium compounds (**FG-a-d**), the chemical shift of the C1 protons varies with the substitutional groups on both N-arms and C=C backbone. The saturated backbone of imidazolinium derivatives of **38e** and **38f** has greatly shifted protons, 9.68 ppm and 9.27 ppm respectively. The signal in the ^{13}C NMR for the C1 carbon (N*C*N) was also recorded at high chemical shift (**38e**: 137.8 ppm, **38f**: 135.3 ppm). These data show that the acidity of the C1 protons depends on the steric demands of the peripheral groups and the degree of saturation of the backbone.

From the comparisons with the literature and analysis of spectral data, the order of relative *p*K$_a$ of the imidazol(in)ium is estimated as follows. (**Figure 3-1**).

pKa: **FG-b > FG-a > FG-c > FG-d > 38e > 38f**

Figure 3-1. Estimated *p*K$_a$ order of *β*-ketoimidazol(in)ium salts **1**.

3.3. Reactivity of imidazolinium salts

3.3.1. **Reaction of 38e and 38f with $MHBEt_3$**

Treatment of either **38e** or **38f** with one equivalent of $NaHBEt_3$ or $KHBEt_3$ in THF yielded a colourless solution, which afforded white solid after filtration and the removal of volatiles under reduced pressure. (**Scheme 3-5**).

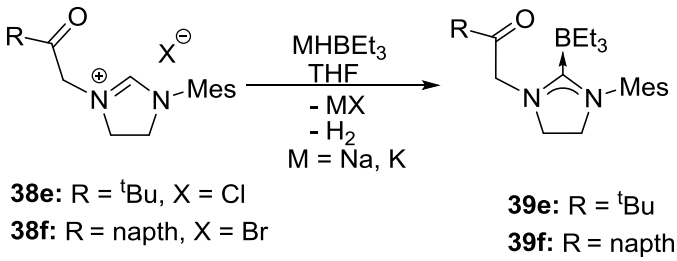

Scheme 3-5. The reaction of **38e** and **38f** towards $MHBEt_3$.

The ^{1}H NMR spectrum of **39e** (**Scheme 3-5**) contains no resonances higher than 7 ppm, which indicates the absence of the imidazolinium proton (9.68 ppm in **38e**). In addition, the α-keto methylene group appears as a sharp singlet at δ = 4.56 ppm (2H) which is different from that of the **38e** at 5.44 ppm, demonstrating that no reduction of the ketone has occurred. In spite of this, a triplet at 1.19 ppm (9H) and a quartet at 0.51 ppm (6H) show the presence of the borane ethyl groups. The ^{13}C NMR spectrum also shows a singlet at δ = 208.8 for the C=O and a broad multiplet at δ = 202.0 ppm for the carbene-borane carbon. The ^{11}B NMR spectrum contains a singlet at -14.1 (**39e**) and -13.9 ppm (**39f**).

X-ray quality crystals of both **39e (Figure 3-2)** and **39f** (**Figure 3-3**) were grown by slow diffusion of hexane into a concentrated toluene solution of the pure product at room temperature.

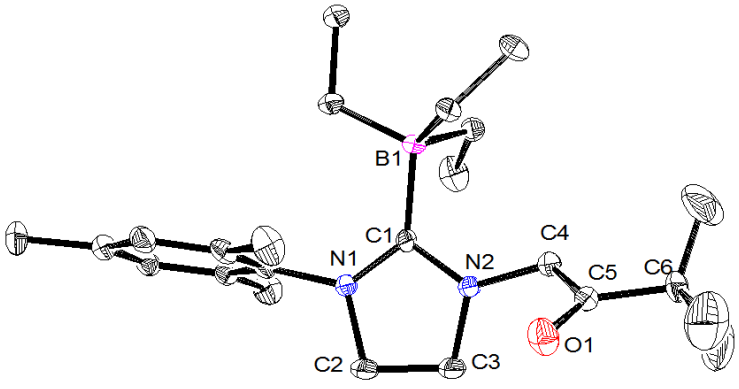

Figure 3-2. Representation of the molecular structure of complex **39e**. Thermal ellipsoids of the atoms are shown at 30% probability. All hydrogen atoms are omitted for clarity.

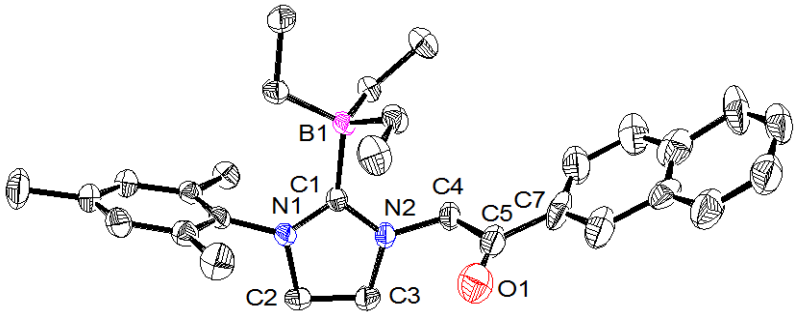

Figure 3-3. Representation of the molecular structure of complex **39f**. Thermal ellipsoids of all the atoms are shown at 30% probability. All hydrogen atoms are omitted for clarity.

The solid-state structures contain a short C=O bond of 1.217(6) Å (**39e**) and 1.208(5) Å (**39f**), indicating the unreacted ketone bond while the C-B bond lengths [**39e**: 1.659(5) Å, **39f**: 1.663(4) Å] fall in line with the reported range of the NHC-borane adducts (*ca*. 1.55-1.68 Å).[8]

Table 3-2. Selected bond lengths and angles of complex **39e** and **39f.**

	39e	**39f**
C1-B1	1.659(5)	1.663(4)
C1-N1	1.321(5)	1.331(4)
C1-N2	1.349(4)	1.345(4)
N2-C4	1.436(5)	1.446(4)
C4-C5	1.524(5)	1.503(5)
C5-O1	1.217(6)	1.208(5)
N1-C1-N2	107.8(3)	107.3(3)
N2-C4-C5	113.0(4)	103.1(2)
C4-C5-O1	119.5(4)	120.9(3)

Treatment of two equivalents of $KHBEt_3$ with **38e** in THF yielded a white suspension. After filtration and the removal of volatiles of the solution under reduced pressure, a colourless oil is obtained (**Scheme 3-6**).

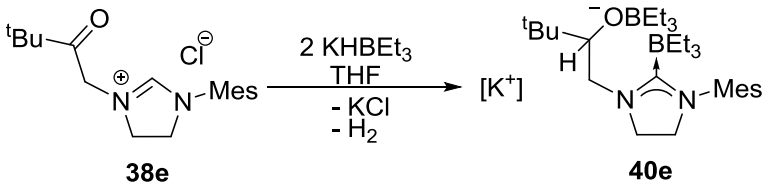

38e **40e**

Scheme 3-6. The reaction of **38e** towards two equivalents of $KHBEt_3$.

The ^1H NMR spectrum of the product contains one singlet at δ = 6.71 ppm which represents the protons on the mesityl group. The *α*-keto methylene groups disappeared while three multiplets at δ = 4.37 ppm (1H), 2.85 ppm (1H), and 2.56 ppm (1H) are observed which is

similar to those in **FI-d**, demonstrating the reduction of the ketone has occurred. Two multiplets at 1.82 ppm (12H) and 0.72 ppm (18H) show the presence of the borane ethyl groups. The ^{11}B NMR spectrum also shows two broad resonance at δ = 23.17 and 5.78 ppm, indicative of two BEt_3 groups of complex **40e**.

3.3.2. **Discussion of differences in the reactions with $KHBEt_3$**

The reactions of this set of six similar *β*-ketoimidazol(in)ium salts described above yield a range of different products depending on the N-atom substituents and on the backbone of carbene precursors. The products of these reactions are summarised in **Figure 3-4**.

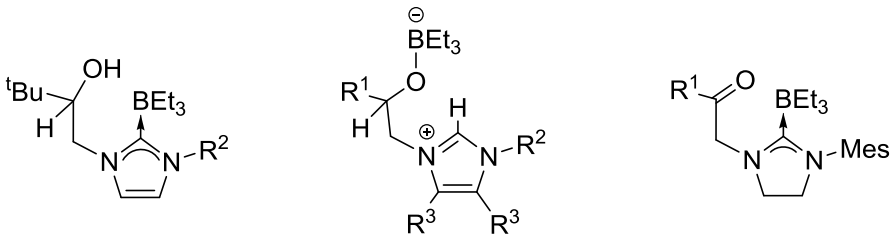

FH-a R^2 = ^{i}Pr
FH-b R^2 = Mes
FI-c R^1 = ^{t}Bu R^2 = ^{t}Bu R^3 = H
FI-d R^1 = nap R^2 = Mes R^3 = Me
39e R^1 = ^{t}Bu
39f R^1 = nap

Figure 3-4. Comparison of the products isolated from the reaction of imidazol(in)ium salts with alkali metal triethylborohydride.

The reaction with the borohydride $MBHEt_3$ with **FG-a-d** results in a reduction of the ketone and addition of the BEt_3 group. The product from **FG-a-b** is an alcohol-carbene-borane, while for **FG-c-d** is a boronate imidazolium compound. In contrast, the ketone in **38e-f** is unreacted, forming the ketone-carbene-borane **39e-f**. The pattern of these reactions does not simply follow a trend according to the relative pK_a of the imidazol(in)ium, which was estimated in **Figure 3-1**. It also depends on the steric demands of the peripheral groups and the backbone.

Compounds **FG-a-d** have the most acidic imidazolium CH group, arguing against the deprotonation of the imidazol(in)ium CH as the first step. Compounds **a-b** have lower steric crowding around the C1 position. These yield carbene-borane species of type **FA**. However, if either the sterics at the N1 position or the pK_a of the C1 proton are increased then the imidazolium borate species **FB** is favoured. With compounds **38e-f** (β-ketoimidazolinium), reduction of the ketone bond was not observed suggesting an alternative mechanism for non-aromatic heterocycles to yield the β-ketocarbene borane species **40e**.

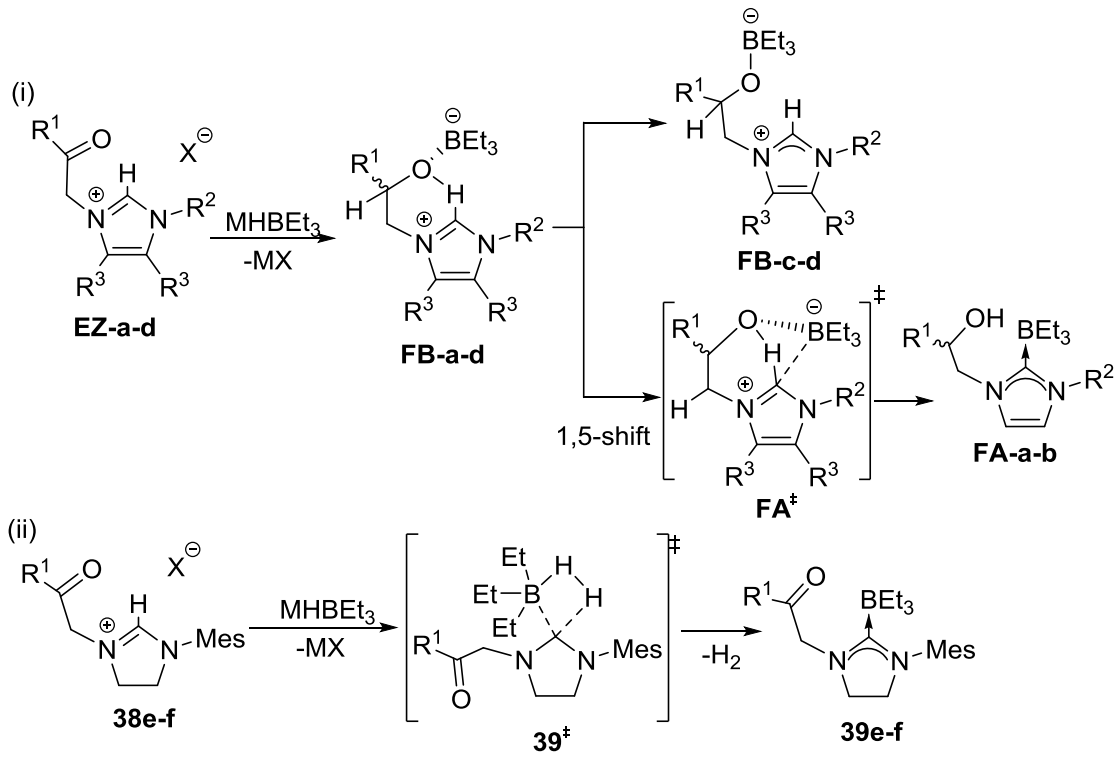

Scheme 3-7. Differences in the reactivity of imidazol(in)ium with $MHBEt_3$ (M = Na, K).

It is proposed that the unsaturated *β*-ketoimidazolium salts **FG-a-d** likely follow the pathway (i) shown in **Scheme 3-7**. Based on the reduction of the ketone, the zwitterionic imidazolium borate **FBa-d** is formed. If the N-R^2 substituent is small or the pK_a of the C1 proton is low (**Table 3-1**), the imidazole borate product of complex **FI-d-d** is formed. Thereafter, when the steric bulk of the R^2 position is sufficiently high to prevent coordination of the BEt_3 fragment in **FA**‡, a 1,5-sigmatropic shift of the highly acidic imidazolium proton to oxygen atom forms a less acidic OH bond and facilitates the formation of the stronger carbene-borane bond, affording complex **FH-a-b** as final products.

The saturated β-ketoimidazolinium salts **38e-f** likely follow pathway (ii) shown in **Scheme 3-7**. It is proposed that the formation of **39e-f** is achieved *via* the addition of $[HBEt_3]^-$ moiety to C1-H bond, forming intermediate (**39**‡) in which the carbon atom adopts a tetrahedral hybridisation. Followed by the elimination of H_2 gas, carbene-borane adducts **39e-f** are obtained. It is clear to see from the intermediate (**39**‡) that the formation of the imidazoline-based transition state may cause the loss of aromaticity of the imidazolinium system. This is expected to have a higher energy barrier for **FG-a-d** than for **38e-f** and therefore is disfavoured.

These results show that the differences between the backbone or substitution groups of the ketoimidazol(in)ium greatly affect the reactivity of the compounds.

3.4. Reaction of imidazolinium salts with MYN"$_4$ (M = Li, K)

It has been shown that after the deprotonation of ketone-tethered proligands with bases such as NaN", the resulting Na-enolate complex can form transition metal (**FJ**, **Scheme 1-38**)[9] and rare earth metal (**FK**, **Scheme 3-8**)[10] enolate-tethered NHC complexes.

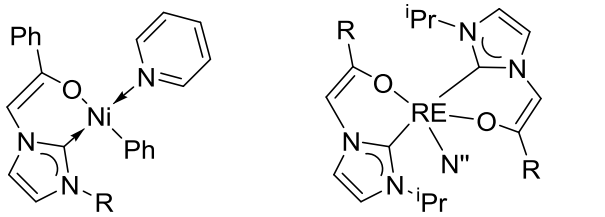

Scheme 3-8. Reported examples of enolate-tethered NHC complexes.

In a modification of a literature procedure,[9, 10] the reaction of **38e** with one equivalent of MYN"$_4$ (M = Li, K) in THF at room temperature yielded a white suspension. After workup, a white solid was obtained (**Scheme 3-9**).

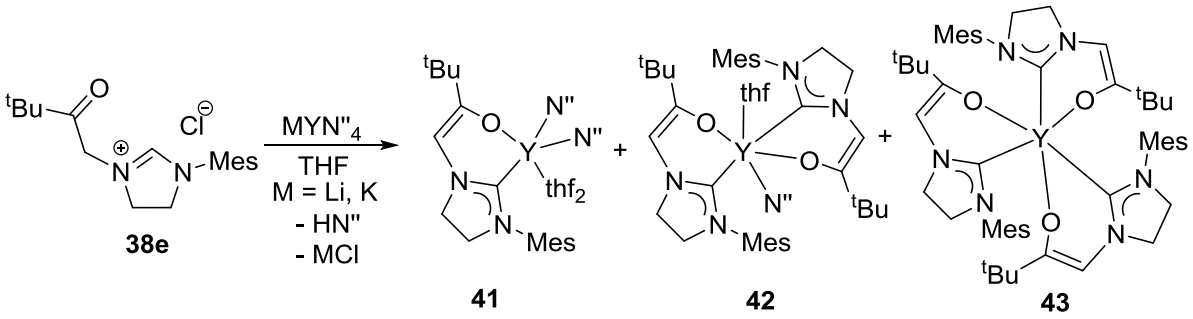

Scheme 3-9. Attempted synthesis of yttrium complexes.

The ^{1}H NMR spectrum of the product shows the disappearance of the resonances for **38e** and the successful deprotonation of the C1 atoms. From the ^{1}H NMR spectrum, three major different sets of resonances for the ligand are observed, which makes it difficult to assign. However, the new resonances for the alkenyl-CH are seen as three major singlets at δ = 6.31, 6.34 and 6.42 ppm respectively. The ^{29}Si NMR spectrum displays broad singlets at -14.6 ppm and two smaller singlets at -8.7 and 6.3 ppm. All these spectral data suggest the formation of mono-, bis- and tris-enolate-tethered NHC complexes **41-43** (**Scheme 3-9**). These complexes showed similar solubility properties and the attempts to isolate pure form of these products through recrystallisation are unsuccessful so far.

3.5. Synthesis of p-aryloxy-tethered imidazolinium salt H_2LX

As discussed in **Chapter 1.5**, due to the mismatch of 'soft' σ-donors (NHCs) and 'hard' Lewis acidic RE elements, NHCs with different tether groups have been developed to bind these metals.[4] The use of a variety of functional groups to tether NHCs to the metal centre has allowed them to stabilise the complexes as well as to bring in rich reactivity in C-H activation,[11] small molecule activation[12] and homogeneous catalysis.[13] Amongst these ligands, alkoxy- and aryloxy- tethers are of great interests as the oxygen anions tend to bound with RE ions to form strong σ bonds which help to stabilise the labile NHC-RE bonds.[14]

Max McMullon from the Arnold group synthesised a series of *ortho*-aryloxy-tethered NHC ligands (**FL**, **Scheme 3-10**) following a procedure reported by Wang and co-workers.[15] These ligands contain an unsaturated imidazole backbone and have been successfully used to synthesise transition metal and RE metal NHC complexes.[16]

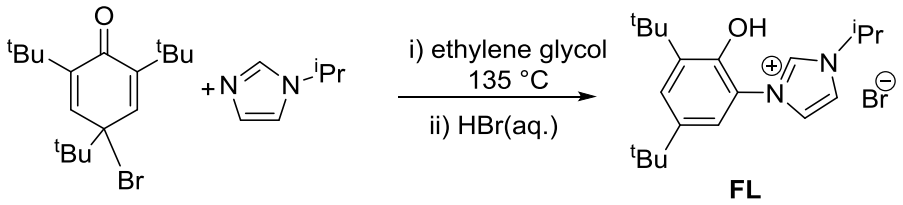

Scheme 3-10. The synthesis of proligand **FL**.

In this part, a *para*-aryloxy-tethered imidazoline ligand is synthesised by two different routes and its reactivity is studied.

Route A:

Following a modification of the route reported by Wang and co-workers,[15] 4-bromo-2,4,6-tri-*tert*-butyl-2,5-cyclohexadien-1-one, N-mesitylimidazoline and ethylene glycol were mixed and then stirred in an N_2 filled Schlenk at 135 °C for 8 hours. After workup and subsequent recrystallisation from chloroform/THF solution, the imidazolinium salt of H_2LBr (**44**, **Scheme 3-11**) was obtained in 15% yield.

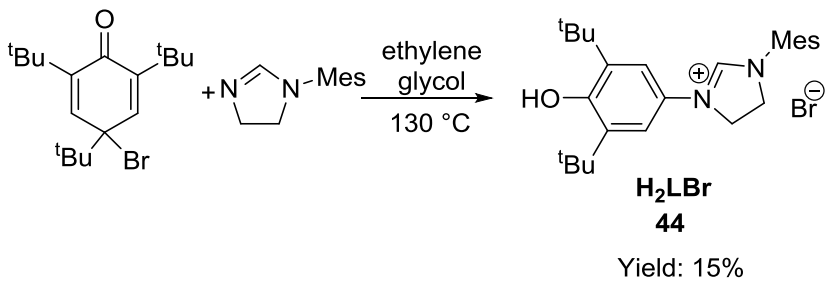

Scheme 3-11. Route **A** for the synthesis of proligand H_2LBr.

The yield was slightly lower than those reported examples.[15] The ^{1}H NMR spectrum of the ligand contains a singlet at 9.55 ppm which can be assigned as the imidazolium proton. Two singlets at 7.30 and 6.97 ppm indicate the phenyl protons while two triplets (4.84 ppm, J = 12.5 Hz, 2H; and 4.51 ppm, J = 12.5 Hz, 2H) are ascribed for the methylene protons on the imidazolinium backbone.

The low yield is due to the formation of various side products amongst which have been reported as 2,4,6-tri-tert-butylphenol (*ca*. 30%), acidified N-substituted imidazolines (*ca.* 20%) and 2-(1,3,5-tri-tert-butyl-4-oxo-2,5-cyclohexadien-1-oxy)ethanol (*ca.* 10%).[15]

An analysis of the mixture of route A also shows a *ca*. 5% yield of the *ortho*-substituted **FL**. Given the similarity of the starting reagents, the two different mechanisms are most likely due to the slight difference of the electron configuration of the backbone of imidazole and imidazoline groups.

Given the low yield of the ligand, another possible pathway was investigated.

Route B:

The synthesis of *ortho*-aryloxy-tethered NHC ligands was reported in 2004 by Grubbs *et al*.[17, 18] Followed by a modified preparation as shown in **Scheme 3-12**, the *para*-substituents **45** (H_2LCl) can be synthesised with an overall yield of *ca*. 20% after several steps of organic synthesis.

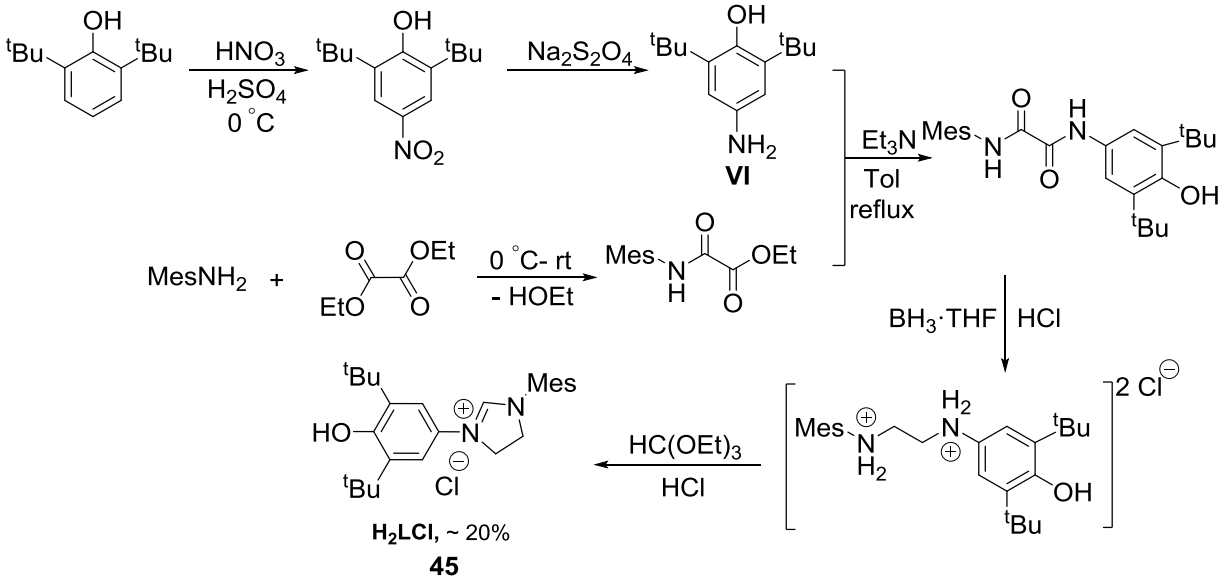

Scheme 3-12. Route B for the synthesis of proligand H_2LCl.

Despite its higher yield of the final product through reactions in route B, the synthesis of the ligand via route A is simpler and the purification is straightforward. Route B is a good method to prepare for ligands with different substitutional groups.

When an aqueous solution of an excess of KPF_6 is added to a chloroform solution of imidazolinium bromide H_2LBr, the product **46** can be obtained through a flash silica column by using DCM/acetone at 9:1 ratio. (**Scheme 3-13**).

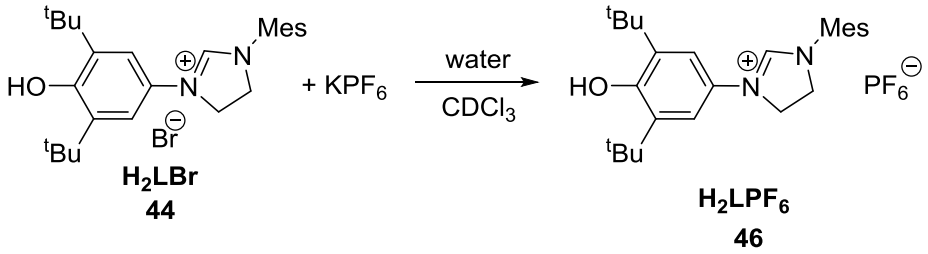

Scheme 3-13. Synthesis of proligand H_2LPF_6.

Crystals of complex **46** are obtained by slow evaporation of a concentrated chloroform solution. The solid-state structure and the selected bond lengths are shown in **Figure 3-5**. In the crystal structure, the C1-N1 and C1-N2 bonds have a similar bond length of 1.293(3) Å and 1.299(4) Å, respectively.

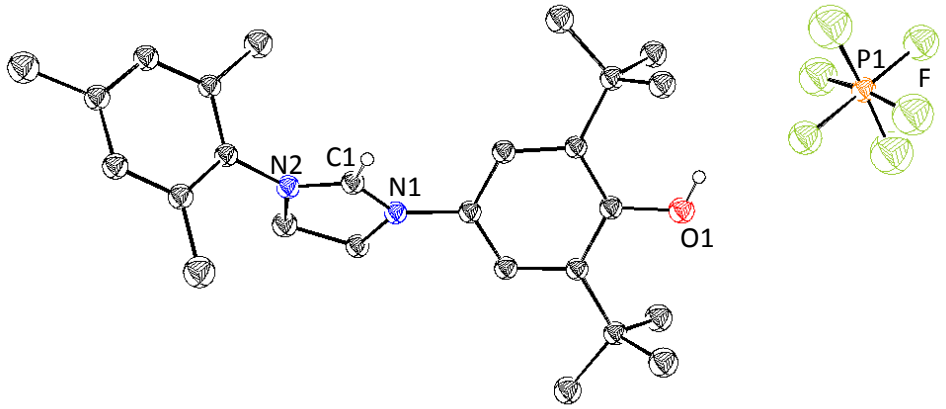

Figure 3-5. Solid-state structure of complex **46**, H_2LPF_6 (displacement ellipsoids are drawn at 30% probability). All hydrogen atoms except on C1 and O are omitted for clarity. Selected bond lengths: C1-N1: 1.293(3) Å, C1-N2: 1.299(4) Å.

3.6. Synthesis of [NaL]$_n$ complex

Treatment of the imidazolinium salt H_2LX (X = Br and PF_6^-) with two equivalents of NaN" in THF, affords a pale yellow solution. After the removal of solvents and volatiles, a colourless solid of complex **47** is obtained at a yield of 80% (**Scheme 3-14**). In the ^{1}H NMR spectrum of the solid are similar to that of complex **47**, where two singlets at δ = 7.82 and 7.01 ppm are assigned to the protons on the two phenyl rings and the two methylene groups on the imidazoline are as triplets at 4.05 and 3.58 ppm, respectively. Two methyl and *tert*-butyl groups are observed with slightly different resonances when compared to the potassium counterpart of complex **47**. However, in the ^{13}C NMR spectrum, the $C_{carbene}$ of **47** is shown as a singlet at a lower frequency of δ = 233.7 ppm when compared to the potassium counterpart **48** (**Scheme 3-15**).

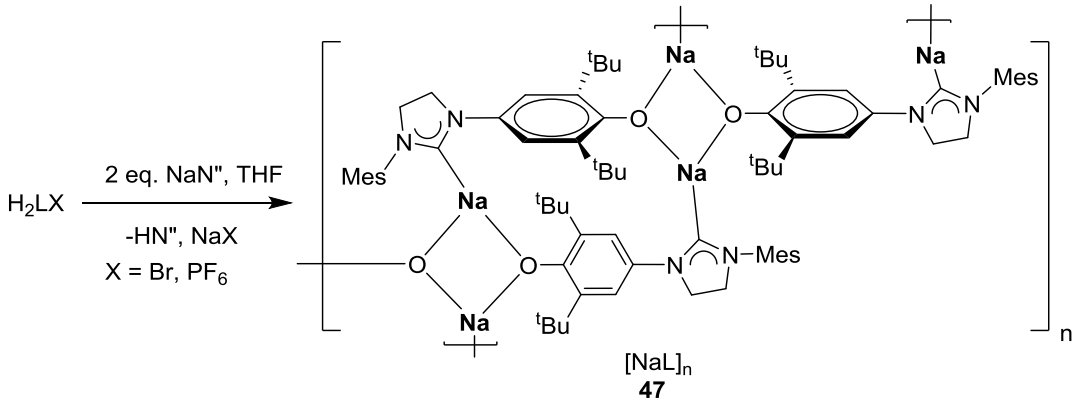

Scheme 3-14. Reaction of H_2LX (X = Br, PF_6) with NaN".

Crystals of complex **47** which were suitable for single crystal X-ray analysis were grown from the concentrated THF solution at room temperature by Dr Catherine Weetman from the Arnold group. The solid-state structure is shown in **Figure 3-6** while selected bond lengths (Å) and angles (°) are provided in **Table 3-3**.

In the solid-state structure, each Na^+ ion is bridged by two phenol oxygen atoms and bonded with one NHC, forming a near-planar trigonal three coordination configuration. This shows a solvent-free structure which is different from complex **48** where two THF molecules are incorporated to give a coordination number of five to the Na^+ centre. The Na-$C_{carbene}$ bond of 2.555(4) Å is 0.1 Å longer than the reported value of 2.451(4) Å in $[Na(IPr)_2][Mg\{N(SiMe_3)_2\}_3]$, (IPr = 1,3-bis(2,6-di-isopropylphenyl)-imidazol-2-ylidene)).[19]

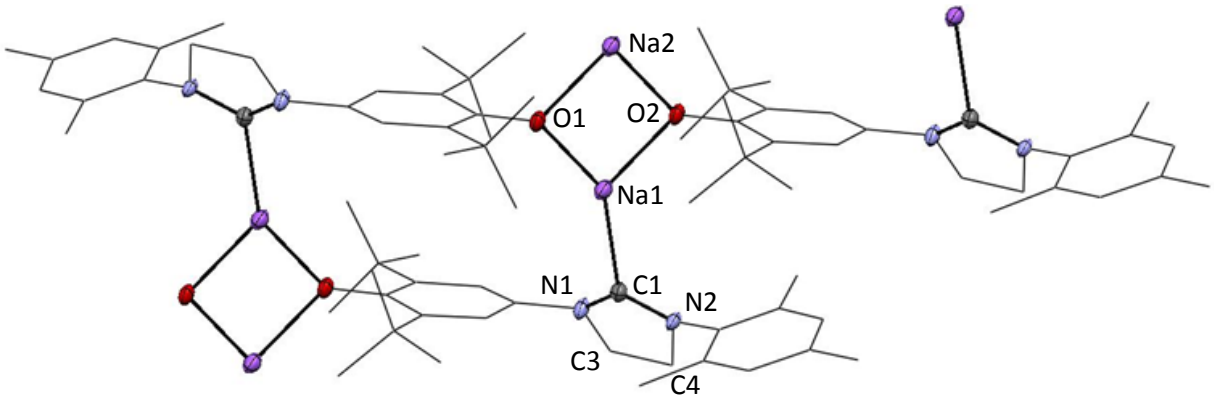

Figure 3-6. Solid-state structure of complex **47** with thermal ellipsoids drawn at 30% probability. All hydrogen atoms are omitted for clarity.

Table 3-3. Selected bond lengths (Å) and angles (°) of **47**.

Bonds	Length (Å)	Angles	°
Na1-C1	2.555(4)	O1-Na1-O2	87.10(10)
Na1-O1	2.243(3)	Na1-O1-Na2	92.90(10)
Na1-O2	2.275(3)	N1-C1-Na2	121.2(3)
C2-C3	1.524(5)	N1-C1-N2	105.9(3)

3.7. Synthesis of $[KL(thf)_2]_n$ complex

Treatment of the imidazolinium salt H_2LX (X = Br and PF_6^-) with two equivalents of KN" in THF affords a pale yellow solution (**Scheme 3-15**).

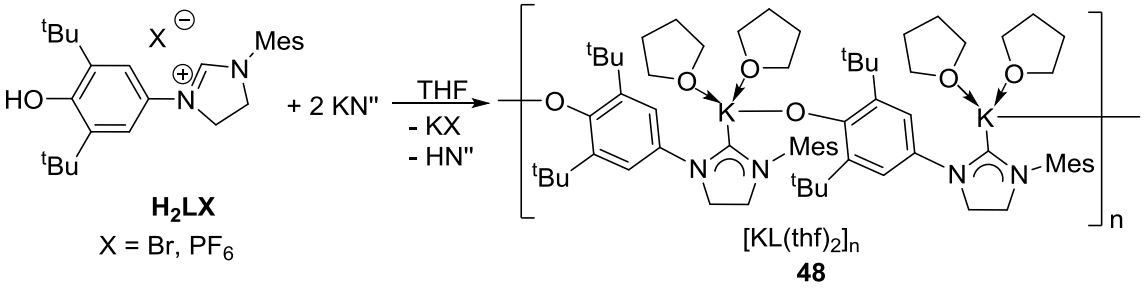

Scheme 3-15. The reaction of H_2LX towards KN".

The ^{1}H NMR spectrum shows a full consumption of the starting material as no imidazolinium-CH protons is observed. In the ^{1}H NMR spectrum, two singlets at δ = 7.79 and 6.93 ppm are assigned to the protons on the two phenyl rings. The two methylene groups on the imidazolinium are displayed as triplets at 4.10 and 3.68 ppm, respectively. Two *ortho*-methyl groups are shown at 2.26 ppm while the *para*-methyl is seen at 2.31 ppm. The *tert*-butyls are recorded at δ = 1.81 ppm. In the ^{13}C NMR spectrum, the $C_{carbene}$ is shown as a singlet at δ = 236.3 ppm, which is at higher frequency compared to the δ = 196.8 ppm resonance in *ortho*-

substituted iridium analogue [K][{OCO}Ir(cod)], (OCO = 1,3-di(2-hydroxy-5-*tert*-butylphenyl)imidazolyl; cod = 1,5-cyclooctadiene).[20]

Single crystals of complex **48** were grown by slow diffusion of hexane into the THF solution at room temperature (**Figure 3-7**). The selected bond lengths and angles are provided in **Table 3-4**. This is the first characterisation of the *para*-phenolate tethered NHC complex of potassium.

In the solid-state structure of complex **48**, each K^+ ion is the centre is four-coordinate which is achieved by bonding to two THF molecules, one phenyl oxygen atom and NHC-carbenic carbon, displaying a distorted tetrahedral configuration. The polymer chain forms a two-dimensional zig-zag shape. The bond length of K-$C_{carbene}$ is 2.968(4) Å which falls in the reported range of 2.844(3) Å in K[{:C[N(2,6-^{i}Pr$_2$C$_6$H$_3$)]$_2$(CH)C}$_2$Mn(Mes)(thf)]·THF[21] and 3.048 Å in [KOCMe$_2$CH$_2$(:C{NCHCHN^{i}Pr})][22]. The terminal K-O_{Ph} bond length of 2.493(3) Å is shorter than those bonds in the phenolate-bridging complex **2^P** and **3^P** in **Chapter 2.2**.

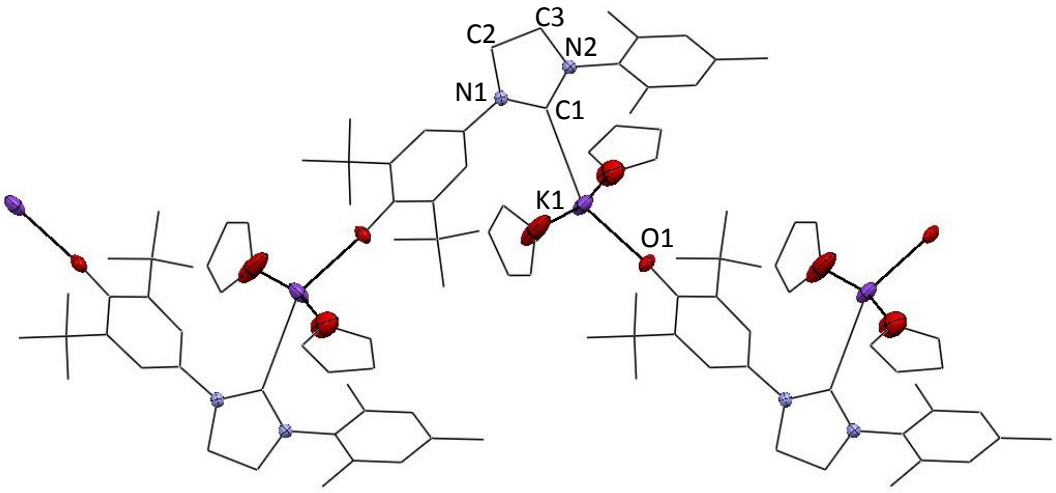

Figure 3-7. Representation of the molecular structure of complex **48**. Thermal ellipsoids of non-carbon atoms are shown at 30% probability. All hydrogen atoms are omitted for clarity.

Table 3-4. Selected bond lengths (Å) and angles (°) of complex **48**.

K1-C1	2.968(4)	C2-C3	1.522(6)
K1-O1	2.493(3)	K1-O2	2.731(5)
C1-N1	1.343(5)	K1-O3	2.699(5)
N1-C1-N2	105.9(4)	C1-N2	1.351(5)
C1-K1-O1	151.02(12)		

Treatment of the imidazolinium salt H_2LBr with two equivalents of KBn (Bn = benzyl) in THF, affords a red solution after being stirred for 4 hours. The ^{1}H NMR spectrum of the product indicates a mixture of several products among which *ca*. 70 % is identified as

potassium complex **48** (**Scheme 3-16**). After the removal of volatiles under reduced pressure, THF is added to extract the solid. The THF solution is then allowed to evaporate in a vial layered with hexane. After a week, colourless crystals of the side product were isolated and characterised as a ring opening product, complex **48**, with a yield of *ca.* 10%.

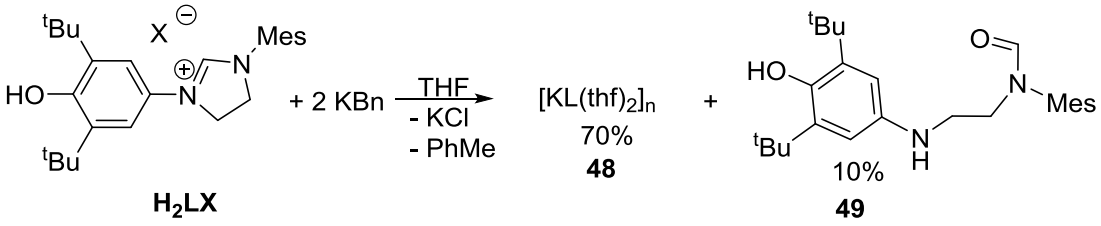

Scheme 3-16. The reaction of H_2LX towards KBn.

The solid-state structure of complex **49** reveals the C1-N2 bond of the ligand has been cleaved, where a ring opening product containing an N-H bond on the N atom and an aldehyde group to the carbon atom is formed. The C1-O2 bond length of 1.230(5) Å confirmed the aldehyde functional group. The relatively shorter C1-N1 bond is considered as a result of the electron delocalisation on the C=O bond. It is proposed that the O atom of the aldehyde group may either come from the trace amount of O_2 in the glovebox or the water in the ligand.

The structure of complex **49** confirms ring opening reaction of the imidazoline group. Given the strength of the C-N bond in aromatic heterocycles (133 kcal/mol estimated in pyridine),[23] the cleavage of the C-N bonds in aromatic heterocycles has been regarded as one of the most difficult cases of ring opening. The reported cases are either involved with transition metal[24, 25] or RE (Sc and Y) alkyl complexes[26]. This result provides a new example of imidazoline ring opening reaction mediated by alkali metal complex.

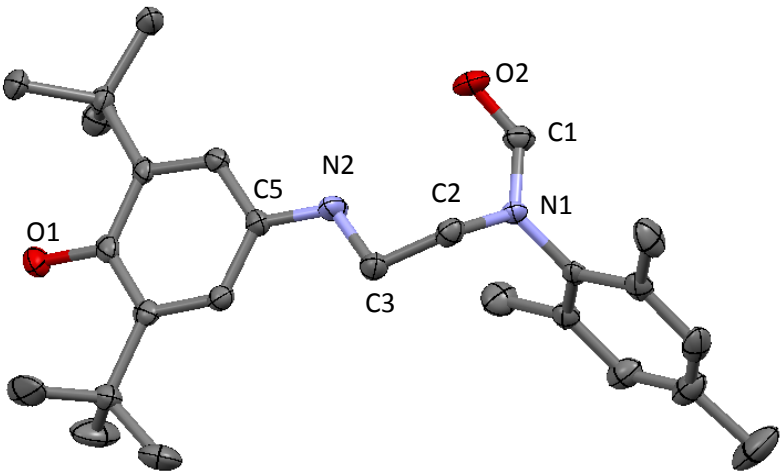

Figure 3-8. Representation of the molecular structure of complex **49**. Thermal ellipsoids of are shown at 30% probability. All hydrogen atoms are omitted for clarity.

Table 3-5. Selected bond lengths (Å) and angles (°) of complex **49**.

C1-O2	1.230(5)	C2-C3	1.499(5)
C2-N1	1.440(5)	C5-N2-C3	120.4(3)
C1-N2	1.337(5)	O2-C1-N2	125.3(4)
C3-N2	1.480(5)	C4-N1-C2	123.1(4)

3.8. Synthesis of $YL_3(KCl)_3(thf)_6$

A pyridine solution of three equivalents $[KL]_n$ was slowly added to a pyridine solution of one equivalent of $YCl_3(thf)_2$ and was left to stir for 8 hours. After the removal of volatiles and followed by washing with hexane, the product **50** was then isolated by filtration as a white powder (**Scheme 3-17**).

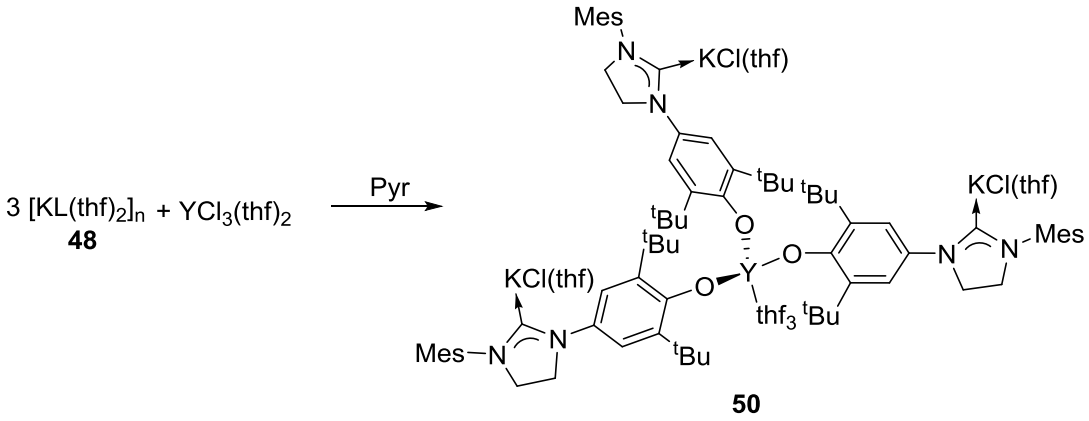

Scheme 3-17. Synthesis of complex **50**, $YL_3(KCl)_3(thf)_6$.

The ^1H NMR spectrum shows two singlets at 7.86 and 6.90 ppm which is slightly shifted compared to resonances of 7.79 and 6.93 ppm in complex **47**. The similar trend is also observed for imidazolinium backbone protons which are observed as broad multiplets at 3.94 and 3.68 ppm. The *meta*-methyl groups remained at 2.26 ppm while the *para*-methyls shifted from 2.31 ppm in complex **47** to 2.18 ppm. The *tert*-butyl groups also shifted to a higher frequency to 1.91 ppm. In the ^{13}C NMR spectrum, the carbene carbon of **47** at $\delta = 236.3$ ppm is no longer present while a singlet resonance at $\delta = 238.2$ ppm could be ascribed for the $C_{carbene}$ of the YL_3 complex **50**. However, there are also several small peaks around the singlet, which could be resulted from the different coordination of the KCl salts in the dimerised or polymerised NHCs. The elemental analysis of complex **50** shows a low percentage of C and H, which may due to the KCl salt incorporation in the complex. Based on this analysis, the molecular formula of complex **50** is calculated as $YL_3(KCl)_3(thf)_6$.

Recrystallisation of this product from THF/hexane mixed solution ended up with the gradual precipitation of KCl salts and no suitable single crystals for the desired product was obtained.

This might due to the labile carbene groups which have various coordination modes to metal ions as observed in its K and Na complexes.

These types of binding of the labile NHC groups are observed in cerium complexes obtained by the oxidation of CeL_3 (L = $[OCMe_2CH_2(1\text{-}C\{NCH{=}CHN^iPr\})]^-$) complexes (**Scheme 1-42**, **Chapter 1**).[27] In the structure of **DU** (**Scheme 3-18**), the cerium cation is coordinated by two bidentate ligands and two monodentate ligands, in which the NHC groups are unbound to the cerium atom.

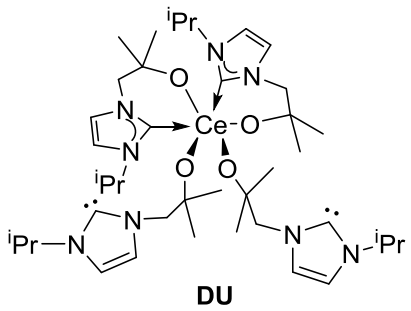

DU

Scheme 3-18. The reported structure of Ce^{IV} NHC complex.

3.9. Attempted synthesis of CeL_3

The treatment of a THF solution of **47** with a THF suspension of 1/3 equivalent of $CeCl_3(thf)_2$, affords a yellow-brown solution with white precipitate after stirring for 8 hours. The mixture was then filtered to afford a clear solution. After the removal of solvents under reduced pressure, hexane was added to precipitate all the products as a pale yellow solid of complex **51** (**Scheme 3-19**). The compounds formed were sensitive to moisture and air. Further workup procedures ended up with the decomposition of the product which caused a colour change from pale yellow to red. The ^1H NMR of the product showed two sets of resonances which suggested two different types of products formed. Attempts to purify the products caused further decomposition.

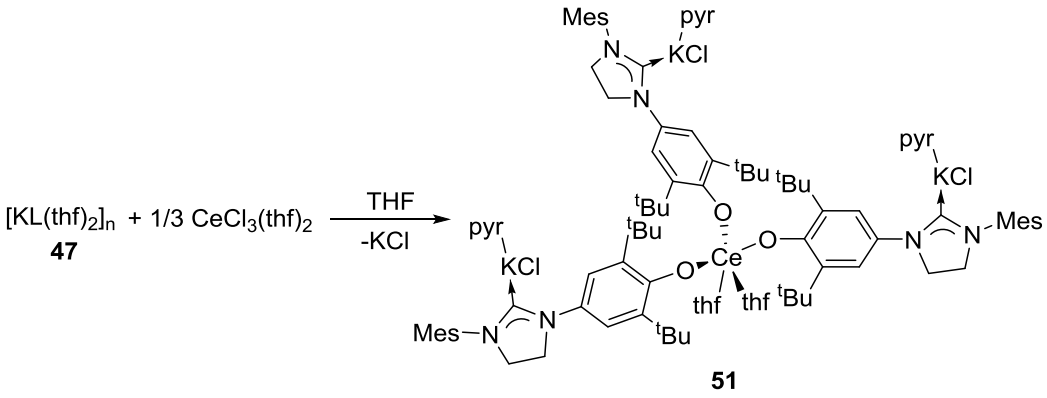

51

Scheme 3-19. Attempted synthesis of Ce complexes.

3.10. Synthesis of LYCp₂

By using a similar approach reported by the Arnold group of making cyclopentadienyl RE NHC complexes,[28] the reaction of $[KL(thf)_2]_n$ with one equivalent of YCp_3 in THF was carried out (**Scheme 3-20**). After the mixture was heated at 50 °C in an oil bath for 8 hours, the colourless precipitate of KCp was formed and the suspension was then filtered to remove the solid. Volatiles were removed under reduced pressure to afford the complex **52** (**Scheme 3-20**) as a beige powder with a yield of 57%.

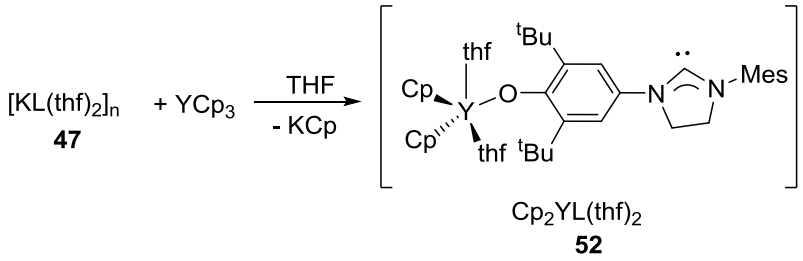

Scheme 3-20. Synthesis of $LYCp_2$.

The ^1H NMR spectrum of the product shows two singlets for phenyl protons at δ = 7.13 and 6.92 ppm. The Cp groups are observed at δ = 6.35 ppm with an integral of 10 protons which show two Cp groups in each molecule. The ^{13}C NMR spectrum also displays a singlet at δ = 216.8 ppm which is accountable for the carbene carbon. However, attempts to grow single crystals of these complexes from THF and pyridine and by different methods were not successful and resulted only in the formation of microcrystalline materials.

3.11. Reactivity of $YL_3(KCl)_3(thf)_6$ towards boranes

As discussed in **Chapter 1**, NHCs are Lewis base and thus can react with Lewis acid to form an acid-base adduct. The first half of this chapter has shown the formation of NHC-borane adducts by reacting NHC precursor with alkali metal triethylborohydride ($MHBEt_3$, M = Na, K) (**Scheme 3-5**).

The Arnold group have previously reported the different chemistry between the bound and unbound carbenes in complex **DU**. The treatment of CeL_4 with borane, 9-BBN (9-borabicyclo[3.3.1]nonane), affords the carbene-borane adduct $[CeL_2(L\text{-}9\text{-}BBN)_2]$ (**DV**, **Scheme 3-21**), which has been characterised by ^{1}H NMR spectroscopy and single crystal X-ray crystallography.[17]

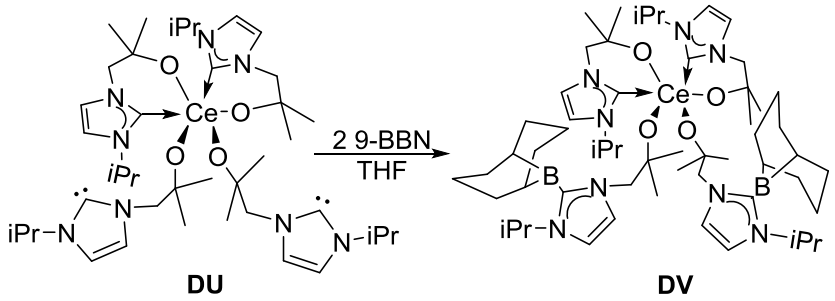

Scheme 3-21. Reported reaction of Ce NHC complexes towards boranes.

In order to test the bonding of the NHC groups in complex **50**, a series of reactions were carried out with boranes, such as $BH_3{\cdot}SMe_2$, 9-BBN and BPh_3.

Treatment of complex **50** with two equivalents of $BH_3{\cdot}SMe_2$ in THF yielded a cloudy suspension instantly (**Scheme 3-22**). After the removal of KCl salts and followed by the removal of volatiles under reduced pressure, a pale yellow oily paste was obtained. The ^{1}H NMR spectrum of complex **53** shows a shift of the phenyl protons to a higher frequency to δ = 7.37 and 6.74 ppm when compared to those in complex **50**. One of the backbone CH_2 group is observed at 3.91 ppm as a triplet while the other set of resonances overlap with the THF solvent at 3.56 ppm. Slightly shifted resonances of protons are observed for the *ortho*- and *para*-methyl groups at 2.13 and 2.10 ppm, respectively. The *tert*-butyl groups showed a shift from 1.91 ppm to 1.75 ppm. The ^{13}C NMR spectrum also showed the consumption of starting carbene complex where no high-frequency $C_{carbene}$ resonance could be detected. This might be due to the coupling of the quadrupolar B atom to $C_{carbene}$ atom which broadens the signal in the ^{13}C spectrum. The signal for boron atom is observed as a broad singlet at -35.6 ppm in the ^{11}B NMR spectrum.

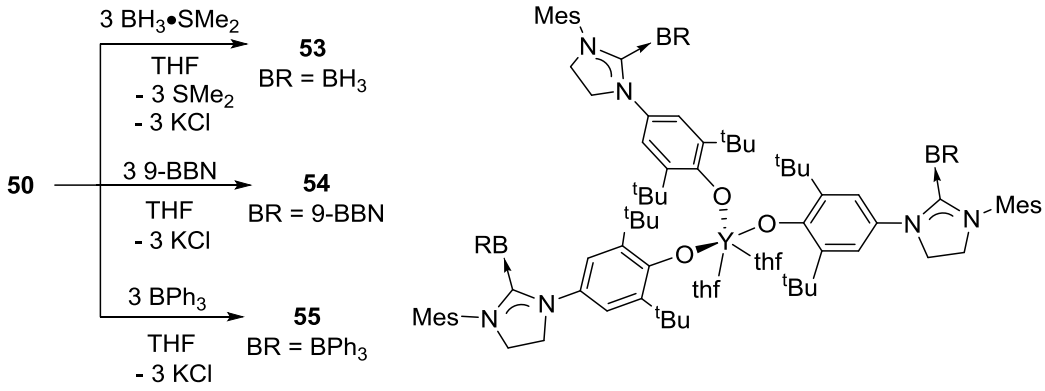

Scheme 3-22. Reactivity of complex **50** towards boranes.

By following the same procedure of making complex **53**, the reaction of complex **50** with three equivalents of 9-BBN affords the corresponding complex **54**. This complex displays phenyl protons at δ = 7.29 and 7.02 ppm in the ^{1}H NMR spectrum. The CH_2 groups of the imidazolinium backbone have shown two triplets at δ = 4.73 (t, *J* = 10.8 Hz, 6H) and 4.27 ppm (t, *J* = 10.8 Hz). This NHC-borane adduct displays a broad singlet at δ = -1.02 ppm in the ^{11}B NMR spectroscopy which is at a higher frequency compared to that of δ = -15.4 ppm in complex **DV** (**Scheme 3-21**).

Treatment of complex **50** with three equivalents of BPh_3 in THF yielded a white suspension from which a white solid was obtained after the removal of salts and volatiles. The ^{1}H NMR spectrum of complex **55** shows multiple shifts of the phenyl protons from δ = 7.54 to 6.29 ppm which can be ascribed to the phenyl rings. The backbone CH_2 groups display resonances to a lower frequency to δ = 3.45 and 3.10 ppm. A similar trend is also observed for the *tert*-butyl groups which show resonances at 1.21 ppm. In the ^{13}C NMR spectrum of this complex, the resonance of the carbon of $C_{carbene}$-B bond could not be identified. The ^{11}B NMR spectrum shows a broad singlet at δ = 4.93 ppm for the NHC-borane adduct.

Attempts to grow single crystals of these complexes from various solvents (THF, benzene and toluene) and by different methods were not successful and resulted only in the formation of microcrystalline materials.

However, after the hydrolysis of the complex **55** (**Scheme 3-23**), crystals of the NHC-borane adduct complex **56** were grown from a concentrated THF solution at room temperature.

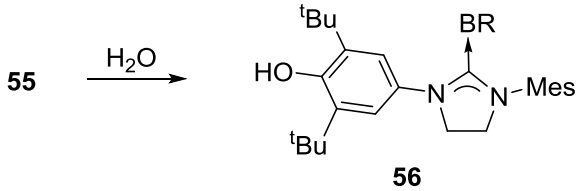

Scheme 3-23. Hydrolysis of the complex **55**.

The solid-state structure and selected bond length (Å) and angles (°) are provided in **Figure 3-9**. The crystal structure of **56** displays a P2(1)/c symmetry with four molecules in the unit cell. The C1-B1 bond length is 1.658(2) Å, which is comparable to those in the carbene-borane adducts: 1.667 Å in $Et_3BC(NMesCH)_2$[29] (**BO**, **Scheme 1-24**) and 1.659(5) Å for complex **39e** and 1.663(4) Å for **39f** (**Table 3-2**).

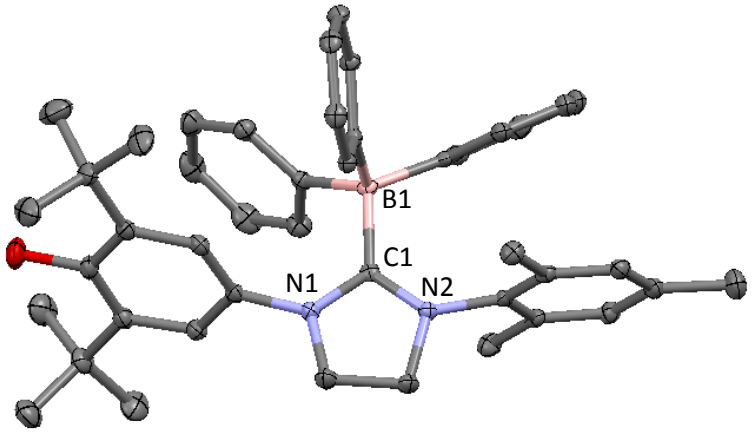

Figure 3-9. Solid-state structure of complex **56**, $HLBPh_3$. Thermal ellipsoids are shown at 30% probability. All hydrogen atoms and solvents are omitted for clarity. Selected bond lengths: C1-B1: 1.658(2) Å, C1-N1: 1.340(2) Å, C1-N2: 1.471(2) Å. Angle: N1-C1-N2: 107.94(14) °.

3.12. Reactivity of $YL_3(KCl)_3(thf)_6$ towards CO_2/CS_2

CO_2 is an abundant, inexpensive natural resource which can serve as C_1 building block for more valuable carbon-containing molecules.[30, 31] Saturated[32] and unsaturated[87] backbone NHCs reversibly react with CO_2 to form imidazolium and imidazolinium carboxylates respectively (**Scheme 1-22**). Both transition metals[33-36] and the f-elements[37-43] have been used for the formation of metal complexes, which can transfer CO_2 to organic substrates such as ketones, aldehydes and alcohols.[44, 45] Some of the complexes have been used to catalyse the co-polymerisation of CO_2/epoxide,[46] cyclotrimerisation of isocyanates[47] and the synthesis of carbonate.[48]

Treatment of complex **50** with CO_2 in THF immediately resulted in the precipitation of a white solid. The ^1H NMR spectrum of the THF solution shows no signal for the starting material and thus the product was proposed to be an NHC-CO_2 adduct of complex **57**, $[Y(L\text{-}CO_2)_3(KCl)_3]_n$ (**Scheme 3-24**).

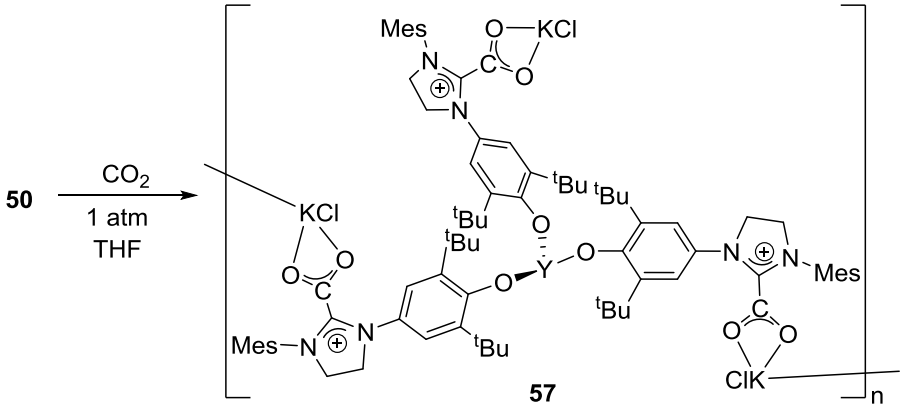

Scheme 3-24. The reaction of complex **50** with CO_2.

The isolated product is slightly soluble in pyridine and an only trace amount of THF is observed. The ^{1}H NMR spectrum shows two sets of ligand environments which have a 2:1 ratio. The protons of imidazolinium backbone are seen as two sets of multiplets at δ = 4.92, 4.47 ppm and δ = 4.87, 4.44 ppm, respectively. The methyl groups also show a similar trend, where two sets of resonances are recorded at δ = 2.33 (*o*-Me), 2.19 ppm (*p*-Me) and δ = 2.25 (*o*-Me), 2.23 ppm (*p*-Me) with a ratio of 2:1.

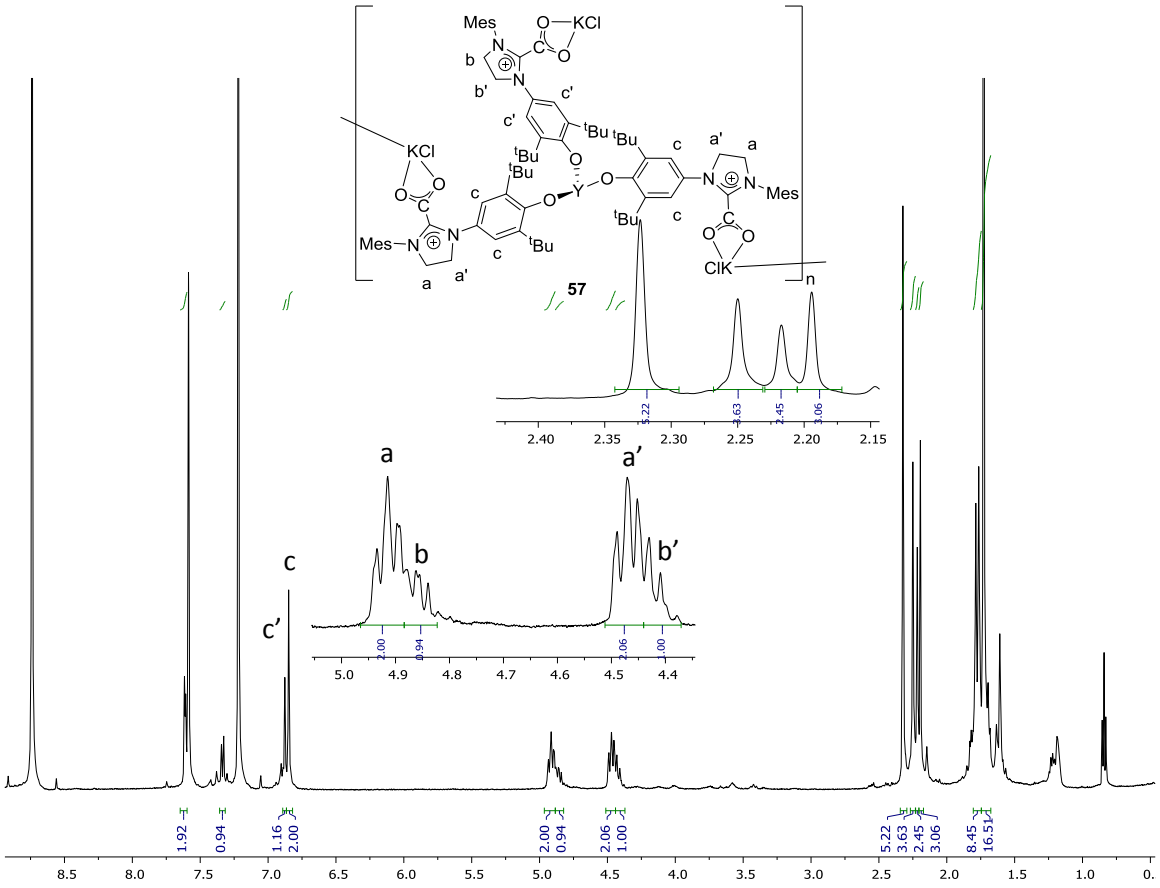

Figure 3-10. ^{1}H NMR spectrum of the reaction of complex **50** with CO_2.

IR analysis (nujol) of the product shows one strong absorption at 1664 cm^{-1} and a weaker absorption at 1687 cm^{-1} which fall in the range from 1630 to 1690 cm^{-1} for NHC-CO_2 adducts.[49-51] These two absorptions can be ascribed to the two different types of COO^- asymmetric stretch in the product. The elemental analysis of the product shows a low percentage of C, H and N elements, which may due to the incorporation of KCl salt which facilities the polymerisation of the complex. These observations suggest the structure of the product **57** as a polymer where two ligands bind to the Y atom and one ligand coordinates with the KCl (**Scheme 3-24**).

As an analogue of CO_2, CS_2 also showed reactivity with RE NHC complexes. The Arnold group have reported that the treatment of scandium tris(alkoxy-tethered NHC) complex $Sc(L)_3$ (**CF**, **Scheme 1-33**) with one equivalent of CS_2 in toluene affords monothiocarboxylate complex $[Sc(L^{CS2})(L)_2]$ (**ED**, **Scheme 1-33**). Reaction with two equivalents of CS_2 in toluene leads to the immediate formation of **ED** followed by the slow formation of bimetallic bithiocarboxylate complex **CE** $\{[ScL(L^{CS2})_2]_2\}$. The addition of more equivalents of CS_2 does not lead to the formation of $Sc(L^{CS2})_3$ but instead, accelerates the rate at which **CE**(**Scheme 1-33**) is formed.[51]

Treatments of complex **50** with either one or two equivalents of CS_2 in THF led to the instant formation of colourless solid. The ^1H NMR spectrum of the products of these reactions shows multiple resonances for the ligand which can hardly be ascribed to a single (or two) product(s). The ^{13}C NMR spectrum also shows similar patterns where several sets of resonances are observed and were unable to be assigned to the products. This can be ascribed to the formation of multiple products when the highly reactive CS_2 is added to the solution. When three equivalents (or excessive) of CS_2 was added to the THF solution of complex **50** (**Scheme 3-25**), a colourless solid was formed immediately.

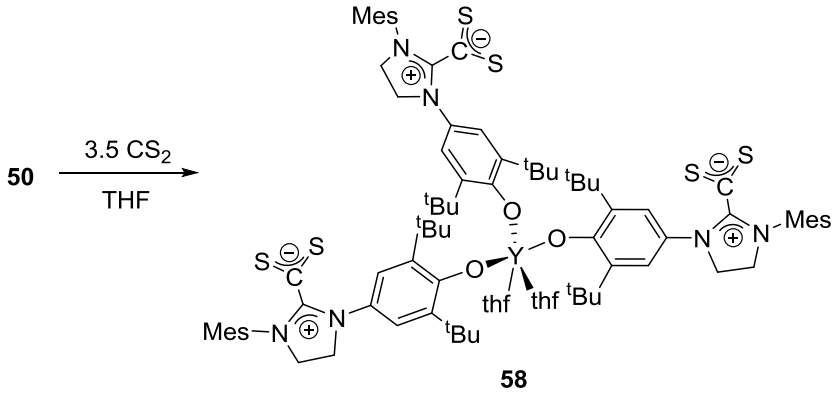

Scheme 3-25. The reaction of complex **50** with CS_2.

The ^1H NMR spectrum of the product in d^5-pyridine shows two sets (1:1) of phenyl protons at δ = 7.93, 6.91 ppm and 7.82, 6.83 ppm, which suggests two environments of the ligands,

respectively. The protons of the imidazolinium backbone also shows the similar patterns where two sets of resonances are observed at δ = 4.74 ppm (d, *J* = 11.4 Hz, 2H), 4.27 ppm (d, *J* = 11.5 Hz, 2H) and 4.57 ppm (d, *J* = 10.3 Hz, 2H), 4.16 ppm (d, *J* = 10.7 Hz, 2H), respectively. The ^{13}C NMR spectrum shows two major singlets at δ = 226.28 and 225.96 ppm, which is similar to that of 226.7 ppm of the dithiocarboxylate group in complex **EE**(**Scheme 1-48**).[51]

Based on these data, the reaction of complex **50** with 3.5 equivalents of CS_2 shows that all of the carbenes should have been reacted. The ^{1}H NMR spectrum indicates the existence of two different environments of the ligands. Due to the difficulty in obtaining its crystal structure, a possible structure of the product is drawn as complex **58** in **Scheme 3-25**.

3.13. References

1. D. Sellmann, W. Prechtel, F. Knoch and M. Moll, *Organometallics*, 1992, **11**, 2346-2348.
2. D. Sellmann, M. Wille and F. Knoch, *Inorg. Chem.*, 1993, **32**, 2534-2543.
3. P. L. Arnold, A. C. Scarisbrick, A. J. Blake and C. Wilson, *Chem. Commun.*, 2001, 2340-2341.
4. P. L. Arnold, S. A. Mungur, A. J. Blake and C. Wilson, *Angew. Chem., Int. Ed.*, 2003, **42**, 5981-5984.
5. P. L. Arnold and I. J. Casely, *Chem. Rev.*, 2009, **109**, 3599-3611.
6. S. She, MSc (Res) Dissertation, The University of Edinburgh, 2012.
7. J. Hamilton, MChem Dissertation, The University of Edinburgh, 2013.
8. F. H. Allen, *Acta Crystallogr B*, 2002, **58**, 380-388.
9. B. E. Ketz, A. P. Cole and R. M. Waymouth, *Organometallics*, 2004, **23**, 2835-2837.
10. Z. Li, M. Q. Xue, H. S. Yao, H. M. Sun, Y. Zhang and Q. Shen, *J. Organomet. Chem.*, 2012, **713**, 27-34.
11. P. L. Arnold, M. W. McMullon, J. Rieb and F. E. Kuhn, *Angew. Chem., Int. Ed.*, 2015, **54**, 82-100.
12. S. Bellemin-Laponnaz and S. Dagorne, *Chem. Rev.*, 2014, **114**, 8747-8774.
13. P. L. Arnold and S. T. Liddle, *Organometallics*, 2006, **25**, 1485-1491.
14. M. Nishiura, F. Guo and Z. M. Hou, *Acc. Chem. Res.*, 2015, **48**, 2209-2220.
15. H. Ren, P. Yao, S. Xu, H. Song and B. Wang, *J. Organomet. Chem.*, 2007, **692**, 2092-2098.
16. M. W. McMullon, Ph.D. Thesis, Exploiting Anionically-Tethered N-Heterocyclic Carbene Complexes for Small Molecule Activation, The University of Edinburgh, 2017.
17. A. W. Waltman and R. H. Grubbs, *Organometallics*, 2004, **23**, 3105-3107.
18. A. W. Waltman, T. Ritter and R. H. Grubbs, *Organometallics*, 2006, **25**, 4238-4239.
19. M. S. Hill, G. Kociok-Kohn and D. J. MacDougall, *Inorg. Chem.*, 2011, **50**, 5234-5241.
20. D. R. Weinberg, N. Hazari, J. A. Labinger and J. E. Bercaw, *Organometallics*, 2010, **29**, 89-100.
21. R. A. Musgrave, R. S. P. Turbervill, M. Irwin and J. M. Goicoechea, *Angew. Chem., Int. Ed.*, 2012, **51**, 10832-10835.
22. P. L. Arnold, M. Rodden and C. Wilson, *Chem. Commun.*, 2005, 1743-1745.
23. U. D. Priyakumar, T. C. Dinadayalane and G. N. Sastry, *Chem Phys Lett*, 2001, **337**, 361-367.

24. A. R. Fout, B. C. Bailey, J. Tomaszewski and D. J. Mindiola, *J. Am. Chem. Soc.*, 2007, **129**, 12640-+.
25. S. D. Gray, K. J. Weller, M. A. Bruck, P. M. Briggs and D. E. Wigley, *J. Am. Chem. Soc.*, 1995, **117**, 10678-10693.
26. C. T. Carver and P. L. Diaconescu, *J. Am. Chem. Soc.*, 2008, **130**, 7558-7559.
27. I. J. Casely, S. T. Liddle, A. J. Blake, C. Wilson and P. L. Arnold, *Chem. Commun.*, 2007, 5037-5039.
28. P. L. Arnold, T. Cadenbach, I. H. Marr, A. A. Fyfe, N. L. Bell, R. Bellabarba, R. P. Tooze and J. B. Love, *Dalton Trans.*, 2014, **43**, 14346-14358.
29. Y. Yamaguchi, T. Kashiwabara, K. Ogata, Y. Miura, Y. Nakamura, K. Kobayashi and T. Ito, *Chem. Commun.*, 2004, 2160-2161.
30. C. M. Rayner, *Org. Process Res. Dev.*, 2006, **11**, 121-132.
31. T. Sakakura, J.-C. Choi and H. Yasuda, *Chem. Rev.*, 2007, **107**, 2365-2387.
32. H. A. Duong, T. N. Tekavec, A. M. Arif and J. Louie, *Chem. Commun.*, 2004, 112-113.
33. D. H. Gibson, *Chem. Rev.*, 1996, **96**, 2063-2096.
34. P. G. Jessop, F. Joó and C.-C. Tai, *Coord. Chem. Rev.*, 2004, **248**, 2425-2442.
35. M. Aresta and A. Dibenedetto, *Dalton Trans.*, 2007, 2975-2992.
36. S. N. Riduan and Y. Zhang, *Dalton Trans.*, 2010, **39**, 3347-3357.
37. F. Calderazzo, G. Dell'Amico, R. Netti and M. Pasquali, *Inorg. Chem.*, 1978, **17**, 471-473.
38. W. J. Evans, C. A. Seibel and J. W. Ziller, *Inorg. Chem.*, 1998, **37**, 770-776.
39. W. J. Evans, D. B. Rego, J. W. Ziller, A. G. DiPasquale and A. L. Rheingold, *Organometallics*, 2007, **26**, 4737-4745.
40. C. Lescop, T. Arliguie, M. Lance, M. Nierlich and M. Ephritikhine, *J. Organomet. Chem.*, 1999, **580**, 137-144.
41. W. J. Evans, K. A. Miller and J. W. Ziller, *Inorg. Chem.*, 2005, **45**, 424-429.
42. I. Castro-Rodríguez and K. Meyer, *J. Am. Chem. Soc.*, 2005, **127**, 11242-11243.
43. O. P. Lam, C. Anthon and K. Meyer, *Dalton Trans.*, 2009, 9677-9691.
44. M. Smiglak, J. D. Holbrey, S. T. Griffin, W. M. Reichert, R. P. Swatloski, A. R. Katritzky, H. Yang, D. Zhang, K. Kirichenko and R. D. Rogers, *Green Chem.*, 2007, **9**, 90-98.
45. I. Tommasi and F. Sorrentino, *Tetrahedron Lett.*, 2005, **46**, 2141-2145.
46. H. Zhou, W.-Z. Zhang, C.-H. Liu, J.-P. Qu and X.-B. Lu, *J. Org. Chem.*, 2008, **73**, 8039-8044.
47. H. A. Duong, M. J. Cross and J. Louie, *Org. Lett.*, 2004, **6**, 4679-4681.

48. Y. Kayaki, M. Yamamoto and T. Ikariya, *Angew. Chem., Int. Ed. Engl.*, 2009, **48**, 4194-4197.

49. B. R. Van Ausdall, J. L. Glass, K. M. Wiggins, A. M. Aarif and J. Louie, *J. Org. Chem.*, 2009, **74**, 7935-7942.

50. E. Brule, V. Guerineau, P. Vermaut, F. Prima, J. Balogh, L. Maron, A. M. Z. Slawin, S. P. Nolan and C. M. Thomas, *Polym Chem-Uk*, 2013, **4**, 2414-2423.

51. P. L. Arnold, I. A. Marr, S. Zlatogorsky, R. Bellabarba and R. P. Tooze, *Dalton Trans.*, 2014, **43**, 34-37.

4. Synthesis and Reactivity of Pyrazolate-Supported Macrocyclic NHC Complexes

This section was carried out in collaboration with Philipp J. Altmann, a PhD student from the Supramolecular Organometallics group of Alexander Pöthig at Technische Universität München. The macrocyclic NHC ligands were provided by them and a brief introduction for the derived complexes are described below.

4.1. Introduction

Various types of macrocyclic NHC ligands have been applied to form robust and stable transition metal complexes which have shown versatile binding modes[1] and properties such as selective recognition of anions or linear molecules.[2]

The synthesis of the pyrazole-supported macrocyclic NHC ligands is rather challenging and was first achieved by Pöthig *et. al.*[3] They have synthesised a series of pyrazole linked cyclophane-like NHC ligand precursors **60**, $H_6L^RX_4$ (R = Me, Et, Pr; X = PF_6, OTf) (**Figure 4-1**), which contain alkyl bridging chains (methylene = L^{Me}, ethylene = L^{Et}, propylene = L^{Pr}) between the imidazolium rings and different substituents on the imidazolium groups (methyl = L^{Me*}). The proligands are obtained with different counterions X^- (X = PF_6 or OTf).

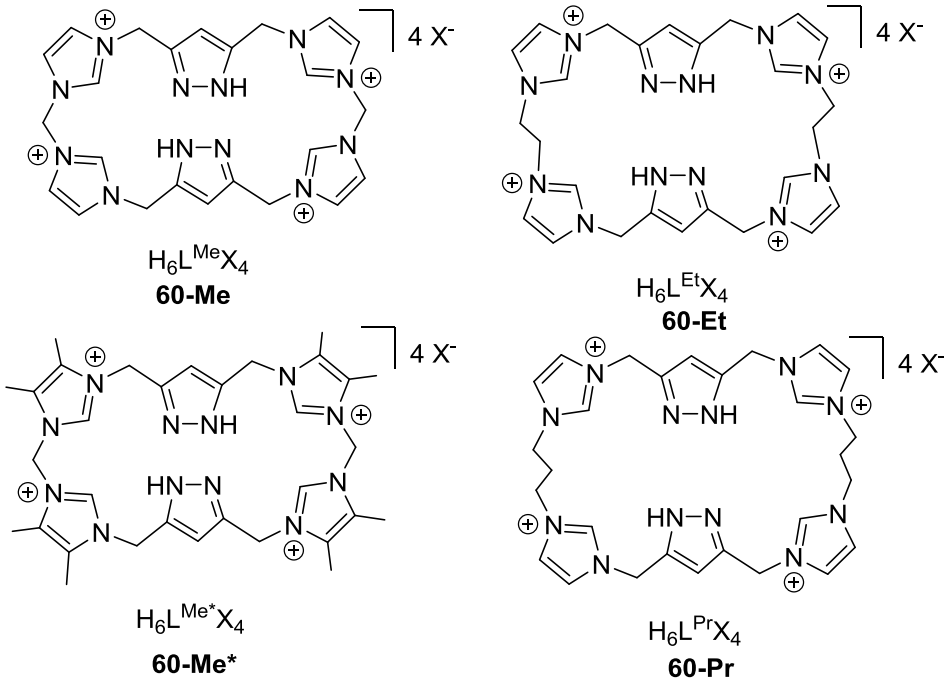

Figure 4-1. Proligands of $H_6L^RX_4$ (R = Me, Et, Pr; X = PF_6, OTf).

It has been reported by Pöthig and co-workers that the treatment of $H_6L^RX_4$ (R = Me, Et; X = PF_6) with caesium carbonate in the presence of bis(triphenylphosphine)nickel(II) chloride produced the dinuclear Ni complex **FM** ($Ni_2L^RX_4$, R = Me, Et; X = PF_6^-) (**Figure 4-2**).[3] Complexes **FM** adopt a bowl-shaped structure with the pyrazole rings at the bottom and the NHC moieties bent upwards to each side to bind the two Ni ions. The two nickel ions are in a slightly distorted square-planar coordination environment.[4]

The reaction of $H_6L^{Me}(PF_6)_4$ with an excess of silver (I) oxide in acetonitrile cleanly affords the octanuclear pillarplex complex **FN** $[Ag_8(L^{Me})_2](PF_6)_4$.[5] Transmetallation reaction of the silver complex **FN** with $(SMe_2)AuCl$ affords gold (I) analogue **FO** $[Au_8(L^{Me})_2](PF_6)_4$.[5]

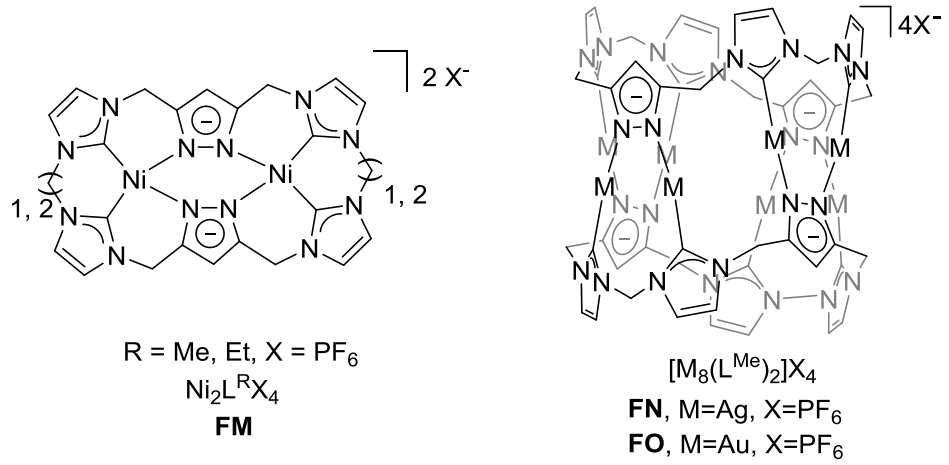

Figure 4-2. Reported synthesis of pyrazolate supported macrocyclic NHC transition metal complexes.

However, RE metal complexes containing macrocyclic NHCs remained undeveloped, and no example has been reported until now.[6] Given the successful synthesis and characterisation of late-transition metal macrocyclic NHC complexes, this type of ligand is thus used to explore the synthesis of RE complexes.

4.2. Synthesis of RE complexes

In order to synthesise the RE complexes with this type of macrocyclic ligand, reactions with different bases (KN", $MgN"_2$ and $CaN"_2$) were investigated.

4.2.1. **Reaction of proligands with KN"**

The treatment of proligand **60-Me** ($H_6L^{Me}X_4$, X = PF_6, OTf) with six equivalents of KN" in pyridine (or MeCN) affords a pale yellow solution. The ^{1}H NMR spectrum of the pyridine solution shows a complete transformation of the KN" into HN" and the absence of the

imidazolium-NCHN protons which suggest the full deprotonation of the imidazolium and pyrazole protons of the proligand (**Scheme 4-1**).

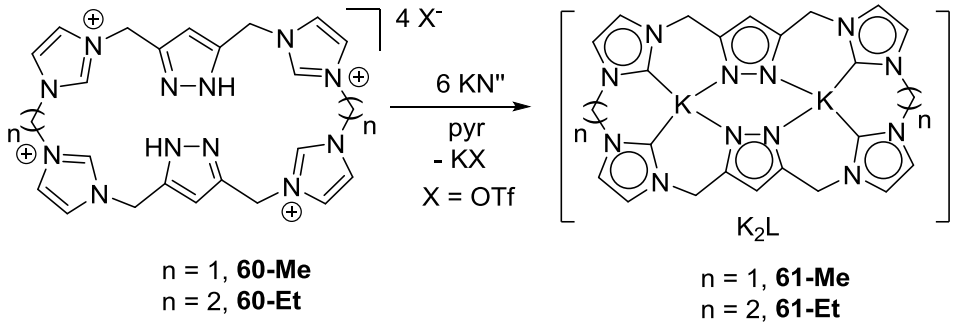

n = 1, **60-Me**
n = 2, **60-Et**

n = 1, **61-Me**
n = 2, **61-Et**

Scheme 4-1. Reaction of proligands **60** with KN".

In the ^{1}H NMR spectrum, the bridging methylene groups between two imidazoles are observed at δ = 6.83 ppm which have shifted to lower frequency compared to that of 7.34 ppm in **60-Me**. A similar trend is also observed for the imidazolium-backbone CH protons which shifted from 8.16 and 7.37 ppm to 6.79 and 6.18 ppm, respectively (**Figure 4-3**). The methylene linkers between pyrazole and imidazole group also shifted to the lower frequency at δ = 5.31 ppm. These methylene groups display a singlet in solution which is different from that of the dinuclear Ni complex **FM** (5.29 (d, ^{2}J = 15.58 Hz) and 5.24 (d, ^{2}J = 15.58 Hz) ppm) where a reduction of the molecular symmetry in solution is observed. This suggests that the symmetry of the ligand is maintained in this complex. The NHC carbene carbon of complex **61-Me** is observed as a singlet at δ = 211.05 ppm which shows a much higher frequency compared to that of 157.6 ppm in nickel complex **FM**. However, the species decomposes gradually in pyridine as examined by ^{1}H NMR spectroscopy.

.

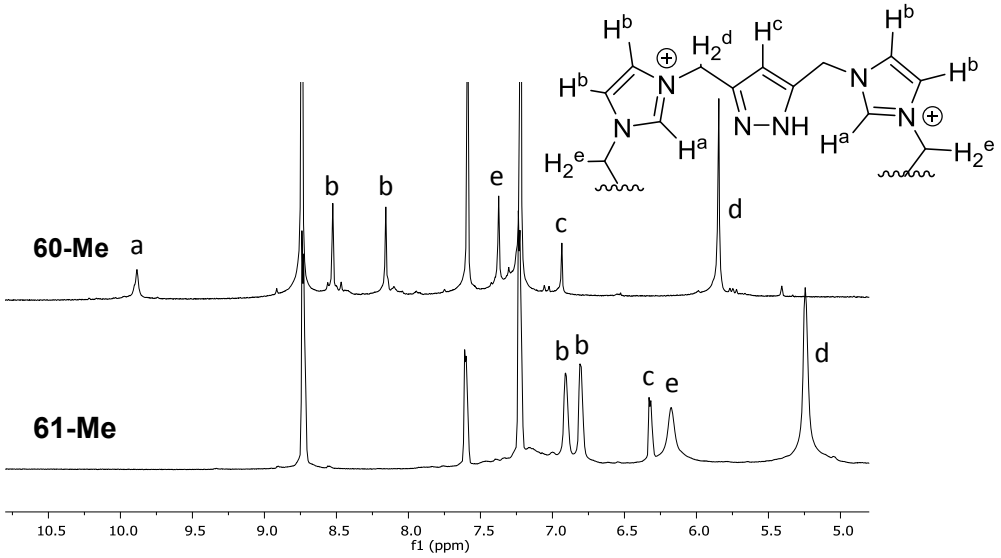

Figure 4-3.^{1}H NMR spectrum (10-5 ppm) of **60-Me** and **61-Me**.

The reaction of the ligand **60-Et** with six equivalents of KN" in pyridine affords a pale yellow solution of complex **61-Et,** [K_2L^{Et}], which shows similar patterns in the ^{1}H and ^{13}C NMR spectrum. This complex decomposes gradually in pyridine which is similar to its analogue.

The solubility of complexes **61-R** (R = Me, Et) is limited in pyridine. When hexane is added to a pyridine solution, the resulting pale yellow solid of complex **61** cannot be fully re-dissolved in pyridine. This complex is stable in pyridine for 12 hours, however, signs of decomposition are observed after being stored for 2 days.

4.2.2. **Reaction of complex 61 with $RECl_3(thf)_2$ (RE = Sc, Y, Ce)**

Due to the instability of complex **61** in pyridine, reactions of complex **61** with $RECl_3(thf)_2$ are carried out *in situ*.

Upon the addition of the pyridine solution of complex **61** into a pyridine solution of two equivalents of $RECl_3(thf)_2$ (RE = Sc, Y, Ce), a white solid is formed immediately. The solid and solution are then separated by filtration. The ^{1}H NMR spectrum of the pyridine solution shows no ligand-signals, but the by-product HN". Attempts to dissolve this solid in organic solvents such as THF, pyridine or MeCN showed no success. The addition of water into the solid causes the hydrolysis of the ligand. Based on these observations, the macrocyclic NHC complexes are most likely to form a polymerised complex **62**, $[LRE_2Cl_4]_x$, which was shown in **Scheme 4-2**.

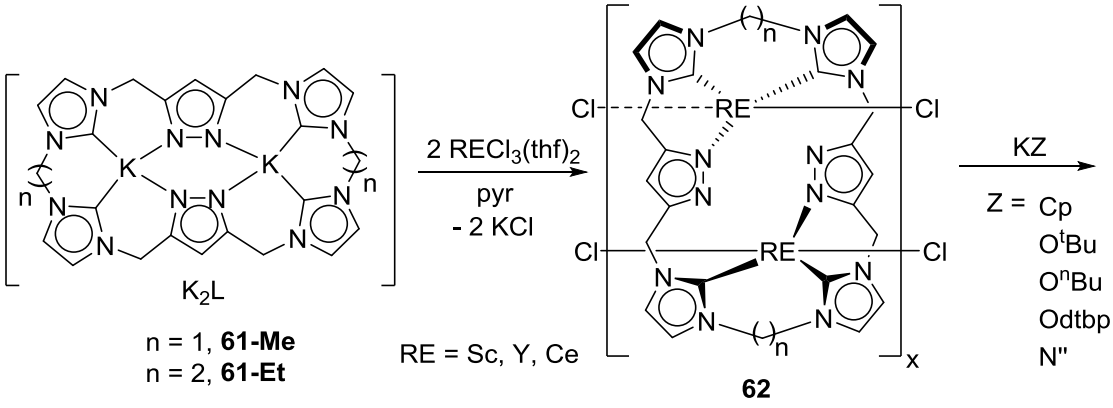

Scheme 4-2. Reactions of complex **61** with $RECl_3(thf)_2$ (RE = Sc, Y, Ce)

Attempts to solubilise the complexes by adding various types of potassium salt KZ (Z = Cp, O^tBu, O^nBu, Odtbp and N") to form LRE_2Z_4 showed no reaction happened. These results show the different properties of the electropositive RE metals with these macrocyclic NHC ligands.

4.3. Reaction proligands with MgN"$_2$

The treatment of proligands **60-R** (R = Me, Et, Pr) with one equivalent of MgN"$_2$ in acetonitrile afford a pale yellow solution. After the removal of volatiles, an oily paste is obtained which afford white solid after being washed with Et_2O (**Scheme 4-3**).

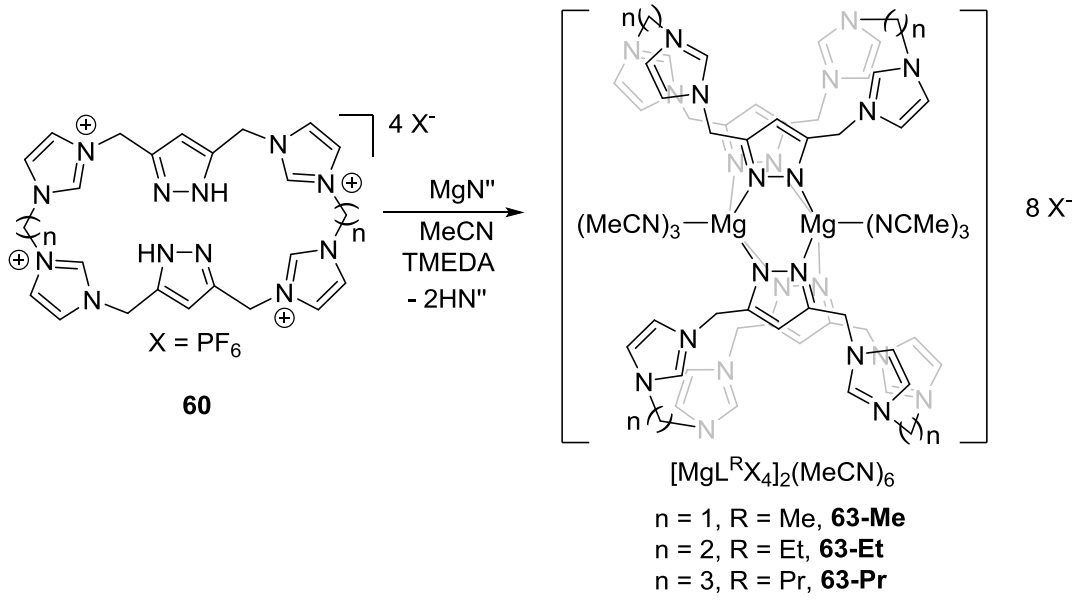

Scheme 4-3. Synthesis of complex **63**, $[MgH_4L^R(PF_6)_4]_2(MeCN)_6$, (R = Me, Et, Pr).

Interestingly, this reaction proceeds cleanly with the presence of two equivalents of tetramethylethylenediamine (TMEDA). However, the TMEDA molecules cannot be seen after being washed by solvents in the work up which suggests the TMEDA is not coordinated in the final products.

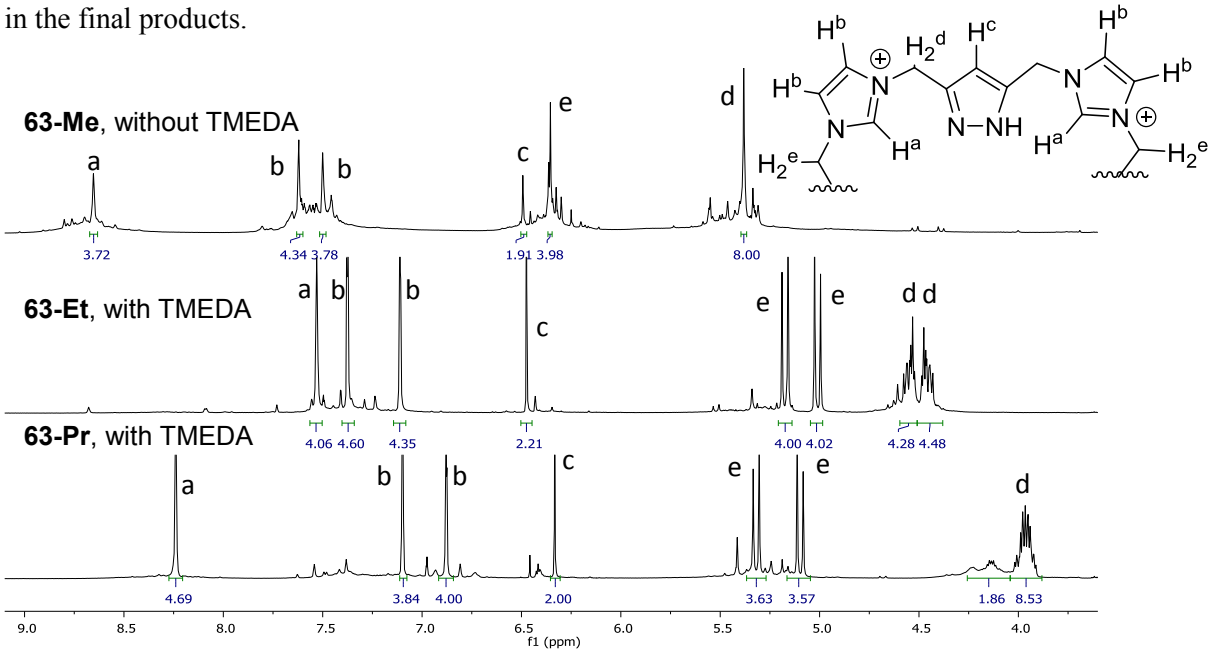

Figure 4-4. ^{1}H NMR spectrum of complex **63-R**, $[MgH_4L^R(PF_6)_4]_2(MeCN)_6$, (R = Me, Et, Pr).

The ^{1}H NMR spectrum of the reaction shows the deprotonation of the pyrazole protons while the imidazolium protons are intact. In the reaction of **60-Me**, the remaining imidazolium protons display a singlet at δ = 8.77 ppm which is at a higher frequency compared to that of 7.53 ppm and 8.24 ppm in complex **63-Et** and **63-Pr**, respectively. The alkyl chains of the complexes show similar splitting patterns with the proligands. All the protons on the imidazolium and pyrazole groups display singlets which suggest the higher symmetries of the complexes are maintained. Based on these observations, the structure of the complex **63-Et** is suggested in **Scheme 4-3** where two Mg^{2+} ions are bridged by four pyrazole N atoms, forming a sandwich-like configuration. It is observed in ^{1}H NMR spectrum that after being stored in MeCN for 2 days, small peaks of new products emerge gradually which shows a sign of decomposition.

Attempts to grow crystals for these complexes have been investigated. In the case of complex **63-Et**, colourless crystals are obtained by Philipp Altmann by diffusion of diethyl ether into a MeCN solution (**Scheme 4-4**). From the single crystal X-ray data, the product is characterised as complex **64-Et**, $Mg_3(L^{Et})_2F_2[PF_6]_8(MeCN)_6$.

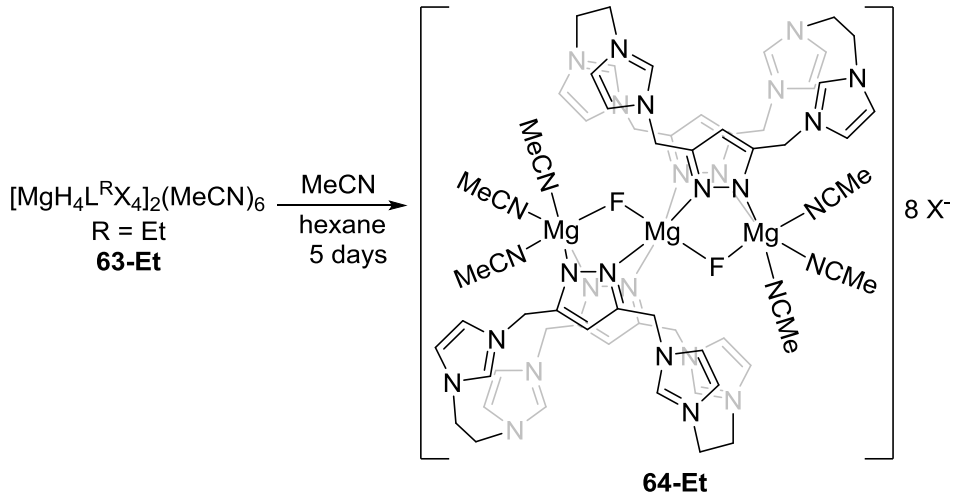

Scheme 4-4. Formation of complex $Mg_3(H_4L^{Et})_2F_2[PF_6]_8(MeCN)_6$.

The solid-state structure and selected bond length (Å) and angles (°) are provided in **Figure 4-5**. The crystals of complex **64-Et** display a C2/c symmetry with four molecules in the unit cell. In the solid-state structure of complex **64-Et**, three magnesium ions are surrounded by two pyrazole ligands with a side-on coordination mode, displaying a distorted octahedral coordination. Each side Mg atom (Mg1 and Mg2) is coordinated by three MeCN molecules and binds to the two nitrogen atoms of the pyrazole ligand at a distance of 2.151(3) Å and 2.169(6) Å, respectively. The two fluorides bridge Mg1 (or Mg3) atom at a distance of 1.940(4) Å which is slightly shorter than that to Mg2 of 1.988(3) Å. These Mg-F bonds are similar to the reported values from 1.953(8) Å in $[BDIMg(\mu\text{-}F)(THF)]_2$ (BDI = κ2-{2,6-^{i}

$Pr_2C_6H_3NCMe\}_2CH)$[7] and 2.017(7) Å in $Mg_3(\mu_3\text{-}F)(\mu\text{-}TFA)_6(OCH_3)_2(py)]_3^-$ anion.[8] The Mg2 atom is surrounded by four pyrazole ligands at the equatorial plane with slightly longer Mg-N bonds (2.185(5) Å 2.235(1) Å). The Mg2 atom also has a distorted octahedral configuration by coordinating two fluorine atoms at the vertex position. In this structure, all the imidazole groups bend to the other side of the pyrazole group, demonstrating a good example of new bonding mode for the macrocyclic NHC ligands. The formation of this complex may due to the fluoride ion abstraction reaction of PF_6 anion which has been documented in the reaction of $Fe(\mu\text{-}^iPrNPPh_2)_3FeE\equiv N^tBu$ with $FcPF_6$ that abstracts the F atom to form fluoride complex $F{-}Fe(\mu\text{-}^iPrNPPh_2)_3FeE\equiv N^tBu$.[9]

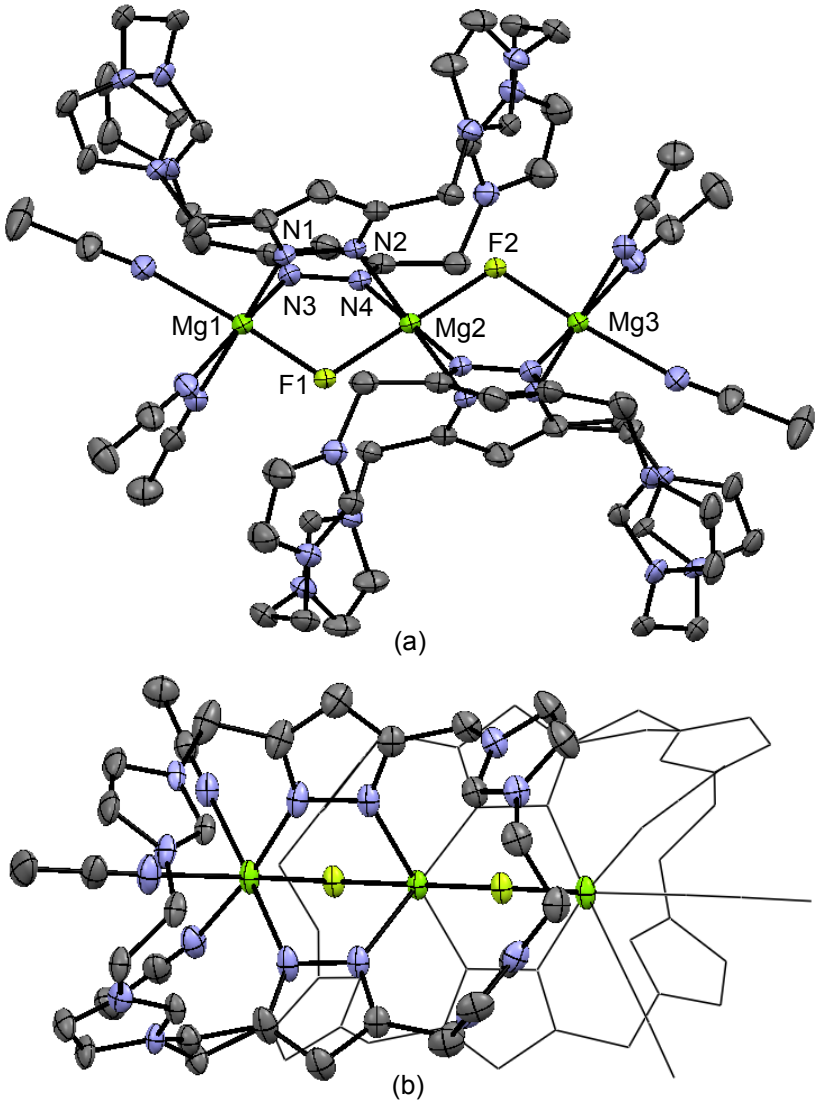

Figure 4-5. Solid state structure view of complex $Mg_3(H_4L^{Et})_2F_2[PF_6]_8(MeCN)_6$ from the side (a) and top (b). Thermal ellipsoids are shown at 30% probability. Hydrogen atoms except those on C1 atom, eight counter ions (PF_6^-) and free solvent molecules are omitted for clarity. Selected bonds (Å): Mg1-N1: 2.151(3), Mg1-N3: 2.169(6), Mg2-N2: 2.235(1), Mg2-N4: 2.185(5), Mg1-F1: 1.940(4), Mg2-F2: 1.988(3). Angle (°): Mg1-F1-Mg2: 112.70(5).

4.4. Reactivity of complex 63-Me

4.4.1. With Ag_2O

It has been shown that Ag_2O can deprotonate all the imidazolium and pyrazole acidic protons, forming pillarplex complex **FN** $[Ag_8(L^{Me})_2](PF_6)_4$ (**Figure 4-2**). In order to synthesise Mg/Ag mixed complexes, reactions of complex **63-Me** with Ag_2O is carried out.

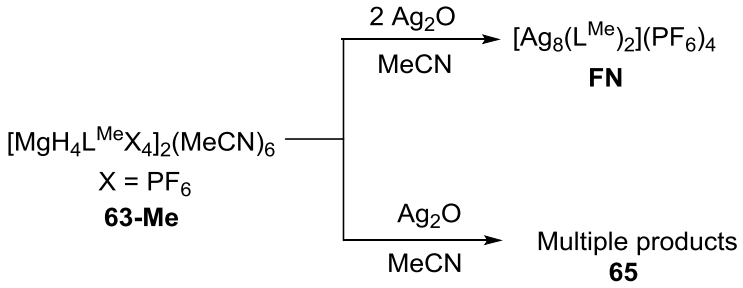

Scheme 4-5. Reactivity of complex **63-Me** with Ag_2O.

The treatment of complex **63** with two equivalents of Ag_2O in MeCN leads to the formation of pillarplex complex **FN**. When only one equivalent of Ag_2O is added, the ^{1}H NMR spectrum shows successful deprotonation of the imidazolium protons. However, multiple products are formed which could not be characterized in detail.

4.4.2. With $SmI_2(thf)_2$ and $UI_4(dioxane)_2$

The reaction of complex **63-Me** with one equivalent of $SmI_2(thf)_2$ affords a greenish brown suspension in MeCN. After the removal of white solid, a dark green-brown solution was obtained. The ^{1}H NMR spectrum of the product shows diamagnetic resonances. The complex can easily be oxidised by a trace amount of oxygen, generating a colourless solution of multiple components (**Scheme 4-6**).

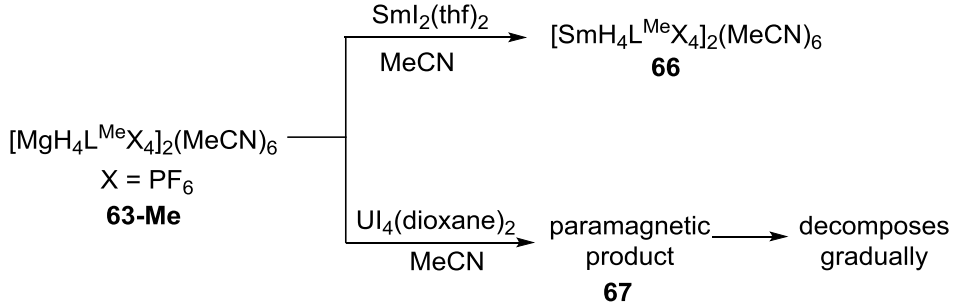

Scheme 4-6. Reactivity of complex **63-Me** with $SmI_2(thf)_2$ and $UI_4(dioxane)_2$.

The reaction of complex **63-Me** with one equivalent of $UI_4(dioxane)_2$ in MeCN affords a yellow suspension from which white solid was then removed by filtration. The ^{1}H NMR

spectrum of the product shows paramagnetically shifted resonances from the range of δ = 61.25 ppm to -19.06 ppm. The complex decomposes quickly and no paramagnetic resonances can be observed after 24 hours (**Scheme 4-6**).

4.5. Reaction of 60-Me with REN"$_3$ (RE = Sc, Ce)

The reaction of two equivalents of REN"$_3$ (RE = Sc, Ce) with one equivalent of **60-Me**(PF_6) affords a pale yellow suspension. After the removal of solid and volatiles and further workup, a pale yellow solid of the product can be obtained at a yield of *ca*. 45% (based on the formation of $LRE_2N"_2(PF_6)_4$).

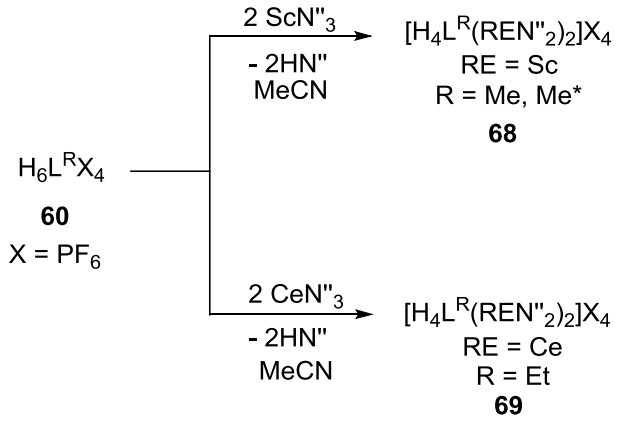

Scheme 4-7. Reaction of **60-Me** with REN"$_3$ (RE = Sc, Ce).

The reaction of **60-Me** with two equivalents of ScN"$_3$ proceeds smoothly in MeCN to form a pale yellow solution. After workup, an off-white solid of the product is obtained. The ^{1}H NMR spectrum of the product shows four singlets of imidazolium NCHN at δ = 8.62, 8.57, 8.50 and 8.45 ppm with an integral of 1H each whilst the pyrazole-NH are deprotonated. The imidazolium-backbone C*H* are seen as triplets at δ = 7.37 (t, *J* = 2.0 Hz) and 7.34 (t, *J* = 2.0 Hz) ppm. All the other protons also display similar pattern which shows an obvious splitting which suggests a deduction of the molecule symmetry. The ^{29}Si NMR shows a singlet at δ = 1.45 ppm for the by-product HN" and -9.39 ppm for the product, respectively.

The methyl analogue of proligand **60-Me*** reacts with two equivalents of ScN"$_3$ in MeCN to form a complex which would demonstrate a similar structure based on the NMR spectroscopy analysis.

The treatment of **60-Et** with CeN"$_3$ exhibits paramagnetically shifted resonances where the shifts of the protons vary from δ = 17.61 to -6.25 ppm. The ^{29}Si NMR of the product is recorded as a singlet at δ = 5.20 ppm (**Scheme 4-7**). These data suggest the formation of a Ce^{III} complex.

4.6. Transmetalation reaction with pillarplex complex

It has been shown that tetranuclear silver(I) macrocyclic NHC complex can be employed as transmetalation agent for the synthesis of nickel(II), palladium(II), platinum(II), and gold(I) derivatives.[10] Since rare earth metal complexes bearing macrocyclic NHC ligands emerged to be difficult to access using aforementioned salt metathesis reactions of alkali or alkaline earth metal complexes, another approach *via* the transmetalation reaction of the silver NHC complexes has been carried out.

The pillarplex complex **FN** $[Ag_8(L^{Me})_2](PF_6)_4$ (**Figure 4-2**) was synthesised according to literature preparations.[5]

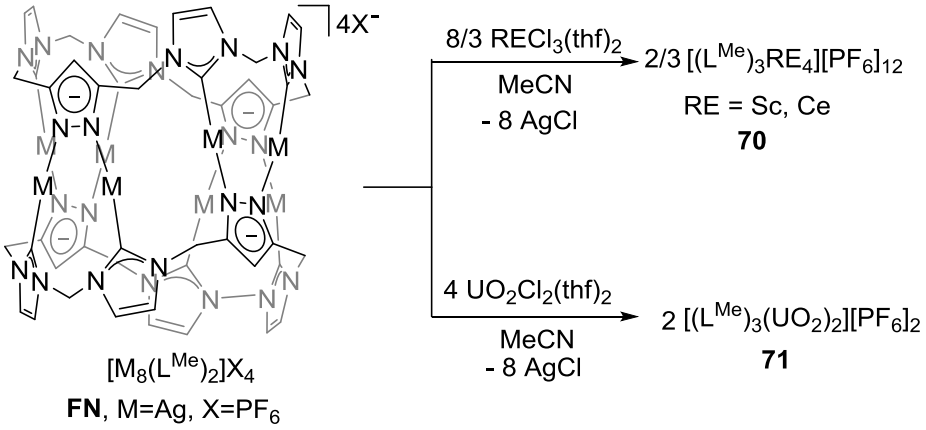

Scheme 4-8. The reaction of pillarplex complex FN $[Ag_8(L^{Me})_2](PF_6)_4$.

The reactions of complex **FN** with $RECl_3(thf)_2$ (RE = Sc, Ce) in MeCN cause an instant formation of white solid (**Scheme 4-8**). And no signal of the starting material can be found in the solution which suggests the full consumption of the reagents. However, the resulting product shows no solubility in organic solvents which prevents them from being structurally characterised.

The uranyl analogues proceed similarly with the RE complexes, which precipitate out immediately and have not been characterised yet (**Scheme 4-8**).

4.7. References

1. P. G. Edwards and F. E. Hahn, *Dalton Trans.*, 2011, **40**, 10278-10288.
2. I. Klawitter, M. R. Anneser, S. Dechert, S. Meyer, S. Demeshko, S. Haslinger, A. Pothig, F. E. Kuhn and F. Meyer, *Organometallics*, 2015, **34**, 2819-2825.
3. P. J. Altmann, C. Jandl and A. Pothig, *Dalton Trans.*, 2015, **44**, 11278-11281.
4. P. J. Altmann and A. Pothig, *Chem. Commun.*, 2016, **52**, 9089-9092.
5. P. J. Altmann and A. Pothig, *J. Am. Chem. Soc.*, 2016, **138**, 13171-13174.
6. M. Poyatos, J. A. Mata and E. Peris, *Chem. Rev.*, 2009, **109**, 3677-3707.
7. H. J. Hao, H. W. Roesky, Y. Q. Ding, C. M. Cui, M. Schormann, H. G. Schmidt, M. Noltemeyer and B. Zemva, *J. Fluor. Chem.*, 2002, **115**, 143-147.
8. J. Noack, C. Fritz, C. Flugel, F. Hemmann, H. J. Glasel, O. Kahle, C. Dreyer, M. Bauer and E. Kemnitz, *Dalton Trans.*, 2013, **42**, 5706-5710.
9. S. Kuppuswamy, T. M. Powers, B. M. Johnson, C. K. Brozek, J. P. Krogman, M. W. Bezpalko, L. A. Berben, J. M. Keith, B. M. Foxman and C. M. Thomas, *Inorg. Chem.*, 2014, **53**, 5429-5437.
10. P. J. Altmann, D. T. Weiss, C. Jandl and F. E. Kuhn, *Chem-Asian J*, 2016, **11**, 1597-1605.

5. Conclusions

A series of bulky tetraphenol-substituted proligands H_4L^R (R = P, PT, M) was synthesised. Through the reaction with four equivalents of KN"(N" = $N(SiMe_3)_2$), a dimerised complex **2**, $[K_4L^P]_2(thf)_{11}$, is synthesised and characterised which exhibits ladder-like structure in the solid state. The salt metathesis reactions of this complex with one equivalent of $RECl_3(thf)_2$ (RE = Ce, Pr) afford bimetallic aryloxide complexes **5**, $[K_2L_2RE_2(thf)_{11}]$ (RE = Ce, Pr), which have one K^+ ion encapsulated between the two phenyl linkers of the ligand. These complexes showed great flexibility to form different structures when treated with different coordinating molecules or solvents. The number of THF molecules coordinating the free K^+ counterion in complexes **5** can be reduced from seven to six without changing the dinuclear core structure. Stronger coordinating molecules such as pyridine and 18-crown-6 also only change the coordination of the free K^+ ion even when heated to 80 °C. However, when the crystals are grown from a THF/hexane solution, the free K^+ ion tend to have less (two) THF molecules coordinating, forcing the K^+ ion to bind between the phenyl rings, forming complexes **8-Ce^R** ($[K(thf)_2K(L^R)_2Ce_2(thf)_3]$, R = P, PT).

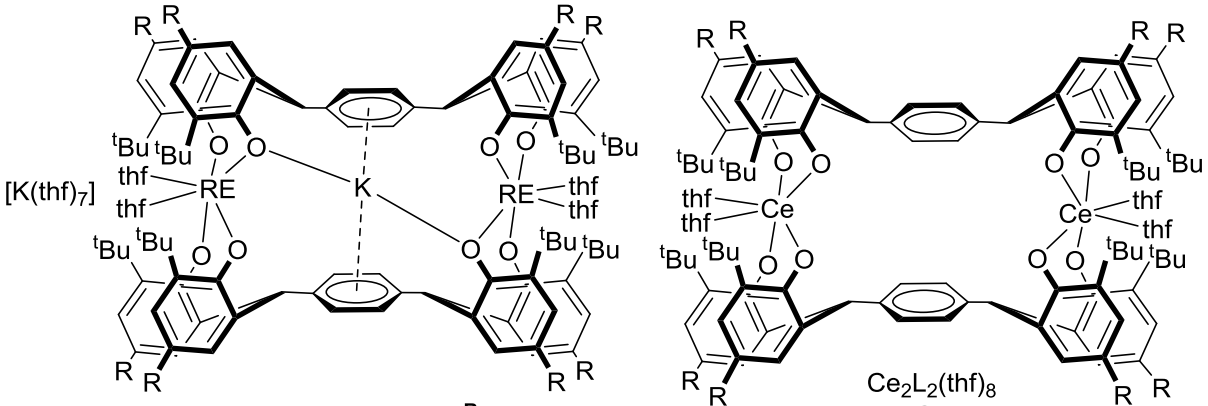

$[K(thf)_7][KL_2RE_2(thf)_4]$, 5-RE^R

5-Ce^P, R = P, RE = Ce
5-Ce^{PT}, R = PT, RE = Ce
5-Pr^{PT}, R = PT, RE = Pr

The complexes of **5-Ce^R** (R = P, PT) are very reactive to oxidants. The reaction of the Ce^{III} complex (**5-Ce^{PT}**) with substrates such as I_2, $CuCl_2$ and HgI_2 lead to the immediate oxidation of Ce^{III} to Ce^{IV}, affording the purple Ce^{IV} dimer **9-Ce^{PT}**, $Ce_2(L^{PT})_2$, which has been structurally characterised. The reaction with $HgCl_2$ and $Hg(OAc)_2$ generates several new products which exhibit paramagnetic resonances in the ^1H NMR spectroscopy. The treatment with Ph_3CCl or 1, 4-benzoquinone or O_2 affords new species which showed different UV-vis absorptions compared to that of complex **9-Ce^{PT}**. The treatment of **5-Ce^{PT}** with $CoCl_2$ or $NiCl_2$ in THF lead to no change of the starting material even when heated at elevated temperature (60 °C).

Thus, the possible redox potential of complex **5-Ce^{PT}** is narrowed in the range of -0.25-+0.27 V (vs SCE). The isolation of Ce^{IV} complexes and the redox chemistry suggest that with the use of these tetraaryloxide ligands L^R, the highly oxidising Ce^{IV} ion can be stabilised.

The reaction of the Pr^{III} complexes (**9-Pr^{PT}**) with I_2 affords a mixture from which a Pr^{III} iodide (**16-Pr^{PT}**) has been isolated and characterised while the other species is still under investigation. From the success isolation of complex **16-Pr^{PT}**, and combined with the redox potential of I_2 (+0.535 V vs SCE), this type of ligand may offer a good environment to stabilise the Pr^{IV} ions.

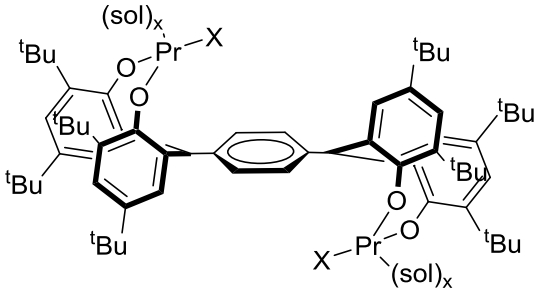

16-Pr^{PT}: X = I, sol = thf, x = 3;
28-Ce^{PT}: X = Cl, sol = py, x = 4;
28-Pr^{PT}: X = Cl, sol = py, x = 4;
31-Ce^{PT}: X = N", sol = null, x = 0;
31-Pr^{PT}: X = N", sol = null, x = 0;

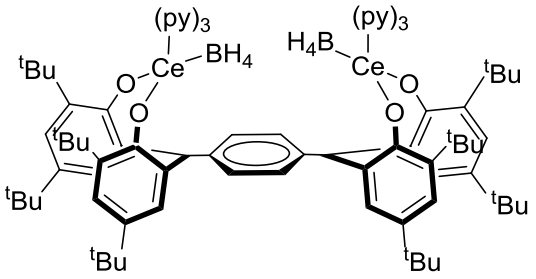

33-Ce^{PT}

The complex **5-Ce^{PT}** also showed reactivity with MeLi or KC_8 in THF to afford species which display paramagnetic resonances in ^1H NMR spectroscopy. The reaction of **5-Ce^{PT}** with four equivalents of KBn (Bn = benzyl) in THF yielded a benzyl-coordinated Ce^{III} complex together with the THF-ring-opening by-product. By changing the solvent of THF with diethyl ether, the reaction affords a polymerised tetra-benzyl Ce^{III} complex. These benzyl-coordinated complexes showed great reactivity towards small molecules such as phenylacetylene, CO_2 and CS_2. These show that the complexes are versatile in bonding modes, and with the functionalisation of the complexes, new chemistry can be brought to the dinuclear core.

Treatment of complex **2^{PT}** with four equivalents of $RECl_3(thf)_2$ (RE = Ce, Pr) in pyridine afforded bimetallic complexes **28**, $(RECl)_2(py)_8(L^{PT})$ (RE = Ce, Pr), which has been characterised as *trans*-configured complexes. and showed reactivity towards silver reagents ($AgPF_6$). Treatment of complexes **28** $(REX)_2(py)_8(L^{PT})$ (RE = Ce, Pr; X = Cl) with two equivalents of KN" yielded the RE amide complexes **31**, which can also be synthesised by the reaction of phenol ligand with two equivalents of CeN"$_3$.

The reaction of complex **2^{PT}** with four equivalents of $Ce(BH_4)_3(thf)_2$ resulted in the formation of salt metathesis product **33-Ce^{PT}**, $L(Ce(BH_4))_2(py)_6$, where the two borohydride groups reside on the same side of the phenyl linker, displaying a '*cis*' configuration which is different

to all the mono-ligand complexes synthesised in this project. This demonstrates the ligand flexibility that enables the metals to reside on the same or opposite sides of the central phenyl bridge.

The reaction of complex $\mathbf{2^{PT}}$ with two equivalents of $(Et_4N)_2CeCl_6$ in THF yielded complex $\mathbf{9\text{-}Ce^{PT}}$ with a 70% yield. And the treatment of $\mathbf{2^{PT}}$ with four equivalents of $(Et_4N)_2CeCl_6$ afforded the Ce^{IV} complex **35**, ($[L^{PT}(CeCl_2)_2(sol)_n$), which reacts with silver reagents AgX (X = CN^-, CNO^-, OCN^- and N_3^-) to form the subsequent cerium complexes with different anions. These show that the tetraaryloxide ligand can be used as a stabiliser to synthesise the Ce^{IV} complexes through salt metathesis reactions.

Preliminary studies on the Ce/Pr complexes ($\mathbf{5\text{-}Ce^{PT}}$/$\mathbf{31\text{-}Ce^{PT}}$/$\mathbf{31\text{-}Pr^{PT}}$) for the catalytic copolymerisation of epoxide/CO_2 are carried out which showed poor activity in this reaction. This suggests that further modifications of the ligand or the complexes need to be considered to catalyse polymerisation reactions.

A series of β-keto-imidazolinium salts H_2LBr {L = $RC(O)CH_2\{CH[NCH_2CH_2NMes]$, R = ^{t}Bu, naphth} were synthesised and reacted with $MHBEt_3$ (M = Na, K) to form carbene-borane adducts complexes **39**, $RC(O)CH_2\{C(BEt_3[NCH_2CH_2NMes]\}$. In these reactions, the ketone groups of the ligands stayed intact which were different from previous results on imidazolium derivatives. The contrasting reactivity of the carbene, borane and alcohol functional groups towards bases show that the differences between the backbone or substitution groups of the ketoimidazol(in)ium greatly affect the reactivity of the compounds.

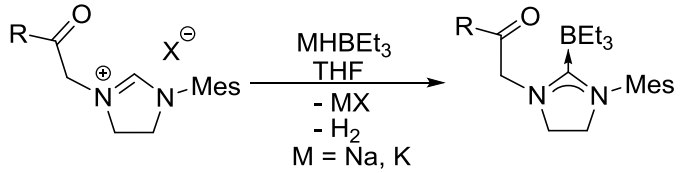

38e: R = ^{t}Bu, X = Cl
38f: R = napth, X = Br

39e: R = ^{t}Bu
39f: R = napth

The *p*-aryloxy-tethered imidazolinium salt H_2LX (L = *N*-3,5-di-*tert*-butyl-4-hydroxyphenyl-N'-mesityl-imidazolinium, X = Cl, Br, PF_6), has been synthesised *via* two different paths. The reactions of this proligand with MN"(M = Na, K) affords two new polymeric NHC complexes of **47** $[NaL]_n$ and **48** $[KL(thf)_2]_n$, respectively. The complex **47** shows a solvent-free polymer with a 3-coordinate Na cation. The potassium analogue displays a 'zig-zag' structure with K^+ ion coordinating to four atoms. This shows that the *p*-aryloxy-tethered NHCs can display varied coordination modes to bind metals with different ionic radii.

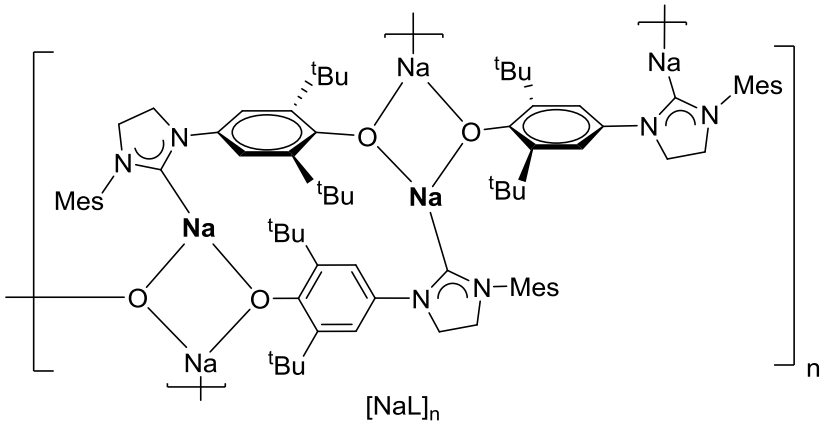

$[NaL]_n$

47

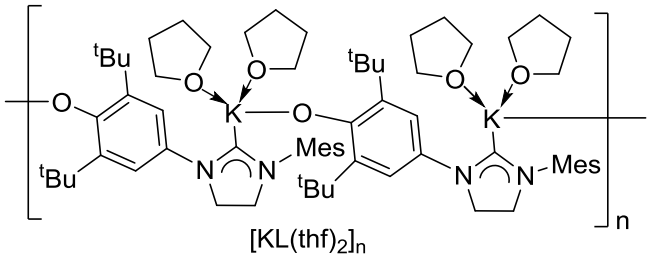

$[KL(thf)_2]_n$

48

The reaction of the complex **48** with 1/3 equivalent of $YCl_3(thf)_2$ yielded complex **50**, $YL_3(KCl)_3(thf)_6$. This NHC complex can react with three equivalents of boranes ($BH_3{\cdot}SMe_2$/9-BBN/BPh_3) which suggest that the carbene groups are facing outside of the metal core. This complex also showed good reactivity to activate small molecules such as CO_2 and CS_2, forming the [NHC-CE_2] adducts (E = O, S).

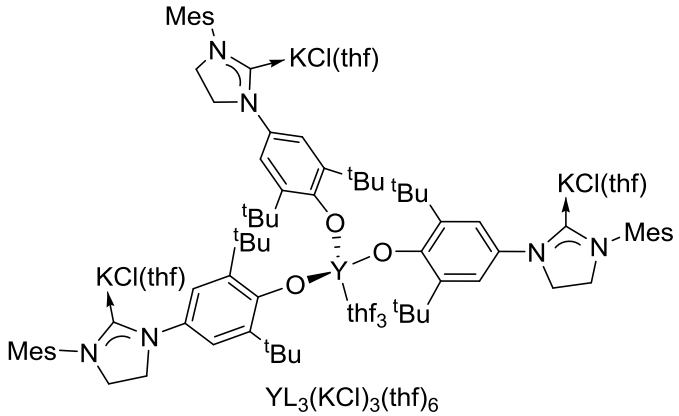

$YL_3(KCl)_3(thf)_6$

50

Macrocyclic NHC based cyclophane proligands **60-R** ($H_6L^RX_4$, L = calix[4]imidazolylidene[2]pyrazolate; R = Me, Et, Pr, Me*; X = PF_6, OTf) react with six equivalents of KN" in pyridine (or MeCN) to afford a series of its potassium complex **61**. However, the resulting complex **61**, $[K_2L]$, decomposes gradually over time. The reaction of complex **61** with two equivalents of $RECl_3(thf)_2$ (RE = Sc, Y, Ce) in pyridine leads to the formation of a white solid which showed no solubility in organic solvents such as THF, MeCN

or pyridine. The other attempts to synthesise the rare earth macrocyclic NHC complexes all ended up with insoluble solid which suggests that these macrocyclic-NHC RE complexes can be made but are difficult to be isolated and characterised.

The treatment of proligands **60-R** (R = Me, Et, Pr) with one equivalent of $MgN"_2$ in acetonitrile affords complex **63-R**, $MgH_4L^RX_4$ (R = Me, Et, Pr; X = PF_6, OTf)) in which only the pyrazole-CH are deprotonated. However, this complex is not very stable in MeCN and decomposes to afford an F-bridged tris-magnesium-bis-ligand complex **64-Et**.

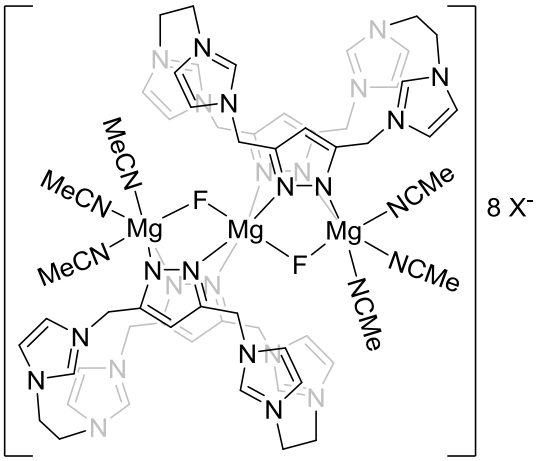

64-Et

These results showed the chemistry of the macrocyclic NHC proligands towards bases and rare earth metal reagents which is different from the reported examples. This suggests these macrocyclic NHCs bind electropositive RE metals in a way which is different to their late-transition metal analogues.

6. Experimental Procedures

6.1. General Experimental

All manipulations were carried out using standard Schlenk techniques under an atmosphere of dinitrogen. Organic solvents (THF, toluene, diethyl ether, acetonitrile and hexane) were dried by using a VAC solvent purification system (SPS), and were degassed and then stored over activated 4 Å molecular sieves prior to use. Deuterated solvents were dried by heating to reflux over potassium (C_6D_6, C_5D_5N, toluene-d_8 and THF-d_8), distilled under reduced pressure, freeze-pump-thaw degassed three times prior to use.

All NMR spectroscopic analyses were recorded at 298K using Bruker Avance III 500.12 MHz spectrometers with ^{1}H NMR spectra recorded at 500.12 MHz, ^{13}C NMR spectra at 125.77 MHz, ^{7}Li NMR spectra at 194.41 MHz, ^{11}B NMR spectra at 160.49 MHz and ^{29}Si NMR spectra at 99.37 MHz, respectively. LiCl, $BF_3{\cdot}(OEt_2)$ and $SiMe_4$, were used to externally reference the relevant spectra. ^{199}Hg NMR was recorded on AVA 400 at 71.309 MHz. The ^{1}H NMR and ^{13}C $\{^{1}H\}$ NMR spectra were referenced internally to residual solvent (^{1}H) or solvent (^{13}C) and are reported referenced to external tetramethylsilane (δ = 0 ppm). Chemical shifts are quoted in δ (ppm) and coupling constants in Hz.

Elemental analyses were performed by Mr Stephen Boyer at the London Metropolitan University. All data are presented in %. All FTIR were recorded using JASCO 410 or JASCO 460 plus spectrometers. Mass spectra were recorded by the mass spectrometry service of Edinburgh University's Department of Chemistry on 12T Bruker SolariX. Fourier Transform Ion Cyclotron Resonance Mass Spectrometry (FT-ICR MS).

X-ray single crystallographic data were collected at 150 K on a Bruker SMART APEX CCD diffractometer using graphite monochromated Mo-$K\alpha$ radiation (λ = 0.71073 Å), at 170 K on an Oxford Diffraction Excalibur diffractometer using graphite monochromated Mo-Kα radiation or at 100 K on an Oxford Diffraction Supernova diffractometer using mirror monochromated Cu-Kα radiation (λ = 1.5418 Å). Using the OLEX 2 suite of programs, all structures were solved using direct methods and refined using a full-matrix least square refinement on $|F|^2$ using SHELXL-97. Unless otherwise stated, all non-hydrogen atoms refined with anisotropic displacement parameters and hydrogen atoms were placed and refined using a riding model.

Standard high-vacuum Schlenk techniques and Vac and MBraun glove boxes were used to manipulate and store air- and moisture-sensitive compounds under an atmosphere of dried and deoxygenated dinitrogen. All gases were supplied by BOC gases UK. All glassware was dried in an oven at 160 °C, cooled under 10^{-3} mbar vacuum and then evacuated or purged with nitrogen. Prior to use, all Fisherbrand® 1.2 μm retention glass microfiber filters and cannula

were dried in an oven at 160 °C overnight and Celite® 545 filter aid was flame dried under vacuum immediately prior to use.

Rare earth chlorides, $RECl_3(THF)_2$ (RE = Sc,[1] Y,[2] Ce,[2] Pr[2] and Eu[2]), were made from the hydrated chlorides according to literature methods. NaN″,[3] KBn,[4] CeN''_3,[5] KN″,[6] LiN″,[7] 1-tert-butylimidazole,[8] 1-mesitylimidazole,[8] 2, 4, 6-tri-*tert*-butyl-4-phenone[9] and the tetraphenol ligands H_4L^R (R = P, PT, M) were synthesised according to literature methods.[10] $CoCl_2$, HgI_2, I_2, XeF_2, and $CuCl_2$ were purchased from Sigma-Aldrich and were used without further purification. $UO_2Cl_2(THF)_2$ was a kind gift from Dr Nicola Bell while MgN''_2 and CaN''_2 were kindly provided by Mr Jordann Wells. The macrocyclic pyrazole-supported NHC ligands were provided by Mr Philipp Altmann and the pillarplex complex $[Ag_8(L^{Me})_2](PF_6)_4$ were synthesised according to literature methods.[11]

6.2. *Experimental for Chapter 2*

6.2.1. **Synthesis of 2^P $(K_4L^P)_2(thf)_{11}$**

A Schlenk flask was charged with H_4L^P (2.00 g, 2.65 mmol) and KN" (2.11 g, 10.60 mmol) and a stirrer bar. THF (10 ml) was added and the resulting yellow solution was stirred for two hours at room temperature. Hexane (5 ml) was subsequently added to precipitate the product as colourless crystals which were isolated by filtration and dried under vacuum. Yield: 2.8560 g (85%).

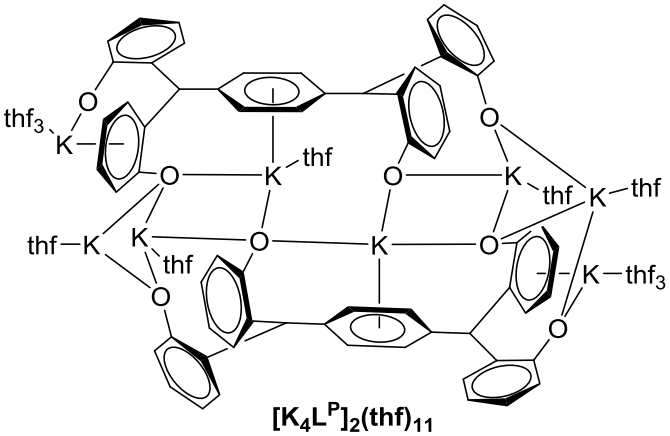

$[K_4L^P]_2(thf)_{11}$
2^P

^{1}H NMR (500 MHz, THF-d_8) δ 7.60 (s, 2H, Ar), 6.70 (s, 2H, Ar), 6.70 (s, 4H, Ar), 6.45 (s, 2H, Ar), 6.31 (s, 2H, Ar), 5.76 (s, 2H, Ar), 2.00 (d, J = 13.4 Hz, 12H, Me), 1.31 (d, J = 34.0 Hz, 36H, ^{t}Bu).

Elemental analysis: Calcd: $C_{144}H_{204}K_8O_{18}$ (2535.93): C, 68.20; H, 8.11. Found: C, 67.09; H, 8.15.

6.2.2. **Synthesis of 3^P $K_{10}(L^P)_2(OSiMe_3)_2$**

To a stirred benzene solution of H_4L^P (0.9234 g, 1 mmol) was added KBn (0.5202 g, 4 mmol). The resulting red solution was stirred for two hours at room temperature. Hexane was

subsequently added to the solution to precipitate the product **2^{P}** as colourless solid with a yield of 72 %, whose identity was confirmed by ^{1}H NMR spectroscopy. The red solution was stored in the freezer at -30 ˚C and tiny colourless crystals of complex **3^{P}** were obtained in a yield of 4%.

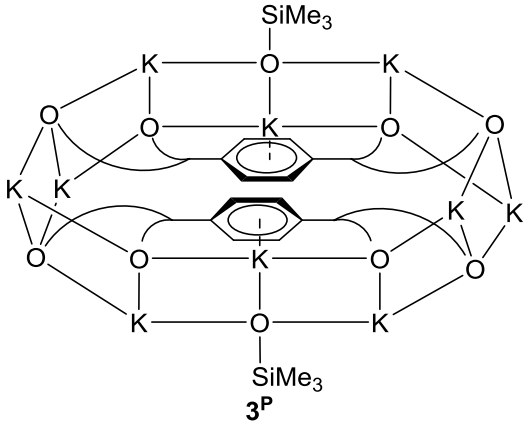

3^{P}

^{1}H NMR (500 MHz, Benzene-d_6) δ 8.06 (d, J = 7.6 Hz, 2H, Ar), 7.69 (d, J = 7.6 Hz, 2H, Ar), 7.20 (d, J = 14.9 Hz, 4H, Ar), 7.06 (d, J = 8.1 Hz, 2H, Ar), 7.01 – 6.95 (m, 2H, Ar), 6.96 – 6.88 (m, 2H, Ar), 6.86 (d, J = 6.2 Hz, 7H, Ar), 5.90 (d, J = 51.0 Hz, 4H, Benzylic-C*H*), 2.34 (d, J = 36.9 Hz, 12H, Me), 2.18 (d, J = 33.0 Hz, 12H, Me), 1.60 (s, 18H, ^{t}Bu), 1.55 (s, 18H, ^{t}Bu), 1.52 (s, 18H, ^{t}Bu), 1.21 (s, 18H, ^{t}Bu).

^{29}Si NMR (99.37 MHz, Benzene-d_6) δ -3.5.

6.2.3. **Synthesis of complex 5-Ce^{P} [K(thf)$_7$][KCe$_2$(L^{P})$_2$(thf)$_4$]**

A THF (5 ml) slurry of $CeCl_3(thf)_2$ (0.3915 g, 10 mmol) was slowly added to a Schlenk flask which contained a THF solution of $K_8L^{P}_2$ (1.268 g, 5 mmol, 10 ml). The mixture was left to stir overnight at room temperature to form a pale yellow suspension. The precipitate was filtered and the volatiles of the yellow solution was removed under reduced pressure. Hexane (5 ml) was added to precipitate the product as white powder. The solid was further washed with hexane and was dried under reduced pressure. Yield: 1.357 g (80%). Colourless crystals of the product were grown from concentrated THF solution at -30 ˚C.

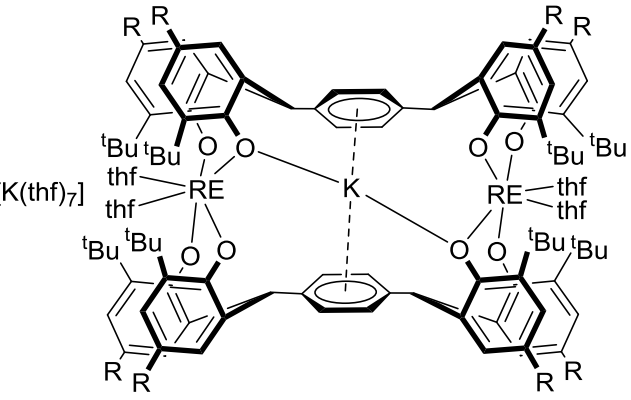

[K(thf)$_7$][KL$_2$RE$_2$(thf)$_4$], 5-RE^{R}

5-Ce^{P}, R = P, RE = **Ce**
5-Ce^{PT}, R = PT, RE = **Ce**
5-Pr^{PT}, R = PT, RE = **Pr**

^{1}H NMR (500 MHz, THF-d_8) δ 9.74 (s, 4H, Ar), 8.89 (s, 4H, Ar), 7.82 (s, 4H, Ar), 5.48 (s, 4H, Ar), 3.77 (s, 12H, Me), 3.45 (s, 36H, ^{t}Bu), 2.00 (s, 12H, Me), -0.35 (s, 36H, ^{t}Bu).

Elemental analysis: Calcd $C_{150}H_{218}Ce_2K_2O_{19}$. C, 67.13; H, 8.19; Found: C, 62.48; H, 8.23.

Note: This Ce^{III} complex is highly reducing and can easily be oxidised by a trace amount of oxygen, thus special care is needed when dealing with these complex. The elemental analysis

obtained does not fit with the calculated results which may due to the rapid and facile decomposition and oxidation of the complex.

6.2.4. Synthesis of complex 5-Ce^{PT} [K(thf)$_6$][KCe$_2$(L^{PT})$_2$(thf)$_4$

Following an analogous procedure to the synthesis of **5-Ce^{P}**, the H_4L^{PT} ligand was used instead to synthesise the **5-Ce^{PT}** analogue in a yield of 82%. Crystals were obtained from a concentrated THF solution at room temperature.

^{1}H NMR (500 MHz, THF-d_8) δ 10.10 (s, 4H, Ar), 9.16 (s, 4H, Ar), 7.92 (s, 4H, Ar), 5.41 (s, 4H, Ar), 3.92 (s, 4H, Ar), 3.82 (s, 36H, ^{t}Bu), 2.47 (s, 36H, ^{t}Bu), 0.96 (s, 36H, ^{t}Bu), -0.61 (s, 36H, ^{t}Bu).

^{13}C NMR (126 MHz, THF-d_8) δ 200.19 (s, Ar), 152.22 (s, Ar), 150.31 (s, Ar), 137.98 (s, Ar), 135.34 (s, Ar), 134.68 (s, Ar), 133.64 (s, Ar), 129.10 (s, Ar), 128.33 (s, Ar), 125.20 (s, Ar), 124.65 (s, Ar), 119.02 (s, Ar), 36.41 (s, ^{t}Bu), 34.50 (s, ^{t}Bu), 34.36 (s, ^{t}Bu), 34.25 (s, ^{t}Bu), 33.11 (s, ^{t}Bu), 32.78 (s, ^{t}Bu), 32.58 (s, ^{t}Bu), 28.67 (s, ^{t}Bu).

Elemental Analysis: Calcd for $C_{148}H_{212}Ce_2K_2O_{13}$. C, 69.50; H, 8.35; Found: C, 68.74; H, 8.17.

6.2.5. Synthesis of complex 5-Pr^{PT} [K(thf)$_6$][KPr$_2$(L^{PT})$_2$(thf)$_4$]

Followed by the similar procedure in the synthesis of complex **5-Ce^{PT}**, the use of $PrCl_3(thf)_2$ lead to the formation of the **5-Pr^{PT}** analogue at a yield of 85% after work up. Crystals were obtained from a concentrated THF solution at room temperature.

^{1}H NMR (500 MHz, THF-d_8) δ 34.58 (s, 4H, Ar), 27.92 (s, 4H, Ar), 26.72 (s, 36H, ^{t}Bu), 13.14 (s, 36H, ^{t}Bu), -2.59 (s, 36H, ^{t}Bu), -11.41 (s, 4H, Ar), -17.64 (s, 36H, ^{t}Bu).

^{13}C NMR (126 MHz, THF-d_8) δ 166.77 (s, Ar), 165.80 (s, Ar), 164.64 (s, Ar), 122.49 (s, Ar), 116.63 (s, Ar), 96.75 (s, Ar), 85.26 (s, ^{t}Bu), 51.27 (s, ^{t}Bu), 47.37 (s, ^{t}Bu), 33.58 (s, ^{t}Bu), 28.92 (s, ^{t}Bu).

Anal. Calcd $C_{160}H_{236}Pr_2K_2O_{16}$. C, 69.28; H, 8.58; Found: C, 68.74; H, 8.17.

6.2.6. Reactions of alkaline earth metal complexes [Ae(L^{PT})$_2$]$_n$ with CeCl$_3$(thf)$_2$

To a THF solution of H_4L^{PT} (0.4617 g, 0.5 mmol, 5 ml) was added a THF solution of $[MgN''_2]_2$ (0.345 g, 1 mmol, 5 ml). The mixture was vigorously stirred for two hours at room temperature, to provide an off-white suspension. The solid was isolated by filtration and was then dissolved in pyridine to form a colourless solution. This solution was then added into a flask containing a pyridine solution of $CeCl_3(thf)_2$ (0.1954 g, 0.5 mmol) to yield a pale yellow-green suspension. The ^{1}H NMR spectra of benzene solutions of the crude product mixture

show many paramagnetically shifted resonances which are different from those in characterised Ce^{III} adducts and could not be readily assigned. No further work-up was carried out.

The reaction with $CaN"_2$ and $SrN"_2$ also produce a mixture which has not been successfully isolated. However, the ^1H NMR spectra of benzene solutions of the crude product mixtures show two sets of paramagnetically shifted resonances which suggest the coordination of the Ce^{3+} ion to the ligand.

6.2.7. Synthesis of complex 6-Ce^P and 6-Ce^{PT} [K(py)$_6$][KCe$_2$(L^P)$_2$(py)$_4$]

0.2684 g (0.1 mmol) of $[K(thf)_7][KCe_2(L^P)_2(thf)_4]$ was dissolved in pyridine (5 ml) and stirred for 2 hours in a Schlenk flask. After volatiles were removed under reduced pressure, 5 ml of hexane was added to the oily residue to precipitate the product **6-Ce** and the supernatant removed by filtration. The white solid was then washed with hexane and dried under vacuum. Pale yellow crystals of **6-Ce** were obtained from a concentrated pyridine solution stored at -30 °C for 5 days. Yield: 0.2644 (82%).

^1H NMR (500 MHz, Pyridine-d_5) δ 10.27 (s, 4H, Ar), 10.20 (s, 4H, Ar), 9.74 (s, 4H, Ar), 5.51 (s, 4H, Ar), 5.44 (s, 4H, Ar), 4.17 (s, 12H, Me), 2.91 (s, 36H, ^{t}Bu), 2.33 (s, 12H, Me), -3.48 (s, 36H, ^{t}Bu).

6.2.8. Synthesis of complex 7-Ce^P [K(18-crown-6)(thf)$_2$][KCe$_2$(L^P)$_2$(thf)$_4$]

0.2684 g (0.1 mmol) of $[K(thf)_7][KCe_2(L^P)_2(thf)_4]$ was dissolved in THF (5 ml) and was added 0.0396 g (0.15 mmol) of 18-crown-6 and was stirred for 2 hours. After solvent was removed under reduced pressure, 5 ml of hexane was added to the oily residue to precipitate the product **7-Ce^P** and filtered off. The white solid was then washed with hexane and dried under vacuum. Colourless crystals were obtained from a concentrated THF solution in freezer at -30 °C. Yield: 0.2018 g (75%).

^1H NMR (500 MHz, THF-d_8) δ 9.76 (s, 4H, Ar), 8.81 (s, 4H, Ar), 7.83 (s, 4H, Ar), 5.45 (s, 4H, Ar), 3.77 (s, 12H, Me), 3.45 (s, 36H, ^{t}Bu), 3.51 (br s, 24H, 18-crown-6), 2.00 (s, 12H, Me), -0.35 (s, 36H, ^{t}Bu).

^{13}C NMR (126 MHz, THF-d_8) δ 197.27, 152.52, 143.56, 138.61, 137.48, 136.38, 129.58, 126.39, 120.21, 68.38, 40.32, 36.54, 34.90, 34.53, 33.52, 33.01, 32.20, 32.02, 27.37, 26.40, 23.28.

6.2.9. Synthesis of complex 8-Ce^{P} and 8-Ce^{PT} [K(thf)$_2$K(L^{PT})$_2$Ce$_2$(thf)$_3$]

The crystals of these complexes were obtained by dissolving complex **5-Ce^{P}** (or **5-Ce^{PT}**) in THF and then layered with an equal volume of hexane. Colourless crystals of the complexes were obtained after the solutions had been stored at room temperature for 3 days.

6.2.10. Oxidation of K$_2$(L^{PT})$_2$Ce$_2$ with I$_2$, CuX$_2$ and HgI$_2$

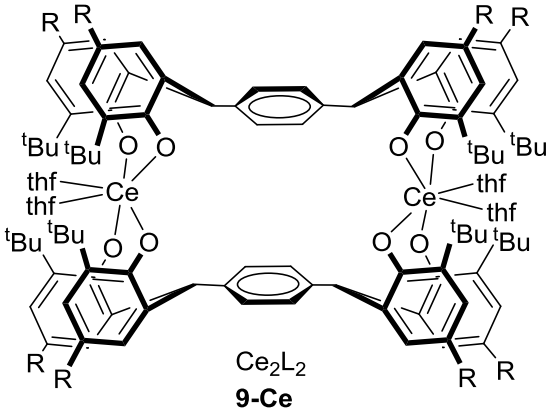

To a stirred THF (5 mL) solution of $K_2L^{PT}{}_2Ce_2$ (0.2858 g, 0.1 mmol) was slowly added a THF solution of oxidant (either $Cu(OTf)_2$ (0.0362 g, 0.1 mmol) or I_2 (0.0253 g, 0.1 mmol) or HgI_2 (0.0454 g, 0.1 mmol)). In each case, the solution changed colour from colourless to dark blue/purple immediately and salts were observed to precipitate. The generated salts were removed by centrifugation then filtration and the solution was transferred to an ampoule to remove volatiles under reduced pressure. Hexane was added to the paste to form a blue powder which was collected and dried under reduced pressure. Crystals of complex **9-Ce^{PT}** were grown by slow diffusion of hexane into a THF solution. Yield: 0.1736 g, 72%.

^{1}H NMR (500 MHz, Benzene-d_6) δ 7.31 (s, 2H, Ar), 6.91 (s, 2H, Ar), 6.79 (s, 4H, Ar), 6.75 (s, 2H, Ar), 6.72 (s, 2H, Ar), 6.49 (s, 2H, Benzylic-C*H*), 2.27 (s, 6H, Me), 2.11 (s, 6H, Me), 1.38 (s, 18H, ^{t}Bu), 0.92 (s, 18H ^{t}Bu).

UV-vis: λ_{max} = 576, 283, 326 nm.

Anal. Calcd. $C_{144}H_{204}Ce_2O_{12}$. C, 71.84; H, 8.54; Found: C, 71.66; H, 8.11.

6.2.11. Reaction of K$_2$(L^{PT})$_2$Ce$_2$ with HgX$_2$

The reaction of $K_2(L^{PT})_2Ce_2$ with $HgCl_2$ was carried out at -30 ˚C. A vial was charged with 0.02850 g (0.01 mmol) **5-Ce^{PT}** in THF-d^8 and was cooled to -30 ˚C. A cold THF-d^8 solution of 2 eq. of HgX_2 (X = Cl, OAc) was then added into the **5-Ce^{PT}** solution with stirring. The colour of the solution changed to dark brown and was then transferred to a Young's tapped NMR tube. The ^{1}H NMR spectrum was collected at 243 K and 298 K on AVA 400.

a: X = Cl. (0.0055 g, 0.02 mmol)

-30 ˚C (243 K): ^{1}H NMR (400 MHz, THF-d_8) δ 13.04 (s, 1H), 10.86 (s, 1H), 10.66 (s, 1H), 9.80 (s, 1H), 9.45 (s, 11H), 8.47 (s, 1H), 7.69 (d, *J* = 44.5 Hz, -2H), 7.51 (s, 1H), 7.31 (s, 3H), 7.19 – 6.65 (m, 11H), 6.47 (t, *J* = 11.1 Hz, 6H), 6.23 (d, *J* = 24.6 Hz, 3H), 6.00 (s, 1H), 5.68

(d, J = 35.1 Hz, 1H), 4.66 (d, J = 7.1 Hz, 1H), 3.01 (s, 15H), 1.93 (s, 11H), 1.67 – 1.45 (m, 48H), 1.45 – 0.91 (m, 107H), 0.58 (s, 13H), 0.33 (s, 14H), -0.36 (s, 14H), -1.94 (s, 18H).

25 °C (298 K): ^{1}H NMR (400 MHz, THF-d_8) δ 7.68 (s, 2H), 7.58 (d, J = 2.4 Hz, 1H), 7.56 (d, J = 2.4 Hz, 1H), 7.43 (d, J = 2.4 Hz, 3H), 7.37 (d, J = 2.4 Hz, 4H), 7.31 (d, J = 2.4 Hz, 5H), 7.08 (dd, J = 7.3, 2.4 Hz, 3H), 7.04 (dd, J = 5.8, 3.0 Hz, 7H), 6.99 (s, 2H), 6.96 (d, J = 8.7 Hz, 4H), 6.91 – 6.75 (m, 25H), 1.57 (s, 46H), 1.52 (d, J = 4.8 Hz, 32H), 1.28 (s, 17H), 1.26 (d, J = 4.5 Hz, 28H), 1.23 (s, 27H), 1.15 (dt, J = 9.7, 4.0 Hz, 101H), 1.10 (s, 12H), 1.05 (s, 16H), 0.99 (s, 16H).

b: X = OAc, (0.0064 g, 0.02 mmol)

The reaction of **5-Ce^{PT}** and $Hg(OAc)_2$ at -30 °C affords a dark blue solution immediately. The ^{1}H NMR spectrum at -30 °C (243 K) shows 10% of paramagnetic product and one major (90%) diamagnetic product.

-30 °C (243 K): ^{1}H NMR (400 MHz, THF-d_8) δ 10.32 (s, 1H), 9.76 – 8.96 (m, 8H), 7.37 (d, J = 2.4 Hz, 4H), 7.34 (d, J = 2.1 Hz, 3H), 6.94 (s, 10H), 6.86 (d, J = 2.5 Hz, 4H), 6.75 (d, J = 2.2 Hz, 1H), 6.73 (s, 2H), 5.49 (s, 2H), 4.62 (s, 3H), 2.40 (d, J = 30.1 Hz, 35H), 1.47 (d, J = 8.0 Hz, 49H), 1.35 – 1.21 (m, 51H), 1.17 (s, 45H), 1.10 (s, 52H), 0.07 (s, 1H).

25 °C (298 K): ^{1}H NMR (400 MHz, THF-d_8) δ 7.33 (d, J = 12.4 Hz, 4H, Ar), 7.07 (s, 4H, Ar), 6.95 (s, 2H, benzylic-CH), 6.88 (s, 4H, Ar), 1.46 (s, 18H, ^{t}Bu), 1.34 (s, 18H, ^{t}Bu), 1.19 (s, 18H, ^{t}Bu), 1.14 (s, 18H, ^{t}Bu).

6.2.12. Reaction of $K_2(L^{PT})_2Ce_2$ with other oxidants

General procedure: To a stirring THF (5 mL) solution of 0.2858 g (0.1 mmol) $K_2L^{PT}{}_2Ce_2$ was slowly added a THF solution of oxidants. The mixture was left to stir for 2 hours. The generated salts were removed by centrifugation and the solution was transferred to an ampoule to remove volatiles under reduced pressure. Hexane (5 ml) was added to the paste, the resulting powder was collected and dried under reduced pressure.

a: Ph_3CCl: 0.0562 g (0.2 mmol). The solution changed to dark brown immediately, and the solid isolated after workup is brown.

^{1}H NMR (500 MHz, Benzene-d_6) δ 7.24 (s, 4H, Ar), 6.85 (d, J = 2.2 Hz, 4H, Ar), 6.83 (s, 4H, Ar), 6.67 (s, 4H, Ar), 4.98 (s, 2H, benzylic-CH), 2.24 (s, 12H, Me), 2.10 (s, 12H, Me), 1.56 (s, 36H, ^{t}Bu), 1.18 (s, 36H, ^{t}Bu).

UV-vis: λ_{max} = 512 nm

b: 1,4-benzoquinone 0.0108 g (0.1 mmol). Dark brown/purple solution and dark brown solid obtained after work up.

^{1}H NMR (500 MHz, THF-d_8) δ 7.28 (s, 4H, Ar), 7.00 (s, 4H, Ar), 6.86 (s, 4H, Ar), 5.97 (s, 4H, Ar), 1.45 (br s, 18H, ^{t}Bu), 1.22 (s, 18H, ^{t}Bu), 1.13 (s, 18H, ^{t}Bu), 1.11 – 0.96 (br s, 9H, ^{t}Bu). UV-vis: λ_{max} = 513 nm

c: O_2.

A Young's NMR tube was charged with a THF-d^8 (1 mL) solution of 0.1430 g (0.05 mmol) $K_2L^{PT}{}_2Ce_2$. The NMR tube was then degassed. Dry air was passed through a drying column and was added to the solution at a pressure of 1 atm. The colour of the solution changed to red-brown immediately. The NMR tube was then vigorously shaken and the mixture was open to the dry air for 1 min. The generated salts were removed by centrifugation and the solution was transferred to an ampoule to remove solvents under reduced pressure. Hexane was added to the paste, the resulting powder was collected and dried under reduced pressure.

^{1}H NMR (500 MHz, THF-d_8) δ 7.67 (s, 4H, Ar), 7.36 (s, 4H, Ar), 7.24 (s, 4H, Ar), 7.08 (s, 4H, Ar), 7.03 (d, J = 8.9 Hz, 4H, Ar), 6.95 (d, J = 10.0 Hz, 16H, Ar), 6.83 (s, 4H, Ar), 1.51 (s, 36H, ^{t}Bu), 1.28 (s, 36H, ^{t}Bu), 1.14 (d, J = 4.8 Hz, 36H, ^{t}Bu), 0.98 (s, 36H, ^{t}Bu).

UV-vis: λ_{max} = 472 nm.

6.2.13. **Reaction of $K_2(L^{PT})_2Pr_2$ with I_2**

A THF (5 mL) solution of 0.2958 g (0.1 mmol) $K_2L^{PT}{}_2Pr_2$ and 0.013g (0.1 mmol) I_2 solid was mixed in a Schlenk flask. The solution was then heated for 8 hours in an oil bath at 60 °C. Upon heating, the solution changed to dark brown gradually and finally turned to dark green. The generated salts were removed by filtration and the solution was transferred to an ampoule to remove volatiles under reduced pressure. Hexane was added to the paste, white powder was filtered and washed with more hexane and then dried under reduced pressure. The green hexane solution was collected and combined together. After the removal of solvents, greenish solid was formed. Crystals of the white material were grown by slow diffusion of hexane into a THF solution. Yield: 0.1027 g, 29%.

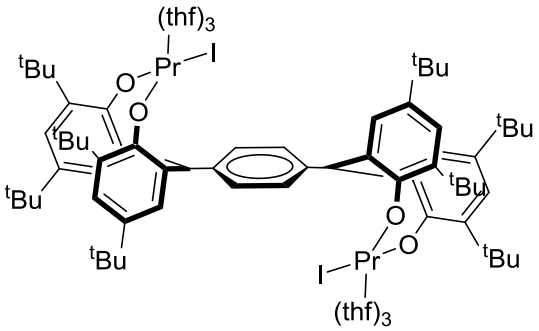

16-Pr^{PT}

^{1}H NMR (500 MHz, THF-d_8) δ 13.67 (s, 4H, Ar), 12.46 (s, 4H, Ar), 10.33 (s, 36H, ^{t}Bu), 5.15 (s, 4H, Ar), 4.48 (s, 2H, Benzylic-C*H*), 1.17 (s, 36H, ^{t}Bu).

Green solution: ^{1}H NMR (500 MHz, THF-d_8) δ 17.94 (s, 4H, Ar), 15.23 (s, 4H, Ar), 11.07 (s, 4H, Ar), 10.85 (s, 18H, Ar), 0.71 (s, 18H), -0.09 (s, 18H, ^{t}Bu).

6.2.14. **Reaction of $K_2(L^{PT})_2Pr_2$ with XeF_2**

To a THF (5 mL) solution of 0.2958 g (0.1 mmol) $K_2L^{PT}{}_2Pr_2$ was slowly added a THF solution of 0.017 g (0.1 mmol) XeF_2 at -30 °C. The solution changed to bright green and then during the stirring, white precipitate gradually come out. The generated solid was then collected and dried under reduced pressure. This product decomposes gradually during work up. Yield: 0.1723 g.

6.2.15. **Reaction of $CuOTf_2$ with 1^P and $CeCl_3(thf)_2$**

Two equivalents of $CuOTf_2$ was added to a THF solution of $\mathbf{2^P}$ to form a brown solution with precipitate overnight. ^{1}H NMR spectrum shows multiple products with no resonance for the starting material. To this suspension was added one eq. of $CeCl_3(thf)_2$ and was allowed to stir for 2 hours. The ^{1}H NMR spectrum of the crude materials shows no reaction occurred.

6.2.16. **Reaction of $K_2(L^P)_2Ce_2$ with KC_8**

To a THF solution of 0.2984 (0.1 mmol) g $K_2L^P{}_2Ce_2$ was added 0.0284 g KC_8 (0.2 mmol). The mixture was left to stir for 12 hours. The colourless solution changed to yellow-green and the solid was filtered off. The yellow solution was then transferred to an ampoule to remove solvents and volatiles under reduced pressure. Hexane was added to the oily paste, and the resulting orange solid was collected and dried under reduced pressure. Yield: 0.1736 g.

^{1}H NMR (400 MHz, Benzene-d_6) δ 21.52 (s, 2H), 14.99 (s, 2H), 11.51 (s, 2H), 6.28 (s, 4H), 2.38 (s, 6H), -1.83 (s, 18H, ^{t}Bu), -2.92 (d, J = 108.6 Hz, 18H, ^{t}Bu), -3.27 – -4.15 (m, 18H, ^{t}Bu), -6.97 (s, 18H, ^{t}Bu).

6.2.17. **The reaction of $K_2(L^P)_2Ce_2$ with MeLi.**

To a THF solution of 0.1560 g (0.05 mmol) $K_2L^P{}_2Ce_2$ was added 0.0044 g (0.2 mmol) MeLi. The mixture was left to stir for 8 hours. The colourless solution changed to red with the constant emission of bubbles. The yellow solution was then transferred to an ampoule to remove solvents and volatiles under reduced pressure. Hexane was added to the oily paste, and yellow solid was collected and dried under reduced pressure. Yield: 0.0836 g.

^{1}H NMR (400 MHz, Benzene-d_6) δ 18.88 (s, 4H), 13.66 (s, 4H), 10.61 (s, 4H), 10.03 (s, 4H), 6.23 (s, 12H), 4.88 (s, 12H), -3.77 (br s, 36H, ^{t}Bu), -5.32 (s, 36H, ^{t}Bu).

6.2.18. **Reaction of $K_2(L^P)_2Ce_2$ with KBn in THF**

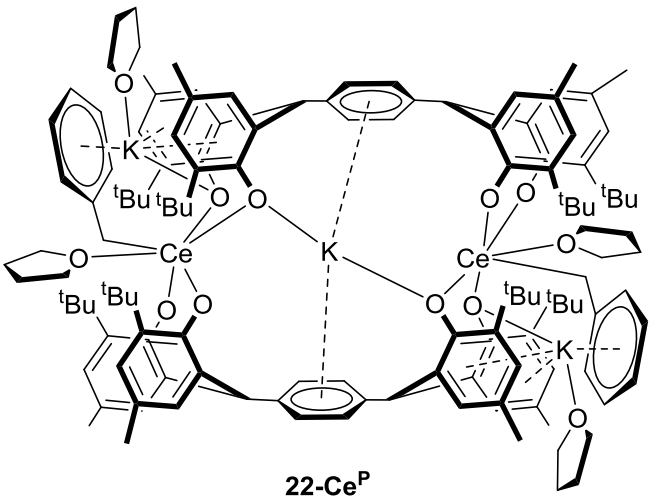

22-Ce^P

To a vigorously stirred THF solution of $K_2L^P{}_2Ce_2$ (0.2684 g, 0.1 mmol) was slowly added THF solution of KBn (0.05210 g, 0.4 mmol). The solution changed to red. The mixture was left to stir for 2 hours and then all solvents were removed under reduced pressure. Hexane was added to form a yellow powder. Washed with hexane and the solid was collected and dried under reduced pressure. X-ray quality single crystals were obtained by diffusion of hexane into THF solution at -30 ˚C. Yield: 0.1473 g (57%).

^{1}H NMR (500 MHz, THF-d_8) δ 9.80 (s, 2H, Ar), 9.11 (s, 2H, Ar), 8.37 (s, 2H, Ar), 7.20 (d, J = 7.5 Hz, 4H, Ar), 7.15 (d, J = 7.5 Hz, 4H, Ar), 7.11 (t, J = 7.3 Hz, 2H, Ar), 6.00 (s, 4H, Ar), 5.66 (s, 2H, benzylic-CH), 4.80 (t, J = 6.8 Hz, 4H, $PhCH_2$), 2.35 (d, J = 6.6 Hz, 18H, ^{t}Bu), 2.21 (s, 12H, Me), 2.14 (s, 12H, Me), 1.78 (s, 18H, ^{t}Bu), 1.15 (s, 18H, ^{t}Bu), -0.16 (s, 18H, ^{t}Bu), -2.27 (s, 18H, ^{t}Bu).

Anal. Calcd. $C_{142}H_{194}Ce_2K_3O_{12}$, C, 68.48; H, 7.85; Found: C, 67.57; H, 7.73.

After allowing the reaction mixture to stir for 2 days, colourless crystals were observed to have formed and a crop was isolated after a week. The crystals are characterised as a THF ring opening product $K_{10}(L^{PT})_2(OCH{=}CHCH_2CH_3)_2(thf)_6$ by X-ray single crystal diffraction and isolated in 20 % yield (0.0860 g).

Follow the similar procedure, the analogue of $KL^{PT}{}_2Ce_2Bn_2$ can also be isolated.

^{1}H NMR (500 MHz, Benzene-d_6) δ 9.50 (s, 4H, Ar), 8.91 (s, 4H, Ar), 7.06 (t, J = 7.5 Hz, 2H, Ar), 7.03 – 6.90 (m, 4H, Ar), 6.04 (t, J = 7.1 Hz, 8H, Ar), 5.54 (s, 4H, trityl CH), 4.83 (s, 4H, Ar), 2.15 (s, 4H, $PhCH_2$), -0.15 (s, 36H, ^{t}Bu), -3.33 (s, 36H, ^{t}Bu).

6.2.19. **Reaction of $K_2(L^{PT})_2Ce_2$ with KBn in Et_2O**

To a vigorously stirred Et_2O suspension of $K_2(L^{PT})_2Ce_2$ (0.2854 g, 0.1 mmol) was slowly added an Et_2O suspension of orange-red KBn (0.05210 g, 0.4 mmol). The solution colour changed to red while the KBn solid disappeared gradually. The mixture was left to stir for 2 hours and then all solvents were removed under reduced pressure. Hexane was added to form yellow solid. After washed with hexane, the solid was collected and dried under reduced pressure. Yellow crystals were obtained by the slow diffusion of an Et_2O solution at room temperature. Yield: 0.2527 g (87%)

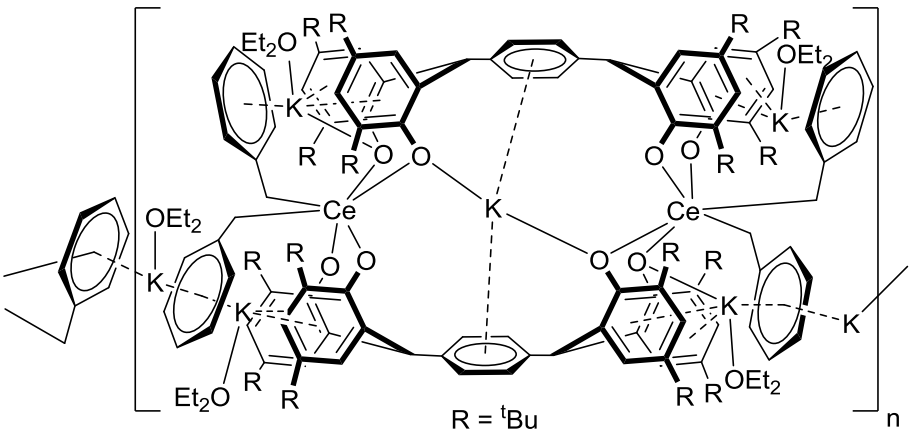

24-Ce^{PT}

^{1}H NMR (500 MHz, Benzene-d_6) δ 9.16 (s, 4H, Ar), 7.07 (t, J = 7.7 Hz, 4H, Ar), 6.99 (d, J = 7.5 Hz, 5H, Ar), 6.31 (s, 4H, Ar), 4.38 (s, 4H, Ar), 3.93 (s, 4H, $PhCH_2$), 2.15 (s, 4H, $PhCH_2$), 2.01 (s, 36H, ^{t}Bu), -2.99 (s, 36H, ^{t}Bu).

6.2.20. **The reaction of $[K_3(L^P)_2Bn_2]$ with PhCCH**

To a vigorously stirred THF solution of 0.2240 g (0.1 mmol) complex **22-Ce^P** was slowly added THF solution of phenyl acetylene (22 μL, 0.2 mmol). The solution changed to yellow-green after the addition. The mixture was left to stir for 4 hours and then all solvents and volatiles were removed under reduced pressure. Hexane was added to form a yellow powder. Washed with hexane and the solid was collected and dried under reduced pressure. Yield: 0.1873 g.

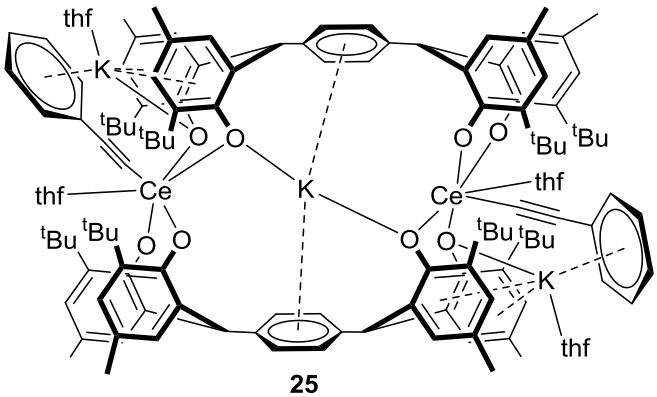

25

^{1}H NMR (500 MHz, THF-d_8) δ 8.68 (s, 4H, Ar), 7.18 (t, J = 7.5 Hz, 4H, Ar), 7.14 – 7.05 (m, 6H, Ar), 6.92 – 6.49 (m, 8H, Ar), 5.97 – 5.85 (m, 4H, Ar), 5.85 – 5.70 (m, 4H, benzylic-CH), 3.49 (s, 18H, ^{t}Bu), 2.30 (s, 12H, Me), 1.93 (s, 12H, Me), 1.72 (s, 18H, ^{t}Bu), 0.05 (s, 18H, ^{t}Bu), -5.11 (s, 18H, ^{t}Bu).

6.2.21. **The reaction of $[K_3(L^P)_2Bn_2]$ with CO_2**

A J-Young Teflon valve NMR tube was charged with a THF-d^8 (1 mL) solution of 0.1120 g (0.05 mmol) complex **22-Ce^P**. The NMR tube was then degassed. CO_2 was then passed through a drying column and was connected to the tube at a pressure of 1 atm at room temperature. White precipitate came out immediately. The NMR tube was then vigorously shaken and the mixture was open to CO_2 air for 30 seconds. The generated white solid was collected by centrifugation and the solution was examined by ^{1}H NMR spectroscopy which showed no resonance for the starting material. Hexane was added to the solid, the resulting powder was collected and dried under reduced pressure with a yield of 0.1028 g (75 % based on CO_2 insertion).

^{1}H NMR (500 MHz, Pyr-d_5) δ 9.82 (s, 4H, Ar), 7.13 (m, 4H, Ar), 6.87 (m, 5H, Ar), 6.39 (s, 4H, Ar), 4.27 (s, 4H, Ar), 2.42 (s, 4H, $PhCH_2CO_2$), 2.21 (s, 12H, Me), 2.14 (s, 12H, Me), 1.95 (s, 18H, ^{t}Bu), 1.27 (s, 18H, ^{t}Bu), -0.25 (s, 18H, ^{t}Bu),-2.89 (s, 18H, ^{t}Bu).

IR(nujol): 1682, 1501, 1378, 1317, 1257, 1208 cm^{-1}

6.2.22. **The reaction of $[K_3(L^P)_2Bn_2]$ with CS_2**

To a THF solution of 0.2245 g (0.1 mmol) complex **22-Ce^P** was added excessive amount of CS_2/touluene solution. The mixture was left to stir for 2 hours to afford a yellow solution. The solvents and volatiles were removed under reduced pressure to form a light yellow paste. Hexane was then added to the oily paste, and light yellow solid was collected and dried under reduced pressure. Yield: 0.1642 g.

^{1}H NMR (500 MHz, THF-d_8) δ 9.75 (s, 2H, Ar), 9.11 (s, 2H, Ar), 8.37 (s, 2H, Ar), 7.28 (d, J = 7.5 Hz, 4H, Ar), 7.17 (d, J = 7.5 Hz, 4H, Ar), 7.08 (t, J = 7.3 Hz, 2H, Ar), 5.94 (s, 4H, Ar), 5.51 (s, 2H, benzylic-CH), 4.74 (d, J = 6.8 Hz, 4H, $PhCH_2$), 2.24 (s, 18H, ^{t}Bu), 1.03 (s, 18H, ^{t}Bu), 0.19 (s, 18H, ^{t}Bu), -2.32 (s, 18H, ^{t}Bu).

6.2.23. **The reaction of $K_2(L^R)Ce_2$ with other substrates**

Treatment of complex **5-Ce^R** (R = P, PT) with one or two equivalents of transition metal chloride $MCl_2(thf)_n$ (M = Fe, Co, Ge, Sm) or $Ni(COD)_2$ in THF showed no change in the ^{1}H NMR spectroscopy. Complex **5-Ce** also did not show any reactivity towards small molecules such as CO_2, CS_2, H_2 or CO under room temperature.

6.2.24. **The synthesis of $L^{PT}Pr_2Cl_2$**

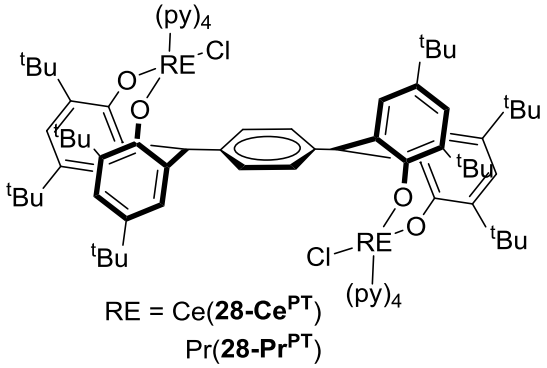

RE = Ce(**28-Ce^{PT}**)
Pr(**28-Pr^{PT}**)

A Teflon-valve ampoule with a magnetic stirrer-bar was charged with H_4L^{PT} (0.9235 g, 1 mmol) and KN" (4eq, 0.7998 g, 0.4 mmol). THF was added (10 ml), the solution was stirred for 1 hour. The resulting yellow solution was slowly added to THF suspension of $PrCl_3(thf)_2$, (2eq, 0.6547 g, 2 mmol). The mixture was left to stir overnight. The solvents were removed by filtration and volatiles in the white solid were removed under reduced pressure. The solids were then extracted by pyridine (2 x 20 ml), after removal of solvents and wash with hexane, white precipitate was collected and dried under reduced pressure. Single crystals suitable for X-ray were grown by vapour diffusion of hexane into a saturated pyridine solution at ambient temperature. Yield: 0.1728 g (90%).

^{1}H NMR (500 MHz, Pyridine-d_5) δ 15.35 (s, 4H, Ar), 14.18 (s, 4H, Ar), 5.33 (s, 4H, Ar), 3.91 (s, 36H, ^{t}Bu), 3.71 (s, 2H, benzylic-CH), 2.30 (s, 36H, ^{t}Bu).

^{13}C NMR (126 MHz, Pyridine-d_5) δ 157.63, 142.01, 132.28, 125.97, 35.51, 34.15, 30.37.

Anal. Calcd. $C_{104}H_{126}Pr_2Cl_2N_8O_4$. C, 65.63; H, 6.67; N, 5.89. Found: C, 65.28; H, 6.56; N, 5.71.

6.2.25. **The synthesis of $L^{PT}CeCl_2$**

Followed by the similar procedure of the synthesis of $L^{PT}PrCl_2$, treatment with $CeCl_3(thf)_2$ led to the formation of the Ce analogue of complex **28**. The yield of this reaction is

^{1}H NMR (500 MHz, Pyridine-d_5) δ 10.62 (s, 4H, Ar), 9.61 (s, 4H, Ar), 5.27 – 4.67 (br s, 4H, Ar), 3.68 (s, 2H, benzylic-CH), 2.03 (s, 36H, ^{t}Bu), 0.20 (s, 36H, ^{t}Bu). ^{13}C NMR (126 MHz, Pyridine-d5) δ 155.91, 140.76, 131.27, 126.54, 35.94, 33.94, 30.49. Anal. Calcd. $C_{104}H_{126}Ce_2Cl_2N_8O_4$. C, 65.57; H, 6.67; N, 5.88. Found: C, 65.31; H, 6.34; N, 5.73.

Note: This complex is readily oxidised by trace amounts of O_2 to afford a brown colour solution which shows diamagnetic resonances in ^{1}H NMR.

6.2.26. **The reaction of $L^{PT}Pr_2Cl_2$ with $AgPF_6$**

0.1905 g (0.1 mmol) $L^{PT}Pr_2Cl_2$ and 0.0562 g (0.2 mmol) $AgPF_6$ was mixed in pyridine and was stirred for 4 hours. The resulting yellow solution was separated from the pale solid of AgCl by filtration. The volatiles in the solution were removed under reduced pressure. The

yellow solids were then washed with hexane and dried under reduced pressure. Yield: 0.1547 g.

^{1}H NMR (500 MHz, THF-d_8) δ 28.35 (s, 1H), 22.49 (s, 1H), 19.47 (s, 4H), 14.78 (s, 1H), 10.73 (s, 1H), 7.51 (s, 8H), 2.51 (s, 26H), 2.39 (s, 2H), 0.30 (d, J = 37.4 Hz, 18H), -3.51 (s, 36H), -3.79 (s, 36H), -4.79 (s, 9H), -5.40 (s, 9H), -24.60 (s, 4H). ^{19}F NMR (471 MHz, Pyridine-d_5) δ -71.30 (d, J = 710.4 Hz).

6.2.27. **The synthesis of $L^{PT}RE_2N"_2$**

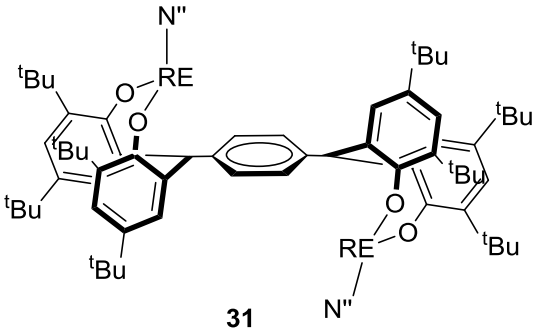

31

a. RE = Pr. To a pyridine solution of 0.1905 g (0.1 mmol) $L^{PT}Pr_2Cl_2$ was added 0.0201 g (0.2 mmol) KN" and was stirred for 4 hours to form a yellow solution. After the removal of the volatiles in the solution, the yellow product was obtained and was then washed with hexane and dried under reduced pressure. Colourless crystal of the product was obtained from a concentrated THF solution. Yield: 0.1670 g (75%).

^{1}H NMR (500 MHz, THF-d_8) δ 22.42 (s, 4H, Ar), 18.46 (s, 4H, Ar), 7.39 (s, 4H, Ar), 3.00 (s, 36H, ^{t}Bu), -8.12 (s, 36H, $SiMe_3$), -12.38 (s, 36H, ^{t}Bu). ^{29}Si NMR (99 MHz, THF) δ -68.49.

Anal. Calcd. $C_{76}H_{122}Pr_2N_2O_4Si_4$. C, 60.04; H, 8.09; N, 1.84. Found: C, 59.47; H, 8.24; N, 1.63.

b. RE = Ce.

^{1}H NMR (500 MHz, THF-d_8) δ 12.65 (s, 4H, Ar), 10.94 (s, 4H, Ar), 7.94 (s, 4H, Ar), 7.15 (s, 2H, benzylic-CH), 1.41 (s, 18H, ^{t}Bu), -1.54 (s, 32H), -2.91 (s, 18H, ^{t}Bu), -5.53 (s, 18H, ^{t}Bu). ^{29}Si NMR (99 MHz, THF) δ -35.77.

Anal. Calcd. $C_{76}H_{122}Ce_2N_2O_4Si_4$. C, 60.04; H, 8.09; N, 1.84. Found: C, 57.47; H, 7.68; N, 1.58.

6.2.28. **The synthesis of $(L^{PT})Ce_2(BH_4)_4$**

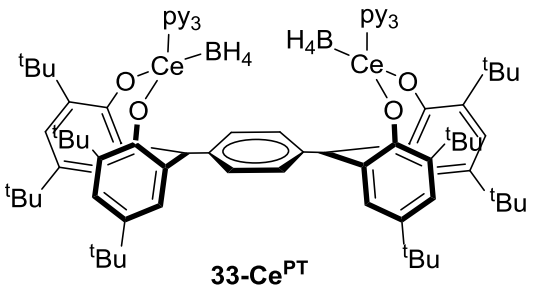

33-Ce^{PT}

A pyridine solution of $K_8L^{P}_2$ 0.1268 g (0.5 mmol) was slowly added to a Schlenk flask which was charged with pyridine solution of 0.1850 g (1 mmol) $Ce(BH_4)_3$. The mixture was left to stir overnight at room temperature to form a light yellow solution. Hexane was added to precipitate the product as white powder. The solid was further washed with hexane and was dried under reduced pressure.

Yield: 0.1341 g (80%). Colourless crystals of the product were grown from concentrated THF solution at -30 ˚C.

^{1}H NMR (500 MHz, Pyridine-d_5) δ 10.49 (s, 4H, Ar), 9.62 (s, 4H, Ar), 4.13 (s, 4H, Ar), 3.69 (t, J = 7.4 Hz, 2H), 2.09 (s, 36H, ^{t}Bu), 0.02 (s, 36H, ^{t}Bu).^{13}C NMR (126 MHz, Pyridine-d_5) δ 196.01, 155.45, 143.24, 141.10, 131.14, 125.67, 68.36, 40.44, 37.24, 35.97, 33.99, 32.27, 30.32, 26.36. ^{11}B NMR (160 MHz, Pyridine-d_5) δ 20.9 (br s).

6.2.29. **The reactions of H_4L with $Ce(BH_4)_3$ to target $(L^{PT})Ce_2(BH_4)_4$**

0.1850 g (1 m mol) of $Ce(BH_4)_3$ reacts with 0.0413 g (0.5 mmol) of H_4L^{PT} in THF with borane acceptors ($P(Cy)_3$, $P(Ph)_3$ or DABCO) to liberate hydrogen gas as verified by ^{1}H NMR spectroscopy. Monitoring these reactions by NMR spectroscopy showed that the reaction proceeds slowly and takes 5 days for completion. The final NMR spectra are similar regardless of the borane acceptor but contain multiple unidentified products. Attempts to crystallize the resulting products resulted in the crystallization of the borane adduct.

^{1}H NMR (500 MHz, Pyridine-d_5) δ 10.70 (s, 4H, Ar), 9.56 (s, 4H, Ar), 4.44(s, 2H, benzylic-CH), 3.54-2.89 (m, 8H, BH_4), 2.17 (s, 36H, ^{t}Bu), -0.08 (s, 36H, ^{t}Bu), -3.48 (s, 4H), -8.36 (s, 18H). ^{11}B NMR (160 MHz, Pyridine-d_5) δ 12.26 (br s).

6.2.30. **The reaction of 2^{PT} with $(Et_4N)_2CeCl_6$**

KN" (0.082 g, 0.44 mmol) and **H_4L^{PT}** (0.100 g, 0.11 mmol) were stirred in THF for 1 hour, resulting in a light yellow solution. This solution was then added into a THF suspension of 0.1195 g (0.22 mmol) $(NEt_4)_2CeCl_4$ and stirred for 2 hours, resulting in a dark purple solution with some precipitate. The precipitate was removed by centrifugation, then the volatiles were removed under vacuum to afford a purple solid. The purple solid was recrystallized in THF at -30°C. Crystals were grown from concentrated THF solution. However, the crystal data were poor and only vague structure of the product can be seen from the poor data which shows the existence of $[(NEt_4)_4L^{PT}Ce_2Cl_8]$.

^{1}H NMR (500 MHz, Pyridine-d_5) δ 8.14 (d, J = 2.3 Hz, 2H, Ar), 8.08 (d, J = 2.4 Hz, 2H, Ar), 7.82 (s, 2H, Ar), 7.60 (s, 2H, Ar), 7.48 (d, J = 2.6 Hz, 2H, Ar), 7.16 (d, J = 2.5 Hz, 2H, Ar), 1.91 (s, 18H, ^{t}Bu), 1.53 (s, 18H, ^{t}Bu), 1.41 (s, 18H, ^{t}Bu), 1.40 (s, 18H, ^{t}Bu).

6.2.31. **Representative CHO-CO_2 copolymerization procedure**

All the manipulations were performed in a glove box under dry nitrogen atmosphere. In a 10 mL glass vial, catalyst (0.011 mmol, 0.033 g for **5-Ce^{PT}** or 0.0168 g for **31-Ce** or 0.0170 g for **31-Pr**) and cyclohexene oxide (5.82 g, 59.4 mmol), and *iso*-propanol (1.7 µL, 0.022 mmol) were mixed and allowed to stir for 5 minutes. This was then transferred to a 25 mL Parr reactor inside the glove box. The properly closed reactor was then taken outside the glove box and fitted with a high-pressure CO_2 line in a fume hood. The reactor was gently purged using CO_2 in order to ensure a complete CO_2 atmosphere inside the reactor. The reactor was then filled with 20 bars of CO_2 and heated up to 80 °C with continuous stirring. The CO_2 pressure was then adjusted to 40 bar. The polymerization stopped after desired time by a rapid cooling of the reactor. The excess carbon dioxide was released. An aliquot was taken from the crude mixture to perform the ^{1}H NMR in order to estimate the conversion and product distribution. The crude polymerization mixture was then precipitated from cold pentane. The precipitated polymer dried under vacuum at 50 °C for 48 hours. The dried polymer was used to perform GPC and other analyses.

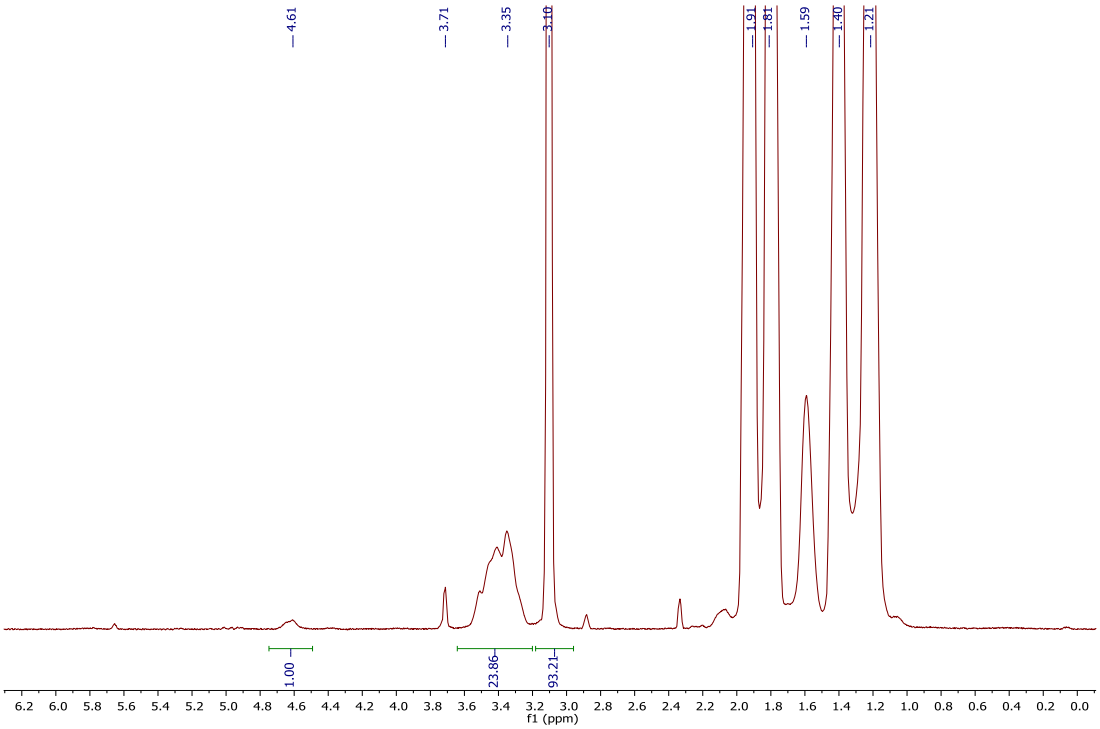

Figure 6-1. ^{1}H NMR spectrum of crude polymerization mixture obtained from the copolymerization of CHO and CO_2 using ($CDCl_3$, 400 MHz) - entry 1, **Table 2-15**.

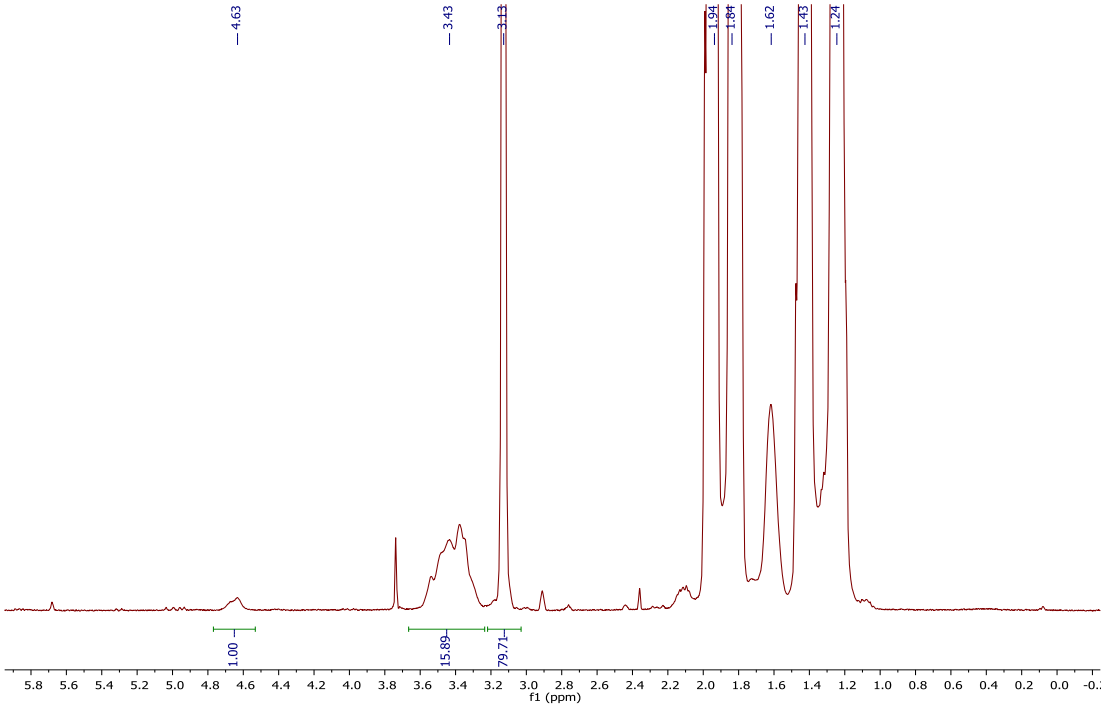

Figure 6-2. ^{1}H NMR spectrum of crude polymerization mixture obtained from the copolymerization of CHO and CO_2 using ($CDCl_3$, 400 MHz) - entry 2, **Table 2-15**.

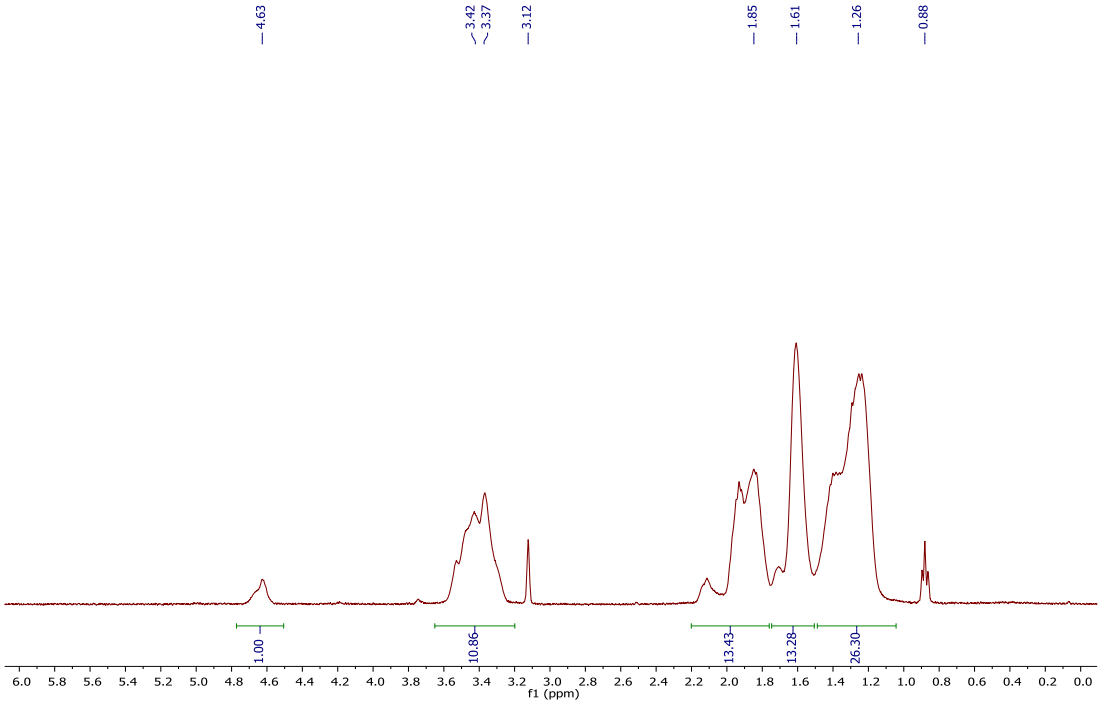

Figure 6-3. ^{1}H NMR spectrum of isolated polycyclohexene oxide obtained from the copolymerization of CHO and CO_2 using ($CDCl_3$, 400 MHz) - entry 2, **Table 2-15**.

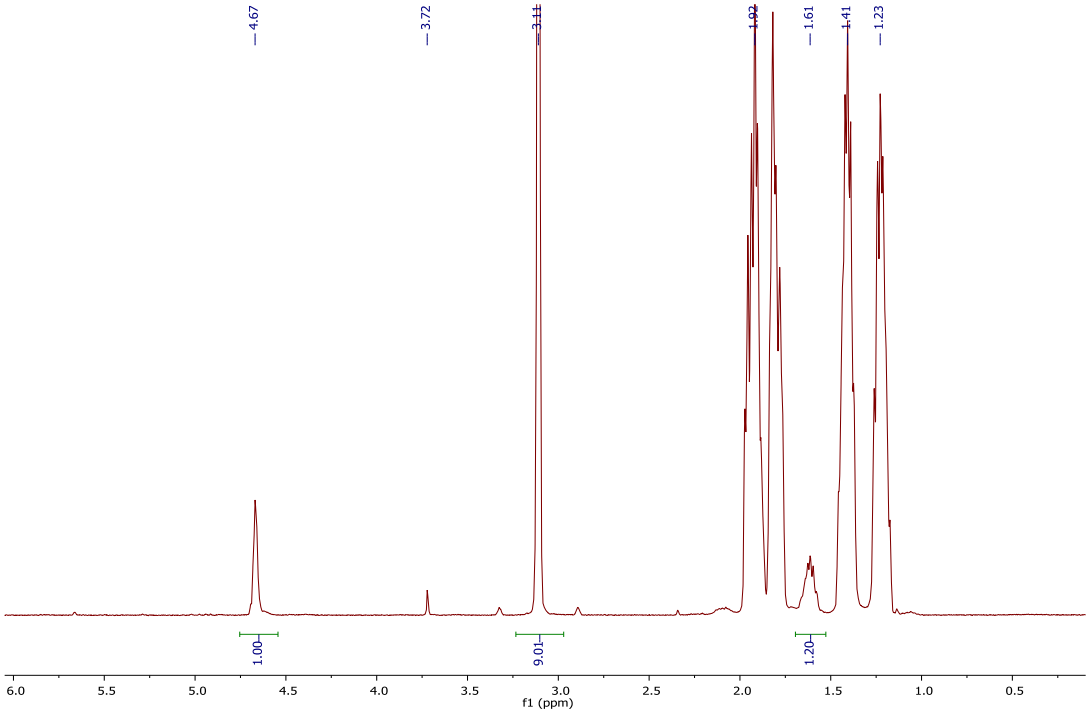

Figure 6-4. ^{1}H NMR spectrum of crude polymerization mixture obtained from the copolymerization of CHO and CO_2 using ($CDCl_3$, 400 MHz) - entry 3, **Table 2-15**.

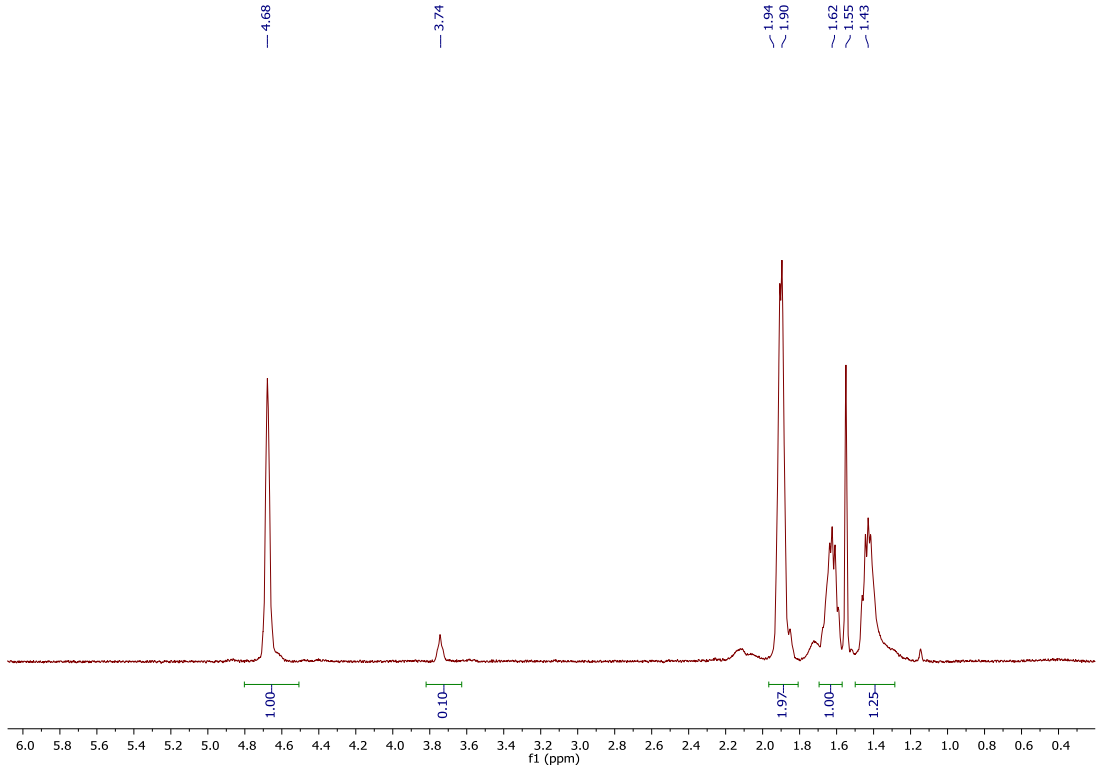

Figure 6-5. ^{1}H NMR spectrum of isolated *cis*-cyclohexene carbonate obtained from the copolymerization of CHO and CO_2 using ($CDCl_3$, 400 MHz) - entry 3, **Table 2-15**.

6.3. Experimental for Chapter 3

6.3.1. **Synthesis of β-ketoimidazolinium salts**

To a toluene solution of N-mesitylimidazolene was added one equivalent of 2-halomethylketone derivative: $RC{=}OCH_2X$, (R = ^{t}Bu, X = Cl; R = naphth; X = Br). After being heated to reflux for 10 hours, a white precipitate formed. After allowing the suspension to cool to room temperature, the precipitate was isolated by filtration and washed with hot hexane to yield compound as a white solid.

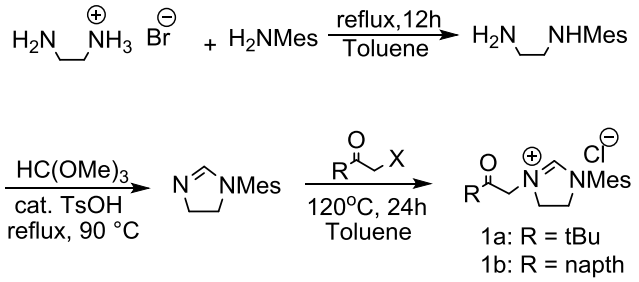

38e: [(tBu)C(O)CH_2{CH[NCH_2CH_2N(Mes)]}]Cl, yield: 83%

Yield: 83 %; ^{1}H NMR ($CDCl_3$, 500 MHz): δ 9.68 (s, 1H), 6.92 (s, 2H, CH), 5.44 (s, 2H, CH_2), 4.16 (s, 4H, CH_2), 2.32 (s, 6H, CH_3), 2.27 (s, 3H, CH_3), 1.25 (s, 9H, $C(CH_3)_3$).

^{13}C NMR (126 MHz, CDCl3): δ 208.6 (C=O), 161.5 (CH), 140.1 (Cq), 135.1 (Cq), 130.5 (Cq), 129.8 (CH), 52.9 (N$\underline{C}H_2$), 51.0 (N$\underline{C}H_2CH_2$N), 49.9 ($NCH_2\underline{C}H_2$N), 43.1 ($\underline{C}(CH_3)_3$), 26.1 ($C(\underline{C}H_3)_3$), 20.9 ($\underline{C}(CH_3)_3$), 17.7 (Ph($\underline{C}H_3)_2$); ESI (+ve) M^+ = 287.21 m/z [M^+-Cl];

Anal. Calcd $C_{18}H_{27}ClN_2O$ (322.88): C, 66.96; H, 8.43; N, 8.68; Found: C, 67.10; H, 8.36; N, 8.61;

IR (CH_2Cl_2) ν_{max}/cm^{-1} 1719 (s); IR (neat) ν_{max}/cm^{-1} 1715(s).

38f [(naphth)C(O)CH_2{CH[NCH_2CH_2N(Mes)]}]Br, yield: 90%

Yield: 90 %; ^{1}H NMR ($CDCl_3$, 500 MHz): δ 9.27 (s, 1H), 8.52 (s, 1H), 7.93 (d, J = 8.4 Hz, 1H), 7.90 (d, J = 8.4, 1H), 7.65 (dd, J = 8.4, 8.4 Hz, 2H), 7.43 (t, J = 7.5 Hz, 1H), 7.34 (t, J = 7.5 Hz, 1H), 6.75 (s, 2H), 5.84 (s, 2H), 4.27 (t, J = 10.6 Hz, 2H), 4.13 – 4.00 (t, J = 10.6 Hz, 2H), 2.19 (s, 6H), 2.12 (s, 3H);

^{13}C NMR (126 MHz, $CDCl_3$): δ 192.7 (CO), 161.1 (CH), 140.3 (C_q), 136.0 (C_q), 135.3 (C_q), 132.4 (C_q), 131.1 (CH), 130.5 (C_q), 130.0 (CH), 129.2 (CH), 128.9 (CH), 127.7 (CH), 127.0 (CH), 123.3 (CH), 54.8 (N$\underline{C}H_2$), 51.2 (N$\underline{C}H_2CH_2$N), 50.5 ($NCH_2\underline{C}H_2$N), 21.0 ($\underline{C}(CH_3)_3$), 18.0 (Ph($\underline{C}H_3)_2$);

ESI (+ve) M^+ = 357.2 m/z [M^+-Br].

6.3.2. **Synthesis of carbene-borane adducts, 39**

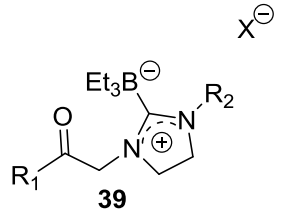

39

R_1 = tBu, R_2 = Mes, X = Cl
R_1 = nap, R_2 = Mes, X = Br

A solution of compound **38** in THF is slowly added diluted THF solution of one equivalent of 1M THF solution of $KHBEt_3$. After stirring for 3 hours at room temperature, the solution is filtered off and the solvents are removed under reduced pressure. Hexane is then added to wash the white solid and then filtered off. The product is dried under reduced pressure. Crystals are obtained by slow diffusion of hexane into a THF solution of **2**.

39e (tBu)C(O)CH_2{CH[NCH_2CH_2N(Mes)]}, yield: 78%

^{1}H NMR (500 MHz, C_6D_6): δ 6.66 (s, 2H), 4.56 (s, 2H), 3.06 – 2.97 (m, 2H), 2.97 – 2.86 (m, 2H), 2.22 (s, 6H), 2.10 – 1.99 (m, 3H), 1.19 (t, J = 7.7 Hz, 9H), 1.01 (s, 9H), 0.51 (q, J = 7.7 Hz, 6H);

^{13}C NMR (126 MHz, C_6D_6): δ 208.8 (C=O), 202.0 (C-B), 137.8 (C_q), 137.6 (C_q), 135.6 (C_q), 129.5 (CH), 53.4 (CH_2), 51.9 (CH_2), 48.2 (CH_2), 43.1 (C_q), 26.5 (CH_3), 21.0 (CH_3), 18.21 (CH_3), 14.98 (CH_2), 12.46 (CH_3);

^{11}B NMR (400 MHz, C_6D_6): δ -14.1.

Anal. Calcd. $C_{24}H_{41}BN_2O$, C, 74.99; H, 10.75; N, 7.29; Found, C, 75.13; H, 10.70; N, 7.41.

39f (naphth)C(O)CH_2{CH[NCH_2CH_2N(Mes)]}, yield: 71%

^{1}H NMR (C_6D_6, 500 MHz,): δ 8.45 (s, 1H, Ar), 8.11 – 8.00 (dd, J = 8.6, 1.7 Hz, 1H, Ar), 7.55 (d, J = 8.1 Hz, 1H), 7.52 (d, J = 8.6 Hz, 1H), 7.49 (d, J = 8.1 Hz, 1H), 7.23 (ddd, J = 8.2, 6.9, 1.3 Hz, 1H), 7.18 (ddd, J = 8.2, 6.9, 1.3 Hz, 1H), 6.68 (s, 2H), 3.25 (ddd, J = 13.5, 9.9, 1.7 Hz, 2H), 3.12 (ddd, J = 13.5, 9.9, 1.7 Hz, 2H), 2.28 (s, 6H), 2.06 (s, 3H), 1.30 – 1.09 (t, J = 7.7 Hz, 9H), 0.60 (q, J = 7.7 Hz, 6H);

^{13}C NMR (126 MHz, C_6D_6): δ 193.1 (CO), 137.5 (C_q), 137.2 (C_q), 135.8 (C_q), 135.3 (CH), 132.6 (C_q), 132.4 (C_q), 129.6 (CH), 129.4 (CH), 129.2 (CH), 128.8 (CH), 128.4 (CH), 126.7 (CH), 123.4 (CH), 54.3 (CH_2), 51.7 (CH_2), 48.7 (CH_2), 20.6 (CH_3), 17.9 (CH_3), 12.1 (CH_3);

^{11}B NMR (400 MHz, C_6D_6): δ -13.9;

Anal. Calcd. $C_{29}H_{37}BN_2O$ (440.44), C, 79.08; H, 8.47; N, 6.36; Found, C, 79.33; H, 8.78; N, 6.05.

6.3.3. **Reaction of 38e with two equivalents of $KHBEt_3$**

A solution of compound **38** in THF is slowly added diluted THF solution of two equivalent of 1M THF solution of $KHBEt_3$. After stirring for 3 hours at room temperature, the solution is

filtered off and the solvents are removed under reduced pressure. Hexane is then added to wash the white solid and then filtered off. The product is dried under reduced pressure.

^{1}H NMR (500 MHz, Chloroform-*d*) δ 6.71 (s, 2H, Ar), 4.37 (m, 1H), 3.77 (m, 2H, C*H*$_2$-imidazoline), 2.85(m, 1H), 2.56(m, 1H), 2.20 (s, 6H), 2.13 (s, 3H), 1.82 (m, 12H), 0.72 (m, 18H, ^{t}Bu), 0.46 – 0.31 (br s, 9H, CH_3).

^{13}C NMR (126 MHz, Chloroform-*d*) δ 156.14, 155.96, 137.77, 129.27, 75.01, 74.17, 59.91, 54.96, 50.68, 36.15, 27.60, 25.77, 25.71, 24.97, 24.81, 24.65, 24.49, 24.33, 18.03, 16.34, 15.31, 11.36, 11.19, 11.08.

^{11}B NMR (400 MHz, C_6D_6): δ 23.17 (br s), 5.78 (br s);

6.3.4. **Synthesis of aryloxy-tethered imidazolinium salt H_2LBr, 44**

Route A.

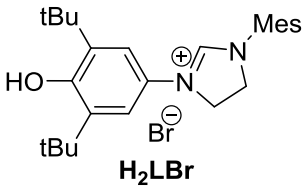

H_2LBr
44

An ampoule was charged with 4-bromo-2,4,6-tri-tert-butyl-2,5-cyclohexadien-1-one (6.8226 g, 20 mmol), N-mesitylimidazoline (7.4285g, 40 mmol) and ethylene glycol (1.1 ml, 20 mmol). The mixture was then heated to 135 ^{o}C for 8 h. After cooling to room temperature, 50 mL of HBr aqueous solution (3 N) was added to the pasty mixture and stirred violently for 2 hours. Chloroform was added to extract (2 x 30 ml) and the organic layer was separated and dried over anhydrous Na_2SO_4. Solvent was removed by rotary evaporator. The brown paste was then washed with THF (3 X 20 mL). After filtration, the product was recrystalised from $CHCl_3$/THF as white solid in 15% yield.

^{1}H NMR (500 MHz, $CDCl_3$): δ = 9.55 (s, 1H, Ar), 7.30 (s, 2H, Ar), 6.93 (s, 2H, Ar), 4.84 (t, J = 12.5 Hz, 2H, C*H*$_2$-imidazoline), 4.51 (t, J = 12.5 Hz, 2H, C*H*$_2$-imidazoline), 2.38 (s, 6H, *o*-CH_3), 2.28 (s, 3H, *p*-CH_3), 1.46 (s, 18H, ^{t}Bu);

^{13}C NMR (126 MHz, $CDCl_3$): δ 155.14 (s), 153.73 (s), 140.18 (s), 137.82 (s), 135.11 (s), 130.71 (s), 129.90 (s), 127.47 (s), 117.00 (s), 76.91 (s), 51.65 (s), 50.79 (s), 34.75 (s), 30.12 (s), 21.03 (s), 18.37 (s).

MS (ESI): m/z = 393.29 (M^{+}-Br).

Route B.

***N*-(2,4,6-Trimethylphenyl)-oxalamic acid, ethyl ester**

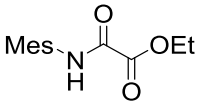

Ethyl chlorooxoacetate (2.73 g, 20.0 mmol) was added dropwise to a solution of 2,4,6- trimethylaniline (2.70 g, 20.0 mmol) and triethylamine (2.02 g, 20.0 mmol) in anhydrous tetrahydrofuran (20 mL) under a

nitrogen atmosphere at 0 °C. The resulting solution was stirred at room temperature for 16 h. The reaction mixture was diluted with ethyl acetate (10 mL) washed with aqueous hydrochloric acid (1.0 M, 2 × 10 mL), saturated sodium hydrogen carbonate (2 × 10 mL) and brine (10 mL), the organic phase was dried over magnesium sulphate and concentrated *in vacuo*. Following recrystalisation from a mixture of hexane and ethyl acetate (9:1 v/v), *N*-(2,4,6- trimethylphenyl)-oxalamic acid, ethyl ester (3.75 g, 15.9 mmol, 78%) was isolated as colourless needles.

^{1}H NMR (500 MHz, $CDCl_3$): δ = 8.36 (s, 1H, NH), 6.95 (s, 2H, Ar), 4.46 (q, *J* = 7.2 Hz, 2H, CH_2CH_3), 2.31 (s, 3H, *p*-CH_3), 2.23 (s, 6H, *o*-CH_3), 1.48 (t, *J* = 7.2 Hz, 3H, CH_2CH_3).

^{13}C NMR (125 MHz, CDCl3): δ = 161.0 (Ar), 154.7 (Ar), 137.7 (Ar), 134.7 (Ar), 129.5 (Ar), 129.1 (CH), 63.6 (CH_2), 20.9 (CH_3), 18.3 (CH_3), 14.0 (CH_3).

2,6-di-*tert*-butyl-4-aminophenol

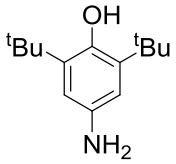

41.27 g (0.2 mol) of 2,6-di-tert-butylphenol was dissolved in 200 ml of ethanol containing 0.15 mol of H_2SO_4. Into this vigorously stirred solution was added a water solution (30 ml) of 17.5 g (0.21 mol) of sodium nitrate over a period of 30 min. The reaction temperature was maintained at 0°C in an ice bath. After 4 hours, 200 ml of water was added to precipitate the nitrosophenol. Purification was accomplished by recrystallization from ethanol/water. Yield 70%. ^{1}H NMR (500 MHz, $CDCl_3$): δ = 8.90 (s, 1H, OH), 7.57 (d, *J* = 2.5 Hz, 1H, Ar), 6.94 (d, *J* = 2.6 Hz, 1H, Ar), 1.34 (s, 9H, ^{t}Bu), 1.32 (s, 9H, , ^{t}Bu).

To an ethanol solution of nitrosophenol (25.1 g, 0.1 mol) was slowly added a concentrated solution of 18.3 g(0.105 mol) sodium hydrosulfite at 50-60°C for 4 hours. The solution was made basic with sodium carbonate and the amino phenol was extracted with ether. The ether was removed and the aminophenol was recrystallized from the ether as yellow solid.

This compound underwent rapid oxidation in contact with air. Thus special care was necessary for the isolation of the product. Yield 62 %.

^{1}H NMR (500 MHz, $CDCl_3$): δ = 6.41 (s, 2H, Ar), 4.63 (s, 1H, OH), 3.42 (s, 2H, NH_2), 1.23 (s, 18H, , ^{t}Bu).

***N*-(4-hydroxy-, 3,5-*tert*-butyl)-*N'*-(2,4,6-trimethylphenyl)-ethanediamide,**

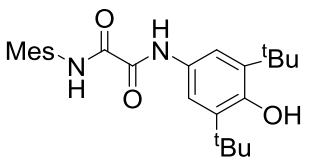

Triethylamine (4.05 g, 40.0 mmol) was added to a suspension of *N*-(2,4,6-trimethylphenyl)-oxalamic acid, ethyl ester (4.71 g, 20.0 mmol) and 2,6-di-*tert*-butyl-4-aminophenol (4.21 g, 20.0 mmol) in toluene (40 mL). The suspension was heated under reflux and then stirred overnight. The reaction mixture was allowed to cool to room

temperature and diluted with ethyl acetate such that any solids were dissolved. The solution was washed with aqueous hydrochloric acid (1.0 M, 2 × 20 mL), the aqueous phase was extracted with ethyl acetate (2 × 20 mL) and the combined organic phase was washed with brine (80 mL) and dried over magnesium sulfate. The solvent was removed under reduced pressure to give a yellow solid with a yield of 80%.

6.3.5. Synthesis of *p*-aryloxy-tethered imidazolinium salt H_2LCl, 45

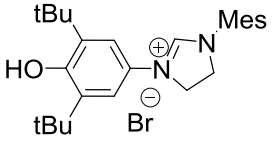

H_2LCl
45

Borane dimethyl sulfide complex (6.08 g, 80.0 mmol) was added dropwise to a solution of N-(4-hydroxy-, 3,5-tert-butyl)-N'-(2,4,6-trimethylphenyl)-ethanediamide (8.201 g, 20.0 mmol) in anhydrous tetrahydrofuran (40 mL) under a nitrogen atmosphere. After 2 hours' stirring, the reaction mixture was heated under reflux for 18 h. Methanol (40 mL) was added slowly to the reaction mixture, followed by concentrated aqueous hydrochloric acid (12 M, 6 mL); the volatiles were then removed under reduced pressure. Triethyl orthoformate (60 mL) was then added, and the resulting mixture heated to 100 °C for 5 hours then allowed to cool to room temperature. The resulting precipitate was collected by vacuum filtration and washed with diethyl ether (3 × 20 mL) to give the product as a white solid at a yield of 54%.

6.3.6. Synthesis of aryloxy-tethered imidazolinium salt H_2LPF_6, 46

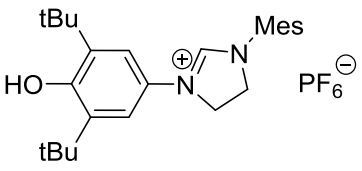

H_2LPF_6
46

An aqueous solution of excessive $NaPF_6$ is added to the chloroform solution of imidazolinium bromide 5. After vigorous stirring for two hours, the organic layer was separated and solvents are removed by rotary evaporator. The product is purified though a flash silica column by using acetone/DCM at 9:1 ratio. Crystals are obtained by diffusing hexane into a concentrated THF solution.

6.3.7. Synthesis of $[KL]_n$, 48

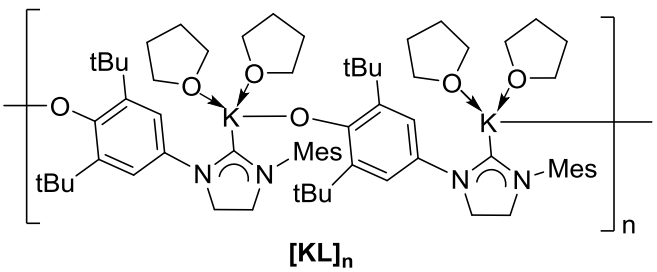

$[KL]_n$
48

To a THF (10 ml) suspension of 5-Br (0.4735 g, 1 mmol) was slowly added a THF (10 ml) solution of KN" (0.4010g, 2 mmol). The mixture was stirred for 4 hours, affording a white suspension. Solids were removed by filtration to afford a light yellow solution. The volatiles were then removed under reduced pressure,

yielding an oily paste which was then washed with hexane, affording $[KL]_n$ as white solid. Crystals were obtained by slow diffusion of hexane into concentrated THF solution. Yield: 0.2736 g, 63%.

^{1}H NMR (500 MHz, Pyr): δ 7.79 (s, 2H, Ar), 6.93 (s, 2H, Ar), 4.10 (d, *J* = 8.6 Hz, 2H, C*H*$_2$-imidazoline), 3.68 (t, *J* = 9.6 Hz, 2H, C*H*$_2$-imidazoline), 2.31 (m, 3H, *p*-Me), 2.26 (s, 6H, *o*-Me), 1.81 (s, 18H, ^{t}Bu).

^{13}C NMR (126 MHz, Pyr): δ 236.32 (s), 169.23 (s), 136.54 (s), 129.79 (d, *J* = 9.6 Hz), 129.09 (s), 126.20 (s), 123.54 (s), 116.77 (s), 51.29 (s), 50.64 (s), 31.18 (s).

Anal. Calcd: $C_{34}H_{52}KN_2O_3$. Elemental Analysis: C, 70.91; H, 9.10; N, 4.86. Found: C, 70.58; H, 9.27; N, 4.73.

6.3.8. **Synthesis of $YL_3{\cdot}(KCl)_3$, 50**

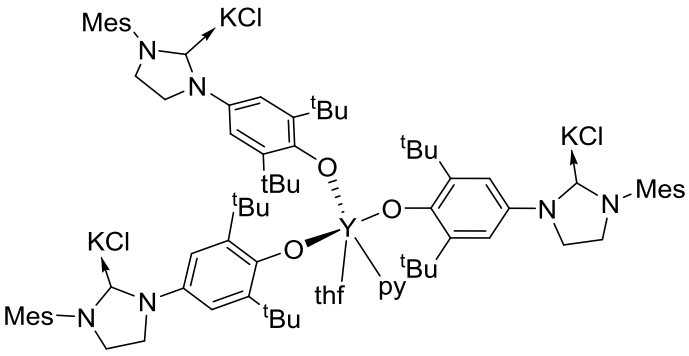

To a THF solution (5 ml) of KL (0.0519 g, 0.09 mmol) was slowly added THF suspension of $YCl_3(thf)_2$ (0.0105 g, 0.03 mmol). The solution changed to brown and was left to stir overnight. The mixture was then filtered off. After the removal of solvents under reduced pressure, hexane was added to form a pale yellow precipitate. Yield: (0.0410 g, 56%)

^{1}H NMR (500 MHz, Pyr) δ 7.86 (s, 2H, Ar), 6.90 (s, 2H, Ar), 3.68 (m, 4H, C*H*$_2$-imidazoline), 2.26 (br s, 6H, *o*-Me), 2.18 (br s, 3H, *p*-Me), 1.91 (s, 18H, ^{t}Bu).

^{13}C NMR (126 MHz, Pyr) δ 238.24 (s), 160.52 (d, *J* = 5.4 Hz), 140.46 (s), 139.31 (s), 138.49 (s), 136.84 (d, *J* = 16.3 Hz), 129.83 (d, *J* = 10.4 Hz), 129.06 (s), 126.22 (s), 114.74 (s), 68.30 (s), 51.53 (s), 48.57 (s), 36.41 (s), 33.65 (d, *J* = 40.8 Hz), 32.94 (d, *J* = 63.2 Hz), 26.28 (s), 21.79 (s), 21.34 (s), 18.55 (d, *J* = 4.4 Hz).

Anal. Calcd: $C_{87}H_{120}Cl_3K_3N_7O_4Y$. Elemental Analysis: C, 63.70; H, 7.37; N, 5.98. Found: C, 62.65; H, 7.70; N, 6.15.

6.3.9. **Reaction of $YL_3{\cdot}(KCl)_3$ with boranes**

a: reaction with $BH_3{\cdot}SMe_2$

Treatment of complex **50** (0.1644 g, 0.1 mmol) with two equivalents of $BH_3{\cdot}SMe_2$ (0.3 ml, 1M in hexane, 0.3 mmol) in THF yielded a cloudy suspension instantly. The KCl salts are

removed by filtration. After the removal of volatiles under reduced pressure, a light yellow oily paste was obtained. Yield: 0.0872 g, 65%.

^{1}H NMR (500 MHz, Benzene-d_6) δ 7.37 (s, 2H, Ar), 6.74 (s, 2H, Ar), 3.91 (m, 2H, CH_2-imidazoline), 2.13 (s, 6H, *o*-Me), 2.10 (s, 3H, *p*-Me), 1.75 (s, 18H, ^{t}Bu). ^{13}C NMR (126 MHz, Benzene-d_6) δ 162.47, 162.43, 121.75, 49.06, 35.92, 32.71, 32.62, 25.85, 25.62, 21.05, 17.97, 17.82. ^{11}B NMR (160 MHz, Benzene-d_6) δ -34.55(br s).

b: reaction with BPh_3

Complex **50** (0.1021 g, 0.69 mmol) was dissolved in THF and triphenylborane (0.055 g, 1.98 mmol, 3 equiv.) was added slowly into the solution. The solution was stirred overnight and the solution turned green. After the removal of volatiles under reduced pressure, the solid was collected by centrifugation and extracted by THF. The resulting product was purified by recrystallisation from THF/hexane mixture. Yield: 0.0812 g, 62%. ^{1}H NMR (500 MHz, Benzene-d_6) δ 7.54 – 7.49 (m, 2H, Ar), 7.45 – 7.40 (m, 5H, Ar), 7.35 – 7.31 (m, 2H, Ar), 7.26 – 7.22 (m, 1H, Ar), 7.01 (t, J = 7.1 Hz, 5H, Ar), 6.98 – 6.93 (m, 4H, Ar), 6.29 (s, 2H), 4.74 (s, 1H, O*H*), 3.50 – 3.35 (m, 2H, CH_2-imidazoline), 3.15 – 3.00 (m, 2H, CH_2-imidazoline), 2.17 (s, 6H, *o*-Me), 1.94 (s, 3H, *p*-Me), 1.21 (s, 18H, ^{t}Bu). ^{13}C NMR (126 MHz, Benzene-d_6) δ 194.83(s, N*C*N, carbene), 152.44(s, Ar), 147.75(s, Ar), 147.52(s, Ar), 147.30(s, Ar), 137.92(s, Ar), 136.76(s, Ar), 136.13(s, Ar), 135.40(s, Ar), 134.61(s, Ar), 133.44(s, Ar), 126.04(s, Ar), 124.28(s, Ar), 123.73(s, Ar), 54.05(s, *C*H_2; imidazoline), 51.51(s, *C*H_2; imidazoline), 34.35(s, Me), 30.00(s, tBu), 20.66(s, Me).^{11}B NMR (160 MHz, Benzene-d_6) δ 4.93(br s).

Colourless crystals obtained from THF solution layered with hexane. It turned out to be the protonated product, $HLBPh_3$.

^{1}H NMR (500 MHz, THF-d_8): δ 7.19 (t, 6H, Ar), 7.12 (s, Ar), 4.27 (dd, J = 12.2 Hz, 2H, CH_2-imidazoline), 4.00 (dd, J = 12.1 Hz, 2H, CH_2-imidazoline).

c: reaction of YL_3 (0.1780 g, 0.1 mmol)with 9-BBN (0.0401 g, 0.3 mmol)follows with the same procedure with a yield of 58%.

^{1}H NMR (500 MHz, Pyridine-d_5) δ 7.29 (s, 6H, Ar), 7.02 (s, 6H, Ar), 4.73 (t, J = 10.8 Hz, 6H, CH_2-imidazoline), 4.27 (t, J = 10.8 Hz, 6H, CH_2-imidazoline), 2.44 – 2.34 (m, 18H), 2.20 (m, 36H), 1.86 – 1.78 (m, 42H), 1.55 (s, 54H, ^{t}Bu). ^{13}C NMR (126 MHz, Pyridine-d_5) δ 173.81, 146.13, 145.91, 145.68, 139.69, 139.49, 139.28, 138.87, 130.34, 126.08, 125.87, 125.67, 111.65, 36.26, 36.12, 34.15, 30.64, 29.95, 26.42, 25.93. ^{11}B NMR (160 MHz, Pyridine-d_5) δ -1.02.

6.3.10. Attempted synthesis of $CeL_3{\cdot}(KCl)_3$

To a THF solution of KL (0.0519 g, 0.09 mmol) was slowly added a THF suspension of 1/3 equivalent $CeCl_3(thf)_2$ (0.0115 g, 0.03 mmol). The solution changed to brown and was left to stir overnight. The mixture was then filtered off. After the removal of solvents under reduced pressure, hexane was added to precipitate all the products as a pale yellow solid. Washed by hexane and solid was dried under reduced pressure. The NMR of the product shown two sets of peaks which indicates two different type of products formed. Further workup on separating these compounds was not successful. These compounds were sensitive to moisture and air. The colour changed immediately after getting exposed to air or moisture.

6.3.11. Attempted synthesis of $LYCp_2$

A THF solution of $[KL(thf)_2]_n$ was slowly added into THF solution of one equivalent of YCp_3. The reaction was then heated at 50 ^oC in oil bath for 8 hours. Colourless precipitate were formed and the suspension was then filtered to remove the solid. Volatiles of the solution were removed under reduced pressure to afford the product as a beige powder. (0.1731g, 57%)

^1H NMR (500 MHz, Pyr-d^5): δ 7.13 (s, 2H, Ar), 6.92 (d, *J* = 4.6 Hz, 2H, Ar), 6.35 (s, 10H, Ar), 3.99 (m, 2H, CH_2-imidazoline), 3.68 (m, 2H, CH_2-imidazoline), 2.29 (s, 6H, *o*-Me), 2.28 (s. 3H, *p*-Me), 1.73 (m, 18H, ^{t}Bu). ^{13}C NMR (126 MHz, Pyr-d^5): δ 216.8 (s), 158.89 (s), 153.22 (s), 151.88 (s), 150.28 (s), 149.19 (s), 129.20 (s), 128.45 (s), 125.56 (s), 113.89 (s), 111.63 (s), 110.55 (s), 110.24 (s), 109.92 (s), 105.34 (s), 35.83 (s), 32.02 (s), 20.45 (s).

6.3.12. Reaction of $YL_3{\cdot}(KCl)_3$ with CO_2

CO_2 was dried by passing through a drying column and was added to a THF (5 mL) solution of 0.1640 g(0.1 mmol) $YL_3{\cdot}(KCl)_3$.White solid came out while stirring. Solid was collected and dried under reduced pressure. Yield: 0.1473 g.

^1H NMR (500 MHz, Pyridine-d_5) δ 7.62 (s, 4H, Ar), 7.61 (s, 2H, Ar), 6.88 (s, 2H, Ar), 6.85 (s, 4H, Ar), 4.91 (m, 4H, CH_2-imidazoline), 4.86 (m, 2H, CH_2-imidazoline), 4.47 (m, 4H, CH_2-imidazoline), 4.43 (m, 2H, CH_2-imidazoline), 2.32 (s, 12H, *o*-Me), 2.25 (s, 6H, *p*-Me), 2.22 (s, 3H, *p*-Me), 2.19 (s, 6H, *o*-Me), 1.78 (d, *J* = 10.9 Hz, 9H), 1.73 (s, 18H, ^{t}Bu).

6.3.13. Reaction of YL_3 with CS_2

A THF (5 mL) solution of 0.1640 g (0.1 mmol) $YL_3{\cdot}(KCl)_3$ was slowly added a diluted THF (3 mL) solution of CS_2 (19 μL, 0.3 mmol). The solution changed from almost colourless to pale yellow, and was stirred for 4 hours. A cloudy suspension was formed and was then filtered

to remove the solid. Volatiles of the solution were removed under reduced pressure to afford the product as a pale yellow powder. (Yield: 0.1420 g).

^{1}H NMR (500 MHz, Pyridine-d_5) δ 7.93 (s, 2H, Ar), 7.82 (s, 1H, Ar), 6.91 (s, 3H, Ar), 6.83 (s, 7H, Ar), 4.74 (d, J = 11.4 Hz, 4H, CH_2-imidazoline), 4.57 (d, J = 10.3 Hz, 2H, CH_2-imidazoline), 4.27 (d, J = 11.5 Hz, 2H, CH_2-imidazoline), 4.16 (d, J = 10.7 Hz, 2H, CH_2-imidazoline), 2.66 (d, J = 15.9 Hz, 23H), 2.29 – 2.21 (m, 16H), 2.14 (d, J = 9.3 Hz, 9H), 1.28 (m, 54, ^{t}Bu).

^{13}C NMR (126 MHz, Pyridine-d_5) δ 226.28 (Carbene), 225.96 (Carbene), 164.78, 140.00, 138.53, 137.87, 137.81, 137.68, 130.54, 130.50, 130.39, 130.35, 130.31, 128.84, 128.65, 128.45, 116.95, 52.29, 52.14, 52.05, 51.14, 49.62, 36.34, 36.28, 36.02, 32.85, 32.75, 32.42, 32.34, 30.92, 30.74, 21.30, 21.24, 19.59, 19.57, 19.54, 17.90.

6.4. Experimental for Chapter 4

6.4.1. **Synthesis of K_2L^R, 61-R.**

a: R = Me.

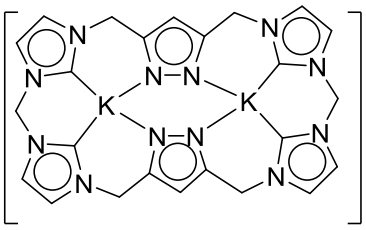

K_2L

61-Me

Calix[4]imidazolylidene[2]pyrazolato hexafluorophosphate, $H_6L^{Me}(PF_6)_4$ (0.1000 g, 0.0939 mmol, and KN" (0.1130 g, 0.5634 mmol) were mixed in 5 mL dry pyridine and stirred for 6 h. The resulting yellow solution was filtered. After addition of 5 ml of hexane, a pale yellow powder precipitated, which was centrifuged, washed with hexane (3 x 5 mL) and dried under reduced pressure. Yield: 0.0642 mg (100% conversion in ^{1}H NMR, isolated with KPF_6). The pyridine solution of the complex shows new peaks in the ^{1}H NMR spectrum in 2 days with resonances for unidentified species emerged.

^{1}H NMR (500 MHz, Pyridine-d_5) δ 6.83 (s, 4H, CH_2), 6.79 (s, 4H, imidazolium-CH), 6.31 (s, 2H), 6.18 (s, 4H, imidazolium-CH), 5.31 (s, 8H, CH_2). ^{13}C NMR (126 MHz, Pyridine-d_5) δ 211.05 (Carbene), 172.42, 121.35, 121.34, 120.33, 120.20, 119.78, 119.66, 118.80, 118.78, 102.95, 72.64, 68.32, 64.91, 58.59, 50.06, 26.30.

B: R = Et

Follow the same procedure as in **61-Me** with $H_6L^{Et}(PF_6)_4$ (0.1020 g, 0.0939 mmol). Pale yellow solid obtained after work up.

^{1}H NMR (500 MHz, Acetonitrile-d_3) δ 6.22 (s, 1H), 5.47 (s, 2H), 5.25 (d, J = 14.9 Hz, 3H), 5.00 (s, 1H), 4.85 (d, J = 9.2 Hz, 11H), 4.71 (d, J = 14.8 Hz, 2H), 4.12 – 4.01 (m, 3H), 3.81 (s, 1H), 3.67 – 3.60 (m, 4H).

6.4.2. Reaction of K_2L^R with $RECl_3(thf)_2$

General procedure: To a pyridine (5 mL) solution of 0.1 mmol K_2L^R (R = Me, Et) was slowly added a pyridine (5 mL) solution of 0.2 mmol (2 equiv.) of $RECl_3(thf)_2$. Upon the addition of the reagents, a white precipitate formed immediately. The suspension was then left to stir for 4 h and was then filtered to separate the white solid and the pyridine solution. ^{1}H NMR spectrum of the solution showed just pyridine and no resonance for the ligand was observed. The solid was washed with pyridine and then dried under reduced pressure to afford the product as a white powder. Attempts to dissolve these solid in organic solvents such as toluene, THF, pyridine or MeCN showed no progress even when heated to 60 °C. Potassium salts KZ (Z = Cp, O^{t}Bu, O^{n}Bu, Odtbp or N") were added to the solid with different stoichiometry (1 -5 equiv.) and the mixture was stirred overnight in pyridine or MeCN. However, no signal for the ligand can be identified in the solution which showed no sign of the formation of complex LRE_2Z_4.

6.4.3. Reaction with $MgN"_2$

General procedure: To a MeCN (5 mL) solution of 0.1 mmol $H_2L^RPF_6$ (R = Me, Et, Pr) was slowly added a MeCN (5 mL) solution of 0.1 mmol (1 equiv.) of $MgN"_2$ (0.0350 g) and 0.1 mmol of TMEDA (0.0120 g). The solution was then stirred for 4 h. After the removal of volatiles, diethyl ether is then added to the paste to form colourless solid which is then filtered and dried under reduced pressure to afford the product complex **60-R** as a white powder.

H2LRPF6 (R = Me): 0.01105 g, yield: 0.01052 g.

^{1}H NMR (500 MHz, Acetonitrile-d_3) δ 8.77 (s, 4H, NC*H*N), 7.65 (s, 4H, imidazolium-CH), 7.45 (s, 4H, imidazolium-CH), 6.42 (s, 2H, pyrazol-CH), 6.30 (s, 2H, CH_2), 5.41 (s, 8H, CH_2).

^{13}C NMR (126 MHz, Acetonitrile-d_3) δ 146.82, 144.39, 139.29, 135.44, 125.20, 123.96, 123.00, 122.72, 104.86, 66.20, 59.88, 58.04, 56.51, 49.54, 46.88, 46.56, 45.82.

$H_6L^{Et}PF_6$: 0.1092 g, yield: 0.0957 g.

^{1}H NMR (500 MHz, Acetonitrile-d_3) δ 7.53 (s, 4H, NC*H*N), 7.38 (s, 4H, imidazolium-CH), 7.11 (s, 4H, imidazolium-CH), 6.47 (s, 2H, pyrazol-CH), 5.17 (d, J = 14.9 Hz, 4H, CH_2), 5.01 (d, J = 14.9 Hz, 4H, CH_2), 4.61 – 4.51 (m, 4H, CH_2), 4.51 – 4.36 (m, 4H, CH_2).

^{13}C NMR (126 MHz, Acetonitrile-d_3) δ 146.17, 136.36, 124.53, 123.25, 106.36, 66.22, 58.41, 56.53, 49.75, 47.58, 46.90, 45.96.

$H_6L^{Pt}PF_6$: 0.1120 g, yield: 0.1024 g.

^{1}H NMR (500 MHz, Acetonitrile-d_3) δ 8.24 (s, 4H, NC*H*N), 7.10 (s, 4H, imidazolium-CH), 6.88 (s, 4H, imidazolium-CH), 6.33 (s, 2H, pyrazole-CH), 5.32 (d, J = 15.1 Hz, 4H, CH_2), 5.10 (d, J = 15.1 Hz, 4H, CH_2), 4.04 – 3.89 (m, 8H, CH_2).

^{13}C NMR (126 MHz, Acetonitrile-d_3) δ 154.7, 136.2, 123.2, 121.6, 57.4, 55.5, 46.5, 46.1, 44.8.

It is observed in ^{1}H NMR spectrum that after being stored in MeCN for 2 days, small peaks of new products emerge gradually. In the case of complex **63-Et**, colourless crystals are obtained by diffusion of diethyl ether into a MeCN solution. From the single crystal X-ray data, the product is characterised as complex **64-Et**, $Mg_3(L^{Et})_2F_2[PF_6]_8(MeCN)_6$.

6.4.4. **Reactivity of complex 63-Me**

The MeCN (5 ml) solution of 0.1 mmol **63-Me** was added into a MeCN (3ml) solution of 0.1 mmol of $SmI_2(thf)_2$ (0.0550 g). The solution changed to dark green immediately and was stirred for 4 hours. After filtration, a dark green-brown solution was obtained. The solution NMR showed a set of new diamagnetic resonances which indicated the formation of a new species. The complex was very sensitive to even trace amount of air, which caused an instant colour change to colourless.

^{1}H NMR (500 MHz, Acetonitrile-d_3) δ 8.08 (s, 2H), 8.00 (s, 2H), 7.85 – 7.77 (m, 4H), 7.68 – 7.63 (m, 2H), 7.55 – 7.48 (m, 4H), 7.17 (d, J = 1.9 Hz, 2H), 6.72 (d, J = 14.9 Hz, 2H), 6.37 (d, J = 14.9 Hz, 2H), 6.13 (s, 1H), 5.83 (s, 2H), 5.64 (d, J = 13.8 Hz, 8H).

The reaction with $UI_4(dioxane)_2$ followed the same procedure to give a yellow green suspension which showed paramagnetic resonances. This complex decomposes quickly and no paramagnetic resonances can be found after being stored for 12 hour.

^{1}H NMR (500 MHz, Acetonitrile-d_3) δ 61.25 (s, 1H), 34.70 (s, 2H), 8.93 (s, 4H), 7.34 (s, 2H), 2.52 (s, 12H), 2.48 (s, 22H), 2.33 (s, 57H), -3.04 (s, 2H), -7.98 (s, 2H), -12.23 (s, 2H), -19.06 (s, 2H).

6.4.5. **Reaction of 60 with ScN"$_3$**

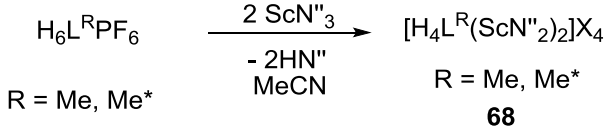

An acetonitrile solution (5 ml) of ScN"$_3$ (0.0526 g, 0.1 mmol, 2 eqiv.) was added into an acetonitrile solution of one equivalent (0.05 mmol) of $H_2L^RPF_6$ (R = Me, Me*, Et) and was stirred for 4 hours. A pale yellow suspension is formed from which white solid was removed

by filtration. After the volatiles were removed under reduced pressure, hexane was added to the pale yellow paste, to give off-white solid.

$H_6L^{Me}(PF_6)$ (R = Me), 0.0550 g, yield: 0.0630 g.

^{1}H NMR (500 MHz, Benzene-d_6) δ 8.62 (s, 1H, NC*H*N), 8.57 (s, 1H, NC*H*N), 8.50 (s, 1H, NC*H*N), 8.45 (s, 1H, NC*H*N), 7.37 (t, *J* = 2.0 Hz, 1H, imidazolium-C*H*), 7.34 (t, *J* = 4.2, 2.0 Hz, 2H, imidazolium-C*H*), 7.33 (br s, 2H, imidazolium-C*H*), 7.28 (br s, 2H, imidazolium-C*H*), 7.24 (t, *J* = 1.9 Hz, 1H, imidazolium-C*H*), 7.21 (t, *J* = 1.9 Hz, 1H, imidazolium-C*H*), 6.18 (d, *J* = 3.5 Hz, 2H, CH_2), 6.15 (s, 1H, pyrazole-C*H*), 6.12 (d, *J* = 3.4 Hz, 2H, CH_2), 6.11 (s, 1H, pyrazole-C*H*), 6.08 (s, 1H), 5.38 (d, *J* = 2.4 Hz, 4H, CH_2), 5.13 (d, *J* = 7.6 Hz, 4H, CH_2).

^{13}C NMR (126 MHz, Acetonitrile-d_3) δ 142.85, 142.71, 138.80, 138.69, 138.61, 138.49, 137.80, 137.71, 137.65, 137.60, 125.01, 124.96, 124.81, 124.77, 123.63, 123.27, 123.24, 123.10, 123.05, 123.03, 108.42, 108.01, 68.24, 59.79, 59.75, 59.70, 48.67, 48.65, 47.22, 47.03, 26.20.

$H_6L^{Me*}(PF_6)$ (R = Me*), 0.0588 g, yield: 0.0487 g.

in MeCN ^{1}H NMR (500 MHz, Benzene-d_6) δ 8.15 (s, 1H, NCHN), 8.03 (s, 1H, NCHN), 7.94 (s, 1H, NCHN), 7.91 (s, 1H, NCHN), 5.91 (s, 2H, pyrazole-CH), 5.22 (d, *J* = 19.6 Hz, 4H, CH_2), 4.98 (d, *J* = 23.7 Hz, 4H, CH_2), 2.08 (d, *J* = 4.2 Hz, 12H, Me), 2.02 (d, *J* = 4.2 Hz, 12H, Me), -0.14 (s, 72H, $SiMe_3$).

^{13}C NMR (126 MHz, Acetonitrile-d_3) δ 142.85, 142.71, 142.57, 138.80, 138.69, 138.61, 138.49, 137.80, 137.71, 137.65, 137.60, 125.01, 124.96, 124.81, 124.77, 123.63, 123.27, 123.24, 123.10, 123.05, 123.03, 108.42, 108.01, 68.24, 59.79, 59.75, 59.70, 48.67, 48.65, 47.22, 47.03, 26.20.

^{29}Si NMR (99 MHz, Benzene-d_6) δ 1.44, -9.49.

6.4.6. **Reaction of 60 with CeN"$_3$**

Follow by the same procedure in the reaction of ScN"$_3$, a colourless solid can be obtained.

^{1}H NMR (500 MHz, THF-d_8) δ 17.61 (s, 1H), 14.10 (s, 2H), 11.93 (s, 2H), 11.77 (s, 2H), 9.08 (s, 3H), 8.66 (s, 3H), 5.23 (s, 2H), 4.84 (s, 4H), 4.48 (s, 4H), -5.74 (s, 11H), -6.25 (s, 30H).

^{29}Si NMR (99 MHz, THF-d_8) δ 5.20.

6.4.7. **Transmetalation reaction with pillarplex complex**

The pillarplex complex $[Ag_8(L^{Me})_2](PF_6)_4$ were synthesised according to literature methods.[11] To the MeCN solution (5 ml) of 0.0250 g (0.01 mmol) pillarplex complex was slowly added

a MeCN solution of $RECl_3(thf)_2$. Upon the addition, white precipitate was formed immediately. The mixture was then stirred for 4 hours and filtered. The solution showed no signal for the ligand while the solid was insoluble in organic solvent.

6.5. Crystal data and structure refinement details

	2^P	**3^P**	**5-Ce^P**
Identification code	P16039_monoclinic	po15010_sq_sq	P15164peakhunting
Empirical formula	$C_{150}H_{217}K_8O_{20}$	C42.5H50.5K2.5O2.5Si 0.5	$C_{82}H_{122}CeKO_{11.5}$
Formula weight	2653.02	713.12	1471.01
Temperature/K	170(2)	170(2)	170(2)
Crystal system	monoclinic	triclinic	monoclinic
Space group	$P2_1/c$	P-1	C2/c
a/Å	22.9449(7)	14.2833(7)	17.6636(3)
b/Å	27.0456(9)	20.3352(7)	33.2740(6)
c/Å	25.5786(8)	31.1458(13)	27.8553(5)
α/°	90	92.629(3)	90
β/°	97.896(3)	92.686(5)	92.6191(17)
γ/°	90	110.294(4)	90
Volume/$Å^3$	15722.5(9)	8456.8(6)	16354.5(5)
Z	4	8	8
$\rho_{calc}g/cm^3$	1.121	1.12	1.195
μ/mm^{-1}	0.278	2.8	0.662
F(000)	5716	3040	6264
Crystal size/mm^3	0.7994 × 0.5264 × 0.1778	0.2611 × 0.1162 × 0.0415	0.5196 × 0.268 × 0.0561
Radiation	MoKα (λ = 0.71073)	Cu Kα (λ = 1.54184)	Mo Kα (λ = 0.71073)
2θ range for data collection/°	5.692 to 48.216	6.612 to 100.872	5.706 to 49.426
Index ranges	$-26 \le h \le 26$, $-31 \le k \le 31$, $-29 \le l \le 29$	$-12 \le h \le 14$, $-20 \le k \le 20$, $-31 \le l \le 31$	$-20 \le h \le 20$, $-39 \le k \le 39$, $-32 \le l \le 32$
Reflections collected	205920	79010	114174
Independent reflections	24952 [R_{int} = 0.1376, R_{sigma} = 0.0947]	17717 [Rint = 0.1468, Rsigma = 0.1279]	13925 [R_{int} = 0.0900, R_{sigma} = 0.0590]
Data/restraints/ parameters	24952/30/1655	17717/189/1767	13925/150/896
Goodness-of-fit on F^2	1.033	1.082	1.065
Final R indexes [I>=2σ (I)]	R_1 = 0.0989, wR_2 = 0.2357	R1 = 0.1452, wR2 = 0.4067	R_1 = 0.0949, wR_2 = 0.2068
Final R indexes [all data]	R_1 = 0.1768, wR_2 = 0.2989	R1 = 0.1739, wR2 = 0.4213	R_1 = 0.1234, wR_2 = 0.2216
Largest diff. peak/hole / e $Å^{-3}$	0.72/-0.51	1.65/-0.64	1.60/-1.11

	5-Ce^{PT}	**5-Pr^{PT}**	**6-Ce^{P}**
Identification code	p16171_mono	PO16012_reint_0p83A	PO16002
Empirical formula	$C_{188}H_{289}Ce_2K_2O_{23}$	$C_{90}H_{138}KO_{10.5}Pr$	$C_{95}H_{109}CeKN_8O_4$
Formula weight	3275.61	1568.01	1606.12
Temperature/ K	170(2)	120.01(10)	120.00(10)
Crystal system	monoclinic	monoclinic	triclinic
Space group	$P2_1/c$	$P2_1/c$	P-1
a/Å	18.81350(10)	18.6073(7)	17.29805(13)
b/Å	31.5876(2)	31.2563(11)	21.51193(16)
c/Å	33.9342(3)	33.684(2)	25.0448(4)
α/°	90	90	97.6409(9)
β/°	101.1900(10)	101.184(5)	103.4543(9)
γ/°	90	90	94.2363(6)
Volume/Å^3	19782.8(2)	19218.7(15)	8930.03(16)
Z	4	8	4
ρ_{calc}g/cm^3	1.1	1.084	1.195
μ/mm^{-1}	0.554	4.661	4.762
F(000)	7020	6720	3376
Crystal size/mm^3	0.21 ×0.17 ×0.13	0.176 × 0.14 × 0.03	0.4897 × 0.2254 × 0.0328
Radiation	MoKα (λ = 0.71073)	CuKα (λ = 1.54184)	CuKα (λ = 1.54184)
2Θ range for data collection/°	5.652 to 60.596	6.256 to 136.502	7.018 to 152.508
Index ranges	-26 ≤ h ≤ 26, -44 ≤ k ≤ 42, -47 ≤ l ≤ 47	-22 ≤ h ≤ 22, -28 ≤ k ≤ 37, -40 ≤ l ≤ 40	-21 ≤ h ≤ 17, -26 ≤ k ≤ 27, -31 ≤ l ≤ 31
Reflections collected	484034	242136	181419
Independent reflections	55385 [R_{int} = 0.0779, R_{sigma} = 0.0608]	35207 [R_{int} = 0.2727, R_{sigma} = 0.1470]	37057 [R_{int} = 0.0832, R_{sigma} = 0.0465]
Data/restraints / parameters	55385/2/1984	35207/0/1895	37057/13/1997
Goodness-of-fit on F^2	1.542	1.207	1.049
Final R indexes [I>=2σ (I)]	R_1 = 0.0776, wR_2 = 0.2159	R_1 = 0.1378, wR_2 = 0.3584	R_1 = 0.0971, wR_2 = 0.2650
Final R indexes [all data]	R_1 = 0.1257, wR_2 = 0.2437	R_1 = 0.2027, wR_2 = 0.4161	R_1 = 0.1045, wR_2 = 0.2733
Largest diff. peak/hole / e Å^{-3}	1.80/-0.85	3.06/-1.89	8.56/-2.51

	5-Ce^{PT}	**5-Pr^{PT}**	**6-Ce^{P}**
Identification code	p16171_mono	PO16012_reint_0p83A	PO16002
Empirical formula	$C_{188}H_{289}Ce_2K_2O_{23}$	$C_{90}H_{138}KO_{10.5}Pr$	$C_{95}H_{109}CeKN_8O_4$
Formula weight	3275.61	1568.01	1606.12
Temperature/K	170(2)	120.01(10)	120.00(10)
Crystal system	monoclinic	monoclinic	triclinic
Space group	$P2_1/c$	$P2_1/c$	P-1
a/Å	18.81350(10)	18.6073(7)	17.29805(13)
b/Å	31.5876(2)	31.2563(11)	21.51193(16)
c/Å	33.9342(3)	33.684(2)	25.0448(4)
α/°	90	90	97.6409(9)
β/°	101.1900(10)	101.184(5)	103.4543(9)
γ/°	90	90	94.2363(6)
Volume/Å^3	19782.8(2)	19218.7(15)	8930.03(16)
Z	4	8	4
ρ_{calc}g/cm^3	1.1	1.084	1.195
μ/mm^{-1}	0.554	4.661	4.762
F(000)	7020	6720	3376
Crystal size/mm^3	0.21 ×0.17 ×0.13	0.176 × 0.14 × 0.03	0.4897 × 0.2254 × 0.0328
Radiation	MoKα (λ = 0.71073)	CuKα (λ = 1.54184)	CuKα (λ = 1.54184)
2Θ range for data collection/°	5.652 to 60.596	6.256 to 136.502	7.018 to 152.508
Index ranges	-26 ≤ h ≤ 26, -44 ≤ k ≤ 42, -47 ≤ l ≤ 47	-22 ≤ h ≤ 22, -28 ≤ k ≤ 37, -40 ≤ l ≤ 40	-21 ≤ h ≤ 17, -26 ≤ k ≤ 27, -31 ≤ l ≤ 31
Reflections collected	484034	242136	181419
Independent reflections	55385 [R_{int} = 0.0779, R_{sigma} = 0.0608]	35207 [R_{int} = 0.2727, R_{sigma} = 0.1470]	37057 [R_{int} = 0.0832, R_{sigma} = 0.0465]
Data/restraints/ parameters	55385/2/1984	35207/0/1895	37057/13/1997
Goodness-of-fit on F^2	1.542	1.207	1.049
Final R indexes [I>=2σ (I)]	R_1 = 0.0776, wR_2 = 0.2159	R_1 = 0.1378, wR_2 = 0.3584	R_1 = 0.0971, wR_2 = 0.2650
Final R indexes [all data]	R_1 = 0.1257, wR_2 = 0.2437	R_1 = 0.2027, wR_2 = 0.4161	R_1 = 0.1045, wR_2 = 0.2733
Largest diff. peak/hole / e Å^{-3}	1.80/-0.85	3.06/-1.89	8.56/-2.51

	7-Ce^{P}	**8-Ce^{P}**	**8-Ce^{PT}**
Identification code	p16002	P15174b_monoclinic	P16106/P16105_ortho
Empirical formula	$C_{138.57}H_{176}Ce_2K_2O_{19.55}$	$C_{149}H_{196.66}Ce_2K_2O_{16}$	$C_{296}H_{424}Ce_4K_4O_{26}$
Formula weight	631.7	2602.15	5115.21
Temperature/K	293(2)	170(2)	170(2)
Crystal system	triclinic	monoclinic	orthorhombic
Space group	P-1	$P2_1/c$	Pbca
a/Å	21.7935(6)	21.2743(5)	31.2721(4)
b/Å	23.1848(7)	20.1178(5)	29.5187(3)
c/Å	24.6660(10)	36.6764(9)	33.7264(4)
α/°	112.342(3)	90	90
β/°	91.967(3)	91.733(2)	90
γ/°	92.513(2)	90	90
Volume/Å^3	11498.9(7)	15690.0(7)	31133.3(6)
Z	2	4	4
ρ_{calc}g/cm^3	0.73	1.102	1.091
μ/mm^{-1}	0.464	0.68	0.682
F(000)	2664	5491	10864
Crystal size/mm^3	0.7227 × 0.5537 × 0.4425	0.3258 × 0.1254 × 0.0631	0.346 × 0.21 × 0.069
Radiation	MoKα (λ = 0.71073)	Mo Kα (λ = 0.71073)	Mo Kα (λ = 0.71073)
2Θ range for data collection/°	5.87 to 54.97	5.662 to 48.216	5.65 to 48.216
Index ranges	-28 ≤ h ≤ 28, -30 ≤ k ≤ 23, -32 ≤ l ≤ 30	-24 ≤ h ≤ 24, -23 ≤ k ≤ 23, -42 ≤ l ≤ 42	-35 ≤ h ≤ 35, -33 ≤ k ≤ 33, -38 ≤ l ≤ 38
Reflections collected	96912	211492	432612
Independent reflections	50164 [R_{int} = 0.0874, R_{sigma} = 0.1520]	24920 [R_{int} = 0.1334, R_{sigma} = 0.0873]	24703 [R_{int} = 0.1407, R_{sigma} = 0.0560]
Data/restraints/ parameters	50164/383/1535	24920/96/1556	24703/61/1525
Goodness-of-fit on F^2	1.592	1.085	1.521
Final R indexes [I>=2σ (I)]	R_1 = 0.1758, wR_2 = 0.4550	R_1 = 0.0937, wR_2 = 0.2685	R_1 = 0.0741, wR_2 = 0.2126
Final R indexes [all data]	R_1 = 0.2584, wR_2 = 0.5091	R_1 = 0.1341, wR_2 = 0.2923	R_1 = 0.1236, wR_2 = 0.2398
Largest diff. peak/hole / e Å^{-3}	9.64/-1.74	2.43/-0.67	2.00/-0.70

	9-Ce^{PT}	**16-Pr^{PT}**	**21**
Identification code	EDPA4	PO17001_refinalized	P16116
Empirical formula	$C_{296}Ce_4O_{24}$	$C_{56}H_{91}IO_8Pr$	$C_{48}Li_3O_5H_{0.25}$
Formula weight	4499.44	1160.09	677.55
Temperature/K	293(2)	293(2)	293(2)
Crystal system	monoclinic	triclinic	monoclinic
Space group	Pn	P-1	$P2_1/n$
a/Å	16.5331(2)	15.3646(9)	13.9569(8)
b/Å	31.1551(4)	15.4365(9)	23.1667(9)
c/Å	36.0837(6)	15.9168(8)	16.0426(11)
α/°	90	95.053(4)	90
β/°	99.828(2)	116.088(5)	115.112(8)
γ/°	90	115.951(6)	90
Volume/Å^3	18313.6(5)	2858.8(3)	4696.8(5)
Z	2	2	4
ρ_{calc}g/cm^3	0.816	1.348	0.958
μ/mm^{-1}	0.531	11.153	0.061
F(000)	4400	1206	1349
Crystal size/mm^3	0.14 × 0.12 × 0.09	0.17 × 0.15 × 0.13	0.12 × 0.08 × 0.07
Radiation	MoKα (λ = 0.71073)	CuKα (λ = 1.54184)	MoKα (λ = 0.71073)
2Θ range for data collection/°	3.202 to 56.75	6.792 to 152.166	5.608 to 60.496
Index ranges	$-21 \le h \le 20$, $-41 \le k \le 41$, $-47 \le l \le 46$	$-16 \le h \le 19$, $-19 \le k \le 18$, $-19 \le l \le 19$	$-19 \le h \le 19$, $-31 \le k \le 32$, $-22 \le l \le 22$
Reflections collected	251030	35153	114312
Independent reflections	74873 [R_{int} = 0.1330, R_{sigma} = 0.1104]	11813 [R_{int} = 0.0792, R_{sigma} = 0.0752]	13229 [R_{int} = 0.2839, R_{sigma} = 0.2902]
Data/restraints/ parameters	74873/10/1245	11813/0/608	13229/0/517
Goodness-of-fit on F^2	3.414	1.069	1.173
Final R indexes [I>=2σ (I)]	R_1 = 0.2758, wR_2 = 0.5468	R_1 = 0.0655, wR_2 = 0.1701	R_1 = 0.1551, wR_2 = 0.2829
Final R indexes [all data]	R_1 = 0.2905, wR_2 = 0.5520	R_1 = 0.0809, wR_2 = 0.1821	R_1 = 0.3670, wR_2 = 0.3509
Largest diff. peak/hole / e Å^{-3}	16.57/-7.20	2.41/-2.34	0.59/-0.33

	22-Ce^{P}	**23**	**24-Ce^{PT}**
Identification code	P16083_monoclinic	P16095_mono	P16116_mono087
Empirical formula	$C_{67}CeK_{1.5}O_6$	$C_{72}H_{101}K_5O_9$	$C_{540}Ce_6K_{23}O_{51}$
Formula weight	1099.44	1306.02	9041.42
Temperature/K	293(2)	293(2)	120.01(10)
Crystal system	monoclinic	monoclinic	triclinic
Space group	C2/c	$P2_1/n$	P-1
a/Å	27.8466(6)	19.6611(6)	18.1836(6)
b/Å	34.9368(8)	17.4375(5)	39.9811(4)
c/Å	17.9267(4)	20.9748(6)	54.5790(10)
α/°	90	90	82.0840(10)
β/°	92.9505(19)	91.523(3)	83.951(2)
γ/°	90	90	81.445(2)
Volume/Å^3	17417.2(6)	7188.5(4)	38717.3(15)
Z	8	4	2
ρ_{calc}g/cm^3	0.839	1.207	0.776
μ/mm^{-1}	0.627	0.358	4.104
F(000)	4292	2800	8866
Crystal size/mm^3	0.18× 0.12 × 0.11	0.12 × 0.08 × 0.07	0.36 × 0.15 × 0.07
Radiation	MoKα (λ = 0.71073)	MoKα (λ = 0.71073)	CuKα (λ = 1.54184)
2Θ range for data collection/°	5.616 to 47.634	5.756 to 58.758	6.608 to 100.87
Index ranges	-31 ≤ h ≤ 31, -39 ≤ k ≤ 39, -20 ≤ l ≤ 20	-26 ≤ h ≤ 26, -23 ≤ k ≤ 23, -28 ≤ l ≤ 27	-18 ≤ h ≤ 16, -35 ≤ k ≤ 39, -54 ≤ l ≤ 54
Reflections collected	145875	124312	285705
Independent reflections	13377 [R_{int} = 0.1717, R_{sigma} = 0.0948]	18067 [R_{int} = 0.2081, R_{sigma} = 0.2286]	80921 [R_{int} = 0.1695, R_{sigma} = 0.1595]
Data/restraints/ parameters	13377/0/681	18067/2/792	80921/2/2445
Goodness-of-fit on F^2	2.237	1.013	1.825
Final R indexes [I>=2σ (I)]	R_1 = 0.1229, wR_2 = 0.3619	R_1 = 0.1012, wR_2 = 0.1994	R_1 = 0.2934, wR_2 = 0.6240
Final R indexes [all data]	R_1 = 0.1686, wR_2 = 0.3783	R_1 = 0.2559, wR_2 = 0.2590	R_1 = 0.3923, wR_2 = 0.6824
Largest diff. peak/hole / e Å^{-3}	3.00/-0.73	0.67/-0.43	3.20/-3.45

	28-Ce^{PT}	**28-Pr^{PT}**	**31-Ce^{PT}**
Identification code	P16191	P16195	P16185a
Empirical formula	$C_{70}H_{89}CeClN_6O_4$	$C_{72}H_{83}ClN_8O_2Pr$	$C_{38.5}H_{61}CeNNaO_2Si_2$
Formula weight	1254.04	1268.82	789.17
Temperature/K	293(2)	293(2)	293(2)
Crystal system	triclinic	triclinic	triclinic
Space group	P-1	P-1	P-1
a/Å	13.9455(2)	13.8885(3)	13.8065(4)
b/Å	14.0906(2)	14.0584(2)	15.6904(5)
c/Å	20.0971(3)	20.1573(3)	19.8224(5)
α/°	76.0300(10)	76.5680(10)	99.632(2)
β/°	80.3200(10)	80.439(2)	107.579(2)
γ/°	61.8470(10)	62.616(2)	103.291(2)
Volume/Å^3	3372.09(9)	3391.09(12)	3852.0(2)
Z	2	2	2
ρ_{calc}g/cm^3	1.235	1.243	0.68
μ/mm^{-1}	0.764	0.807	0.644
F(000)	1316	1326	824
Crystal size/mm^3	0.373 × 0.129 × 0.111	0.12 × 0.12 × 0.08	0.465 × 0.368 × 0.276
Radiation	MoKα (λ = 0.71073)	Mo Kα (λ = 0.71073)	MoKα (λ = 0.71073)
2Θ range for data collection/°	5.82 to 58.754	5.868 to 60.572	6.034 to 48.216
Index ranges	-19 ≤ h ≤ 19, -19 ≤ k ≤ 18, -27 ≤ l ≤ 27	-18 ≤ h ≤ 19, -18 ≤ k ≤ 18, -28 ≤ l ≤ 28	-15 ≤ h ≤ 15, -18 ≤ k ≤ 18, -22 ≤ l ≤ 22
Reflections collected	74594	83658	64514
Independent reflections	16549 [R_{int} = 0.0440, R_{sigma} = 0.0452]	18379 [R_{int} = 0.0634, R_{sigma} = 0.0635]	12235 [R_{int} = 0.0412, R_{sigma} = 0.0350]
Data/restraints/ parameters	16549/0/791	18379/24/745	12235/31/510
Goodness-of-fit on F^2	1.025	0.941	2.263
Final R indexes [I>=2σ (I)]	R_1 = 0.0378, wR_2 = 0.0837	R_1 = 0.0478, wR_2 = 0.1248	R_1 = 0.1939, wR_2 = 0.5027
Final R indexes [all data]	R_1 = 0.0521, wR_2 = 0.0904	R_1 = 0.0711, wR_2 = 0.1427	R_1 = 0.2247, wR_2 = 0.5314
Largest diff. peak/hole / e Å^{-3}	0.66/-0.66	0.81/-0.61	5.73/-1.37

	33-Ce^{PT}	**39e**	**39f**
Identification code	P17023	P13135B	exp_1480
Empirical formula	$C_{232}H_{296}B_4Ce_4N_{20}O_9$	$C_{24}H_{41}BN_2O$	$C_{30}H_{39}BN_2O$
Formula weight	4112.59	652.76	454.44
Temperature/K	293(2)	170.15	153.15
Crystal system	triclinic	triclinic	triclinic
Space group	P-1	P-1	P-1
a/Å	19.7117(3)	9.2340(19)	8.1720(4)
b/Å	23.3826(4)	11.811(3)	8.6088(3)
c/Å	25.9038(6)	12.577(3)	20.0510(8)
α/°	82.210(2)	69.63(2)	81.502(3)
β/°	74.578(2)	70.562(19)	84.547(4)
γ/°	82.7970(10)	76.389(19)	68.047(4)
Volume/Å^3	11353.2(4)	1201.5(4)	1292.75(10)
Z	2	2	2
ρ_{calc}g/cm^3	1.203	1.804	1.167
μ/mm^{-1}	0.845	0.107	0.069
F(000)	4304	684	492
Crystal size/mm^3	0.462 × 0.176 × 0.055	0.17 × 0.16 × 0.08	0.7199 × 0.483 × 0.1416
Radiation	MoKα (λ = 0.71073)	MoKα (λ = 0.71073)	MoKα (λ = 0.71073)
2Θ range for data collection/°	5.702 to 51.364	6.68 to 59.5	5.988 to 50.698
Index ranges	-24 ≤ h ≤ 23, -28 ≤ k ≤ 28, -31 ≤ l ≤ 31	-12 ≤ h ≤ 11, -11 ≤ k ≤ 15, -15 ≤ l ≤ 14	-9 ≤ h ≤ 9, -10 ≤ k ≤ 10, -24 ≤ l ≤ 24
Reflections collected	177897	4846	20429
Independent reflections	43075 [R_{int} = 0.1102, R_{sigma} = 0.1338]	3474 [R_{int} = 0.0645, R_{sigma} = 0.1219]	4734 [R_{int} = 0.0326, R_{sigma} = 0.0329]
Data/restraints/ parameters	43075/288/2537	3474/18/262	4734/2/313
Goodness-of-fit on F^2	1.034	1.02	1.032
Final R indexes [I>=2σ (I)]	R_1 = 0.0761, wR_2 = 0.1801	R_1 = 0.0892, wR_2 = 0.2225	R_1 = 0.0889, wR_2 = 0.2403
Final R indexes [all data]	R_1 = 0.1478, wR_2 = 0.2155	R_1 = 0.1547, wR_2 = 0.2740	R_1 = 0.1109, wR_2 = 0.2582
Largest diff. peak/hole / e Å^{-3}	2.66/-1.00	0.43/-0.30	1.28/-0.42

	47	**48**
Identification code	P16052	p15081
Empirical formula	$C_{26}H_{35}N_2NaO$	$C_{34}H_{51}KN_2O_3$
Formula weight	414.55	574.86
Temperature/K	293(2)	293(2)
Crystal system	triclinic	monoclinic
Space group	P-1	$P2_1/n$
a/Å	8.6969(7)	11.5409(3)
b/Å	12.2469(10)	16.2694(5)
c/Å	12.7912(9)	17.8385(6)
α/°	73.287(7)	90
β/°	79.755(6)	91.020(3)
γ/°	69.269(7)	90
Volume/Å^3	1215.95(18)	3348.88(18)
Z	2	4
ρ_{calc}g/cm^3	1.132	1.14
μ/mm^{-1}	0.084	0.192
F(000)	448	1248
Crystal size/mm^3	0.2435 × 0.2358 × 0.1035	0.8209 × 0.1225 × 0.1218
Radiation	MoKα (λ = 0.71073)	Mo Kα (λ = 0.71073)
2Θ range for data collection/°	6.266 to 41.628	6.128 to 41.632
Index ranges	$-8 \le h \le 8$, $-12 \le k \le 12$, $-12 \le l \le 12$	$-11 \le h \le 11$, $-16 \le k \le 16$, $-17 \le l \le 17$
Reflections collected	12583	43429
Independent reflections	2543 [R_{int} = 0.0759, R_{sigma} = 0.0638]	3489 [R_{int} = 0.0522, R_{sigma} = 0.0257]
Data/restraints/ parameters	2543/0/280	3489/0/360
Goodness-of-fit on F^2	1.069	1.029
Final R indexes [I>=2σ (I)]	R_1 = 0.0589, wR_2 = 0.1294	R_1 = 0.0707, wR_2 = 0.1767
Final R indexes [all data]	R_1 = 0.0880, wR_2 = 0.1428	R_1 = 0.0851, wR_2 = 0.1868
Largest diff. peak/ hole / e Å^{-3}	0.23/-0.17	0.57/-0.41

	49	**56**
Identification code	P16041_tetra	p15131
Empirical formula	$C_{26}H_{37}N_2O_2$	$C_{176}H_{204}B_4N_8O_4$
Formula weight	409.57	2538.7
Temperature/K	293(2)	293(2)
Crystal system	tetragonal	monoclinic
Space group	$P\text{-}42_1c$	$P2_1/c$
a/Å	20.3895(5)	12.6433(3)
b/Å	20.3895(5)	14.6551(3)
c/Å	12.0239(6)	20.8923(5)
α/°	90	90
β/°	90	106.141(2)
γ/°	90	90
Volume/Å^3	4998.7(4)	3718.52(15)
Z	8	1
ρ_{calc}g/cm^3	1.088	1.134
μ/mm^{-1}	0.068	0.066
F(000)	1784	1368
Crystal size/mm^3	0.572 × 0.1315 × 0.0689	0.9772 × 0.3226 × 0.1392
Radiation	MoKα (λ = 0.71073)	MoKα (λ = 0.71073)
2Θ range for data collection/°	5.608 to 48.206	5.918 to 48.814
Index ranges	$-23 \le h \le 23$, $-23 \le k \le 23$, $-13 \le l \le 13$	$-14 \le h \le 14$, $-17 \le k \le 17$, $-24 \le l \le 24$
Reflections collected	64490	66452
Independent reflections	3968 [R_{int} = 0.1583, R_{sigma} = 0.0636]	6110 [R_{int} = 0.0549, R_{sigma} = 0.0294]
Data/restraints/ parameters	3968/1/284	6110/0/442
Goodness-of-fit on F^2	1.04	1.031
Final R indexes [I>=2σ (I)]	R_1 = 0.0612, wR_2 = 0.1243	R_1 = 0.0453, wR_2 = 0.0962
Final R indexes [all data]	R_1 = 0.0797, wR_2 = 0.1324	R_1 = 0.0636, wR_2 = 0.1035
Largest diff. peak/hole / e Å^{-3}	0.18/-0.16	0.25/-0.17

6.6. References

1. G. B. Deacon, T. Feng, P. C. Junk, B. W. Skelton, A. N. Sobolev and A. H. White, *Aust J Chem*, 1998, **51**, 75-89.
2. G. B. Deacon, T. Feng, P. C. Junk, B. W. Skelton, A. N. Sobolev and A. H. White, *Aust. J. Chem.*, 1998, **51**, 75-89.
3. C. R. Krueger and H. Niederpruem, *Inorg. Chem. Synth.*, 1966, **8**, 15-19.
4. M. Schlosser and J. Hartmann, *Angewandte Chemie International Edition in English*, 1973, **12**, 508-509.
5. D. C. Bradley and J. S. Ghotra, *Inorg. Chim. Acta*, 1975, **13**, 11-16.
6. W. J. Evans, D. B. Rego and J. W. Ziller, *Inorganic Chemistry*, 2006, **45**, 3437-3443.
7. M. W. Rathke, *Org. Syn.*, 1973, **53**, 66-69.
8. A. A. Gridnev and I. M. Mihaltseva, *Synth. Commun.*, 1994, **24**, 1547-1555.
9. M. R. Johnston, M. J. Latter, R. N. Warrener, M. Golic, D. McKavanagh and D. Margetic, 2000.
10. J. A. L. Wells, M. L. Seymour, M. Suvova and P. L. Arnold, *Dalton Trans.*, 2016, **45**, 16026-16032.
11. P. J. Altmann and A. Pothig, *J. Am. Chem. Soc.*, 2016, **138**, 13171-13174.